Photophysics and photochemistry of pyrazolotriazole azomethine dyes.

Thomas, Jonathan David

Photophysics and Photochemistry of Pyrazolotriazole Azomethine Dyes

by

Jonathan David Thomas

A thesis submitted to the University of Wales in partial fulfilment of the requirements for the degree of Doctor of Philosophy in Chemistry

Department of Chemistry
University of Wales, Swansea
August 2004

DECLARATION

This work has not previously been accepted in substance for any degree and is not being concurrently submitted in candidature for any degree.

Signed ..... (candidate)

Date 22/9/04

This thesis is the result of my own investigations, carried out at the Department of Chemistry, University of Wales, Swansea from October 2000 to September 2003. Other sources are acknowledged by footnotes giving explicit references.

Signed ..... (candidate)

Date 22/9/04

I hereby give consent for my thesis, if accepted, to be available for photocopying and for inter-library loans after expiry of a bar on access approved by the University of Wales on the special recommendation of the Constituent Institution/University College concerned.

Signed ..... (candidate)

Date 22/9/04

For Clare

Acknowledgements

It only seems like yesterday when I first walked into lab 426 of the (then) Chemistry Dept. and was told in no uncertain terms, to 'Tidy this lab up'. Not the most auspicious of beginnings, but then as I'd learn over the next 3 years, there's a lot more to research than ground breaking science! Making friends, going places, laughing (lots), shouting, farting, hours in a blackened room, moving laboratory paraphernalia, hours in front of Excel, tea drinking, travelling, thinking about something so hard that your head hurts, drinking beer to help you forget about the thing which makes your head hurt only to wake up with a worse headache than the original.

Throughout the whole experience I've been guided by Dr Peter Douglas, and I cannot thank him enough for his patience, assistance, enthusiasm, expertise and ability to organise a 'team building day' at the drop of a hat. The amount of times when he would have been well within his rights to give me a slap is probably into double figures but he never did, although he did shoot me on more than one occasion! Also I must thank Dr Chris Winscom at Kodak for his knowledge and input into this project. His ability to explain concepts and keep me on the right track has been invaluable.

Thanks also to Dr Dave Clark at Harrow for all of his guidance regarding dye synthesis. Dr Chris Morley and Dr Bill Bentley have also provided answers to many questions throughout the course of this study, while Dr Michael 'Monsieur' Garley was always on hand to offer advice particularly on all matters PC-like and the life cycle of the Indonesian land crab.

Special thanks must also be given to Prof Sergio Seixas and Joao Pina at the University of Coimbra for the opportunity to run the singlet oxygen quenching and single photon counting experiments. Obrigado! Also I'd like to thank Leanne Nicholls for her help with the acid titration experiments, Dr James Padfield for his assistance with the M.O. calculations and Prof Cameron Jones of Cardiff University for the x-ray crystallography data.

As for the 4th floor superteam at Swansea, a special mention first for Big Chris, he of the superhuman weight loss and the mockney accent. The number of times that the

two of us laughed is impossible to count, but moving the coffin (twice) was definitely one of funniest things I have ever done. Special thanks also to Rachel, Kay and Kath Mainwaring, for always being on hand to offer assistance and to laugh with us (or was it at us?). Thanks also to project students for generally adding to the great atmosphere that was always present, and also to Jon Jones for being a fellow scouse supporter on the top floor!

A special mention too for the tea room crew, Kath-O, Stevie G., Rhian, and Y Fachgen Watson. The lively discussions were always one of the high points of the day. Thanks also to John 'The master' Lewis, John Tregembo, Myron, Stan, Gareth, Mike Turner, Mike Manning and Eileen for all of their help and assistance. Also a big thank you to Tim Churchill for all his help with the printing of this thesis.

Finally I'd like to thank Mum and Dad, Chris and Em, Steve and Sarah and most of all my long suffering wife Clare, for always being there to help me and to give support when I most needed it. Diolch o galon.

And finally, why did I do it? To quote the great man:

"Mainly because it's a challenge....."

Geraint Pillock

Summary

The synthesis and physical and photochemical characterisation of a series of pyrazolotriazole azomethine (PT) dyes, varying only in the substituent in the R_6 position, with absorption maxima stretching from 546-633 nm, *i.e.* from the magenta to the cyan, has been carried out. X-ray crystallography confirms that the most stable conformer of the dyes is *syn* with respect to the azomethine bond, and shows that in the solid state the dyes are planar, with zero twist angle about the azomethine bond

Singlet state studies give the extinction coefficients of the dyes to be between 5.0-6.6 $\times 10^4$ mol^{-1} dm^3 cm^{-1}, and show quantum yields of fluorescence to be 2.0-6.3 $\times$ 10^{-4} at room temperature. At 77 K these increase to *ca.* 0.6-1. Singlet lifetimes have been calculated using the Strickler Berg equation and the emission quantum yields. These range from *ca.* 1-3.9 ps with dyes carrying strongly electron withdrawing and electron donating substituents giving longer lifetimes than those with electroneutral substituents.

Using laser flash photolysis it has been found that the rate at which PT dyes isomerise from the less stable *anti* isomer to *syn* can be catalysed by the addition of acid and therefore the protonation of the azomethine bond. The rate of protonation and isomerisation is not affected by the R_6 substituent (which controls dye hue) but rather by the solvent environment.

Triplet energy transfer measurements from porphyrin and phthalocyanine sensitisers give the triplet energies of the PT dyes to be 88-115 kJ mol^{-1}. Singlet oxygen luminescence has measured the rate of oxygen quenching by the dyes studied to be in the range 0.13-1.89 $\times$ 10^8 mol^{-1} dm^3 s^{-1}. Quantum yields of fade have been found to be in the range of 0.4-11.1 $\times$ 10^{-6} in oxygen and 0.2-8.9 $\times$ 10^{-7} in nitrogen.

Abbreviations and Symbols

Abs	Absorbance
A_{irr}	Irradiated area
AM1	Austin method 1
CAP	Chloroaluminium phthalocyanine
CCD	Charge coupled device
CI	Chemical ionisation
DPBF	Diphenylisobenzofuran
EI	Electron ionisation
EPA	diethylether:isopentane:ethanol (2:5:5 v/v)
E_T	Triplet energy
E_T (30)	Solvent polarity parameter
EtOH	Ethanol
ε	Extinction coefficient
GaNC	Gallium naphthalocyanine
HID	High intensity daylight
HOMO	Highest occupied molecular orbital
HPLC	High performance liquid chromatography
IR	Infrared
isc	Intersystem crossing
K_a	Deprotonation equilibrium constant
k_{diff}	Diffusion controlled rate constant
k_{en}	Pre-exponential factor
k_{ic}	Rate constant for internal conversion
k_{isc}	Rate constant for intersystem crossing
k_{obs}	Rate constant (observed)
k_{ox}	Rate constant for oxidation
k_{qt}	Quenching rate constant
k_{rad}	Radiative rate constant
λ_{max}	Wavelength at maximum absorbance
LDR	Light dependent resistor

LUMO	Lowest unoccupied molecular orbital
M.O.	Molecular orbital
NMR	Nuclear Magnetic Resonance
NOE	Nuclear Overhauser Effect
P_{acid50}	- log [acid] for 50% protonation of dye
PDP	*p*-dodecylphenol
PdTPP	Palladium tetraphenylporphyrin
PM3	Parameterisation method three
PPD	*p*-phenylene diamine
PT	Pyrazolotriazole azomethine
QDI^+	Quinonediimine cation
Φ_{fade}	Quantum yield of fade
Φ_{fl}	Quantum yield of fluorescence
RT	Room temperature
SANS	Simulated artificial north skylight
SENS	Sensitiser
S_n	Singlet state
SnNC	Tin naphthalocyanine
SSC	Small scale coater
τ	Lifetime
TFAA	Trifluoroacetic acid
THF	Tetrahydrofuran
T_n	Triplet state
TPP	Tetraphenylporphyrin
UV	Ultra violet
Vis	Visible
v/v	Volume to volume
w/w	Weight for weight
ZnTPP	Zinc tetraphenylporphyrin

Contents

Chapter 1

Introduction

1.1 Introduction to photography

Mankind's desire for reproducing scenes and images can be appreciated by noting ancient art on cave walls and the fact that one of the most ancient forms of written communication, hieroglyphics, involved the use of pictures/images as a precursor to words and letters.

A modern form of this communicative technology is photography, which is an integral part of 21st century life. The speed at which images can now be reproduced is truly staggering with 50-billion colour photographic prints [1] processed each year. The history and science behind these photographic images is well documented, and many of the principles which are integral to photography have changed little since their discovery hundreds of years ago.

The earliest forms of photographic technology were based on the *camera obscura*, a device that throws an optical image of a view onto a flat surface by means of a pin hole [2], and which could be used as a tool for sketching objects. Two Frenchmen, Nicephore Niepce and Louis Jacques Monde Daguerrre were among the first to try and make optical images permanent by utilising this basic *camera obscura*. Daguerre formed a light sensitive surface of silver salts by using a silvered copper plate which had been treated with iodine vapour. Daguerre produced an image that could be observed after treatment of the exposed salts with mercury vapour (the mercury deposits onto the exposed silver salts), so as to provide a positive image. These images came to be known as 'daguerrotypes'.

The development of positive/negative photography with which we're familiar now was made by William Henry Fox Talbot. He also used light sensitive silver salts, but unlike Daguerre who produced a positive image Talbot produced a negative (*i.e.* dark where the positive was light and vice versa) image. He did this by exposing paper that had been impregnated with silver salts to the image of a scene focussed through a lens. By experimenting with various fixatives and developers, Fox Talbot discovered the 'latent image', the invisible precursor to the useful visible image which appears upon photographic development [3]. Utilising his discoveries Fox Talbot produced in the early 1840's the first textbook containing photographs 'The Pencil of Nature'. Although the processing of the early pioneering black and white photographers has

been refined many of the principles are the same now as 200 years ago, and as early as 1876 Louis Ducos du Hauron who has been described as the 'father of colour photography' [1] was granted a patent which contains a forecast of many processes that are now integral to modern photographic technology.

Colour photography had its infancy in the work of physicists who were interested in the characteristics of light. De Dominis noted in 1611 that most colours seen by the eye could be simulated by the superposition of blue, green and red light beams [4].

1.1.1 Additive Colour

"Adding together" light of these three primary colours in transmitted light results in white light. The absence of these colours is black. Other colours can be formed by mixing of the three different colours at different intensities. For example when red and green light are mixed the result is yellow, similarly mixing of green and blue results in cyan, and red and blue, magenta. Mixing the light beams at varying intensity results in a wide range of colours. Figure 1.1 shows the effect of mixing three primary colours in additive colour systems.

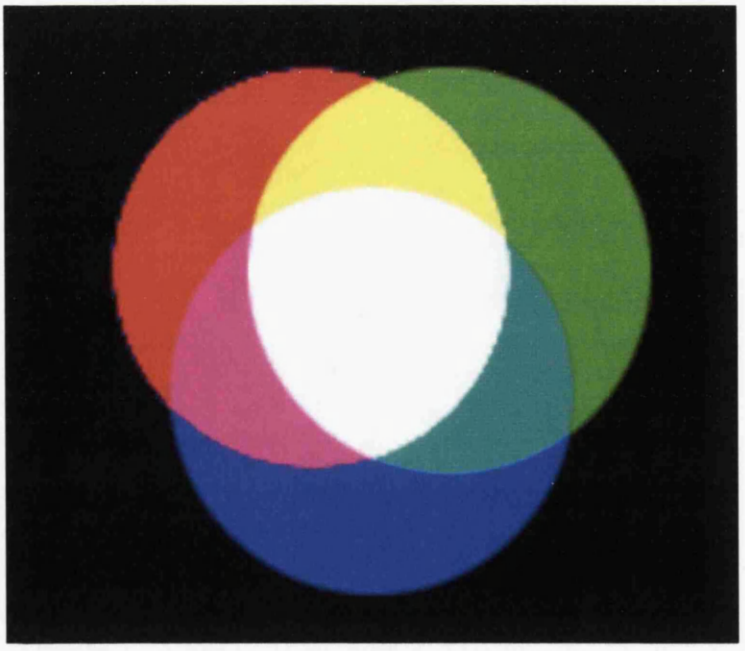

Figure 1.1: Additive colour arrangement.

This additive system was the first system to be utilised for colour photography. Scottish physicist, James Clark Maxwell produced the first colour photographic image from a negative of silver positive images that had been subjected to light produced from three projectors containing filters of the three primary 'additive' colours [5, 6].

This system was developed further and photographic systems created based on additive primaries by using very small red, green or blue filter particles adsorbed onto silver halide on a suitable support. Some of the processes that used the additive system included the Lumieres Autochrome and Dufaycolour processes as well as other screen processes. "Additive primaries" were also used in the Keller-Darion and Kodacolor processes. In comparison to the compact technology that we're familiar with today, the system used to produce additive colour photographs was cumbersome and complex. The process used a system of three primary colour filters in front of the camera lens, which resulted in separation of the colour contents of the scene/image. These separated signals were registered in different areas of the silver halide emulsions resulting in a positive silver image available for projection. Projection of white light through this image in silver recreated the original image in colour. There is an inherent problem with the additive method. The filters used in additive methods transmit only a third of the visible spectrum so that when two primary colour filters are superimposed on each other there is no transmission of light and the result is black, and therefore each of the three colour records must be recorded separately. 'Additive' methods now use either a side-by-side, spatial location of the primary elements, or a time sequential presentation whereby blue, green and red pictures are projected in rapid succession [7]. Other applications for this system include instant film processes and colour computer monitors [8].

1.1.2 Subtractive Colour

Additive colour theory relies on the presence of a light source and the mixing of different colours (wavelengths) of light to produce a variety of colours. Subtractive colour theory starts with the presence of all the colours in white light and relies on pigments or dyes to remove red, green or blue from the white light to provide the required colour. It differs from the additive process in that these subtractive primaries transmit two thirds of the visible spectrum and only remove a third (note figure 1.2).

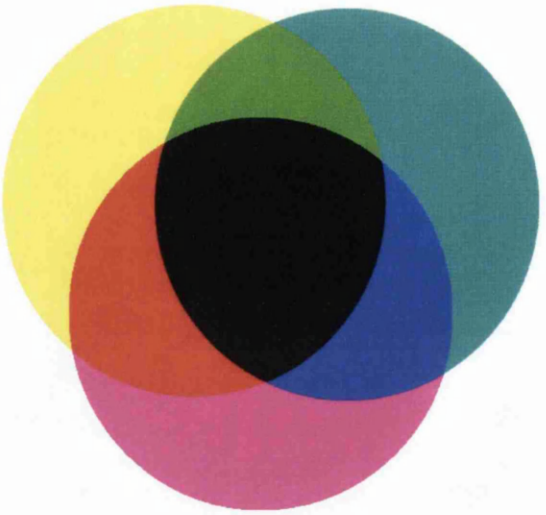

Figure 1.2: Subtractive colour arrangement.

While red, green and blue are the primary colours for additive processes, their complementary colours, magenta, cyan and yellow are the primary colours for subtractive processes. Cyan (an equal mixture of blue and green in additive terms) absorbs red light leaving blue and green transmitted. Magenta (an equal mixture of red and blue in additive terms) absorbs green light leaving red and blue transmitted. Yellow (an equal mixture of red and green in additive terms) absorbs blue light leaving red and green transmitted. When all three subtractive primary colours are combined the result is black.

Colour reproduction using the subtractive process was initially utilised to provide slides for viewing with a projector. Kodachrome® film was developed for cinematography in 1935 and the system named the 'integral tripack' (a tripack is the name given to the system where three layers, each sensitive to a primary colour are coated one over the other so that the distance between layers is a 'fraction' of one-thousandth of an inch [9]) resulted in the development of the technology that we see in today's colour films. By 1936 the Kodachrome® film was being marketed for use in slide preparation with miniature cameras [9]. This was followed by the 'negative films' of Kodacolor® in 1943 and Ektacolor® in 1948; these were the first mass-marketed

colour negative films for paper colour prints. The subtractive systems used to produce coloured prints today work on the same scientific principles as these methods developed around 60 years ago.

1.2 The future of silver halide or 'conventional' colour photography

A major development in photography was the production of the CCD (charge coupled device) digital camera which became generally available in the mid to late 90's, although the technology that it utilises has been around for almost 40 years [10]. In a digital CCD camera the imaging photons are converted into photoelectrons *via* a silicon based CCD [11].

A cursory examination suggests that digital photography offers significant advantages over silver halide technology. For example, the image taken on a digital camera can be instantly viewed, and if it is not acceptable that 'photo' can simply be deleted and a better one taken. Also the image, once stored on CCD, can be manipulated (*e.g.* enlarged, retouched or cropped) on a PC and directly printed on a conventional inkjet printer at home thus preventing the need for development as is needed for images from a silver halide negative.

Much work has been done in comparing the relative merits of digital and silver halide imaging. Tani [12, 13] suggests that silver halide technology can potentially become more cost effective than digital technology. He identifies the drawbacks of digital imaging as the time consuming nature and comparative high cost (*e.g.* replacement inks for inkjet printers) of printing the digital image, and the 'pixelation' of digital images when they're enlarged.

Two other aspects of the final image of concern to the consumer are the quality of colour reproduction, (which is usually not so good for home printed images from digital cameras as compared to professionally printed colour prints) and the stability of the image. Research into the 'light-fastness' of the final prints [14,15] of inkjet and silver halide systems has shown that both sets of dyes are affected by their environment and both are prone to similar degradation pathways.

Although the image quality of digital photographs printed professionally *via* an inkjet system is similar to that of the 'traditional' silver halide system there are still some fundamental problems regarding image durability in digital systems that need to be overcome. Dye–based inks, which are those most commonly used in inkjet applications, give images which are significantly less light stable than those which can be obtained photographically, although pigment-based inkjet colourants can give images of excellent light stability [16].

Some image scientists suggest that the future of photography revolves around improving the capability of silver halide systems by 'improving the sensitivity and image quality of silver halide emulsions' [12]. At present, a combination of both silver halide and digital technology can be used, where digital images are transferred onto 'conventional' silver halide paper to produce high quality prints [17].

1.3 General principles of photography

1.3.1 Collecting the image, the importance of light sensitive silver halide

Even though photographic technology is now almost 200 years old the light sensitive silver halide materials (AgX, where X is Cl, I or Br) used are basically the same. A modern day camera film is made up of silver halide crystals suspended in gelatin coated onto a plastic backing [18] to form a light sensitive emulsion*. Opening the shutter on a camera allows photons to fall on some of the crystals and photoinduced electron transfer from Br^- to Ag^+ then occurs. The Ag atoms so produced migrate through the crystal and cluster together forming a developable centre on the crystal. These clusters of Ag atoms make up the latent image. In order to make this image visible a chemical "developer" is used which reduces those crystals that have been exposed, but not the unexposed crystals, to silver.

Figure 1.3 shows transmission electron microscope images of silver halide grains.

---

* A photographic emulsion is a dispersion of photosensitive solid microcrystals in a protective colloid, or a photosensitive layer coated on a support, not as in colloid science where an emulsion is a colloidal system of 2 or more immiscible liquids [19].

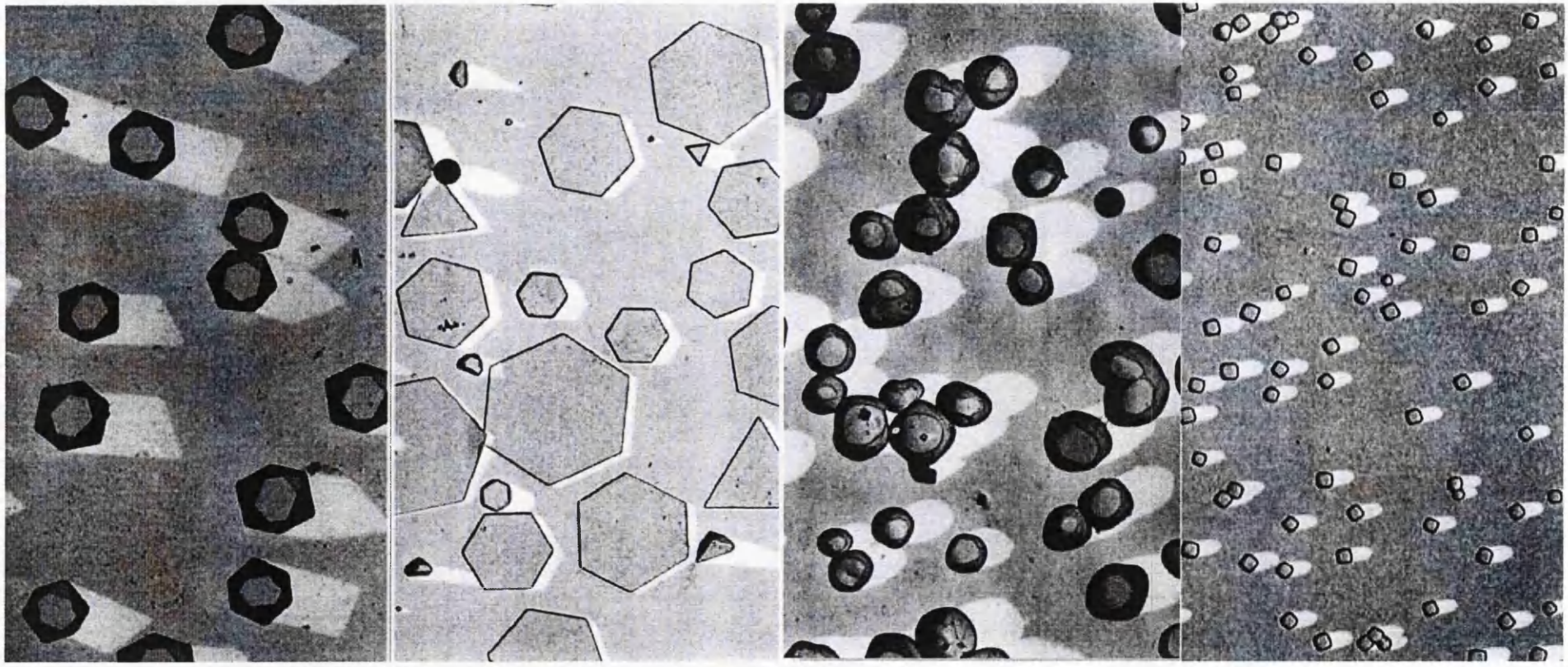

Figure 1.3: TEM images of silver halide crystal grains. (Thanks to Dr Gareth Evans.) The geometry can be varied by controlling the concentration of silver and halide during the crystallisation process. Different geometries have different light sensitive properties.

The latent image needs to be formed in high quantum yield, be sufficiently long lived, and also be easily converted into a useable form in a convenient chemical or physical process [20]. The silver atoms of the latent image act as catalytic sites for the reduction of Ag^+ to Ag. The reaction is autocatalytic, and proceeds until the entire grain is converted to metallic silver *i.e.* 'developed' [21].

1.3.2 The latent image

It is generally accepted that the mechanism by which the latent image forms is that proposed by Gurney and Mott [22, 23].

The stages of the mechanism can be summarised as follows:

1) A silver halide lattice absorbs photons of light, which results in promotion of photoelectrons from the valence band to the conduction band.
2) The promoted photoelectrons and interstitial silver ions migrate to preferential sites in the halide, resulting in the formation of silver atoms due to reduction of the silver cation.
3) This free silver atom then traps subsequently produced electrons resulting in the production of more free silver ions in the vicinity of the original site of photodecomposition.
4) Specks of silver grow near the preferential site.
5) Holes left behind by the electron are also mobile, and they diffuse towards the surface of the halide grain and react to form free halogen.
6) Aggregation processes continue by collection at the same site of additional photoelectrons and additional mobile silver ions.

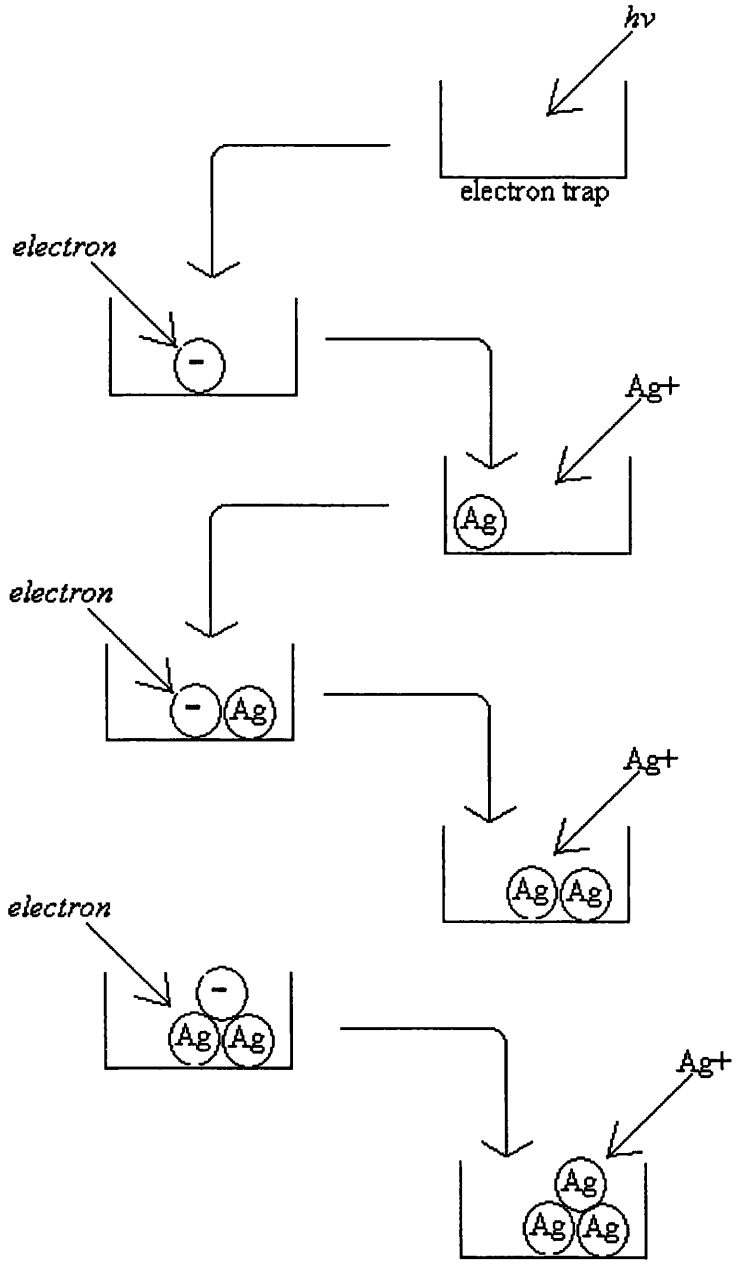

Figure 1.4: Schematic representation of the Gurney-Mott process [21].

The sensitivity of photographic silver emulsions can be greatly enhanced by the presence of labile sulphur or reducing groups within the gelatin in which the silver halide is suspended. It is thought that this increase in sensitivity is due to the formation of silver sulphide that can act as a more efficient electron trap.

1.3.3 Colour registration

The latent image described above would be that corresponding to light absorbed by the silver halide crystals alone *i.e.* the UV and blue spectral region. For colour reproduction, or any response to other wavelengths such as that required for panchromatic black and white film, colour sensitisation is required. This is achieved by use of dyes adsorbed onto silver halide grains which absorb light in selected spectral regions and which transfer the record of that absorption event to the silver halide grain by formation of a latent image. The first recorded example of a photosensitized reaction was by Vogel in 1873 [24] and it has since been termed "spectral sensitisation".

The characteristics of spectral sensitisation are as follows:

1) Only dye adsorbed onto the silver halide surface is effective.
2) The spectral region of sensitisation corresponds to the absorption spectrum of the adsorbed dye.
3) The latent images formed by intrinsic absorption and by spectral sensitisation are of essentially the same nature [4].

The high efficiency of the sensitisation process points towards electron transfer as being the dominant mechanism, although energy transfer may also be a factor. Examples of sensitising dyes include cyanines, pinacyanol and heterocyclic polymethine dyes [20].

1.3.4 Processing of the latent image

The developing agent used to convert the latent image into a useable image is usually an alkaline solution of a reducing agent. The clusters of silver atoms which make up the 'latent image' catalyse the reduction of those silver halide crystals exposed to light. The developing agent used in colour processing must meet the following criteria.

1. It must be a reducing agent for silver ions.
2. It should be a compound that is capable of reducing exposed silver halide grains at a higher rate than unexposed grains.
3. It must react with a coupler to form a light stable image dye.

The redox potential of the developer/oxidised developer system must be more negative than that of the silver halide/silver system, in order for electron transfer to occur from the developer to the silver halide to produce metallic silver.

In terms of formation of image dyes from 1H-pyrazolo [5,1-c]-1,2,4-triazoles (PT) in colour photography, the initial stage involves the oxidation of the *p*-phenylenediamine developer (PPD) and its subsequent reaction with the coupler in the presence of a silver halide to form an image dye. The steps can best be summarised as follows (note figure 1.5):

1) PPD is oxidised to the quinonediimine cation (QDI^+) by silver halide after AgX has absorbed a photon of light. The rate of this reaction is dependent on the degree of latent image present on the silver halide grain, that is the reaction is catalysed by the exposed silver halide grains which contain a metallic silver latent image [25].
2) QDI^+ then diffuses into the oleophilic droplet containing the coupler.
3) Due to the fact that the pH in its surrounding environment has been tailored so that the coupler exists in its anionic form a nucleophilic addition reaction takes place between the anionic coupler and the cationic oxidised developer. (The coupler contains a ballast group which anchors it in place while the reaction occurs with the (comparatively) smaller developer molecule.)

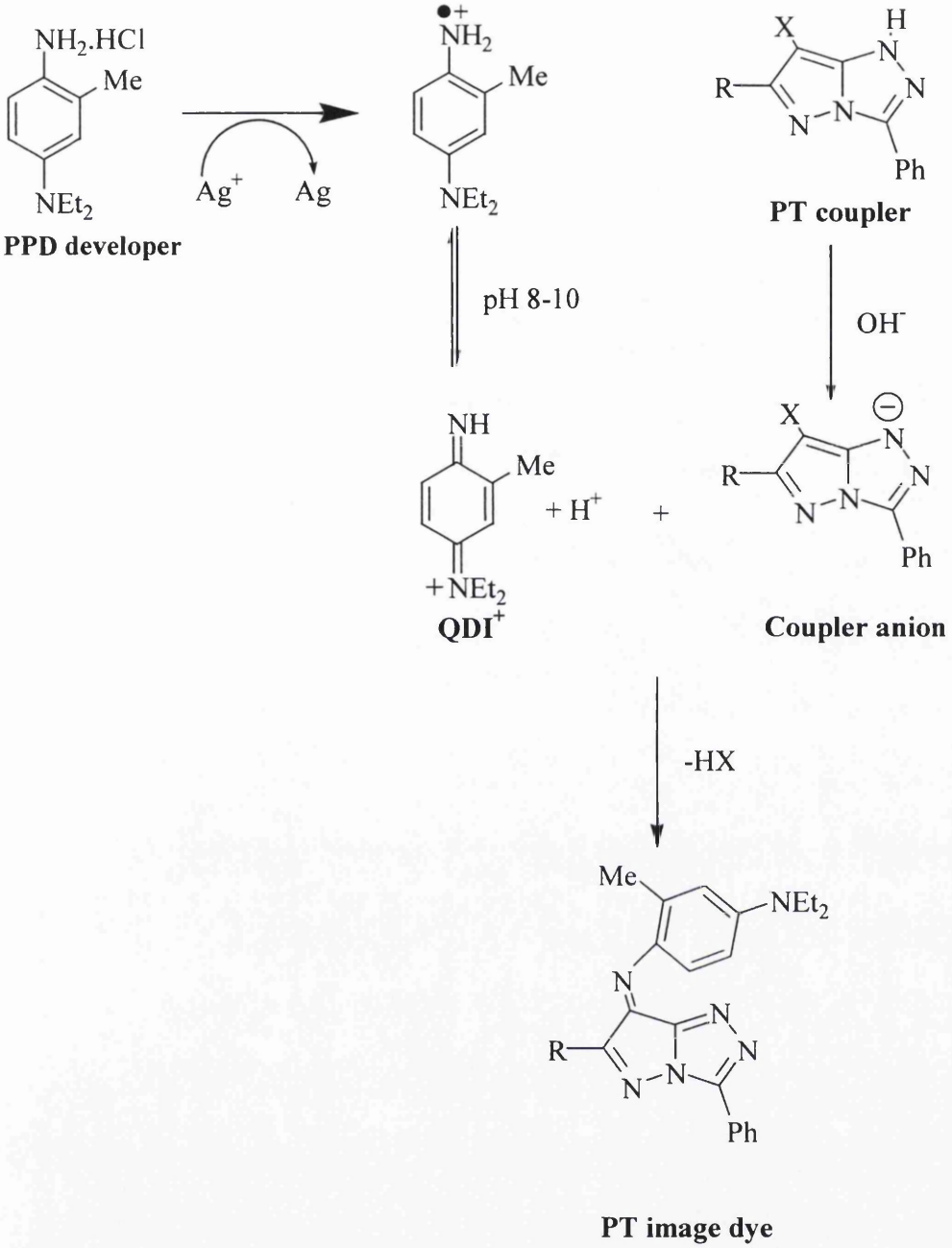

Figure 1.5: Image dye formation. Silver halide catalysed reaction between anionic coupler and cationic developer.

1.4 Couplers used in photographic coatings

Modern colour photographic systems consist of at least three layers of silver halide, each spectrally sensitised to a different primary spectral region. The top layer is sensitive to blue light and therefore contains a yellow dye forming coupler. Below this layer is a yellow filter which prevents any blue light (as silver halide is naturally sensitive to blue light) affecting the bottom 2 layers. The next layer is sensitive to green light and upon exposure and development will form a magenta image dye while the bottom layer is sensitive to the remaining red light and will contain a cyan coupler.

The couplers which form the final image dye are dissolved in oleophilic oil droplets and dispersed in gelatin in uniform manner, along with the silver halide crystal grains and other components to form the emulsion [26]. Paper or film base is the usual substrate onto which the three colour recording layers are arranged in a multilayer format [4].

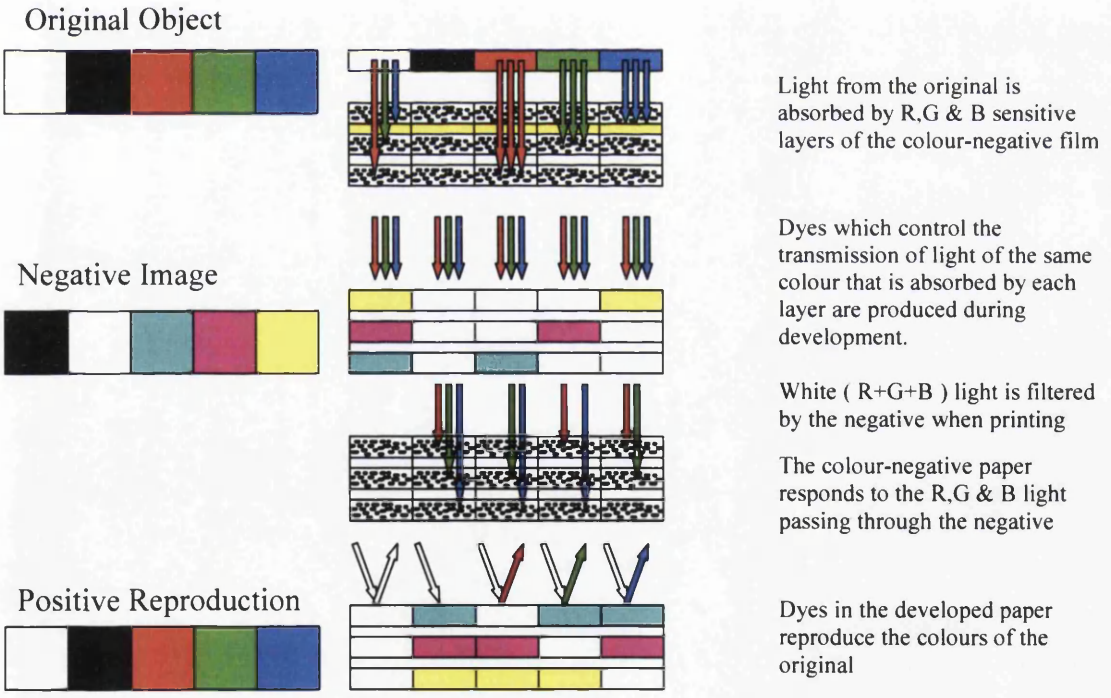

Figure 1.6: Simple schematic of the subtractive system which leads to the formation of a colour negative which is then developed to yield the final image.

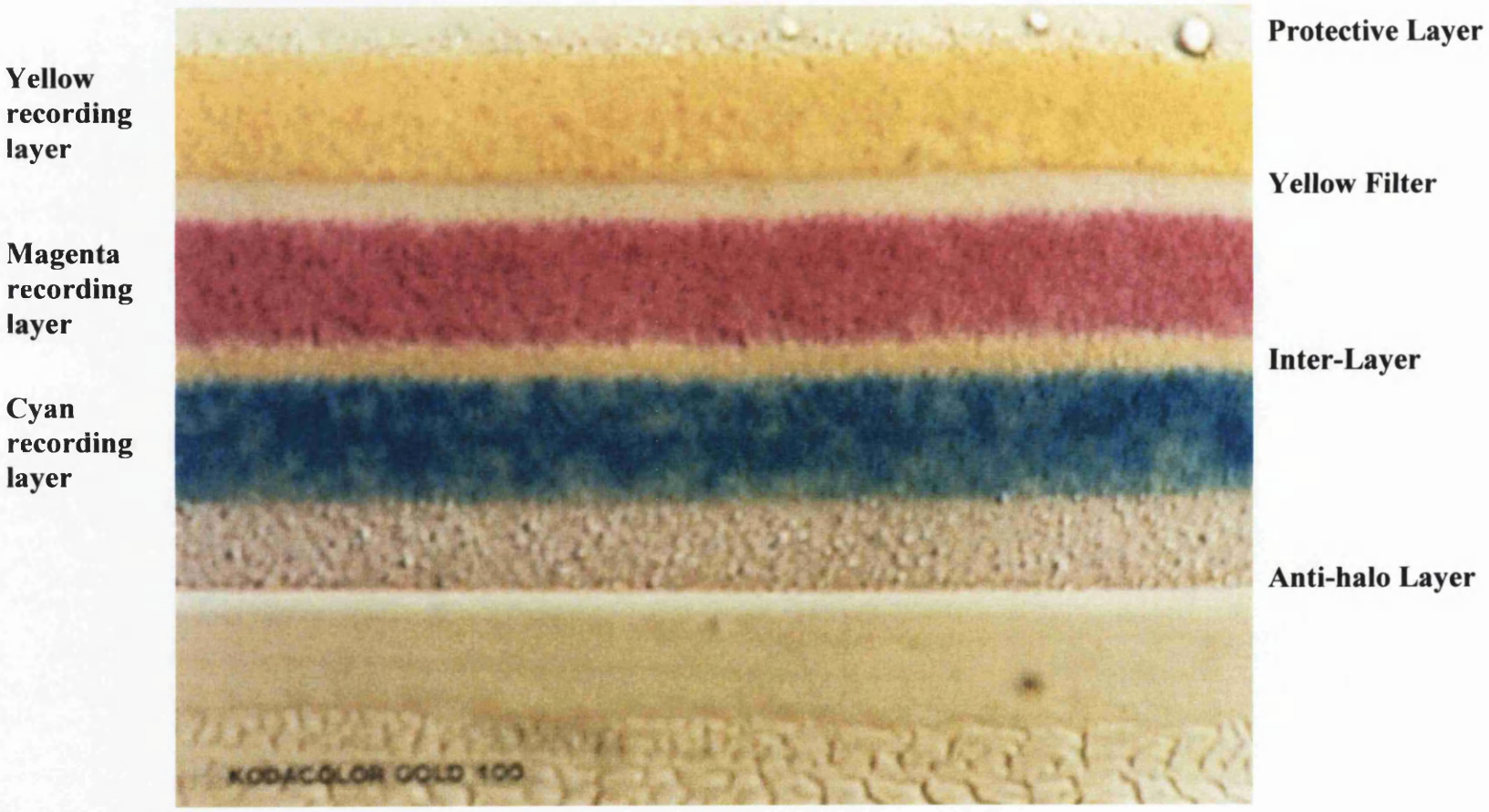

Figure 1.7: Cross-section of processed Kodacolor Gold® 100.

After exposure to light the film is then developed. This converts the latent image to metallic silver and the oxidised developer produced reacts with the coupler to produce dye [27] (figure 1.5). Removal of undeveloped silver halide after this stage will then result in the formation of a colour negative, which can be further processed to provide a positive print.

For couplers to work efficiently in photographic systems they need to react efficiently with the developer, be dispersed easily into the photographic emulsion, and form light stable image dyes. Thousands of couplers have been synthesised and characterised [28] and their respective properties well documented [29-31].

1.4.1 Yellow couplers

Couplers of this class usually contain an active open chain methylene group [32] (X-CH_2-Y). 1,3-dicarbonyl compounds such as benzoylacetanilides (see figure 1.8) and malondiamides are commonly used as yellow couplers [31]. Yellow azodyes have also been formed by coupling benzoisooxalones with the appropriate developer.

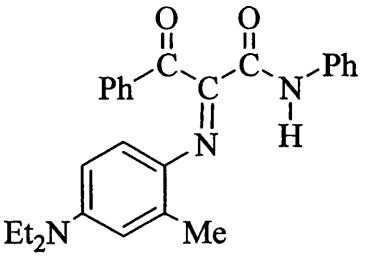

Figure 1.8: Typical 1,3-dicarbonyl image dye.

1.4.2 Magenta couplers

Magenta couplers usually contain either a cyanoacetyl derivative of a cyclic system, or a heterocyclic ring system containing an active (-CH_2-) component as part of the ring system [27]. The pyrazolone ring system is the most common magenta coupler, but pyrazolotriazole couplers, which are the subject of this thesis, are finding increasing use.

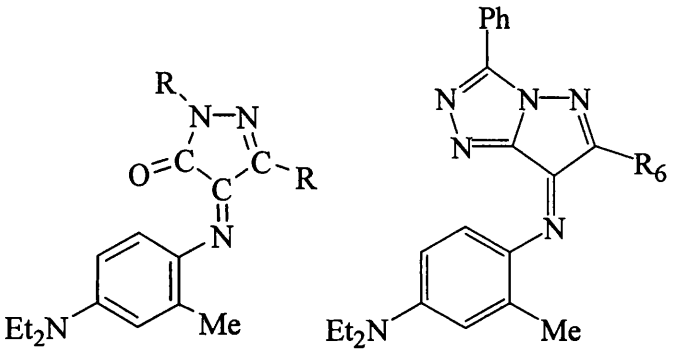

Figure 1.9: Magenta pyrazolone (left) and pyrazolotriazole azomethine image dyes.

1.4.3 Cyan couplers

Cyan couplers are almost exclusively derived from phenol or α-naphthol.

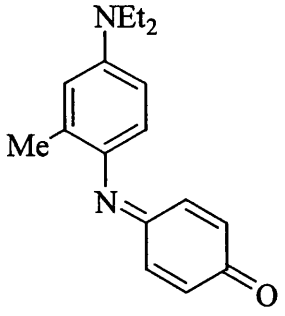

Figure 1.10: Typical indoaniline azomethine image dye.

1.5 Photochemical and photophysical processes of organic molecules

1.5.1 Fundamental laws

Some of the key photochemical concepts are now around 100 years old. Beer improved upon an equation first developed by Lambert, to formulate the 'Beer-Lambert Law' in 1852. The equation links the concentration of an absorbing material with the amount of light absorbed.

$$\log_{10} (I_o/I) = \varepsilon.C.l = \text{ABSORBANCE} \qquad \textbf{1.1}$$

(where ε is the molar extinction coefficient, C the concentration and l the path length of the cell used.)

The 'first law of photochemistry' was formulated by Grotthus and Draper in the early 1800's:

'*Only light absorbed by a molecule can bring about a photochemical change*'.

This was developed further to give the Stark-Einstein law:

'*A molecule which undergoes a photochemical change does so as the result of the absorption of a single quantum of light energy*' [33],

although with the advent of high intensity lasers exceptions to this rule such as two photon absorption can now be observed [34].

1.5.2 Absorption of light

Coloured materials absorb light in the visible region of the electromagnetic spectrum. The initial product of the absorption process is an excited state formed by the promotion of an electron to a level of higher energy.

The energy difference (ΔE) between the lowest excited state (E_2) and the ground state (E_1) is proportional to the frequency of the absorbed light, as shown below where h is Planck's constant, υ is the light frequency, c is the speed of light and λ the wavelength of light:

$$\Delta E = (E_2-E_1) = h\upsilon = hc/\lambda \qquad \textbf{1.2}$$

For most organic molecules the bonding (σ,π) and non-bonding (n) orbitals are full, while the corresponding antibonding (σ^*,π^*) orbitals are empty. The electronically excited state is reached by promotion of an electron from a bonding orbital to a higher energy anti-bonding orbital. The energy gap between the respective ground and excited states usually follows the following pattern in a given molecule:

a) $\sigma \rightarrow \sigma^*$; large energy gap, high energy transitions, absorptions in the UV region.

b) $\pi \rightarrow \pi^*$; lower energy than (a), most common transitions for organic dyes, with absorption of light in the visible region.

c) $n \rightarrow \pi^*$; longer wavelength transitions than (a) or (b), usually still in the visible region.

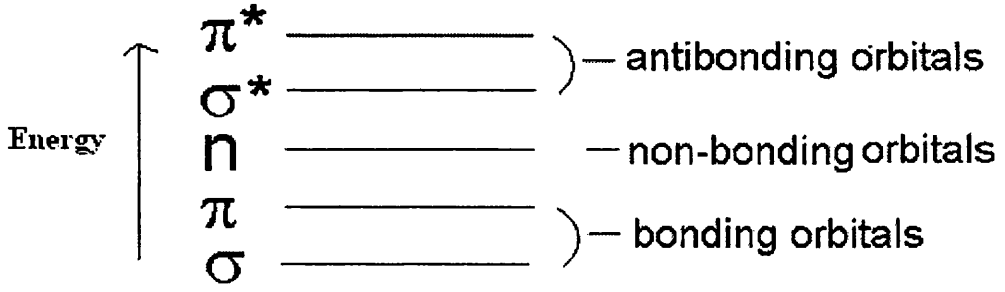

Figure 1.11: Electronic molecular energy levels.

These transitions can give rise to different excited states depending on the spin multiplicity of the molecule. For most organic molecules these are:

1) The singlet (S) state, for which electrons are paired with antiparallel spins.
2) The triplet (T) state, which contains two unpaired electrons with parallel spins.

The triplet state, as the name implies is composed of three states which are degenerate in the absence of an electric/magnetic field.

Two important rules/principles are Hund's rule:

'Electrons with parallel spins have a lower energy than a corresponding pair with opposed spins' and Pauli's principle:

'No more than two electrons may occupy any orbital, and if two do occupy it their spin directions must be opposed.'

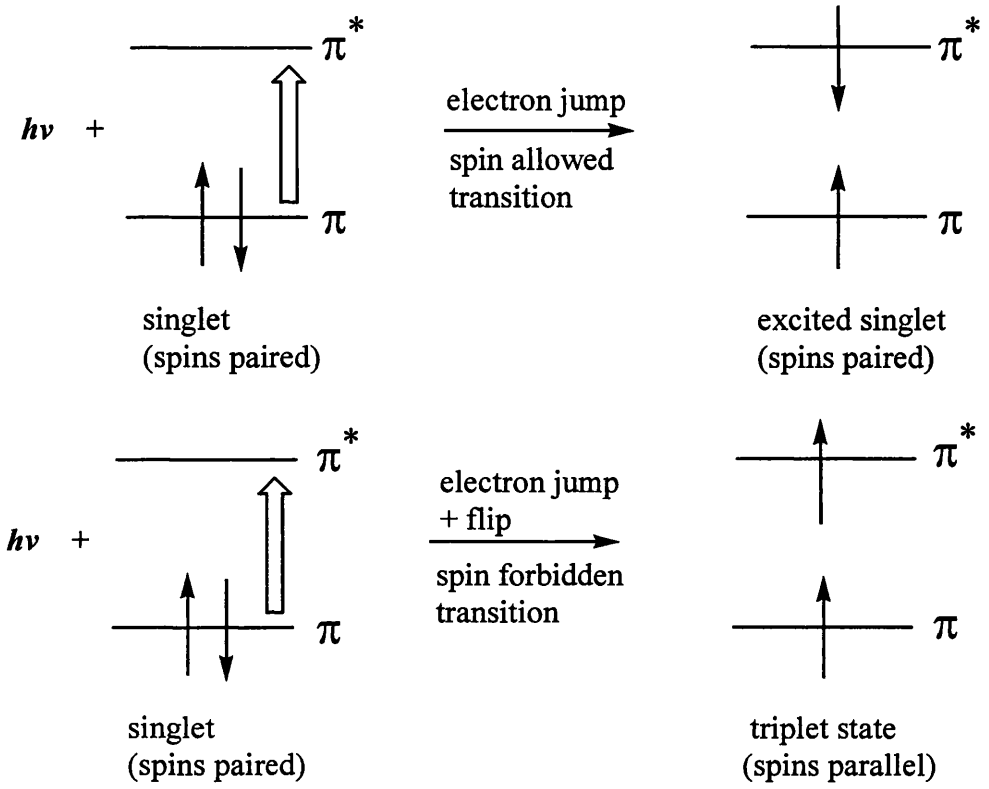

Figure 1.12: Orbital energy level diagram for a $\pi \rightarrow \pi^*$ transition in an organic molecule [35].

The absorption process and the various intramolecular processes that occur post excitation are best summarised by a Jablonski diagram as shown in figure 1.13.

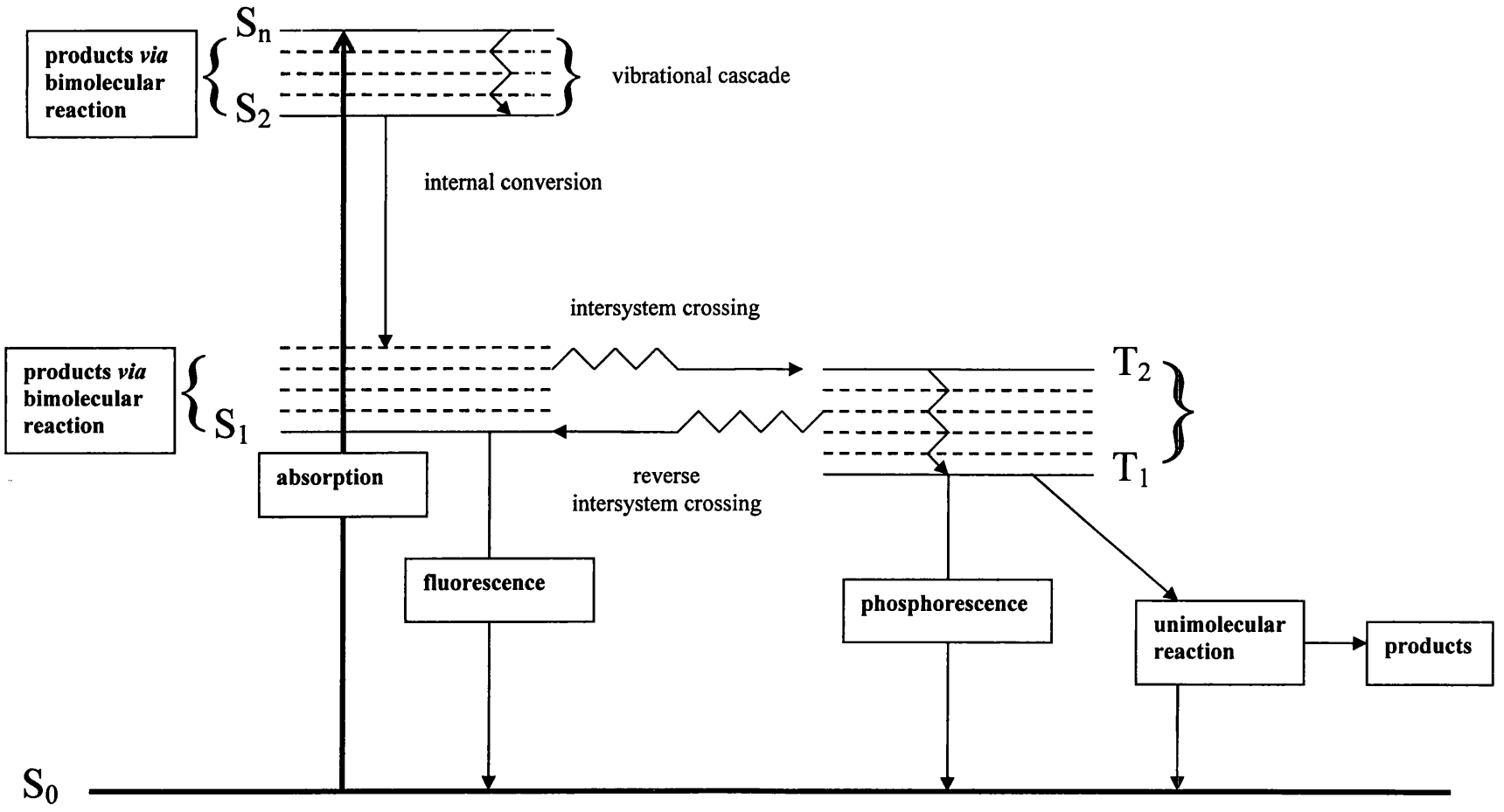

Figure 1.13: Jablonski diagram summarising intramolecular processes that occur after absorption, rotational states are not shown.

1.5.3 Deactivation of excited states by intramolecular processes

According to the Franck-Condon principle the promotion of the molecule to higher vibrational states occurs so quickly that the nuclear configuration of the molecule does not change [36]. Furthermore the spin selection rule means that transitions involving the simultaneous absorption of a photon and a change in electron spin are, for organic molecules made up of first row atoms, strongly forbidden. It follows, since for most molecules of this type the ground state is a singlet, that the initial product of photon absorption is an excited upper singlet state (S_n) which may also be vibrationally excited. Deactivation of this excited state may involve the following processes (illustrated by the Jablonski diagram, figure 1.13).

1) Vibrational relaxation (or 'cascade') to the lowest vibrational level of the state.
2) Internal conversion where a transition occurs between states of the same spin multiplicity *e.g.* $S_2 \rightarrow S_1$.
3) Intersystem crossing - a 'spin forbidden' transition from singlet to triplet states.
4) Reverse intersystem crossing - a 'spin forbidden' transition from triplet to singlet states.
5) Deactivation *via* molecular torsion, isomerisation or dissociation (unimolecular reaction).
6) Fluorescence - a radiative transition between S_n and S_0 states, which is spin allowed.
7) Phosphorescence - a 'forbidden' radiative transition, between states of different spin multiplicity *e.g.* $T_1 \rightarrow S_0$.

There is a general relationship between the extinction coefficient for absorption and the radiative rate constant for emission. A high absorption efficiency implies a rapid radiative rate. The fluorescence radiative rate constant can be calculated using the Strickler-Berg equation [37]. For dyes with high extinction coefficients, of the order of 10^4-10^5 mol^{-1} dm^3 cm^{-1}, such as those under investigation here, the fluorescence radiative rate constant is typically 10^8-10^9 s^{-1}, and the radiative lifetime a few ns.

The radiative rate constant for the spin forbidden process of phosphorescence is typically many orders of magnitude smaller. Hence phosphorescence is rarely observed in fluid solution because collisional intermolecular quenching by impurities and solvent molecules competes very effectively with emission as deactivation mechanisms for triplet states in fluid solution. In many cases freezing out these collisional processes and "locking" the molecule in an organic glass at 77K allows the detection of phosphorescence.

1.5.4 Deactivation of excited states by intramolecular torsion

The fluorescence quantum yield (Φ_{fl}) is a measure of the relative rate constant for radiative deactivation of the singlet state by fluorescence (k_{rad}) and that for all other deactivation processes (Σk).

$$\Phi_{fl} = k_{rad}/\Sigma k \qquad \textbf{1.3}$$

A low quantum yield implies either efficient ISC, IC or some other efficient mode of deactivation, such as isomerisation. (Molecular torsion can be an extremely efficient method for deactivation of excited states.) Generally, flexible molecules such as azo-dyes, and azomethine dyes, have low quantum yields of fluorescence due to the flexibility around the N=N or C=N bond, and the corresponding deactivation *via* molecular torsion or flexibility in the excited state, what Turro calls the "free rotor" effect [35].

1.5.5 Deactivation of excited states by intermolecular processes

Deactivation by intermolecular processes is usually termed quenching because these processes quench emission from the excited state. They can be classified as either physical quenching or chemical quenching depending upon whether or not the quenching process results in chemical change. Physical quenching of the excited state of a dye results in both dye and quencher returning to their ground states [7]; in chemical quenching one of them is altered chemically.

For the work presented in this thesis one mode of physical quenching is very important, namely energy transfer and particularly triplet-triplet energy transfer. (One mode of chemical quenching is also important, and that is chemical quenching of

singlet oxygen, but here it is the oxygen molecule which in an excited state and it is the dye which is the quencher, and so discussion of this will be left until a more general discussion of dye degradation by the self-sensitised singlet oxygen route.)

1.6 Energy Transfer in photochemical systems

1.6.1 Introduction

Energy transfer can take place from either singlet or triplet excited states. Higher singlet and triplet states rapidly relax to the S_1 and T_1 states *via* vibrational cascade and internal conversion; therefore we need only consider energy transfer from these first two states. There are three mechanisms for excited state energy transfer: radiative, Förster and exchange.

1.6.2 Radiative mechanism

The radiative mechanism is often described as trivial as it can be easily rationalised and understood by considering photophysical emission and absorption processes. An excited donor molecule (D*) emits a photon which can then be accepted by a ground state acceptor (A) [21].

$$D^* \rightarrow D + h\nu \qquad \textbf{1.4}$$

$$A + h\nu \rightarrow A^* \qquad \textbf{1.5}$$

For this method of energy transfer to be favoured within a system, a high quantum yield of emission from the donor, high concentration and extinction coefficients for the acceptor and good overlap between the emission and the absorption of donor and acceptor are required [27]. The need for a high extinction coefficient in the acceptor means this process is strictly limited to energy transfer to a singlet-singlet transition, and the high emission quantum yield generally limits it, for organic molecules in fluid RT solution, to energy transfer from a singlet-singlet transition, *i.e.* singlet-singlet energy transfer overall.

1.6.3 Förster mechanism of energy transfer

Also called resonance or Coulombic energy transfer this mechanism involves the movement of an electron from the LUMO to the HOMO of the excited state donor which simultaneously facilitates the promotion of an electron from the HOMO to the LUMO of the ground state acceptor (A). There is no exchange of electrons and at no point in the process is there any need for orbital overlap, *i.e.* collision, between the donor and acceptor. The mechanism is driven by perturbations between the oscillation of the D* electron inducing a dipole in the A electron. Energy transfer by this route can occur across distances of tens of nm, and it is often described as a 'long range' interaction [21].

Efficient Förster energy transfer requires an acceptor transition with a high oscillator strength, *i.e.* absorption coefficient, and as such it is, for most organic dye molecules, limited to energy transfer into an acceptor singlet-singlet transition. Since the energy transfer process of most interest to this thesis is triplet-triplet energy transfer we will not discuss Förster energy transfer further.

1.6.4 Exchange energy transfer

This method is fundamentally different from Förster energy transfer in that the mechanism is driven by collision or physical interaction between the excited donor and acceptor.

The lower part of figure 1.14 displays how the transferral of the electron from the LUMO of the excited donor to the LUMO of the acceptor corresponds with the simultaneous movement of an electron from the HOMO of the acceptor to the HOMO of the donor. This exchange occurs due to the overlap between the electron clouds of the donor and acceptor during collision. The collision causes a continuous potential energy surface to form between the donor and the acceptor on which the energy transfer reaction occurs; an energy transfer reaction with this mechanism of interaction is said to proceed adiabatically. For this to occur both donor and acceptor involved in the collision need to correlate in terms of (mainly) electron spin and orbital momentum [38].

The primary limitations on energy transfer by this mechanism are energetics and spin conservation. Both singlet-singlet and triplet-triplet energy transfer is possible. This is the most common mechanism for triplet-triplet energy transfer in solution, and it is this mechanism which is relevant to the work presented in this thesis.

Since energy transfer requires collision the maximum rate in fluid solution corresponds to the diffusion controlled rate (where the maximum rate is given by $k_d/(1 + k_{-d}/k_{en})$; if k_{en} is adequately large this reduces to k_d as will be shown later in Section 6.2.1). This is the expected rate if the donor triplet energy is much higher than that of the acceptor. When the donor-acceptor energy gap is small or when the acceptor triplet energy is higher than that of the donor the rate will be less than the diffusion controlled value.

The dependence of energy transfer rate on the donor-acceptor energy gap, orbital overlap criteria, and any structural reorganisation required of donor and/or acceptor during reaction is given by the Balzani equation [39]. This will be discussed in more detail in chapter 6 where results from studies of triplet-triplet, and singlet oxygen energy transfer processes are discussed.

1.6.5 Other forms of intermolecular deactivation

1.6.5.1 Electron transfer quenching

Other mechanisms of excited state deactivation include electron transfer which is a mechanism of chemical quenching which generates an oxidised/reduced donor/acceptor radical ion pair. This occurs by electron transfer and molecular collision is required. The maximum rate is limited by diffusion, and the rate is also controlled by energetic considerations *i.e.* the redox potentials of the acceptor and donor, and also any need for structural reorganisation upon oxidation/reduction of either donor or acceptor. It is possible that once formed in the solvent cage the radical ion pair rapidly deactivates by reverse electron transfer. In this case there is no resultant chemical change and the quenching process is classified as "physical quenching" [35].

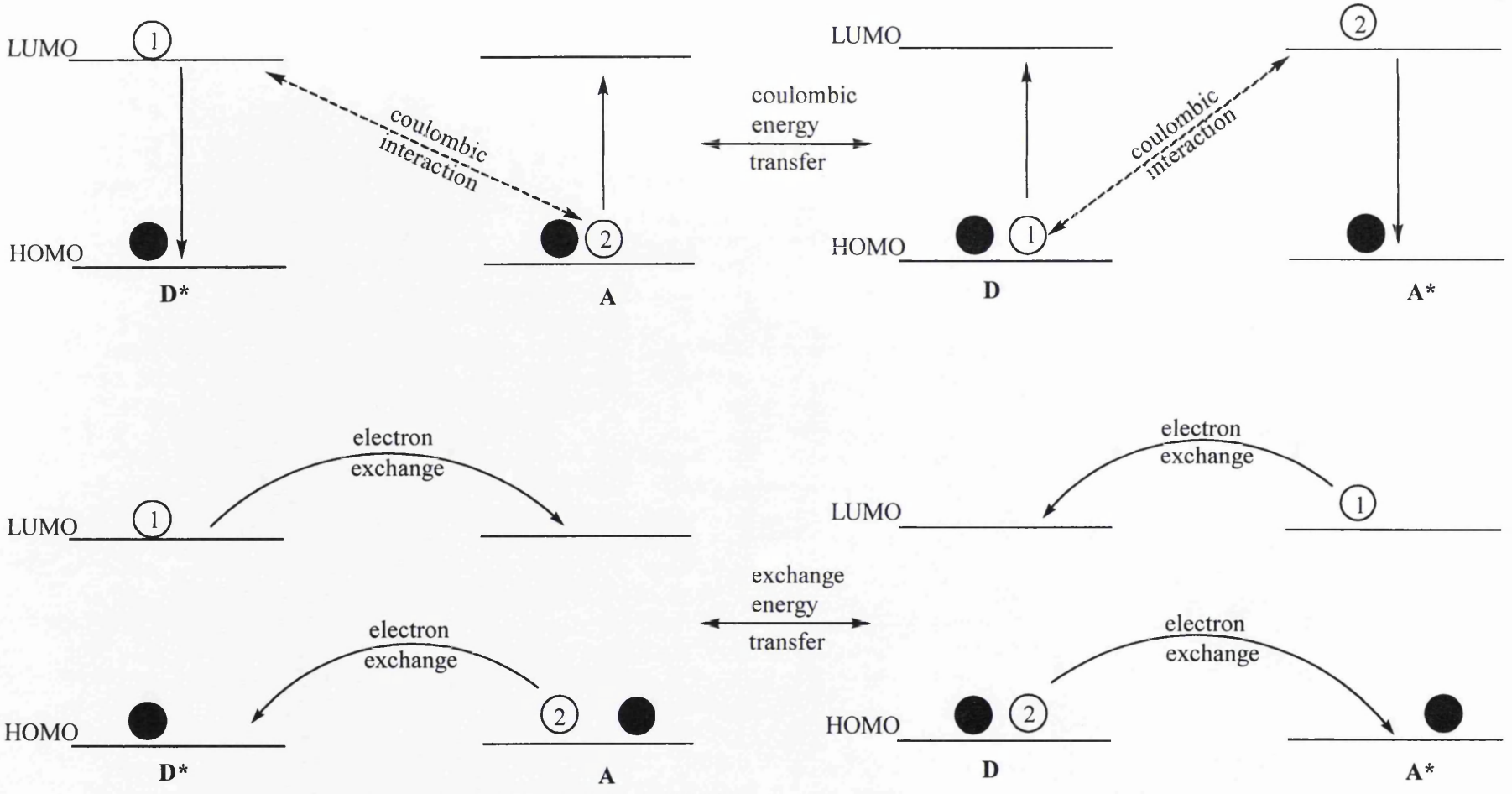

Figure 1.14: Orbital comparison of (top) Förster and (bottom) exchange energy transfer [35].

(D=Donor, A=Acceptor, LUMO=lowest unoccupied molecular orbital, HOMO=highest occupied molecular orbital)

1.7 A summary of the photochemistry and photophysics of pyrazolotriazole azomethine dyes

1.7.1 Absorption and emission characteristics

Bailey was the first to synthesise pyrazolotriazole azomethine (PT) dyes [40]. When compared to the related pyrazolone azomethine dyes [41, 42], he noted that, in general, PT dyes have higher extinction coefficients, no secondary blue absorption and a sharper 'cut off' at longer wavelength absorption. (Note figures 1.15 and 1.16.) Unlike pyrazolones, PT dyes do not exhibit two distinct electronic transitions in the visible spectral region, but rather a single electronic transition which can be resolved into vibrational fine structure (particularly in non-polar solvents).

Bailey also noted the effect that substituents on the pyrazolotriazole ring system have on final dye hue, with electron donating groups at the 6-position (note figure 1.9) producing magenta dyes and electron withdrawing groups forming cyan dyes.

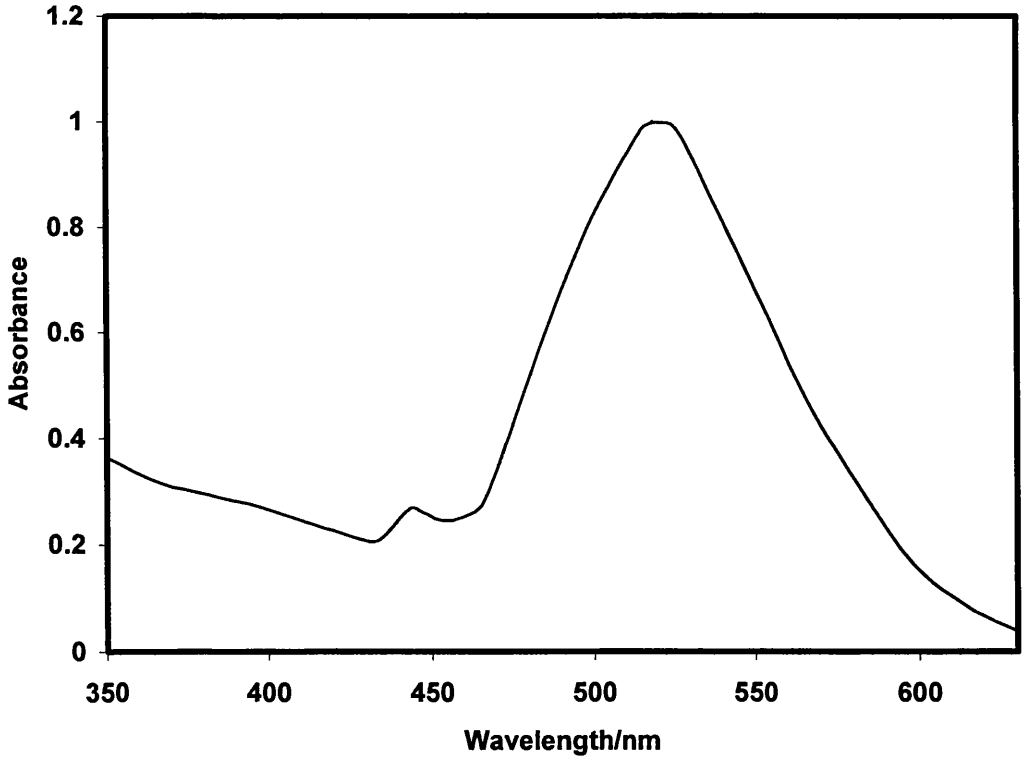

Figure 1.15: Typical absorption spectrum of a magenta pyrazolone azomethine image dye.

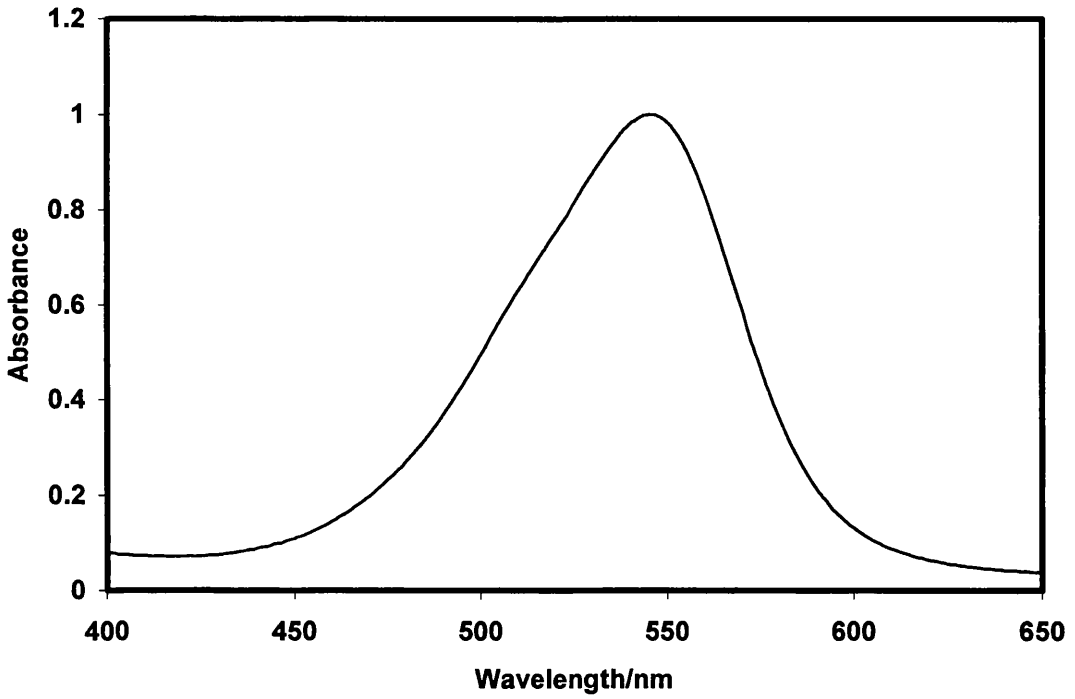

Figure 1.16: Typical absorption spectrum of a magenta pyrazolotriazole azomethine image dye.

The quantum yields of fluorescence of PT dyes in solution at room temperature are low (*ca.* 1×10^{-4}) [43] but these increase dramatically when the dyes are locked in organic glasses at low temperature to give yields of close to 1 at 77 K [44]. This has been attributed to the prevention of molecular torsion/isomerisation as the dye is prevented from movement around the azomethine bond in the frozen glass matrix.

In a detailed analysis of the excited states of PT dyes Wilkinson and co-workers assigned picosecond transients to the deactivation of the S_1 potential energy surface during photoisomerisation [45, 46]. More recent work has focussed on further characterisation of the S_1 potential energy surface and fluorescence emission from 'hot' molecules as the S_1 state relaxes to the state minimum [47]. Evanescent wave-induced fluorescence has also been used to study PT dye aggregation due to the changing of substituents on the pyrazolotriazole ring system [48]. Mikoshiba *et al.* showed that stability of PT dyes is also dependent on their respective oxidation potentials [49].

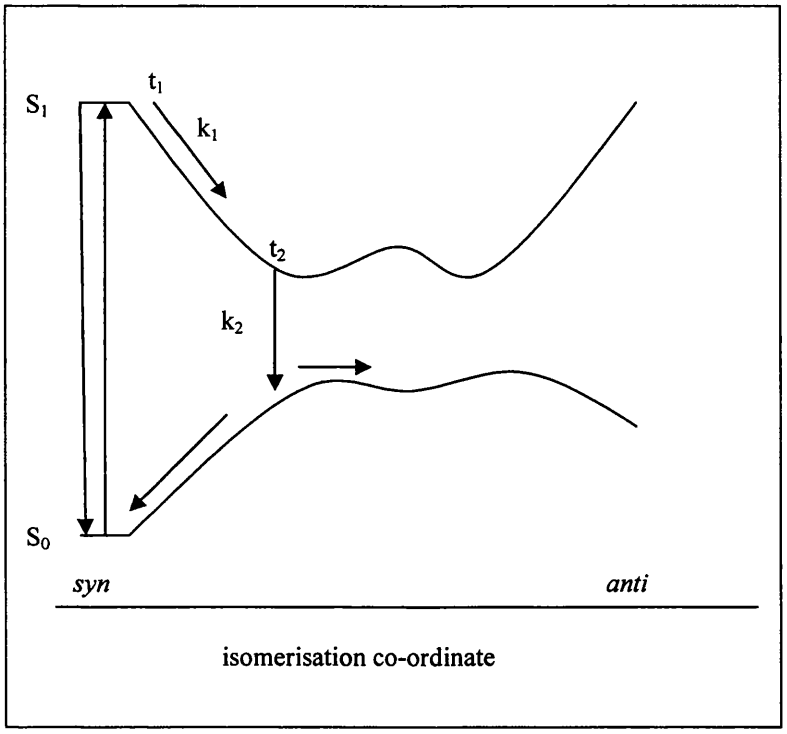

Figure 1.17: Potential energy surfaces used to model the photophysical behaviour of azomethine dye transients (t_1 and t_2) on the S_1 potential energy surface [45].

1.7.2 Triplet energy estimations

The determination of the triplet energy levels of PT dyes is particularly difficult due to the absence of any detectable phosphorescence even at low temperatures. Similar problems with pyrazolones were overcome by using indirect methods of energy transfer using low energy triplet sensitisers such as chrysene, isoviolanthrene and pentacene [50]. This technique has been used with magenta PT dyes to give estimations of triplet energies in the 100-120 kJ mol^{-1} range [51] and also with cyan indoanilines to give triplet energy estimations of 87-94 kJ mol^{-1} [52].

1.7.3 Configuration and photoisomerisation

The configuration of pyrazolotriazole azomethine dyes in solution has been studied by NMR [53] and NOE NMR spectroscopy. There is no evidence from NMR spectra for two isomers in solution, and therefore it is estimated that the equilibrium constant for isomerisation to give the less stable isomer is < 0.01. NOE shows that the 6-Me PT dye exists in the *syn* conformation in $CDCl_3$ [54]. It is assumed that this is the case for all PT dyes .

Isomerisation about the C=N azomethine bond for pyrazolones has been described in some detail by Herkstroeter [55-57]. PT dyes also undergo photoinduced isomerisation. Flash excitation generates a mix of the *syn* and *anti* isomers which decays over the μs to s timescale to give the thermally stable composition.

Douglas and Clark have examined the effects of substituent and solvent on the rate of isomerisation of PT dyes [58]. They concluded that the rate of photoisomerisation is mainly dependent on steric crowding around the azomethine bond. For example the rate of isomerisation when the 6-substituent is a H atom (k_{isom} = 2.69 s^{-1}) is much slower than that for the bulkier 6- tertiary butyl group (3.2 × 10^6 s^{-1}).

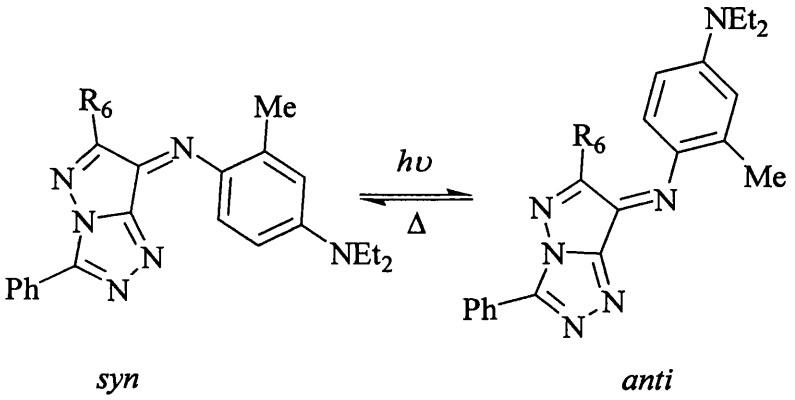

Figure 1.18: Photoisomersiation of a PT dye. Differences in R_6 subsituent have a large effect on the rate of photoisomerisation.

It is clear that one of the main reasons for the inherent photostability, and lack of RT fluorescence of PT dyes is their ability to undergo molecular torsion and photoisomerise. This enables the flexible molecule to remove excess energy rapidly and efficiently through an easily accessible route.

A summary of PT dye characteristics is given in table 1.1. Data for other azomethine dyes is included for comparison.

Characteristic	Yellow	Magenta	Cyan	Azine
	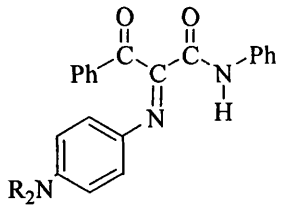	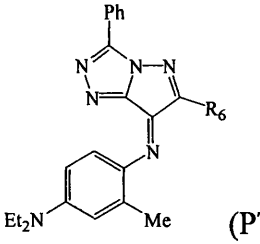 (PT)	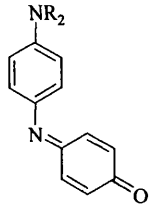	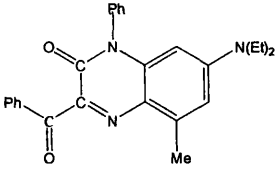
1st excited state energy/kJ mol^{-1}	280-285 [59]	210-241 (P) [40] 200-242 (PT) [40]	173-193	
1st excited state lifetime RT **77K**		*ca.* 2 ps (PT) [46] *ca.* 60 ps (PT) [46]	*ca.* 200-800 fs [27]	
Quantum yield of fluorescence RT **77K**		*ca.*1 × 10^{-4}(PT) [43] *ca.* 0.7-1 (PT) [44]	2-8 × 10^{-5} [27] 1-8 × 10^{-3} [27]	
1st excited triplet state energy (T_1) / kJ mol^{-1}	91-105 [59]	67-138 (P)[57] 100-118 (PT) [43]	87-94 [27]	180-192 [50]
2nd excited triplet state energy (T_2) /kJ mol^{-1}	161-168 [59]			
1st excited triplet state lifetime		*ca.*10 ns [43,46]	<5 μs [27]	50-83 μs [50]
Triplet quantum yield		*ca.*0.04 (PT) [43]	Low [27]	
Isomerisation quantum yield		*ca.*0.04 (PT) [43]	Low [27]	
Photodegradation quantum yields		10^{-6}-10^{-7} [59]		

Table 1.1: Summary of the photochemical and photophysical characteristics of azomethine dyes: P = pyrazolone, PT = pyrazolotriazole [27].

1.7.4 Interaction between PT dyes and ground state and singlet oxygen

The interaction of singlet oxygen with PT dyes is discussed at length in chapters 6 and 7 of this thesis. The importance of singlet oxygen in both photochemical and photobiological systems is shown by the sheer volume of work published discussing its mechanisms of formation and interaction with organic molecules [60-63].

The interaction of the dyes with oxygen is important to their photostability, since photodegradation is thought to proceed *via* an oxidative route [64].

In terms of its interaction with PT dyes the following scheme has been postulated to describe the various interactions occurring between dye and both ground state and singlet oxygen [51].

$$DYE + h\nu \rightarrow {}^1DYE^* \quad \textbf{1.6}$$

$${}^1DYE^* \rightarrow {}^3DYE^* \quad \textbf{1.7}$$

$${}^3DYE^* \rightarrow ISOMER \rightarrow DYE \quad \textbf{1.8}$$

$${}^3DYE^* + {}^3O_2 \rightarrow DYE + {}^1O_2^* \quad \textbf{1.9}$$

$${}^1O_2^* + DYE \rightarrow {}^3O_2 + ISOMER \rightarrow {}^3O_2 + DYE \quad \textbf{1.10}$$

$${}^1O_2^* + DYE \rightarrow [DYE\ DEGRADATION] + {}^3O_2 \quad \textbf{1.11}$$

There have been a number of studies of singlet oxygen generation and quenching by azomethine dyes and it has been found that, in general, these compounds are inefficient singlet oxygen sensitisers [52, 59, 65] but very effective singlet oxygen quenchers [51, 52, 64].

The low yields of singlet oxygen produced by these dyes upon irradiation in oxygenated fluid solution suggests a low triplet yield and short triplet lifetime [51]. In their early work, Herkstroeter *et al.* [50, 56, 57] suggested that both energy transfer and electron transfer were important in singlet oxygen quenching by azomethine dyes. Although there was no evidence for electron transfer products both mechanisms were thought important primarily because yellow azomethines were good singlet oxygen quenchers and at the time they were thought to have triplet energies which where much higher than singlet oxygen. However in their most recent work Herkstroeter and

Abu-Hasanayn show that yellow azomethines have low lying triplet states and they now interpret the quenching of singlet oxygen by these compounds in terms of an energy transfer mechanism [59].

Fade studies into the mechanisms of PT dye degradation have also been noted [66] and Kucybala *et al.* [65] in an investigation into the photobleaching of both pyrazolone and PT dyes reported that the bleaching rate was greatly increased when the rotation of the azomethine bond was restricted.

1.8 Mechanisms of dye fade

The mechanisms for the fading of photographic image dyes can be divided into light and dark fade. When prints are kept at constant temperature some dark fade processes may occur particularly if, during the printing process, factors such as the presence of impurities, residual material and pH have not been carefully controlled [66-68].

However, many prints are not kept in a dark environment at a constant temperature and instead they are displayed and are therefore also subject to photodegradation.

Measuring, or trying to 'model' conditions in a typical home environment is a contentious issue. Work by Andersen and coworkers has defined 120 lux as the representative light intensity to be used when monitoring light fade experimentally over a long period of time [69, 70]. (A lux is the International Standard (SI) unit of measure for luminous flux density at a surface. One lux equals one lumen per square metre.) Rapid fade studies enable a comparison between light intensity and dye stability to be made [25].

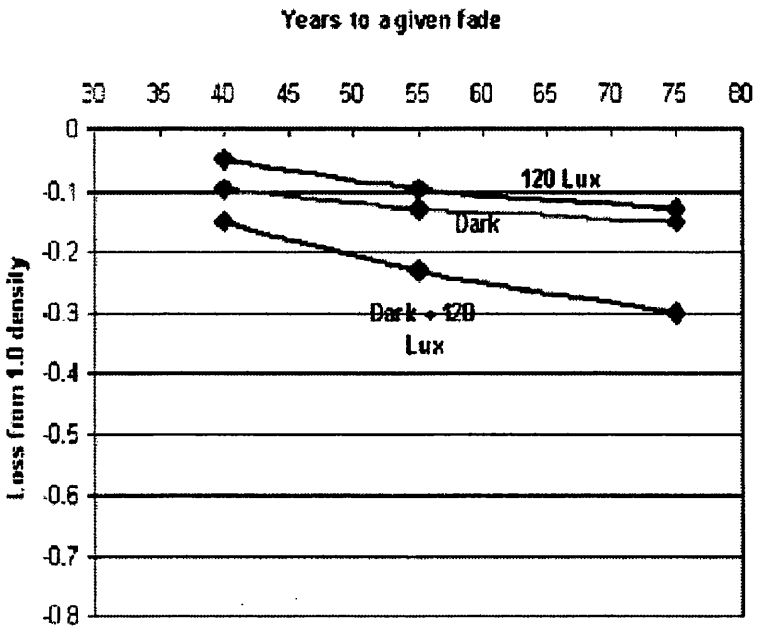

Figure 1.19: Relationship of light and dark fade with typical home illumination [71].

1.9 Thesis overview

The aim of this work is to study the fundamental photochemistry and photophysics of a range of PT dyes with hues that range from magenta to cyan. Magenta PT's are already used in producing the final photographic image and it is important to deduce whether cyan PT's, which are structurally identical apart from the R_6 substituent, share the same photochemical/photophysical properties which render their magenta analogues useful photographic dyes.

Chapter two describes the experimental techniques used during the course of this study. Conformational and ground state spectroscopic studies as well as methods for synthesising the model dye series are reported in chapter three. Chapter four considers fundamental singlet state properties for the dye series, both at room temperature and at 77K. Chapter five discusses the effect that protonation has on dye isomer kinetics. Chapter six describes studies of triplet energy transfer measurements and singlet oxygen quenching. Chapter seven acts as a concluding chapter for the thesis providing results from studies of dye fade in pre-formed dye coatings, and bringing together data from the rest of the thesis in an attempt to identify those photochemical features which may be important in determining the rate of dye fade in photographic coatings.

1.10 References

1) J.H.Coote, *The Illustrated History of Colour Photography*, **1993**, Fountain Press, London.
2) H.Baines, *The Science of Photography*, 4th Ed., **1971**, Fountain Press London.
3) A full background to the photographic process can be obtained from '*The Theory of the Photographic Process*' (4th Ed.) by T.H.James.
4) E.J.Wall, *History of Three Colour Photography*, **1958**, American Photographic Publishing Co., Boston, Massachussetts.
5) J.C.Maxwell, *Trans. Roy. Soc. Edinburgh*, **1857**, 21, 275.
6) J.C.Maxwell, *Proc. Roy. Soc.*, **1859**, 60, 404.
7) S.M.Townsend, *PhD thesis*, **1992**, University of Wales Swansea.
8) S.H.Liggers, K.J.McCarthy and J.A.Stella, *J. Imag. Technology*, **1984**, 10, 1.
9) C.E.K.Mees, *From Dry Plates to Ektachrome Film*, **1961**, Ziff-Davis Publishing Company, New York.
10) W.S.Boyle and G.E.Smith, *The Bell System Technical Journal*, **1970**, 49, 587.
11) T.V.Higgins, *Laser Focus World*, December **1994**, 53.
12) T.Tani, *Journal of Imaging Science and Technology*, **1998**, 42, 1.
13) T.Tani, *Journal of Imaging Science and Technology*, **1995**, 39, 31.
14) H.Wilhelm and C.Bower, *The Permanence and Care of Color Photographs-Traditional and Digital Color Prints, Color Negatives, Slides and Motion Pictures*, 1st Ed., **1993**, Grineel: Preservation Publishing Company.
15) H.Wilhelm. 'With New Pigmented Inks, Dye based Inks and Inkjet Papers, An Unprecedented New Era Has Begun in Color Photography'. *International Association of Fine Art Digital Printmakers Meeting* March 1999-updated June 2000. New York:Wilhelm Imaging Research.
16) A.Lavery, *Imaging Sci. J.*, **2002**, 50, 125.
17) Fujifilm annual report, 'The Development of Digital Imaging', **2002**.
18) C.E Wayne.and R.P.Wayne, *Photochemistry Primer*, Oxford University Press, UK.
19) D.J.Shaw, *Introduction to Colloid and Surface Chemistry*, 3rd Ed., **1980**, Butterworth and Co., UK.
20) J.D.Coyle, R.R.Hill and D.R.Roberts, *Light, Chemical Change and Life*, **1982**, Open University Press, UK.

21) R.P.Wayne, *Principles and Applications of Photochemistry,* **1988,** Oxford University Press, UK.

22) R.F.Gurney and N.F.Mott, *Proc. Roy. Soc. Ser. A*, **1938**, 164, 15.

23) N.F.Mott., *Electronic Processes in Ionic Crystals*, **1948**, Clarendon Press, Oxford

24) H.W.Vogel, *Berichte*, **1873**, 6, 1302.

25) C.K.Parmar, *PhD thesis,* **2001**, Imperial College of Science, Technology and Medicine.

26) R.W.G.Hunt, *The Reproduction of Colour in Photography, Printing & Television,* 4th Ed., **1987,** Fountain Press, London.

27) R.J.Berry, *PhD thesis,* **1998**, University of Wales Swansea.

28) L.F.A.Mason, *Photographic Processing Chemistry,* **1975,** (2nd Ed.), The Focal Press, London.

29) A.G.Tull, *Brit. J. Photogr.*, **1938**, 85, 647.

30) P.W.Vittum, A. Weissberger, *J.Photogr. Sci.*, **1954**, 2, 81.

31) P. Bergthaller, *Imaging Sci. J.*, **2002**, 50, 153.

32) R.L.M.Allen, *Colour Chemistry,* **1971**, Thomas Nelson and Sons Ltd., London.

33) W.H.Horspool, *Aspects of Organic Photochemistry,* **1976,** Academic Press Inc., London.

34) R.O.Kan, *Organic Photochemistry,* **1966,** McGraw-Hill Book Company, New York.

35) N.J.Turro, *Modern Molecular Photochemistry*, **1991**, University Science Books, USA.

36) P.W.Atkins, *Physical Chemistry,* 1st Ed., **1977,** Oxford University Press, UK.

37) S.J.Strickler and R.A.Berg, *J. Chem. Phys.*, **1962,** 814.

38) R.P.Wayne, *Photochemistry*, **1971**, Butterworth & Co., England.

39) V.Balzani, F.Bolletta, F.Scandola, *J. Am. Chem. Soc.*, **1980**, 102, 2152.

40) J.Bailey, *J. Chem. Soc. Perkin Trans. 1,* **1977**, 2047.

41) G.H.Brown, B.Graham, P.W.Vittum and A.Weissberger, *J. Am. Chem. Soc.*, **1951**, 73, 919.

42) W.F.Smith Jr., *J. Phys. Chem.*, **1964**, 68, 1501.

43) P.Douglas, *J. Photogr. Sci.* **1988**, 36, 83.

44) P.Douglas, S.M.Townsend, P.J.Booth, B.Crystall, J.R.Durrant and D.R.Klug, *J. Chem. Soc. Faraday Trans.*, **1991**, 87, 3479.

45) F.Wilkinson, D.R.Worrall, R.S.Chittock, *Chem. Phys. Letters,* **1990**, 174, 416.

46) F.Wilkinson, D.Worrall, D.McGarvey, A.Goodwin, A.Langley, *J. Chem. Soc. Faraday Trans.* **1993**, 89, 2385.

47) D.Kondakov, *J. Chem. Soc., Perkin Trans. 2*, **2001**, 953.

48) C.K.Parmar, G.Rumbles and C.J.Winscom, *Phys. Chem. Chem. Phys.*, **2002**, 4, 1766.

49) H.Mikoshiba, M.Tanaka, S.Kybochura, *Journal of the Society of Photographic Science and Technology of Japan,* **2000,** 63, 322.

50) W.G.Herkstroeter, *J. Am. Chem. Soc.,* **1975**, 97, 3090.

51) P.Douglas, S.M.Townsend, R.Ratcliffe, *J. Imag. Sci.,* **1991**, 35, 211.

52) R.J.Berry, P.Douglas, M.S.Garley, T.Jolly, D.Clarke, H.Moglestue, H.Walker, C.J.Winscom, *J. Photochem. Photobiol. A : Chem.*, **1999**, 120, 33.

53) P.J.S.Pauwels, *J. Am. Chem. Soc.,* **1967**, 89, 580.

54) P.Douglas, C.Couture, D.Clarke, D.Reed, I.H.Sadler, T.Wear, *J. Chem. Soc. Perkin Trans. 2,* **1994**, 1295.

55) W.G.Herkstroeter, *Mol. Photochem.,* **1971**, 3, 181.

56) W.G.Herkstroeter, *J. Am. Chem. Soc.,* **1973**, 95, 8686.

57) W.G.Herkstroeter, *J. Am. Chem. Soc.,* **1976**, 98, 330.

58) P.Douglas and D.Clarke, *J. Chem. Soc. Perkin Trans. 2*, **1991**, 1363.

59) Faraj Abu-Hasanayn and W.G.Herkstroeter, *J. Phys. Chem. A*, **2001**, 105, 1214.

60) A.H.Thomas, C.Lorents, A.L.Capparelli, C.G.Martinez, A.M.Braun and E.Oliveros, *Photochem. Photobiol. Sci.*, **2003**, 2, 245.

61) M.Tarr and D.P.Valenzenzo, *Photochem. Photobiol. Sci.*, **2003**, 2, 355.

62) C.Schweitzer and R.Schmidt, *Chem Rev.*, **2003**, 1685.

63) F.Wilkinson, W.P.Helman and A.B.Ross, *J. Phys. Chem. Ref. Data*, **1995**, 24, 663.

64) W.F.Smith Jr.,W.G.Herkstoeter and K.L.Eddy, *J. Am. Chem. Soc.*, **1975**, 97, 2764.

65) Z.Kucybala, I.Pyszka, B.Marciniak, G.Hug, J.Paczkowski, *J. Chem. Soc. Perkin Trans. 2*, **1999**, 2147.

66) W.F.Smith Jr.,W.G.Herkstoeter and K.L.Eddy, *Photogr. Sci. Eng.*, **1976**, 20, 140.

67) U.Nickel, *J. Imag. Technol.,* **1986**, 12, 181.

68) K.Sakanoue and N.Furutachi, *J. Phot. Sci.*, **1988**, 36, 79.

69) S. Anderson and G. Larson, *J. Imag. Technol.*, **1987**, 13, 49.

70) S. Anderson and R. Anderson, *J. Imag. Technol.*, **1991**, 17, 127.

71) Information obtained from Kodak R&D website, www.kodak.com, January 2004.

Chapter 2

Experimental

2.1 Materials

CHEMICAL	SUPPLIER	GRADE
Acetone	Fisher	AR
Acetonitrile	Fisher	HPLC
Chloroaluminium phthalocyanine (CAP)	Eastman chemicals	
Chloroform (anhydrous) stabilised with amylenes	Aldrich	99%
Chloroform (anhydrous) stabilised with 0.5-1% ethanol	Aldrich	99%
1-Chloronaphthalene	Aldrich	
Cresyl violet	Eastman chemicals	Laser Grade
Deuterated chloroform	Aldrich	
Diethyl ether	Fisher	
Dimethylsulfoxide	Lancaster	99%
Ethanol	Fisher	AR
Gallium naphthalocyanine	Aldrich	
Gelatin	Kodak	Photographic
Isopentane	Aldrich	99%
Methanol	Fisher	HPLC
Methylcyclohexane	Aldrich	Spectroscopic
Methylene blue	Aldrich	
Nitrogen	BOC	
p-Dodecylphenol	Aldrich	
Palladium tetraphenylporphyrin	Aldrich	
Phenalenone	Aldrich	
Potassium bromide	Fisher	
Propan-2-ol	Fisher	
Rhodamine B	Kodak	Laser grade
Sodium dodecyl sulphate	BDH	Biochemical
Tetrahydrofuran (THF)	Aldrich	AR
Tetraphenylporphyrin	Avocado	

Tin naphthalocyanine	Aldrich	
Toluene	Fisher	
Trifluoroacetic acid	Aldrich	Spectroscopic
Water	Fisher	HPLC
Zinc phthalocyanine	Koch Light	
Zinc tetraphenylporphyrin	Aldrich	

2.1.1 Procedure for reporting experimental details

General experimental techniques are reported here, while more detail is provided in the relevant chapters.

2.1.2 Triplet energy measurements - solubility considerations

Due to the poor solubility of some naphthalocyanine triplet energy sensitisers in ethanol the technique outlined by Berry [1] was used to prepare solutions of tin and gallium naphthalocyanines free of aggregation. These sensitisers were dissolved in 1-chloronaphthalene with refluxing at 180°C for 2-3 hrs.

The 6-CN dye also has poor solubility in ethanol, and therefore acetone was the solvent of choice for the energy transfer experiments for this dye with all sensitisers (except tin and gallium naphthalocyanine.)

2.2 Dyes available for study

In total nine PT dyes, differing only in the substituent at the 6 - position, were chosen for study. This dye set was chosen because it provided a range of dyes with absorption maxima ranging from *ca.* 546-633 nm in ethanol *i.e.* from magenta to cyan.

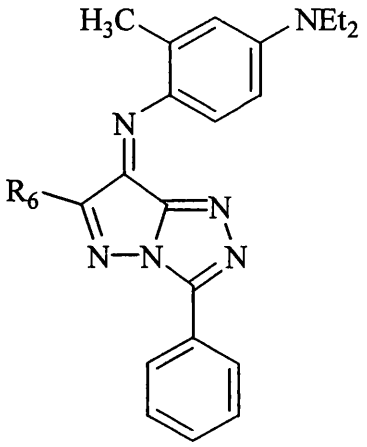

Figure 2.1: Structure of the dyes available for study.
R_6 = ^{t}Butyl, OMe, Me, Ph, H, CO_2Et, $CONH_2$, COOH, and CN.

Four were synthesised by the author using the methods outlined in section 3.1, and the other five, those for which R_6 is: H, CN, CO_2Et, OMe and ^{t}Butyl, were provided by Kodak Research Division, Kodak Ltd., Headstone Lane, Harrow, Middlesex, UK, HA1 4TY. (Throughout the course of this work the dyes will be referred to by the position and nature of the substituent, *i.e.* the dye with an ester group in the 6 - position is referred to as 6-CO_2Et.)

2.3 Spectroscopic techniques

2.3.1 Infrared

Infrared spectra were recorded on a PC controlled Perkin Elmer spectrophotometer. Samples were prepared by grinding a small amount of dye (<5 mg) into dry potassium bromide which was then compressed to form a disk. The effects of dye concentration on the IR spectra was studied by increasing the amount of potassium bromide in the mixture.

2.3.2 Steady state UV/Vis absorption spectroscopy

2.3.2.1 RT measurements

A number of UV/Vis spectrophotometers were used during the course of this study. For the RT studies recorded in chapter 4, and the isomerisation experiments in chapter 5 a PC controlled Perkin-Elmer Lambda 9 UV/Vis/NIR double beam spectrophotometer was used.

For the studies described in chapters 4 and 6 a PC controlled Perkin-Elmer Lambda 15 UV/Vis double beam spectrophotometer was used. Spectra of the preformed dye coatings were measured by placing the coating under a brass mask so that it fitted directly onto a thermostatted 1 cm quartz cuvette (note section 2.4).

2.3.2.2 77K measurements

For 77K absorption spectra dye samples were made up in EPA (a 2:5:5 mixture of ethanol:isopentane:diethyl ether) at a concentration of *ca.* 2×10^{-5} mol dm^3. The dye sample was placed in a *ca.* 3 mm NMR tube which was plunged into a liquid nitrogen - filled quartz phosphorimeter dewar. The dewar was arranged such that the sample could be placed reproducibly in the optical path of the Lambda 9 spectrophotometer by use of a custom - built Teflon dewar holder.

2.3.3 Fluorescence measurements

The basic components that make up a fluorimeter are given in figure 2.3. A Perkin Elmer MPF-44E spectrofluorimeter was used for the room temperature measurements and a Jobin-Yvon JY3 D spectrofluorimeter was used for the 77K measurements. Slit widths were 5 nm for RT studies and 4 nm for emission and excitation studies at 77K. Both spectrofluorimeters used 150 W xenon arc lamps and Hammamatsu R928 photomultipliers. (The lamp profile is shown in figure 2.4.)

Fluorescence excitation spectra were corrected for excitation intensity using methylene blue and rhodamine B quantum counters in ethylene glycol using the method described by Demas *et al.* [2].

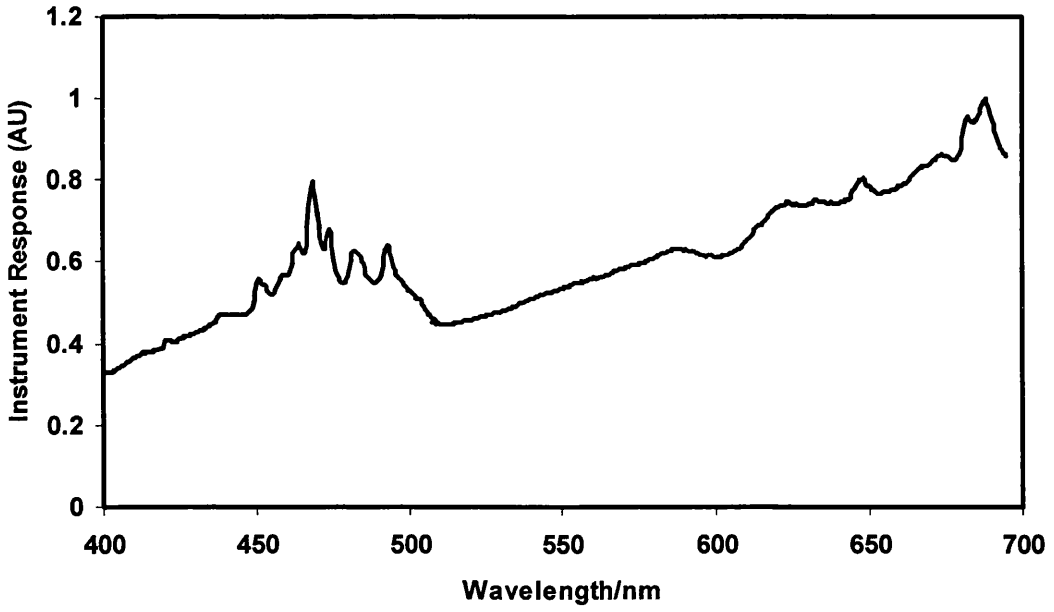

Figure 2.2: Wavelength dependence of excitation intensity obtained using methylene blue and rhodamine B 'quantum counters'.

Emission spectra were corrected by using cresyl violet as standard and the spectrum obtained was compared to that corrected by Magde *et al.* [3]. Any correction factors needed to the spectrum were then used for the emission spectra of the PT dyes.

The fluorescence quantum yield (ϕ_{fl}) of an unknown sample ϕ_u can be estimated by relating it to the known quantum yield (ϕ_{ref}) of a reference sample [2]. The following expression was used:

$$\phi_u = \phi_{ref} \ (Fl_{ref}/Fl_u).(I_u/I_{ref}).(n_u/n_{ref})^2.(P_{ref}/P_{unknown}) \qquad \textbf{2.1}$$

where Fl is the fraction of the light absorbed at the exciting wavelength, I is the integrated emission intensity in energy units corrected for both instrument response and self absorption, and n is the refractive index. P is the optical excitation power, *i.e.* intensity at the excitation wavelength.

The references for 77K measurements were cresyl violet [3] and 6-^{t}Butyl PT [4]. For fluorescence work at RT Rhodamine B was used.
The radiative rate constant, k_{rad}, for each dye was calculated from the Strickler - Berg equation [5], *i.e.*

$$k_{rad} = 2.88 \times 10^{-9}.n^2.\nu_{fl}^3.\int \varepsilon.d\,(\ln\nu_{abs}) \qquad \textbf{2.2}$$

Where n is the refractive index of the medium, ν_{fl} is the mean reciprocal emission wavelength, $\int \varepsilon.d\,(\ln\nu_{abs})$ is the absorption integral, calculated from the area of a plot of extinction coefficient against the natural log of the frequency.

The observed rate constant for radiative deactivation of the singlet state, k_{fl}, was then calculated using k_{rad} and Φ_{fl} as follows:

$$k_{fl} = (k_{rad}/\Phi_{fl}) \qquad \textbf{2.3}$$

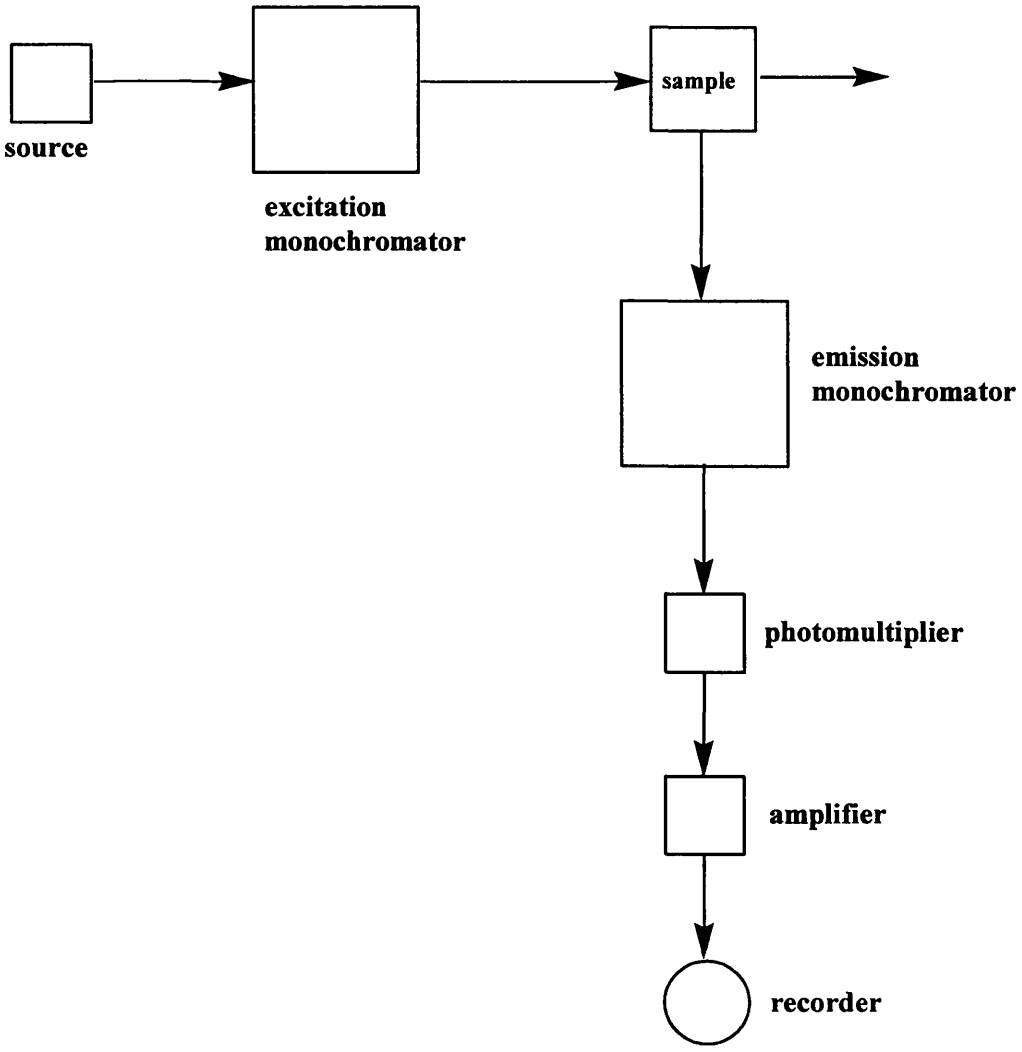

Figure 2.3: Components of a fluorimeter [6].

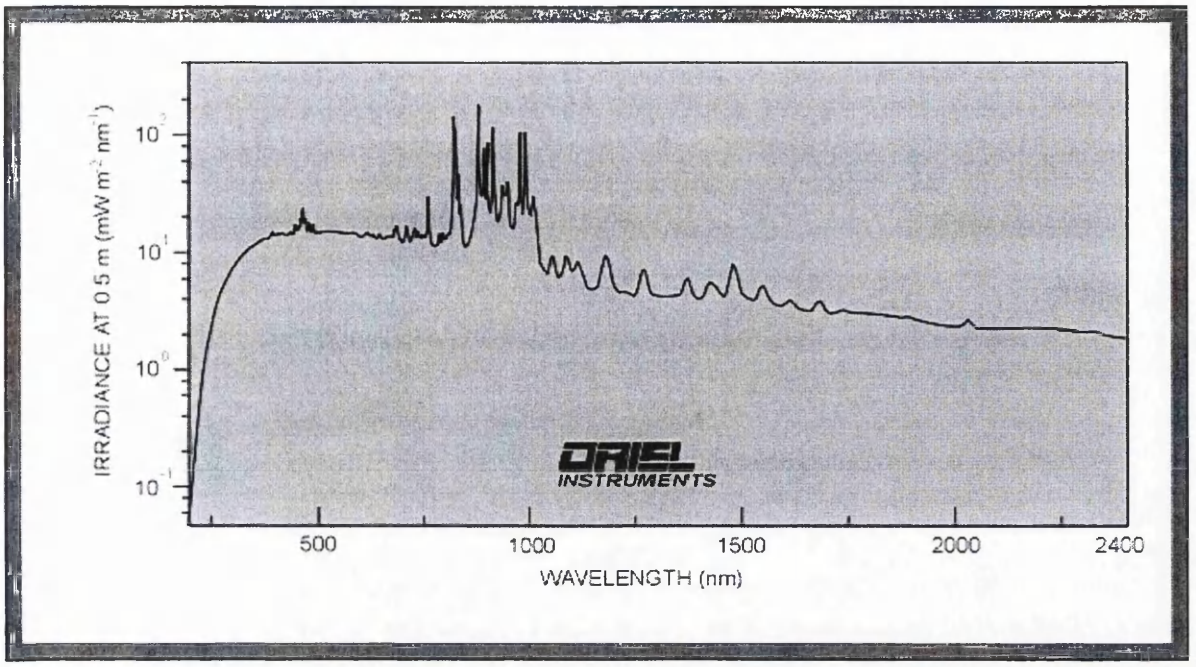

Figure 2.4: Lamp profile for Oriel 150W xenon arc [7].

2.3.4 Single photon counting

Fluorescence decay measurements were carried out at the Chemistry Department of the University of Coimbra. The instrument used was a home-built time-correlated single photon counting apparatus with: an N_2 filled IBH 5000 coaxial flashlamp as excitation source, Jobin-Yvon monochromator, Philips XP2020Q photomultiplier, and Canberra Instruments Time-to-amplitude converter and Multichannel Analyser. Alternate measurements (1000 counts per cycle), of the pulse profile at 337 or 356 nm and the sample emission were performed until 1-2 x 10^4 counts at the maximum were reached [8]. The fluorescence decays were analysed using the modulating functions method of Striker [9]. I would like to thank Dr Seixas De Melo and Joao Pina at the University of Coimbra, Portugal for allowing me to use this equipment and also for their invaluable assistance in carrying out this work.

2.3.5 Flash photolysis

Nanosecond flash photolysis experiments were carried out using 532 or 355 nm radiation from an Nd/YAG laser (Spectron Lasers) and an Applied Photophysics Laser Kinetic Spectrometer. The unfocussed excitation beam was ~ 1 cm in diameter, with a pulse duration of ~ 16 ns, and pulse energy of ~ 15 mJ. Samples were contained in 1 cm or 0.5 cm cells and the transmission monitored at 90° to the excitation pulse. Transient kinetic data were recorded on a Gould OS4072 digital oscilloscope and transferred *via* a Picolog data logger to a PC for kinetic analysis.

A pulsed xenon arc source was used as monitoring beam for studies in the microsecond time domain, and either this lamp in continuous mode, or a stabilized 100 W tungsten lamp, was used for studies in the millisecond time range.

2.3.6 Singlet oxygen luminescence

Singlet oxygen quenching rates were measured using equipment in the laboratories of the Chemistry Department of the University of Coimbra. Singlet oxygen was generated by excitation of phenalanone using Applied Photophysics laser flash photolysis equipment pumped by the third harmonic of a Nd:YAG laser (Spectra Physics) with excitation wavelength of 355 nm [10]. The phosphorescence decay of singlet oxygen was monitored at 1270 nm. The emission was detected using a cooled Hamamatsu R5509-42 detector.

I would like to thank Dr Seixas De Melo and Joao Pina at the University of Coimbra, Portugal for allowing me to use this equipment and their invaluable assistance in carrying out this work.

2.3.7 NMR and mass spectrometry

^{1}H NMR spectra were recorded by Mr M.Nettle on a Bruker AC spectrometer at 400 MHz using tetramethylsilane as an internal standard. All samples were run in deuterated chloroform.

Mass spectra were recorded by Mr G.Llewellyn at the EPSRC Mass Spectrometry Centre at the University of Wales Swansea using low resolution EI/CI techniques on a VG analytical Quattro II triple quadrupole mass spectrometer.

2.4 Fade studies

2.4.1 HID and rapid fade systems

Irradation using a high intensity daylight (HID) source is the method commonly used to measure the lightfastness of dyes in photographic systems. This method has been previously employed by Parmar [11] and Townsend [12] in photochemical studies of pyrazolotriazole azomethine dyes. Unfortunately photographic dyes are so stable that HID experiments can take weeks to complete.

'Rapid fade' experiments, as used in this study are less time consuming, and, provided experimental conditions are carefully monitored and duplicated, experiments can be completed in days rather than the week required when using HID. A comparison of the emission profiles of a rapid fade and the HID system is given in figure 2.5.

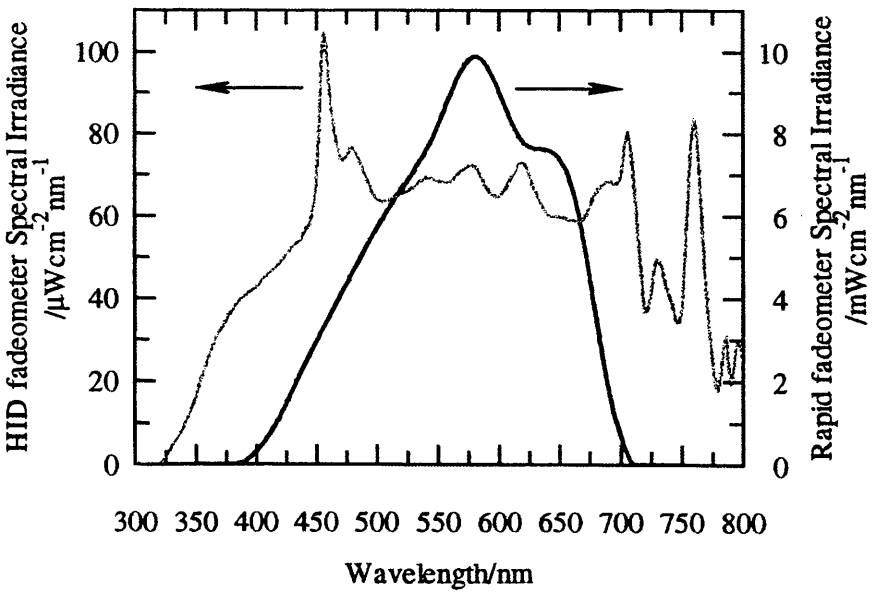

Figure 2.5: Comparison between the emission profile of a rapid fade and the HID system [10]. (Note that the irradiance is given in units of mW cm^{-2} nm^{-1} for the rapid fade apparatus, and μW cm^{-2} nm^{-1} for the HID fade apparatus.)

2.4.2 Rapid fade apparatus

The light source was a 150 W quartz-halogen lamp the output of which was passed through filters and a 1 metre liquid light pipe (diameter 8.5 mm) in order to remove UV and IR light. The liquid light pipe was then fitted into a custom made cuvette holder and positioned so that it is 3.5 mm from the preformed dye coating which is held in place on the front face of a 1 cm cuvette by a brass 'mask'. The cuvette holder also contained a gas inlet so that gases could be flushed through at a constant rate so that the atmosphere around the coating could be controlled. An optical fibre attached to a light dependent resistor was also positioned on the front face of the cuvette holder so that the light intensity could be monitored and kept constant throughout the experiment.

The brass 'mask' left a circular cross section that was exposed to the light source and the decrease in absorbance of this area of the coating was measured over time using a Perkin-Elmer Lambda 15 UV/Vis spectrophotometer. The temperature of the cuvette

was kept constant at 23(±1)°C by circulating water from a thermostatted water bath into the cuvette.

A schematic of the apparatus is given in figure 2.6.

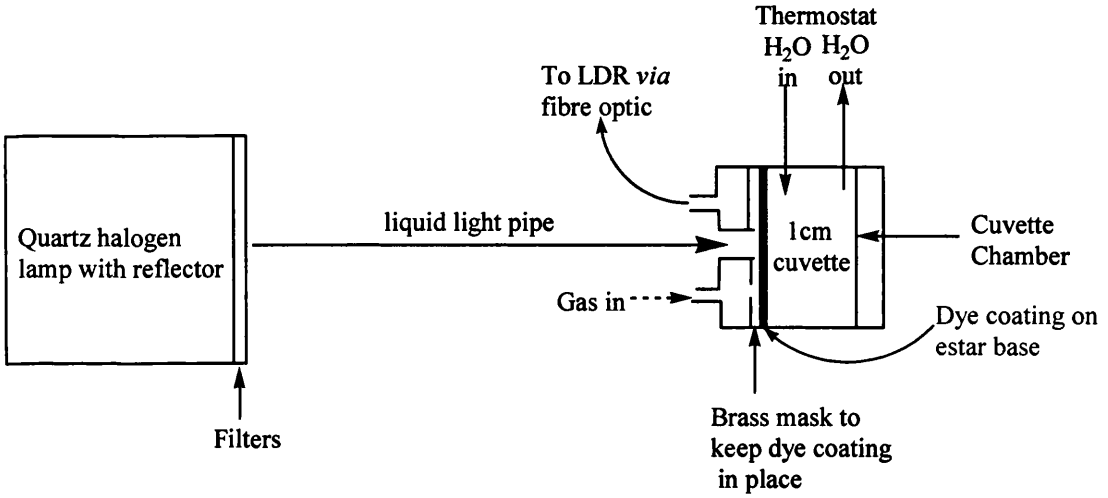

Figure 2.6: Schematic of rapid fade apparatus.

2.5 References

1) R.J.Berry, *PhD Thesis*, **1998,** University of Wales Swansea.

2) J.N.Demas and G.A. Crosby, *J. Phys. Chem.*, **1971**, 75, 991.

3) D.Magde, J.H.Brannon, T.L.Cremers and J.Olmsted, *J. Phys. Chem.*, **1979**, 75, 1991.

4) P.Douglas, S.M.Townsend, P.J.Booth, B.Crystall, J.R.Durrant and D.R.Klug, *J. Chem. Soc. Faraday Trans.*, **1991**, 87, 3479.

5) S.J.Strickler and R.A.Berg, *J. Chem. Phys.*, **1962,** 814.

6) D.A.Skoog, D.M.West and F.J.Holler, *Fundamentals of Analytical Chemistry,* 7th Ed., **1996**, Thomson Learning, Inc., London, UK.

7) Oriel Catalogue or website www.oriel.com, **2003**.

8) J.Seixas de Melo and P.F.Fernandes, *J. Mol. Struct.*, **2001**, 565, 69.

9) G.Striker, V.Subramniam, C.A.M. Seidel and A.Volkmer, *J. Phys. Chem. B*, **1999**, 103, 8612.

10) J.Seixas de Melo, F.Elisei, C.Gartner, G.G. Aloisi, R.S. Becker, *J. Phys. Chem. A*, **2000**, 104, 6907.

11) C.K.Parmar, *PhD Thesis*, **2001**, Imperial College of Science, Technology and Medicine.

12) S.Townsend, *PhD Thesis*, **1991**,University of Wales Swansea.

Chapter 3

Synthesis, ground state characterisation and structural studies of PT dyes

3.1 Synthesis of 6-$CONH_2$, 6-Ph, 6-COOH and 6-Me PT dyes

3.1.1 Introduction

Pyrazolo [5,1-c]-1,2,4-triazole azomethine (PT) dyes are formed by a coupling reaction between a pyrazolotriazole coupler and a *p*-phenylenediamine derivative developer. Pyrazolo [5,1-c]-1,2,4-triazole couplers were first synthesised by Bailey [1] *via* the oxidative cyclisation of pyrazole-hydrazones. Alternative methods include the extrusion of sulphur from triazolothiadiazines [2] and cyclisation of pyrazolyl-amidoximes [3].

The following dyes, 6-H, 6-CN, 6-CO_2Et, 6-OMe and 6-^{t}Butyl were provided by Kodak Ltd. The 6-Ph, 6-COOH and 6-Me dyes were synthesised by the author using a simple coupling reaction with a *p*-phenylenediamine developer (see **3.1.4**) and the respective PT couplers which had been prepared previously by Kodak Ltd. (note scheme 2.1).

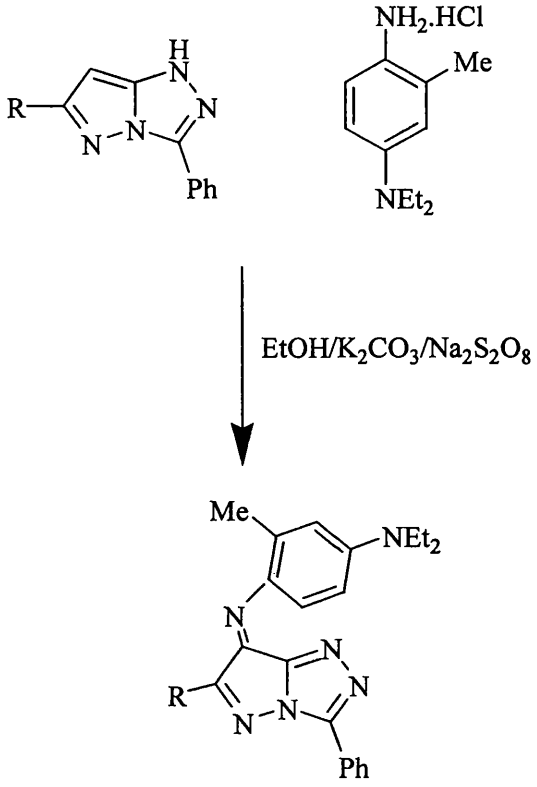

Scheme 2.1

Where R is Ph, COOH and Me yields were 67%, 38% and 61% respectively.

For the 6-$CONH_2$ dye a modification of the sulphur extrusion route to pyrazolotriazole couplers, followed by oxidative coupling with *p*-phenylenediamine was used as described in **3.1.2- 3.1.4** below.

3.1.2 Synthesis of triazolothiazine 6-$CONH_2$ intermediate

A stirred mixture of 4-amino-3-phenyl-trazolin-5-thione **1** (42.5 g 0.22 mol) and of ethyl bromopyruvate (47.7 g 0.24 mol) (approx. 1:1 molar ratio) was refluxed for 2-3 hours in ethanol on a steam bath. The resultant product was left to cool and the solvent was removed by rotary evaporation to leave the triazolothiadiazine ester hydrobromide salt **2** (57.4 g, 70.6% yield).

Salt **2** (33.7 g 0.11 mol) was dissolved in ethanol (250 ml) and an excess (30 ml) of aqueous ammonia was added. The solution was warmed on a steam bath for 5-10 minutes, and then stirred at room temperature (22-24°C) for a further hour. The precipitate was then collected by filtration and washed with ethanol to yield the triazolothiadiazine amide **3** (17 g, 72%), the structure of which was confirmed by IR spectroscopy and mass spectrometry.

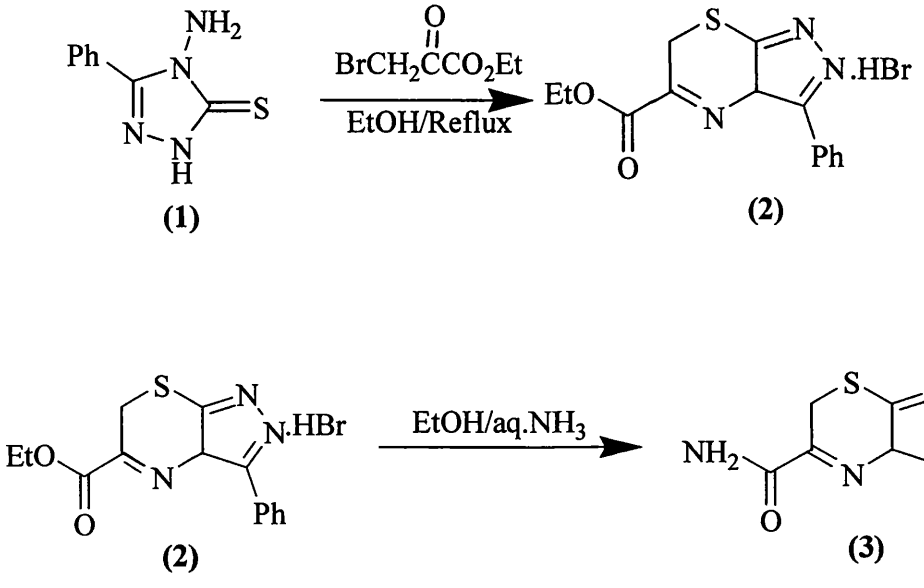

Scheme 2.2

3.1.3 Synthesis of PT coupler with $R_6 = CONH_2$

Triazolothiadiazine amide **3** (11.5 g, 0.044 mol), triphenylphosphine (35 g, 0.15 mol) and acetic anhydride (8 ml, 0.08 mol) was refluxed for *ca.* 12 hr in toluene (50 ml). The solution was filtered to give the di-acetylated pyrazolotriazole intermediate **4** (9 g, 65.3%) of, the structure of which was confirmed by IR spectroscopy and mass spectrometry.

All of product **4** was dissolved in 4:1 methanol/tetrahydrofuran solution (25 ml) and stirred at room temperature. A solution (50 ml) of potassium hydroxide (5.6 g in 50 ml water) was added dropwise over a period of 10 minutes. The mixture was stirred for 30 minutes. The precipitate was collected by filtration, washed with dilute hydrochloric acid, and dried to give the pyrazolotriazole coupler **5** (3.5 g, 53.2%). The structure was confirmed by IR spectroscopy and mass spectrometry.

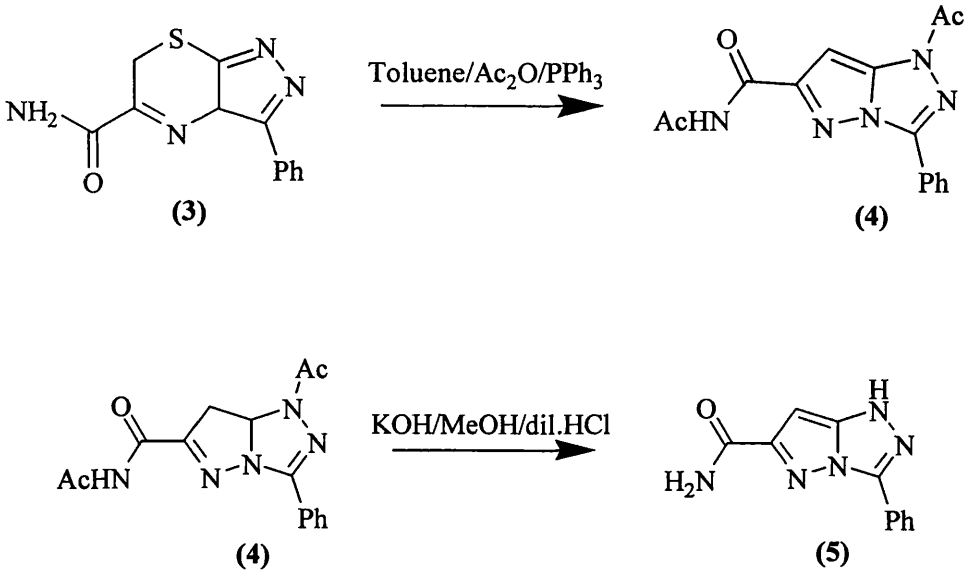

Scheme 2.3

3.1.4 Dye formation

Coupler **5** (3.5 g, 0.015 mol) was dissolved in ethanol. *p*-Phenylediamine developer (4.29 g, 0.02 mol) was then added with stirring at room temperature. An aqueous solution (30 ml) of potassium carbonate (6 g) and potassium persulphate (4 g) was added to the initial mixture and the resultant solution was heated on a steam bath and stirred for *ca.* 1 h. The product was collected by filtration and washed with dilute hydrochloric acid, then recrystallised from ethanol to give the PT azomethine dye, compound **6** as a blue amorphous solid (2.3 g, 38.2%).

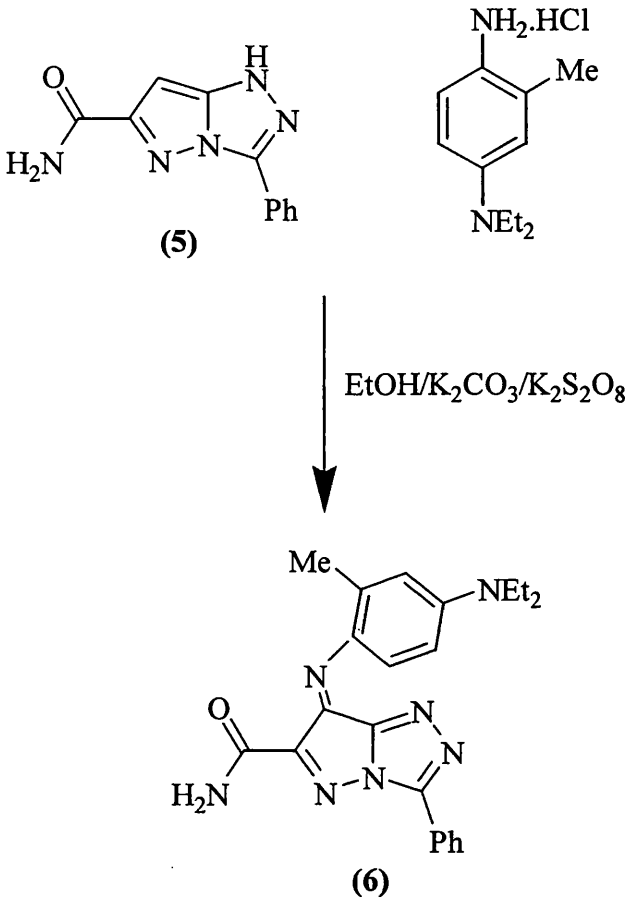

(5) **(6)**

Scheme 2.4

3.2 Dye characterisation

The following four tables give data from NMR spectroscopic and mass spectrometric analyses for the four dyes synthesised. Full spectra are given in the appendix. Elemental analysis for the 6-Me dye is also given.

Table 3.1: Spectroscopic data for 6-Me.

a) ^{1}H NMR

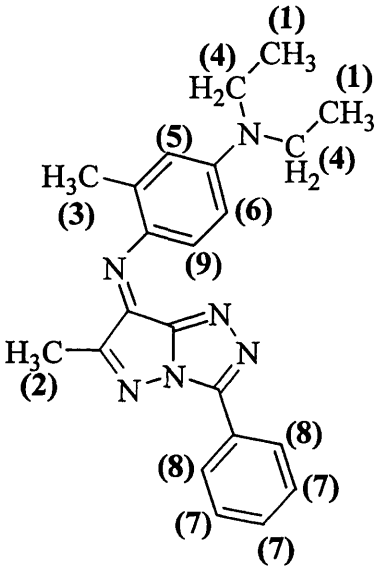

Proton No.	*Chemical shift and structure*
H-1 developer ethyl CH_3 group	1.2(t)
H-2 R_6 substituent on coupler	2.5(s)
H-3 methyl group adjacent to azomethine bond on developer	2.6(s)
H-4 developer ethyl CH_2 group	3.5(m)
H-5 proton on developer phenyl group	6.6(d)
H-6 proton on developer phenyl group	6.8(dd)
H-7 m,p protons on phenyl moiety on coupler	7.5(m)
H-8 o-protons on phenyl moiety on coupler	8.3(m)
H-9 proton adjacent to azomethine bond on developer	9.25(d)

(s-singlet, d-doublet, dd-double doublet, t-triplet, m-multiplet)

b) Mass spectrum (CI): Molecular ion present at m/z 372.3.

c) Elemental analysis: Calculated: C 70.97%, H 6.45%, N 22.58%.

Found: C 70.04%, H 6.49%, N 22.24%.

Table 3.2: Spectroscopic data for 6-Ph.

a) ^{1}H NMR

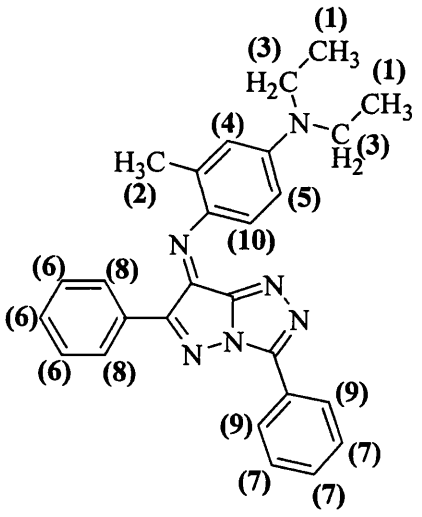

Proton No.	*Chemical shift and structure*
H-1 developer ethyl CH_3 group	1.3(t)
H-2 methyl group adjacent to azomethine bond on developer	2.6(s)
H-3 developer ethyl CH_2 group	3.5(m)
H-4 proton on developer phenyl group	6.7(d)
H-5 proton on developer phenyl group	6.8(dd)
H-6 m,p protons on R_6 substituent	7.4(m)
H-7 m,p protons on phenyl moiety on coupler	7.5(m)
H-8 o-protons on R_6 substituent	8.2(m)
H-9 o-protons on phenyl moiety on coupler	8.3(m)
H-10 proton adjacent to azomethine bond on developer	9.4(d)

b) Mass spectrum (CI): Molecular ion present m/z at 434.3.

Table 3.3: Spectroscopic data for 6-$CONH_2$.

a) ^{1}H NMR

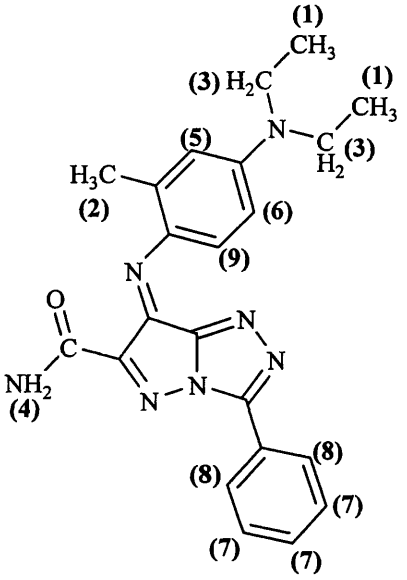

Proton No.	*Chemical shift and structure*
H-1 developer ethyl CH_3 group	1.5(t)
H-2 methyl group adjacent to azomethine bond on developer	2.6(s)
H-3 developer ethyl CH_2 group	3.5(m)
H-4 amide protons on R_6 substituent	6.1(m)
H-5 proton on developer phenyl group	6.7(d)
H-6 proton on developer phenyl group	6.9(dd)
H-7 m,p protons on phenyl moiety on coupler	7.5(m)
H-8 o-protons on phenyl moiety on coupler	8.5(m)
H-9 proton adjacent to azomethine bond on developer	9.5(d)

b) Mass spectrum (CI): ion present at m/z 402.3 representative of the quasi molecular ion ($M+H^+$) [4].

Table 3.4: Spectroscopic data for 6-COOH.

a) ^{1}H NMR

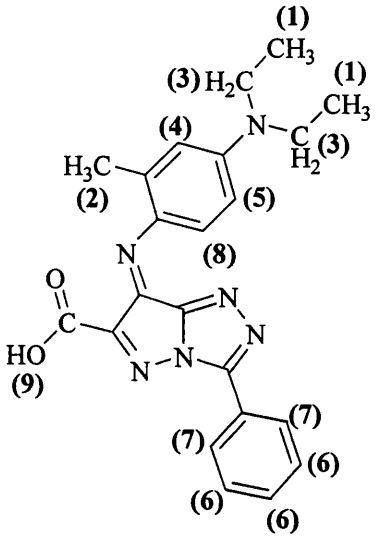

Proton No.	*Chemical shift and structure*
H-1 developer ethyl CH_3 group	1.2(t)
H-2 methyl group adjacent to azomethine bond on developer	2.6(s)
H-3 developer ethyl CH_2 group	3.5(m)
H-4 proton on developer phenyl group	6.6(d)
H-5 proton on developer phenyl group	6.8(dd)
H-6 m,p protons on phenyl moiety on coupler	7.5(m)
H-7 o-protons on phenyl moiety on coupler	8.3(m)
H-8 proton adjacent to azomethine bond on developer	9.5(d)
H-9 hydroxyl proton on carboxylic acid R_6 substituent	*Exchanged in solution-no signal*

b) Mass spectrum (CI): Molecular ion present at m/z 402.2.

3.3 Ground state studies

3.3.1 NMR spectroscopy

The position of the nmr signal assigned to the developer proton adjacent to the azomethine bond (shown as H* in figure 3.1) is of interest. Azomethine dyes can exist in *syn* or *anti* configurations and they undergo *syn-anti* photoisomerisation (figure 3.1). Pauwels has used the position of the resonance of the analogous H* proton in the pyrazolone azomethine dyes as a diagnostic tool in determining absolute configuration [5, 6]. Douglas *et al.* [7] used NOE studies of this proton to show that PT dyes exist in the *syn* conformation in solution (figure 3.1).

Figure 3.2 shows that there is some correlation between λ_{max} and the chemical shift of H* which may suggest that the perturbing influence of R_6 on the ring current of the [5,5] heterobicycle affects the NMR properties of this proton. This may be due to a decrease in electron density in the pyrazolotriazole ring system when the R_6 substituent is electron withdrawing (e.g. 6-CO_2Et) which leads to the H* proton becoming more strongly deshielded and therefore shifted downfield.

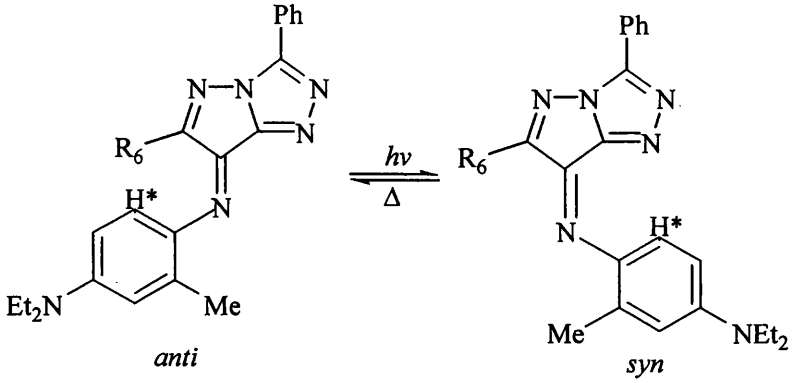

Figure 3.1: PT dye isomerism. NOE studies of proton H* show that the *syn* conformation is the preferred arrangement in room temperature solution.

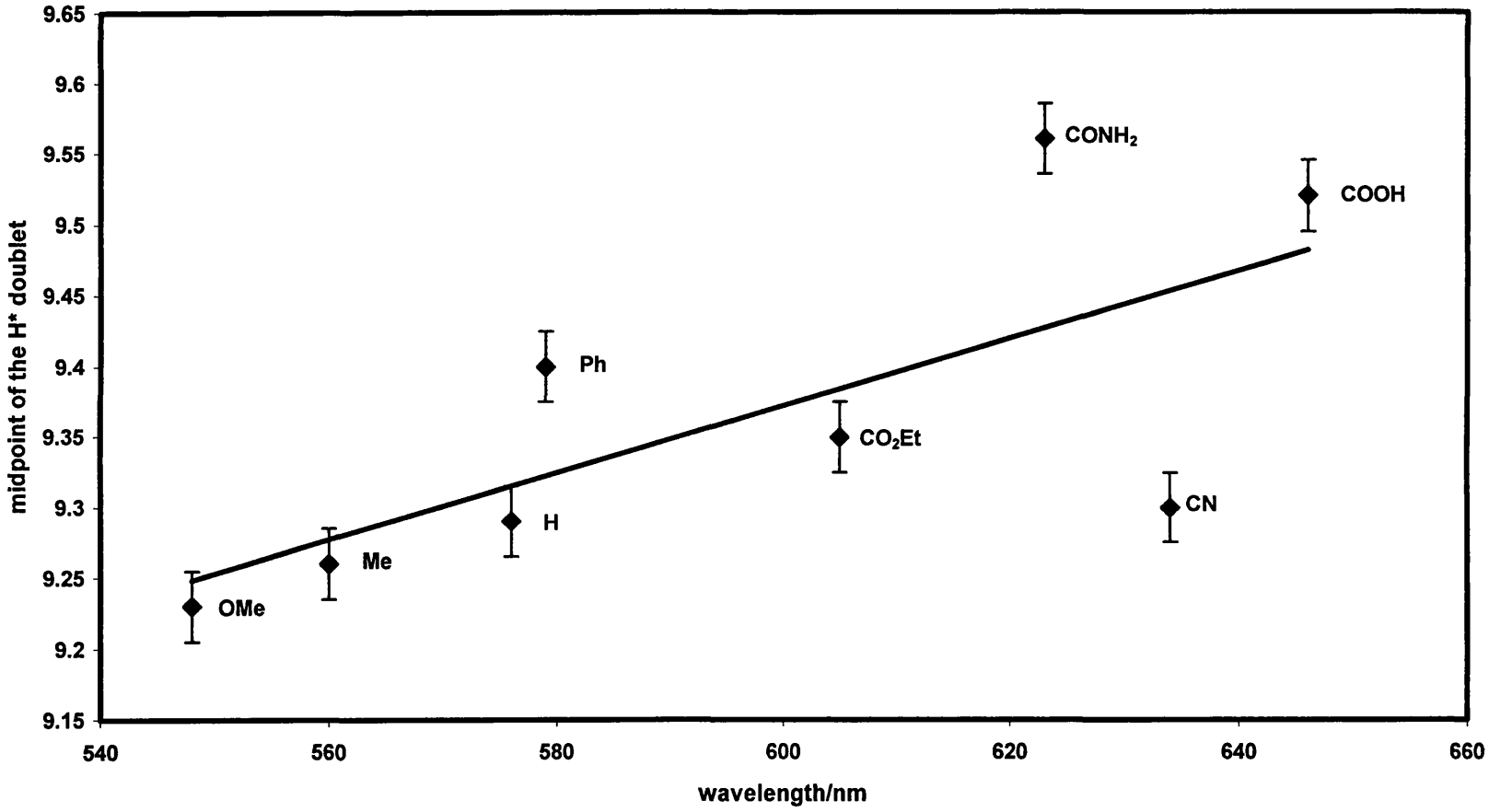

Figure 3.2: The correlation between the chemical shift of H* in $CDCl_3$ and the λ_{max} of the dye in $CHCl_3$.

3.3.2 X-ray crystallography

Fortunately, the 6-Me dye gave crystals of suitable quality for x- ray analysis. The molecular structure is shown in figure 3.3. Crystallographic data are given in table 3.5. The crystal packing is shown in figure 3.4.

Temperature	150(2) K
Wavelength	0.71073 Å
Crystal system	Monoclinic
Space group	C2/c
Unit cell dimensions	a = 19.5222(4) Å alpha = 90 deg.
	b = 16.6104(3) Å beta =123.8811(12) deg.
	c = 14.2768(3) Å gamma = 90 deg.
Volume	3843.44(13) Å ^3
Z	8
Density (calculated)	1.287 Mg m^3
Absorption coefficient	0.080 mm^{-1}
F(000)	1584
Crystal size	0.30 × 0.05 × 0.05 mm
Theta range for data collection	2.99 to 26.12 deg.
Index ranges	-24 ≤h ≤ 24, -20 ≤ k ≤ 20, -17 ≤ l ≤17
Reflections collected	35577
Independent reflections	3804 [R(int) = 0.1836]
Absorption correction	None
Max. and min. transmission	0.9960 and 0.9763
Refinement method	Full-matrix least-squares on F^2
Data / restraints / parameters	3804 / 0 / 253
Goodness-of-fit on F^2	0.979
Final R indices [I>2sigma(I)]	R1 = 0.0598, wR2 = 0.1186
R indices (all data)	R1 = 0.1276, wR2 = 0.1401
Extinction coefficient	0.0040(5)
Largest diff. peak and hole	0.253 and -0.308 e $Å^{-3}$

Table 3.5: Crystal data and structure refinement for the 6-Me dye.

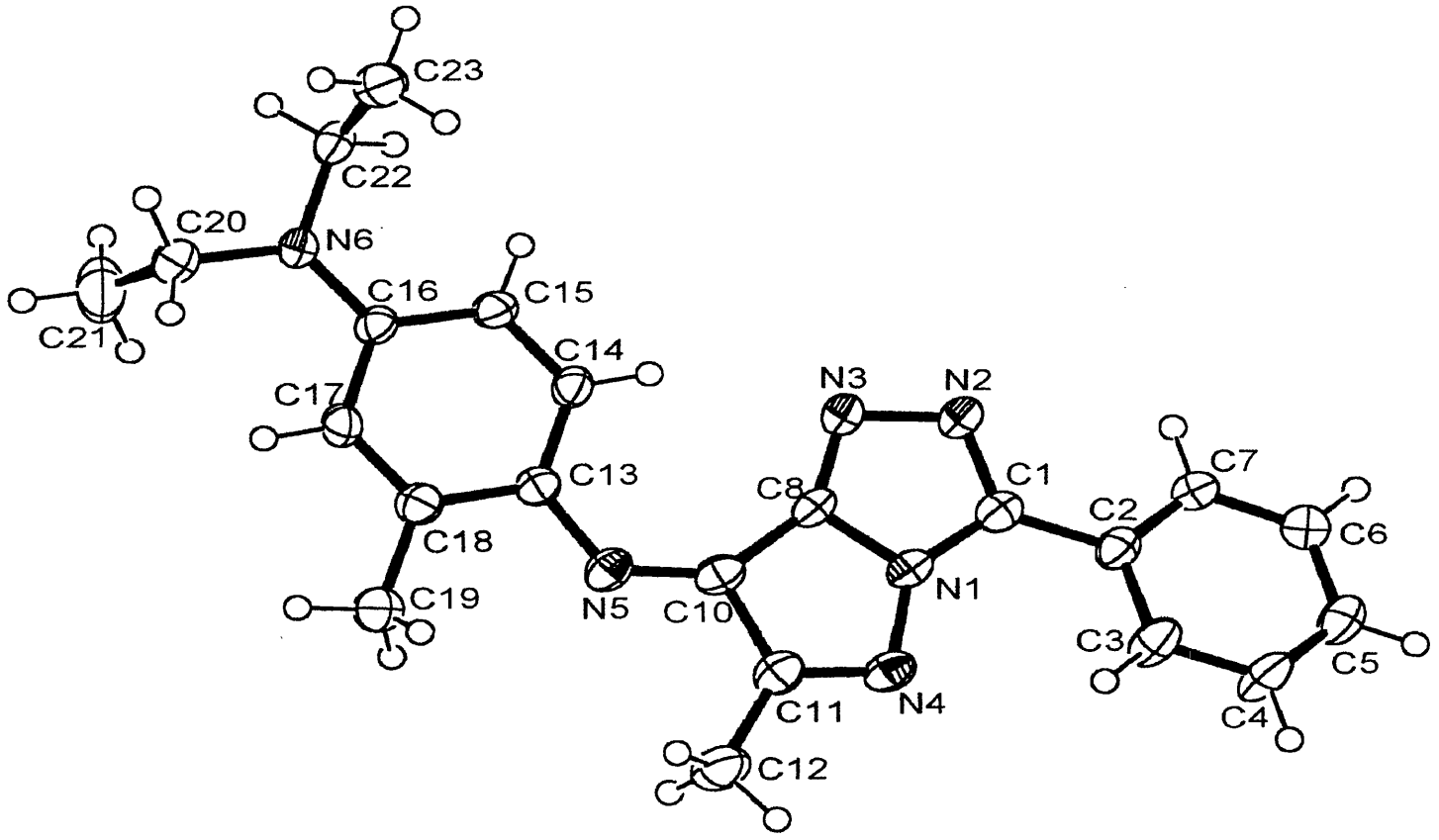

Figure 3.3: X-Ray crystal structure of the 6-Me dye (C and N atoms are numbered, and positions of H atoms are also given).

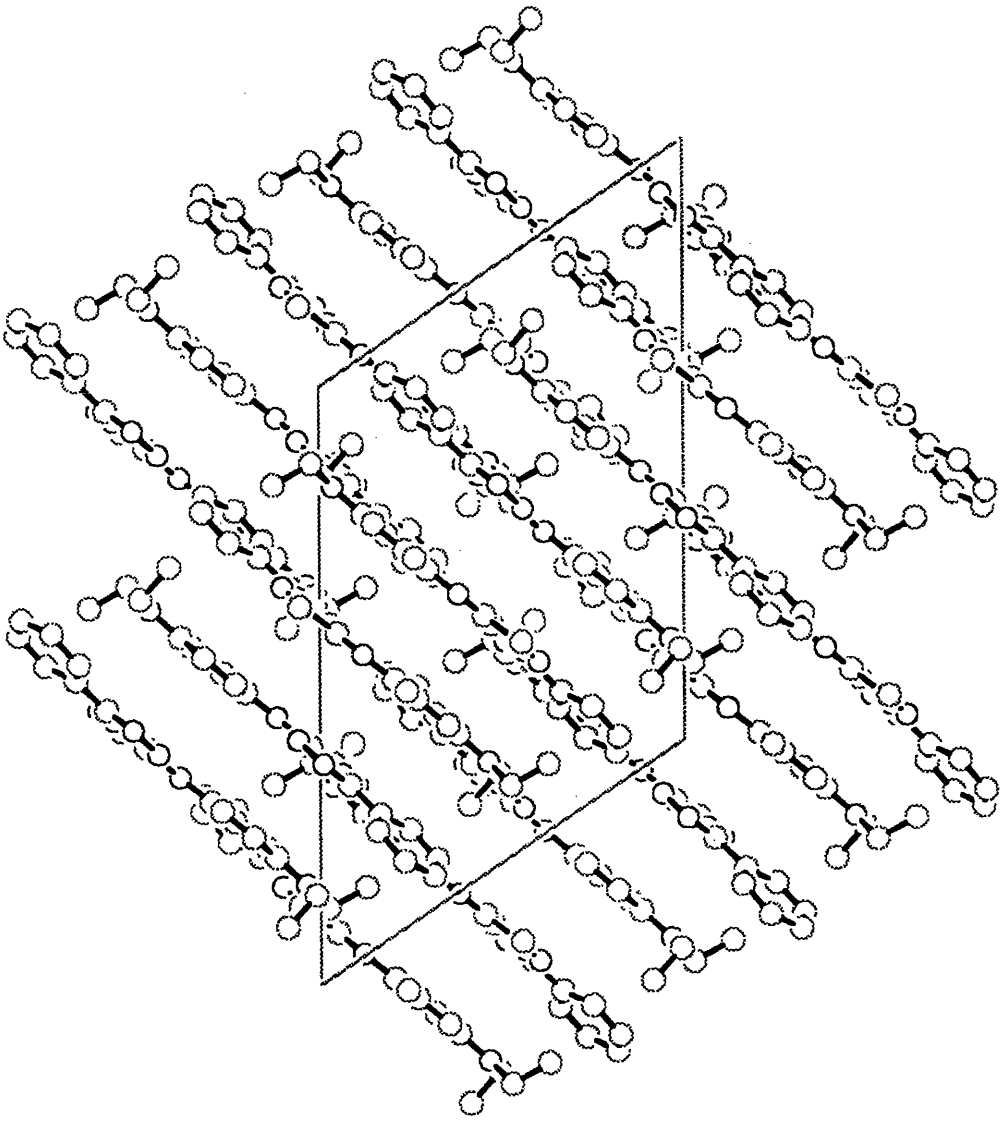

Figure 3.4: Crystal packing of the 6-Me dye.

It is worth noting that in the solid state the dye is in the *syn* configuration and that it is planar except for the ethyl groups on the developer where one of the terminal CH_3 groups points up and the other points down with respect to the plane of the rest of the molecule.

3.3.3 Molecular orbital calculations

Figures 3.5 and 3.6 show the calculated minimum energy ground state configurations for 6-Me and 6-CN dyes, obtained using CNDO-VS [8]. AM1 (Austin Method 1) and PM3 (Parameterisation Method 3) methods were used to optimise the geometry [9]. (Thanks to Dr James Padfield for his assistance with this work.)

For both dyes the *syn* arrangement is more stable than *anti* by *ca.* 17 kJ mol^{-1}, results which are consistent with the detection of only one isomer in the NMR spectra, and NOE studies [7]. In the calculated minimum energy conformation the developer and coupler rings are twisted at an angle of 40° for the 6-Me dye and 32° for the 6-CN dye.

A comparison between calculated transition energies (given in nm) and absorption maxima in hexane gives:
6-Me, calculated 572 nm, observed 542 nm;
6-CN, calculated 623 nm, observed 622 nm.
The predicted and experimental values are in good agreement for both dyes, with the values for the cyan 6-CN dye being remarkably close.

Also shown are the relative electron densities in the ground and excited states. Red indicates a positively charged atom (relative to the neutral atom) while blue represents a negatively charged atom. The relative amount of charge is indicated by the radii of the coloured circles. The essence of the transition is the transfer of electron density, primarily from the coupler group but with some contribution from the carbon atom at the 6-position of the PT ring, to the azomethine nitrogen and the PT nitrogen at the 5-position of the PT ring. There is little change in electron density at the 3-position. These calculations are in line with the observation that a change of substituent at the 6-position makes a big difference to hue, with electron withdrawing groups shifting it

to lower energy, whereas the effect on the hue of the substituent at the 3 position is very small [1].

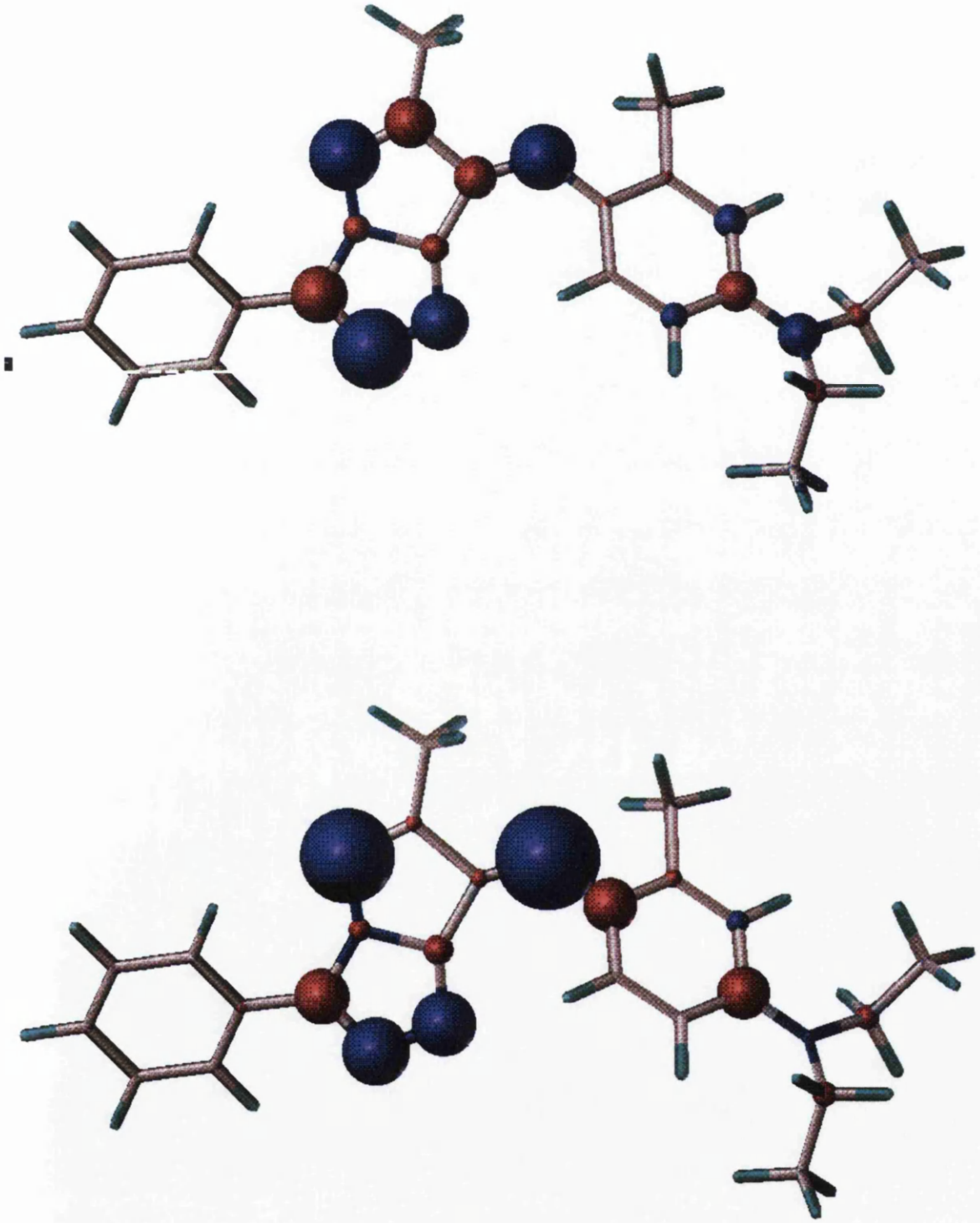

Figure 3.5: Ground state (top) and excited state (bottom) charge densities for the 6-Me dye (Red = +ve/ Blue = -ve).

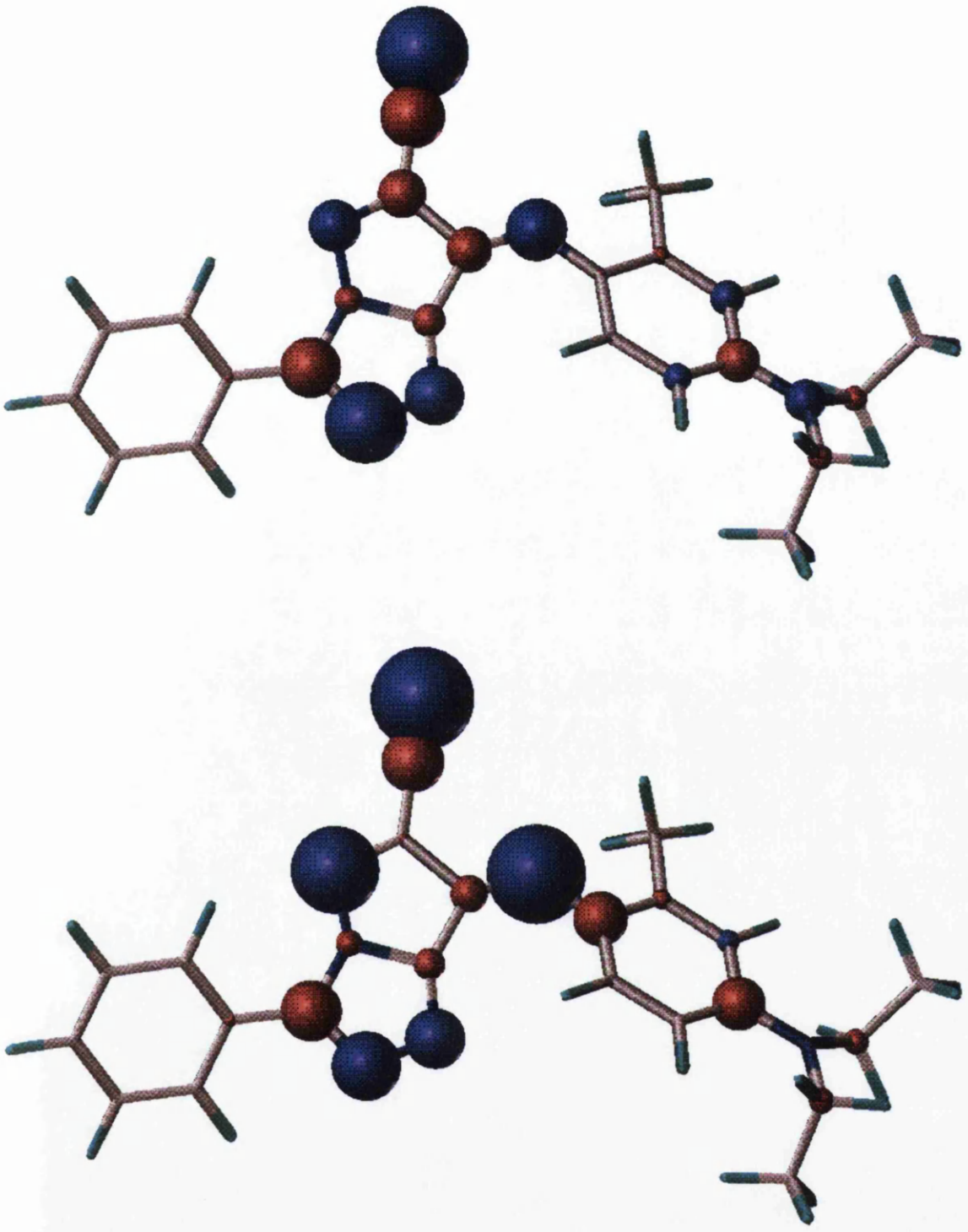

Figure 3.6: Ground state (top) and excited state (bottom) charge densities for the 6-CN dye (Red = +ve/ Blue = -ve).

Table 3.6 compares the bond lengths obtained from molecular orbital calculations with those measured from the x-ray crystal structure.

Parameter	gas phase		hexane		x-ray data
	AM1	PM3	AM1	PM3	
N(1)-C(1)	1.403	1.392	1.402	1.389	1.356(3)
N(1)-N(4)	1.355	1.421	1.356	1.422	1.411(3)
N(2)-N(3)	1.321	1.333	1.322	1.336	1.391(3)
N(4)-C(11)	1.333	1.322	1.333	1.324	1.304(3)
N(5)-C(13)	1.401	1.420	1.403	1.421	1.370(3)
C(1)-C(2)	1.456	1.454	1.456	1.455	1.466(3)
C(10)-C(11)	1.541	1.515	1.541	1.515	1.474(3)
C(18)-C(19)	1.484	1.487	1.484	1.487	1.505(3)
N(1)-C(8)	1.452	1.417	1.452	1.415	1.358(3)
N(2)-C(1)	1.381	1.370	1.381	1.371	1.335(3)
N(3)-C(8)	1.351	1.345	1.350	1.344	1.326(3)
N(5)-C(10)	1.281	1.287	1.280	1.287	1.307(3)
N(6)-C(16)	1.392	1.448	1.389	1.446	1.367(3)
C(8)-C(10)	1.481	1.462	1.481	1.463	1.460(3)
C(11)-C(12)	1.475	1.476	1.474	1.475	1.491(3)

Table 3.6: Comparison of selected bond lengths (Å) obtained from molecular orbital calculations and x–ray crystallography respectively.

In the crystalline state the molecules are essentially planar, *i.e.* there is a developer-coupler twist angle of *ca.* 0°. The M.O. calculations for the free isolated dye show the angle to be *ca.* 40°. This difference presumably arises due to the intermolecular forces in the crystalline state. This may also explain the relatively large difference between the calculated bond lengths obtained from the M.O. calculations and those observed in the solid state for the C_{13}-N_5 bond, which is the bond about which the developer-coupler will twist. The indication that these forces are sufficient to force planarity when the free isolated dye has a significant developer-coupler twist angle suggests a relatively shallow potential energy curve along the twist angle.

3.4 Aggregation studies

3.4.1 Absorption studies

It has been noted by workers in Kodak Ltd. that the UV/Vis spectra of the 6-COOH dye shows unusual solvent dependent features and that the absorption maximum of the 6-$CONH_2$ dye is at a longer wavelength than expected based on the electronegativity of this substituent. It was suggested by D.Clarke and C.Winscom of Kodak Ltd. that aggregation might be the reason for the unusual behaviour of these dyes; this may also be a factor in terms of photostability [10]. While the UV/Vis spectra of the dyes are discussed in more detail in chapter 4 it was important at this early stage in the work to investigate this suggestion of aggregation of the dyes in solution, and a study of the concentration dependence of the UV/Vis absorption spectra of the 6-COOH and 6-$CONH_2$ PT dyes in a polar, ethanol, and non-polar, toluene, solvent was undertaken.

3.4.1.1 Results and discussion

The absorption spectra for the 6-$CONH_2$ PT dye (shown in figures 3.7 and 3.8) showed only one absorbing species in both ethanol and toluene, with the more polar solvent pushing dye hue bathochromically (this will be discussed in more detail in chapter 4). Concentration does not affect the shape or position of the spectrum in either solvent. There is no evidence for any aggregation equilibria over the concentration range *ca.* 2×10^{-4} to 5×10^{-6} mol dm^{-3}. While this does not prove that in this concentration range the dye is present as a monomer, it is unlikely that any aggregation equilibria will lie so far in favour of the aggregate in both polar and non-polar solvents to be undetected across this concentration range.

The situation is not as clear for the 6-COOH dye. In most cases carboxylic acids form stable dimers, so stable that usually in some solvents the monomer cannot be detected [11]. Figure 3.9 shows that the concentration does not affect the shape and position of the spectra in ethanol implying that only the monomer is absorbing.

However, in toluene as the concentration is decreased it seems that two species are resolving into one, which implies that in non-polar solvents the equilibrium favours the dimer at high concentrations.

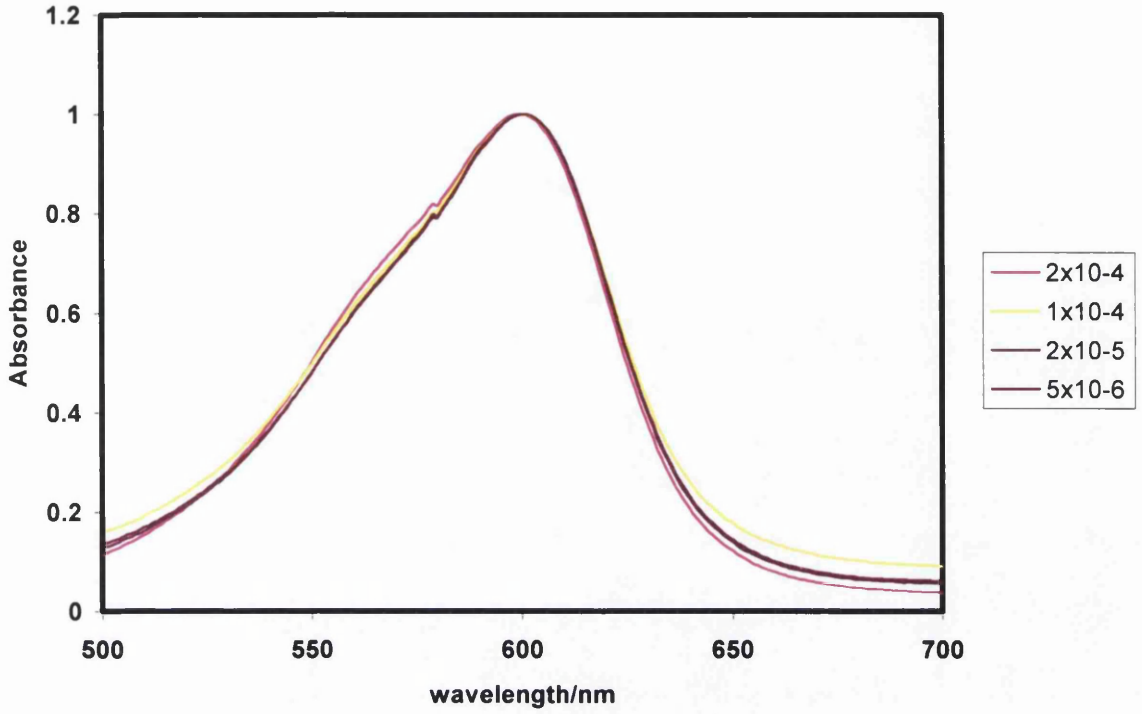

Figure 3.7: Normalised spectra of the 6-$CONH_2$ dye at various concentrations in toluene. (Legend shows concentration in mol dm^{-3}.)

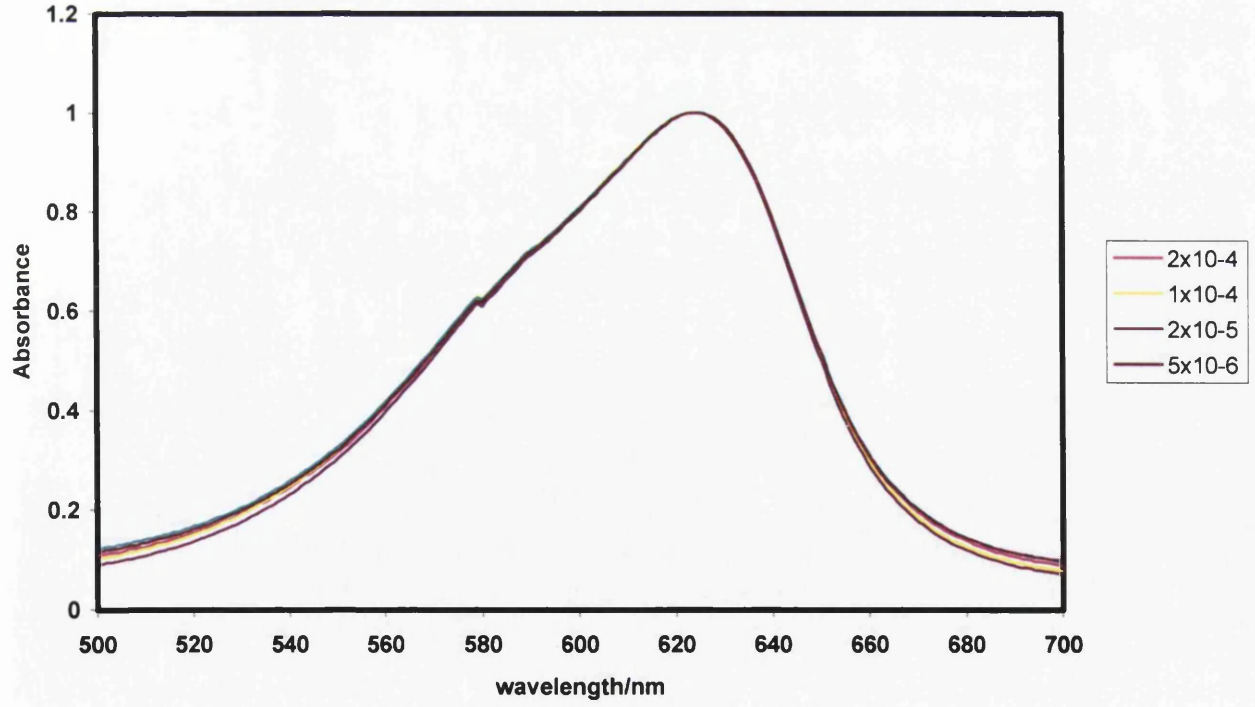

Figure 3.8: Normalised spectra of the 6-$CONH_2$ dye at various concentrations in ethanol. (Legend shows concentration in mol dm^{-3}.)

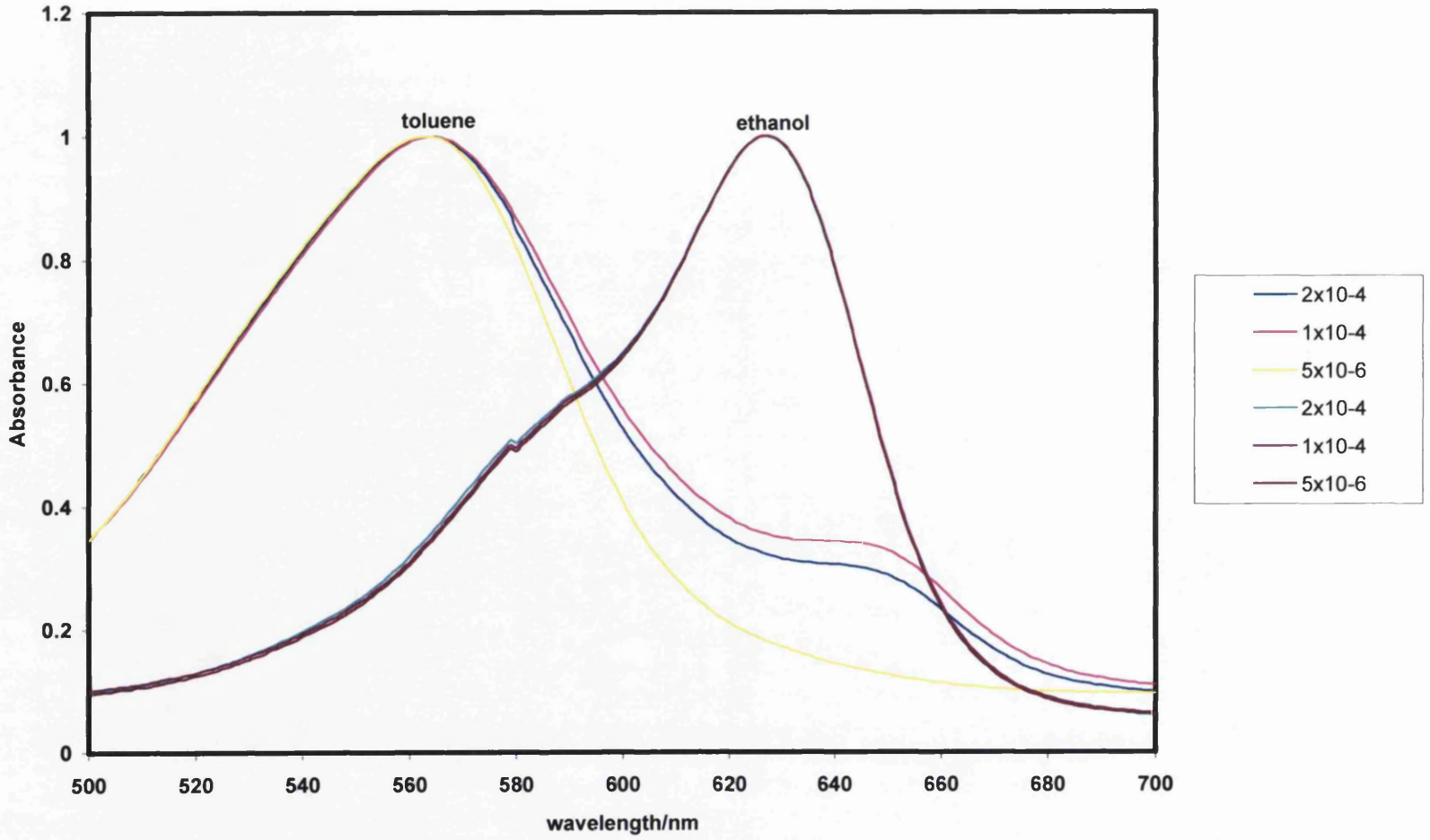

Figure 3.9: Normalised spectra of the 6-COOH dye at various concentrations in ethanol and toluene. (Legend shows concentration in mol dm^{-3}.)

3.4.2 Infrared

Infrared spectra for the dyes were also obtained in order to investigate whether the dyes may be hydrogen bonding and therefore aggregating/dimerising. (These spectra are given in the appendix.)

3.4.2.1 6-CO_2Et

In carbonyls a weakening of the carbon-oxygen double bond results in the signal moving to a lower frequency [12]. One of the factors that can cause this is the effect of β–conjugation on the C=O vibration. The frequency for the carbonyl vibration in saturated esters is around 1735 cm^{-1} [13]; the value obtained for the 6-CO_2Et dye is 1715 cm^{-1} which correlates well with the effect of the N=C bond present in the pyrazolotriazole ring system, β to the ester substituent. There is no evidence of any association occurring between CO_2Et moieties.

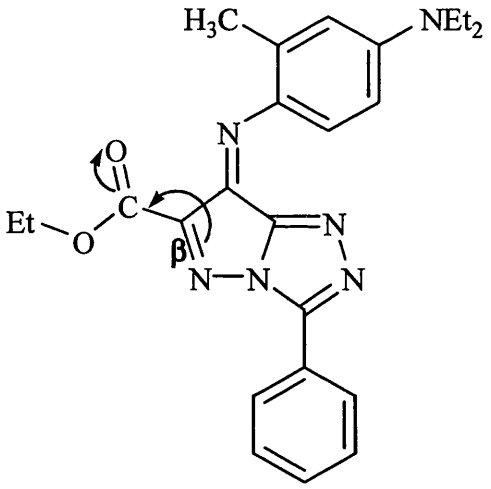

Figure 3.10: Effect of β-conjugation on C=O stretching frequency in the 6-CO_2Et dye.

3.4.2.2 6-$CONH_2$

There is no obvious evidence of association. The stretching frequency for the C=O functionality is at a slightly higher frequency than expected, at 1690 cm^{-1}; this can be attributed to the conjugation effect of the double bonds present in the pyrazolotriazole system.

3.4.2.3 6-COOH

The stretching frequency present at 1760 cm^{-1} is characteristic of monomeric carboxylic acids. The absence of any bands in the 1700-1725 cm^{-1} region suggests that the dimer is not present. A closer inspection of the peak shows some broadening which may suggest some association occurring between the COOH functional groups.

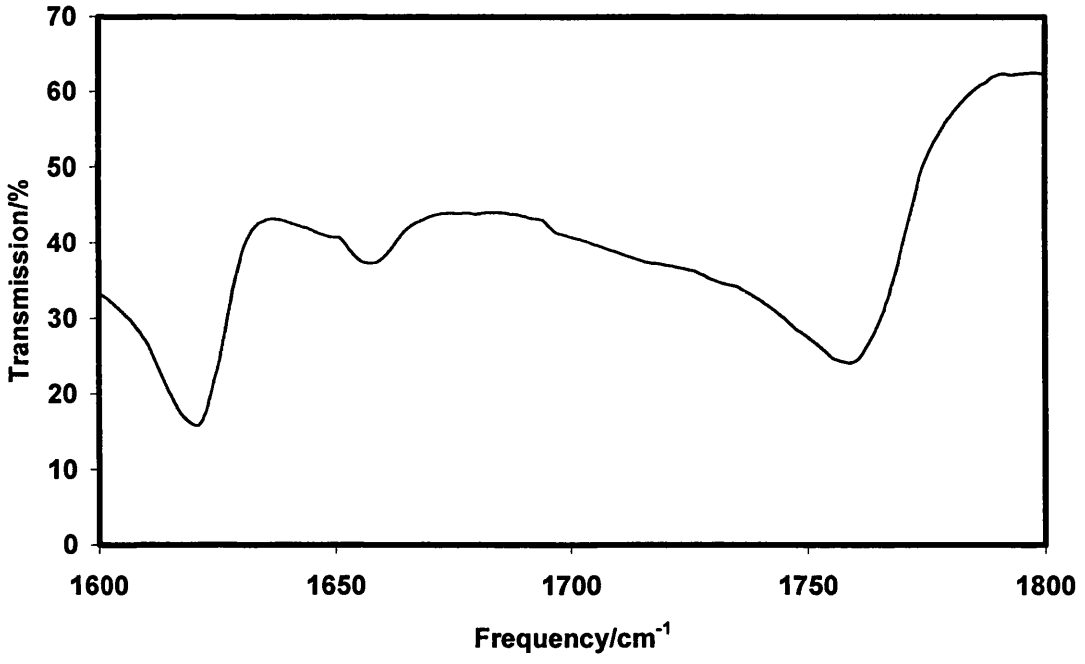

Figure 3.11: Broadening of stretching frequency at 1760 cm^{-1} possibly due to association between COOH groups.

3.5 Conclusions

The dyes synthesized for study vary only by the substituent at the 6-position of the pyrazolotriazole azomethine [5,5] heterobicycle ring system. The substituents vary in terms of their electron donating/withdrawing effects which have a direct effect on dye hue, giving hues which stretch from the magenta into the cyan.

Infrared studies suggest that no association occurs in the solid state for the 6-CO_2Et and 6-$CONH_2$ dyes. The broadness of the characteristic stretching frequency for the 6-COOH dye implies that although the monomer predominates, some dimer may be present.

NMR spectroscopic studies provide a tentative relationship between the R_6 substituent and the chemical shift of a characteristic proton adjacent to the azomethine bond.

Structural and molecular orbital studies agree with previous work in that the most stable conformer is *syn* with respect to the azomethine bond, and also that in crystalline form the 6-Me dye is essentially planar. M.O. calculations indicate the lengthening of the C-N bond (in the gas phase and in solution) about which molecular flexion occurs; this is reasonable as molecular flexibility would be restricted in the solid state leading to a shortening of the bond.

3.6 References

1) J.Bailey, *J. Chem. Soc. Perkin Trans. 1,* **1977**, 2047.

2) W.Landon, Kodak Ltd. Research disclosure, August 1974, p.39.

3) P. Bergthaller, *Imaging Sci. J.,* **2002**, 50, 153.

4) J.R.Chapman, *Practical Organic Mass Spectrometry,* **1995,** John Wiley and Sons, UK.

5) P.J.S.Pauwels, *J. Am. Chem. Soc.,* **1967**, 89, 580.

6) E.B.Knott and P.J.S Pauwels, *J. Org. Chem.* **1968**, 33, 2120.

7) P.Douglas, C.Couture, D.Clarke, D.Reed, I.H.Sadler, T.Wear, *J. Chem. Soc. Perkin Trans. 2*, **1994**, 1295.

8) J.O.Morley, M.H.Charlton, R.Docherty, D.J.McGeein, *J. Chem. Soc. Faraday Trans.*, **1993**, 89, 1671.

9) J.Padfield, *PhD Thesis*, University of Wales, **2003**

10) C.K.Parmar, *PhD thesis,* **2001**, Imperial College of Science, Technology and Medicine.

11) P.Suppan and N.Ghoneim, *Solvatochromism,* **1997**, RSC information services, UK.

12) D.L.Pavia, G.M.Lampman, G.S.Kriz, *Introduction to Spectroscopy*, **1996**, Saunders College Publishing, Florida, USA.

13) D.H.Williams and I.Fleming, *Spectrosopic Methods in Organic Chemistry*, **1997**, McGraw-Hill Publishing Company, London, UK.

Chapter 4

Room temperature and low temperature singlet state characterisation

4.1 Introduction

In photographic terms the singlet states of an image dye are vitally important, as dye hue is influenced primarily by the most probable S_0-S_n electronic transition (λ_{max}), and the molar absorptivity of image dyes needs to be high in order for effective silver to image dye conversion.

PT dye hue can be 'tuned' by varying the R_6 substituent [1-3]. Electron donating groups in the 6-position on the pyrazolotriazole ring system (*e.g* 6-OMe) give a dye with a magenta hue, while electron withdrawing groups in this position (*e.g* 6-CN) push the hue well into the cyan. This can be seen in the absorption spectra for the six dyes used in this study (figure 4.1), and also from a correlation of absorption maxima and Hammett functions in figure 4.2. (The six dyes were chosen from the nine available on the basis of dye hue and steric considerations.)

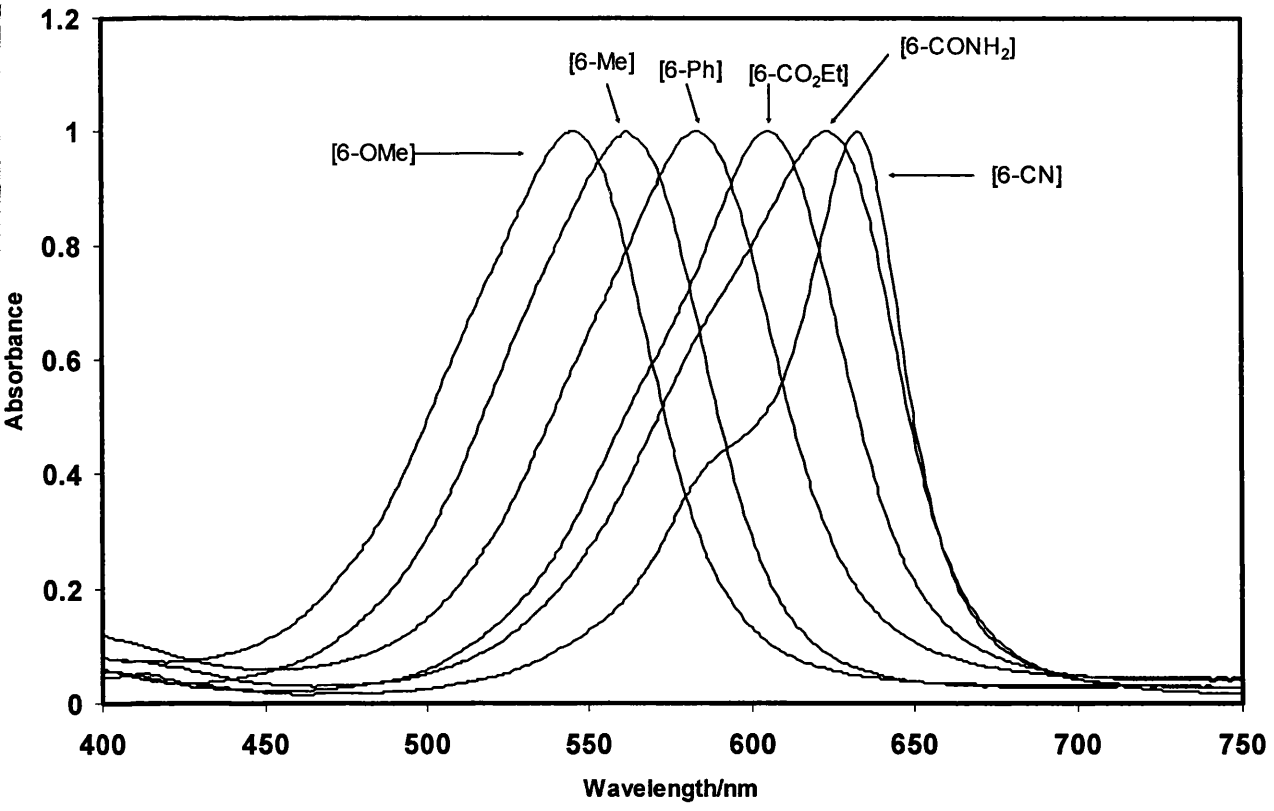

Figure 4.1: Normalised absorption spectra for six PT dyes in ethanol.

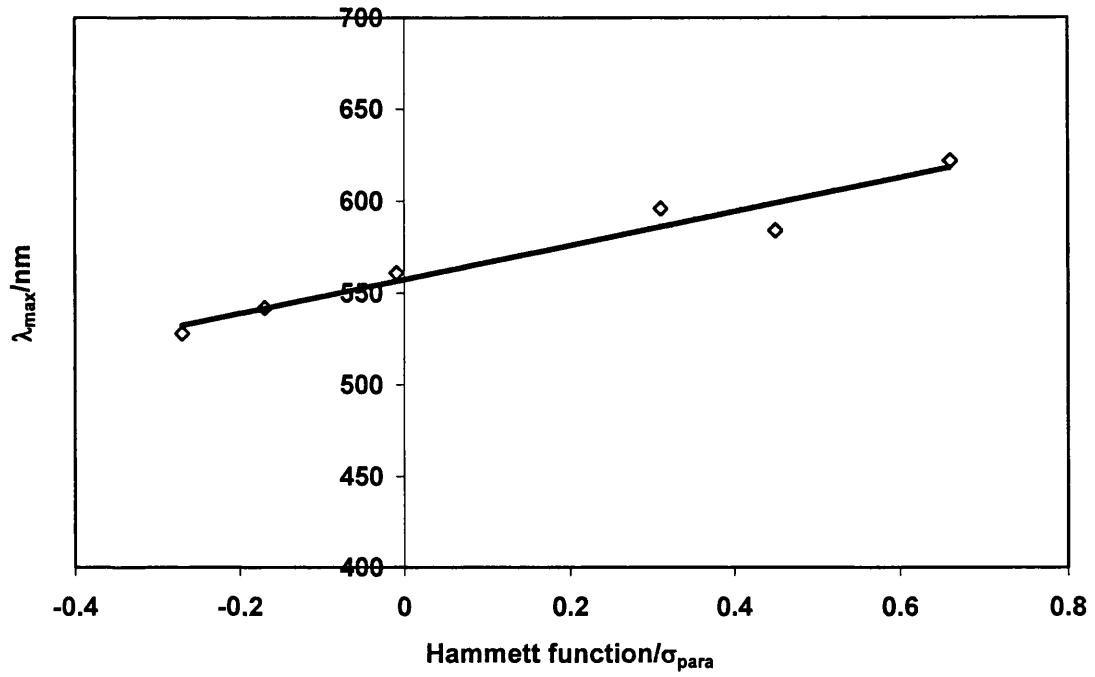

Figure 4.2: Correlation between σ_{para} Hammett parameters and absorption maxima in methylcyclohexane for the dyes studied ($R^2 = 0.939$).

4.2 77 K absorption characterisation

4.2.1 Introduction

Furya *et al.* [4] studied the effects of low temperature on PT dyes in EPA. Berry comprehensively studied the effects of decreasing temperature on indoaniline dyes [5], and he observed a narrowing of absorption spectra as well as a bathochromic shift in absorption maxima as the temperature decreased.

For PT dyes at RT in solution the discreet vibrational bands are generally masked and transitions over a range of energies 'overlap' each other. This combined with interaction between the excited state of the dye and the solvent environment results in characteristic broadening of the spectrum [6].

77 K absorption studies are useful as they help resolve vibrational band structure. At low temperatures the population distribution in energy levels becomes narrower

compared to those recorded at room temperature where the population distribution of energy levels is wider [7].

4.2.2 Experimental

Absorption spectra at RT and 77 K were recorded using a Perkin Elmer Lambda 9 UV/Vis/NIR spectrophotometer. The solvent of choice was EPA (a 2:5:5 mix of ethanol:isopentane:diethyl ether) as this consistently provided the best glass at 77 K [2].

About 1 ml of dye solution (*ca.* $2x10^{-5}$ mol dm^{-3}) was added to a quartz tube with an internal diameter of 3 mm. This was then plunged directly into liquid nitrogen held in a custom made quartz dewar. In order to consistently align all samples correctly in the beam of the spectrophotometer a PTFE fitting was made which enabled safe attachment of the dewar to the base of the spectrophotometer and correct alignment during the experiment.

4.2.3 Results and discussion

The absorption maximum for all of the dyes shifts bathochromically upon cooling to 77 K and ε_{max} increases. The absorption spectrum becomes sharper with a relatively well defined vibrational progression becoming evident (figures 4.3-4.8). A comparison of the integrated area of the absorption band shows that the transition probability does not change significantly upon cooling.

Table 4.1 summarises the RT and 77 K frequency maxima, as well as the difference in energy between the frequency at maximum absorption and the shoulder (which is more clearly resolved at 77 K) on the high energy side of the spectrum.

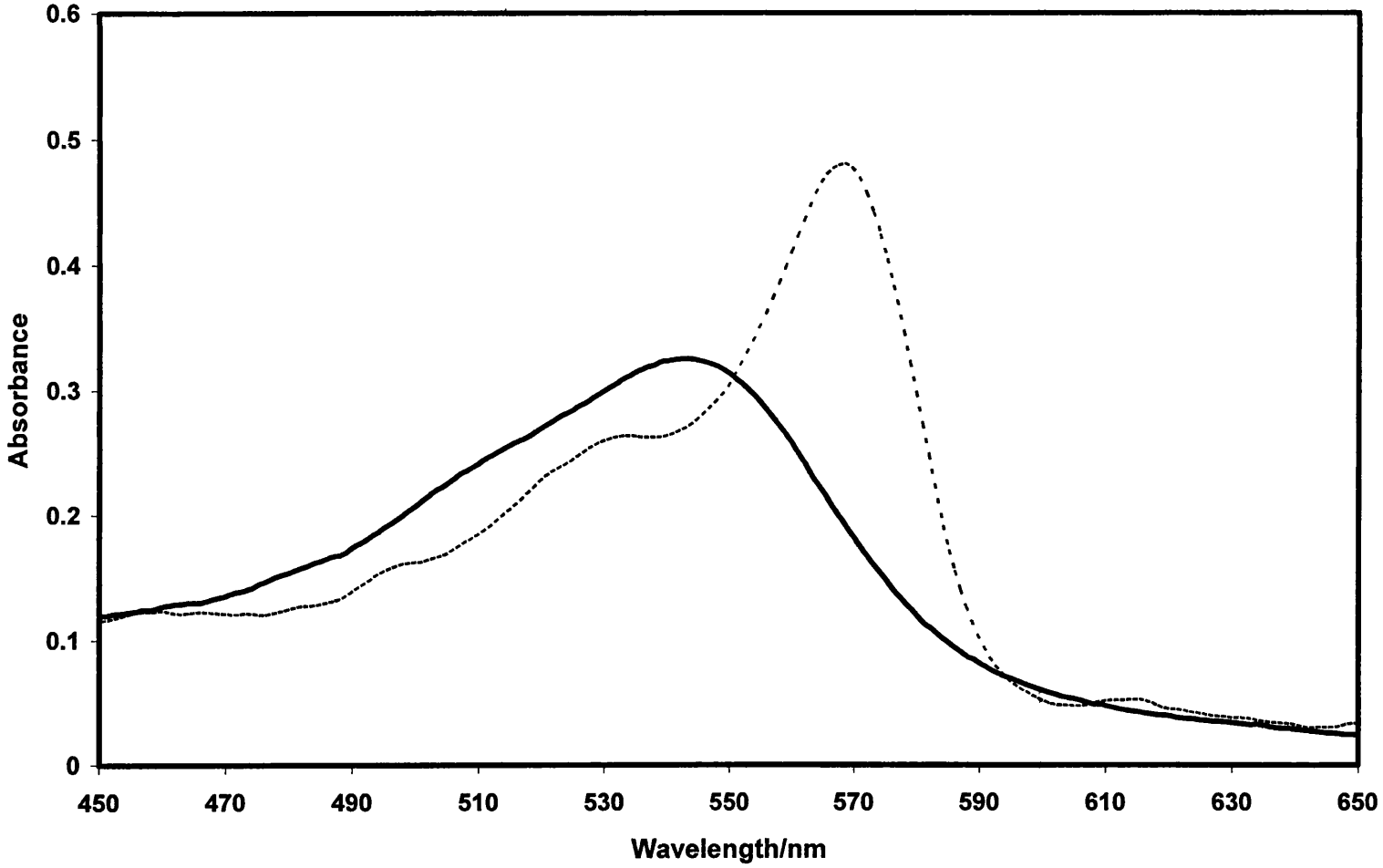

Figure 4.3: Absorption spectra for 6-OMe at room temperature (solid bold line) and 77 K (dashed line).

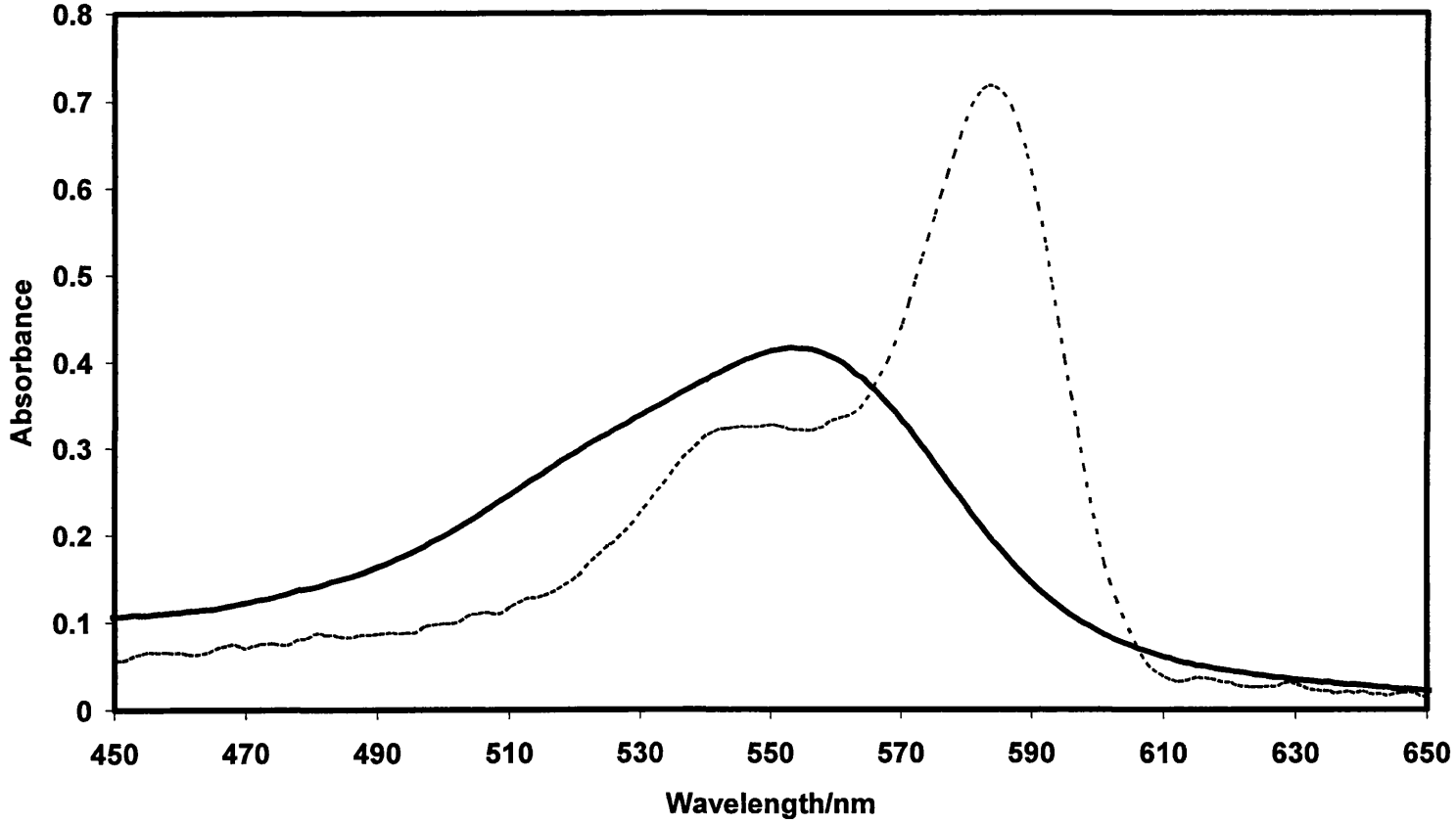

Figure 4.4: Absorption spectra for 6-Me at room temperature (solid bold line) and 77 K (dashed line).

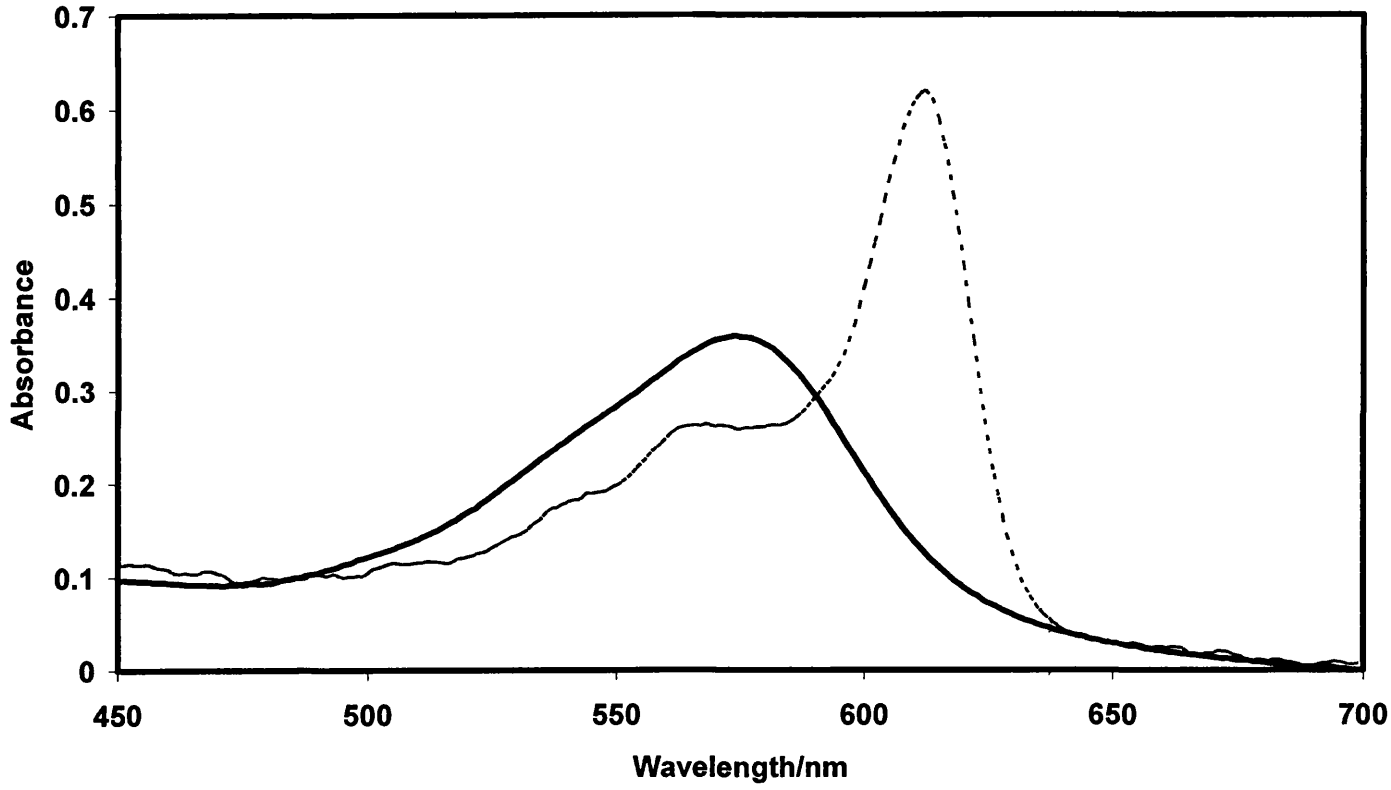

Figure 4.5: Absorption spectra for 6-Ph at room temperature (solid bold line) and 77 K (dashed line).

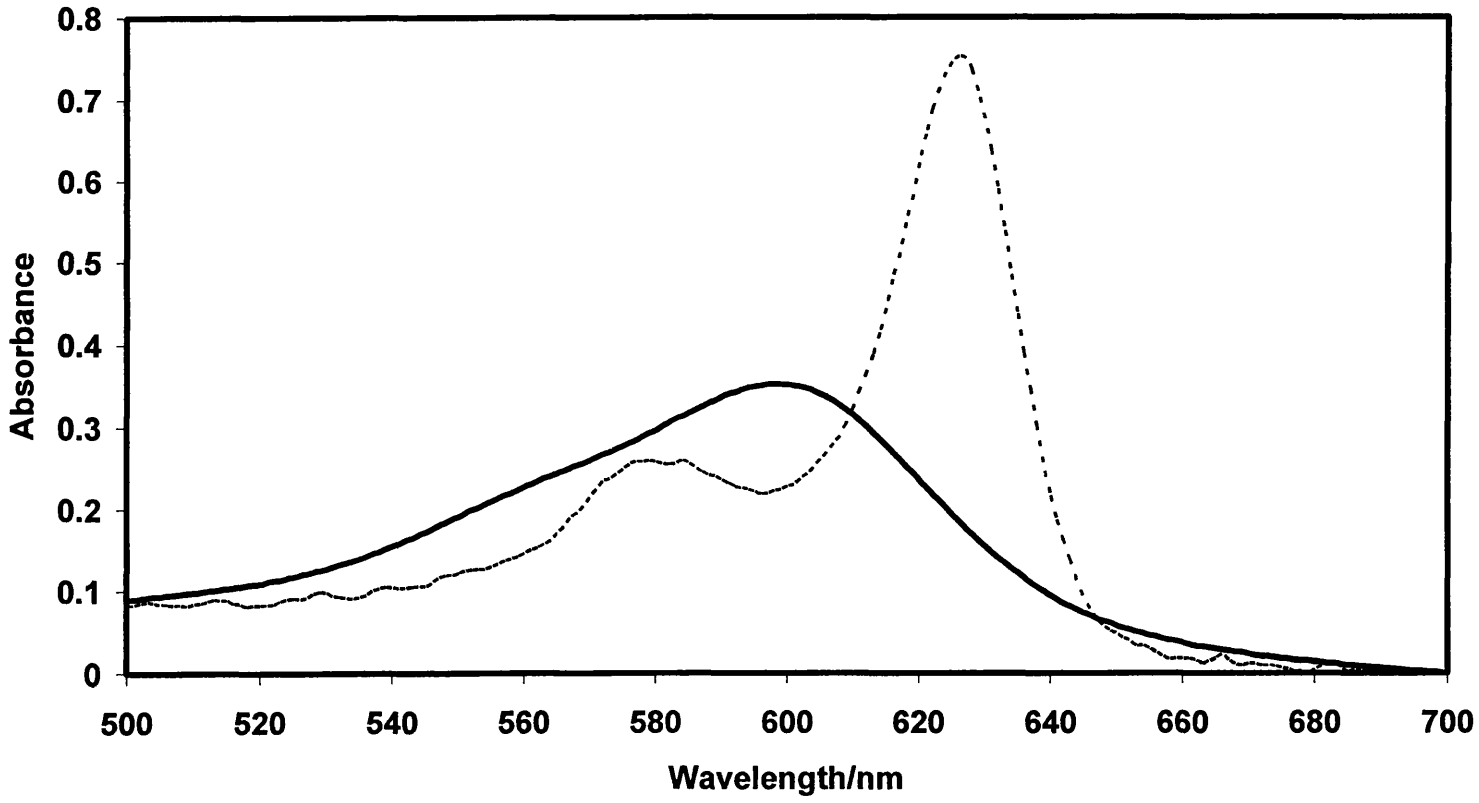

Figure 4.6: Absorption spectra for 6-CO_2Et at room temperature (solid bold line) and 77 K (dashed line).

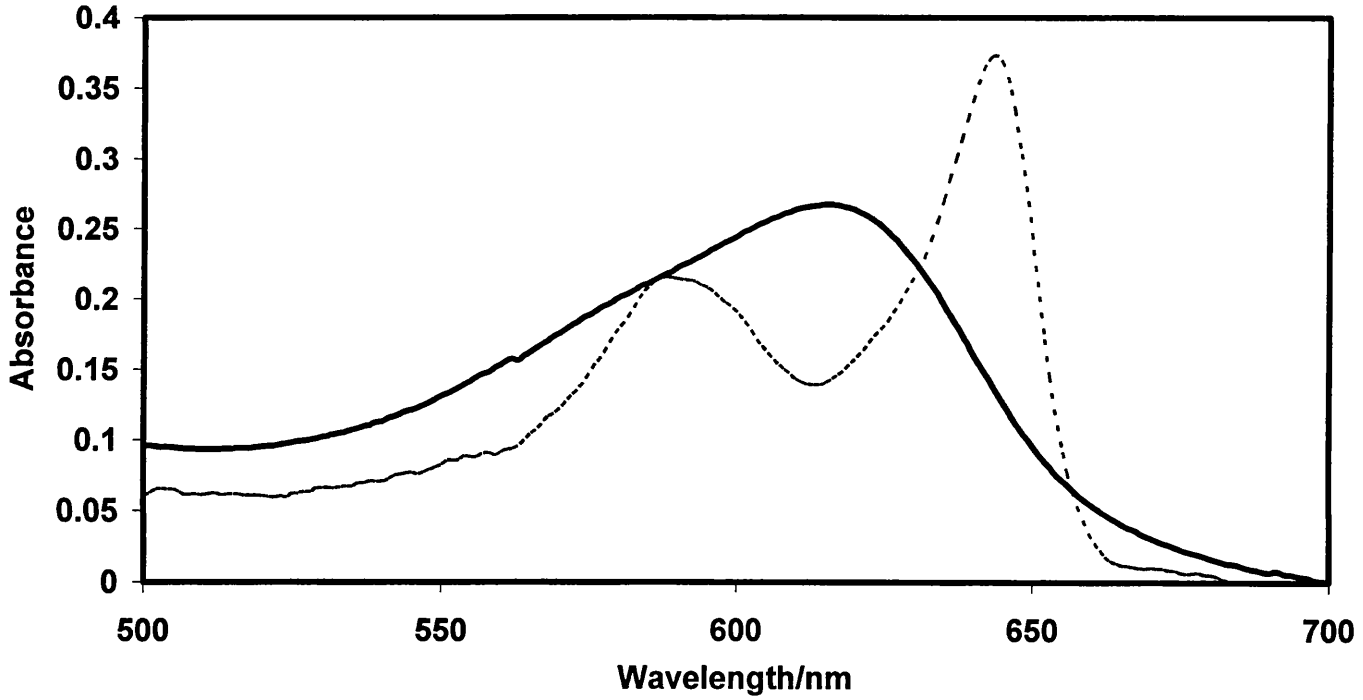

Figure 4.7: Absorption spectra for 6-$CONH_2$ at room temperature (solid bold line) and 77 K (dashed line).

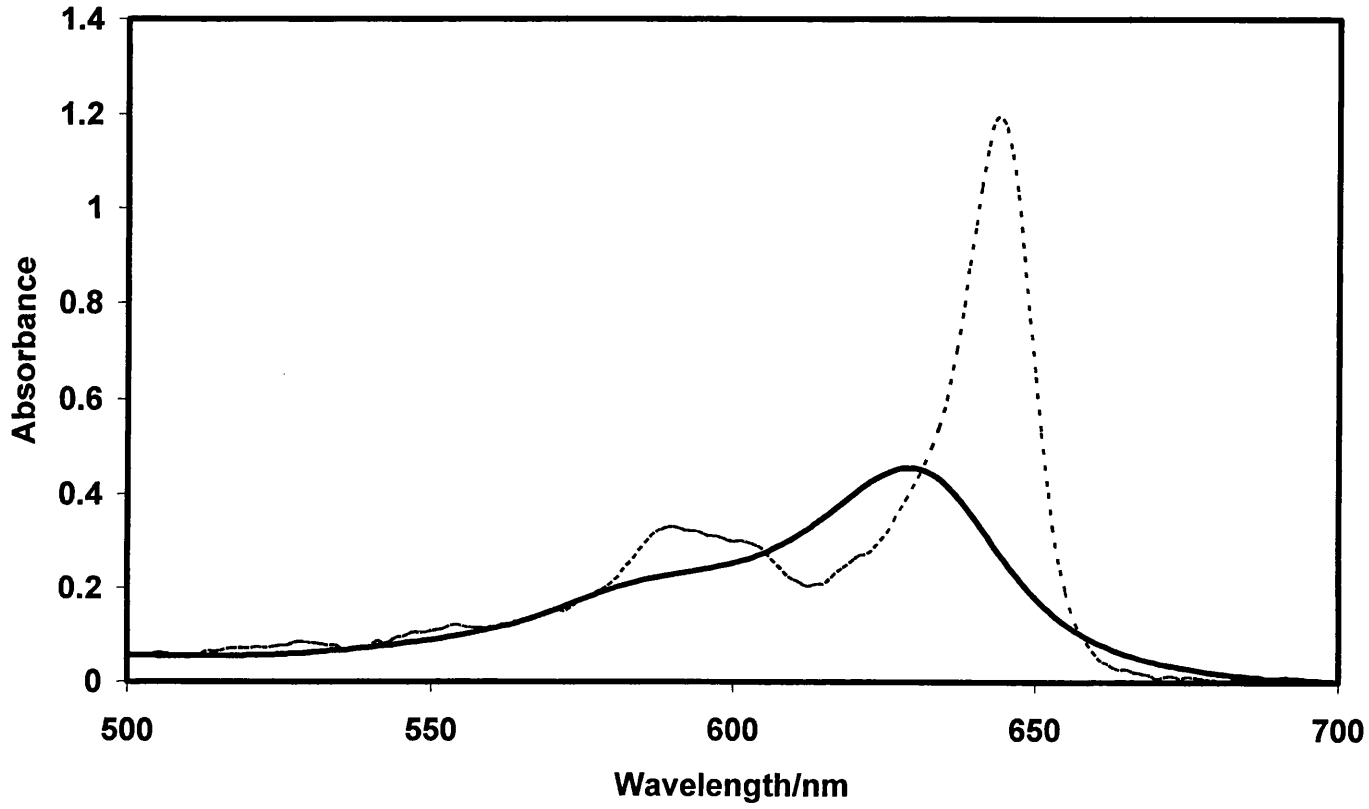

Figure 4.8: Absorption spectra for 6-CN at room temperature (solid bold line) and 77 K (dashed line).

At all temperatures the solvent-solute interaction needs to be considered [8]. Recent work by Boxer and Bublitz [9] has shown that the polarities of frozen glasses are significantly higher than those of the corresponding liquids at room temperature. This, together with the shift in distribution of conformers around the twist of the azomethine bond explains the bathochromic shift of all the dyes at 77K as this is characteristic for PT dyes when the polarity of the solvent medium is increased [1,2].

The vibrational spacing in an absorption spectrum is characteristic of the dye excited state [6]. Although the data are far from precise there does appear to be a trend in that both electron donating and electron withdrawing substituents give larger excited state vibrational spacings than substituents with a small or neutral electronic effect.

The data suggest that either an electron donating or withdrawing group has a similar effect in terms of compressing the excited state potential energy surface, and therefore widening the vibrational intervals relative to dyes with electro-neutral substituents which are postulated to have shallower potential energy wells in the excited state.

4.3 77 K emission and excitation spectra

4.3.1 Introduction

In an organic glass at 77 K, PT dyes are locked in a rigid matrix and therefore the molecular flexion around the azomethine bond is inhibited. At these low temperatures a major route for deactivation of the excited state is fluorescent emission from the S_1 state and, for those predominantly magenta PT dyes studied to date, fluorescence quantum yields close to 1 have been measured at 77 K [10].

4.3.2 Experimental

Fluorescence emission and excitation were recorded using the same quartz dewar described in section 4.2.2 positioned in a Jobin-Yvon JY3D spectrofluorimeter. Data were collected *via* a Picolog data logger connected to a PC for ease of analysis.

Samples were prepared with absorbances of <0.1 (in the 3 mm quartz tube) at the excitation wavelength, which was 520 nm for 6-OMe and 6-Me dyes and 580 nm for the remainder of the dye series. Emission slits were 8 nm and excitation slits were 4 nm.

Excitation spectra were corrected by using methylene blue and rhodamine B quantum counters using the method outline by Demas *et al.* [11]. Emission spectra were corrected for photomultiplier response (see section 2.3.3). Uncorrected and corrected emission spectra for 6-Me and 6-CO_2Et are shown in figures 4.9 and 4.10.

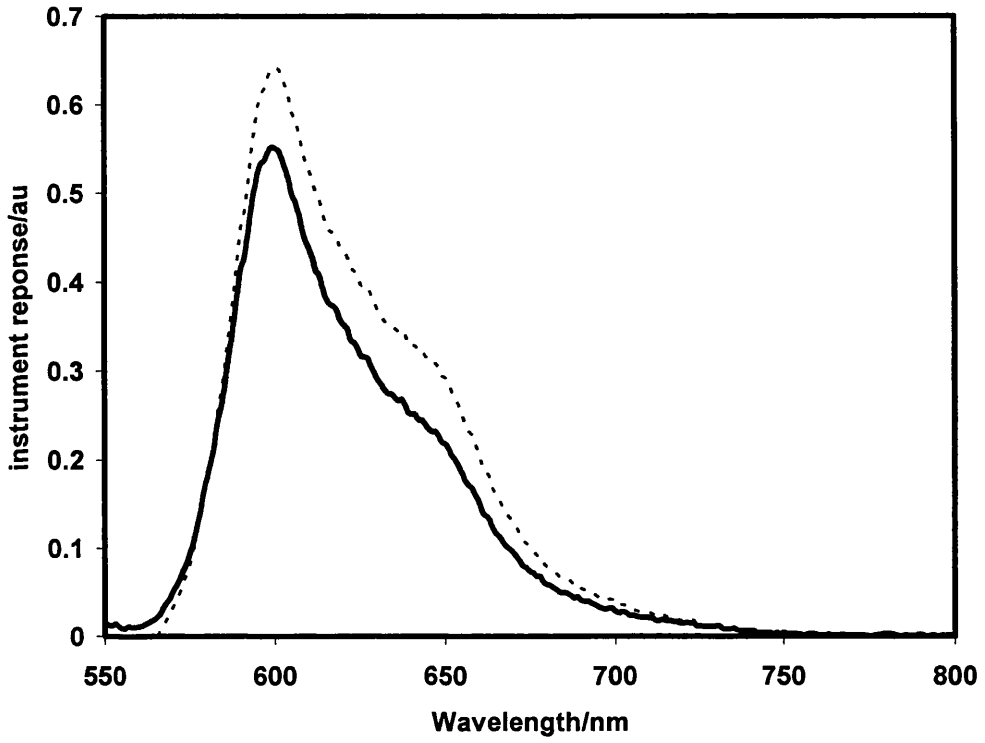

Figure 4.9: Uncorrected (bold lines) and corrected (dashed line) emission spectra for 6-Me.

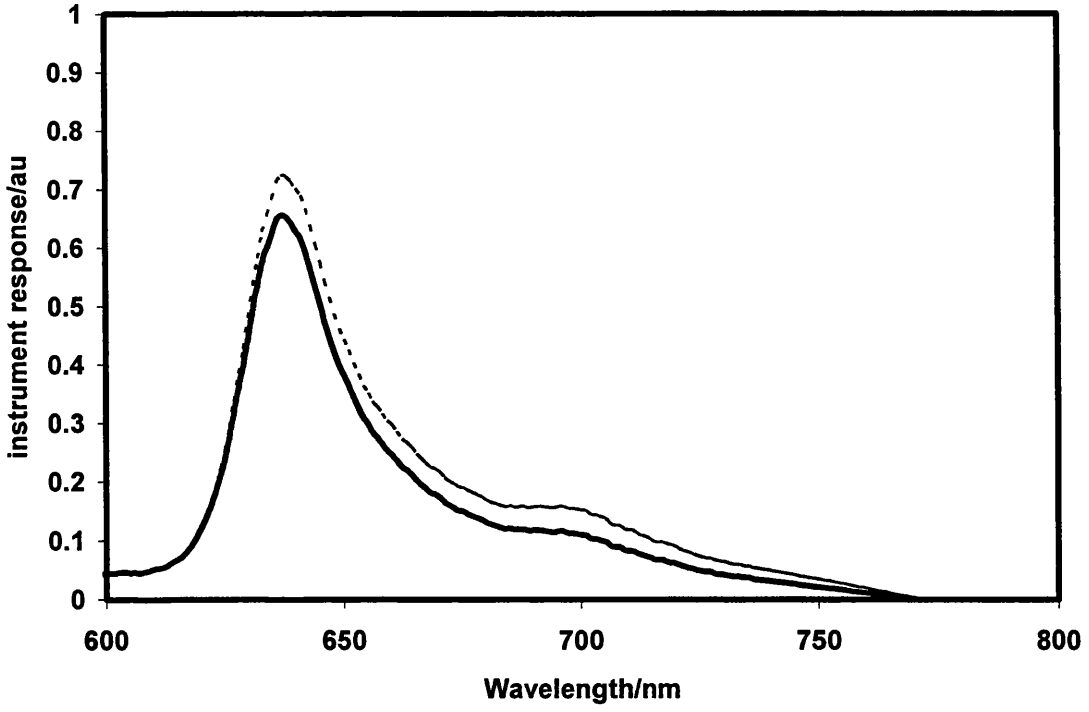

Figure 4.10: Corrected (dashed line) and uncorrected (bold line) emission spectra for 6-CO_2Et.

There are many difficulties with fluorescence standards at 77 K [12], a problem compounded by difficulties in finding standards for use in the spectral range in which PT dyes emit. However two suitable standards were found for this work, 6-^{t}Butyl PT dye and cresyl violet. 6-^{t}Butyl PT (77 K Φ_{fl} = 0.9 (±0.1) [10]) was used as a standard for studies with the magenta dyes 6-OMe and 6-Me. For the cyan dyes cresyl violet (RT Φ_{fl} = 0.54 [13], 77 K Φ_{fl} =0.9 (±0.1)) was used as reference.

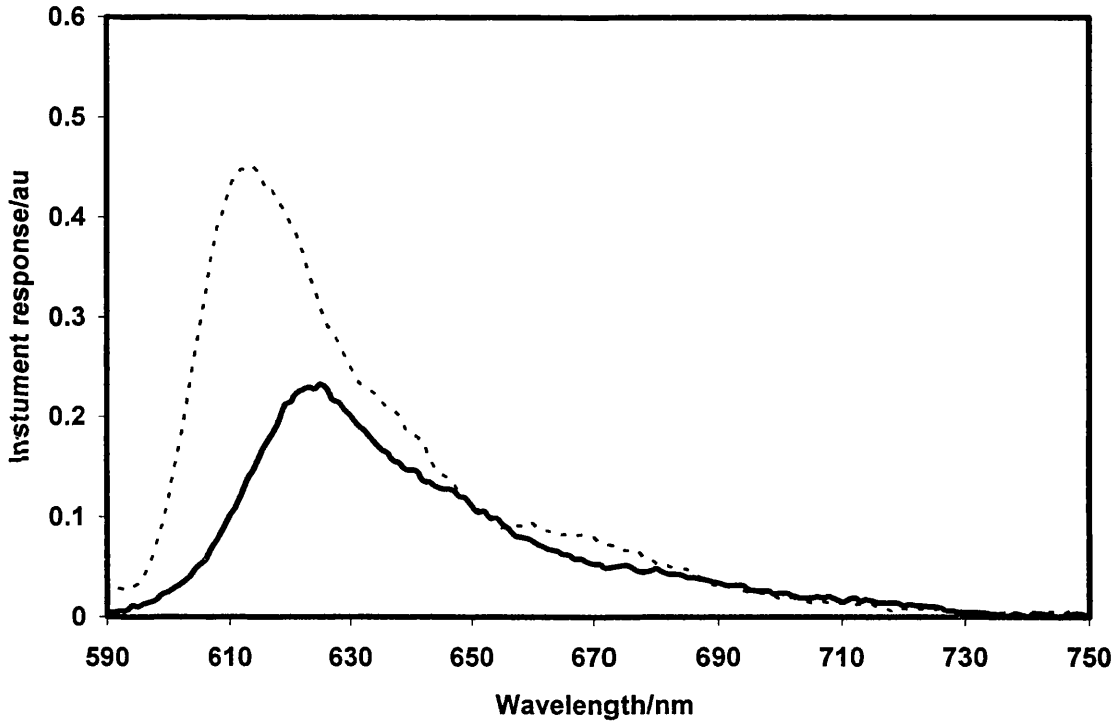

Figure 4.11: Corrected, room temperature (solid line) and 77 K emission spectra (dashed line) of cresyl violet.

4.3.3 Results and discussion

As would be expected, the emission spectra are roughly mirror images of the excitation spectra [14] (see figures 4.12-4.17).

The energy difference between the vibrational bands of the emission spectrum gives information about the ground state potential energy curve. As the data in table 4.1 show there is little systematic variation in ground state vibrational spacing. This suggests that the depth and shape of the ground state potential energy wells do not vary as much across the dye series when compared to the excited state.

Dye	λ_{max} emission (nm)	Φ_{fl} at 77K (*ca.*10%)	Stokes shift (±1 nm)
6-OMe	573	1.1*	2
6-Me	599	1*	17
6-Ph	618	1*	8
6-CO_2Et	639	0.9#	20
6-$CONH_2$	651	0.7#	1
6-CN	651	0.6#	3

* 6-^{t}Butyl PT dye as standard [6], # cresyl violet as standard [15].

Table 4.2: Summary of 77 K Φ_{fl} for the dye series.

The data show a clear trend: as the wavelength of the emission and excitation maxima increases the quantum yield of fluorescence decreases (figures. 4.18 and 4.19). There is a trend also in terms of the Stokes shift, with the largest shift evident for dyes with mid range λ_{max} values *i.e.* 6-Me, 6-Ph and 6-CO_2Et dyes, while a smaller shift is present for substituents which are significantly electron donating or withdrawing and have absorption maxima at either side of the λ_{max} range .

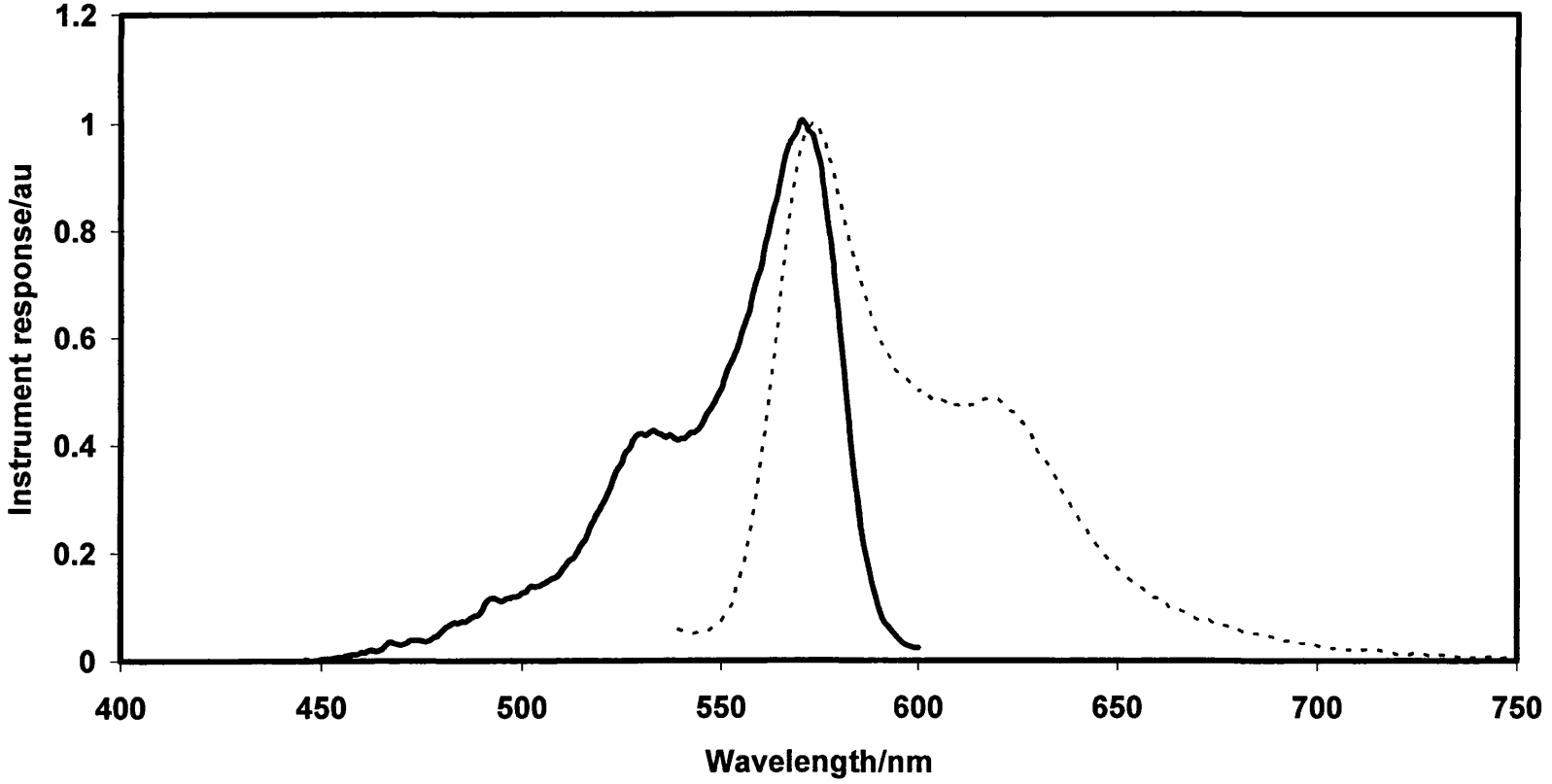

Figure 4.12: Normalised 77 K excitation (solid line) and emission (dashed line) spectra for 6-OMe in EPA. Excitation and emission bands have been removed.

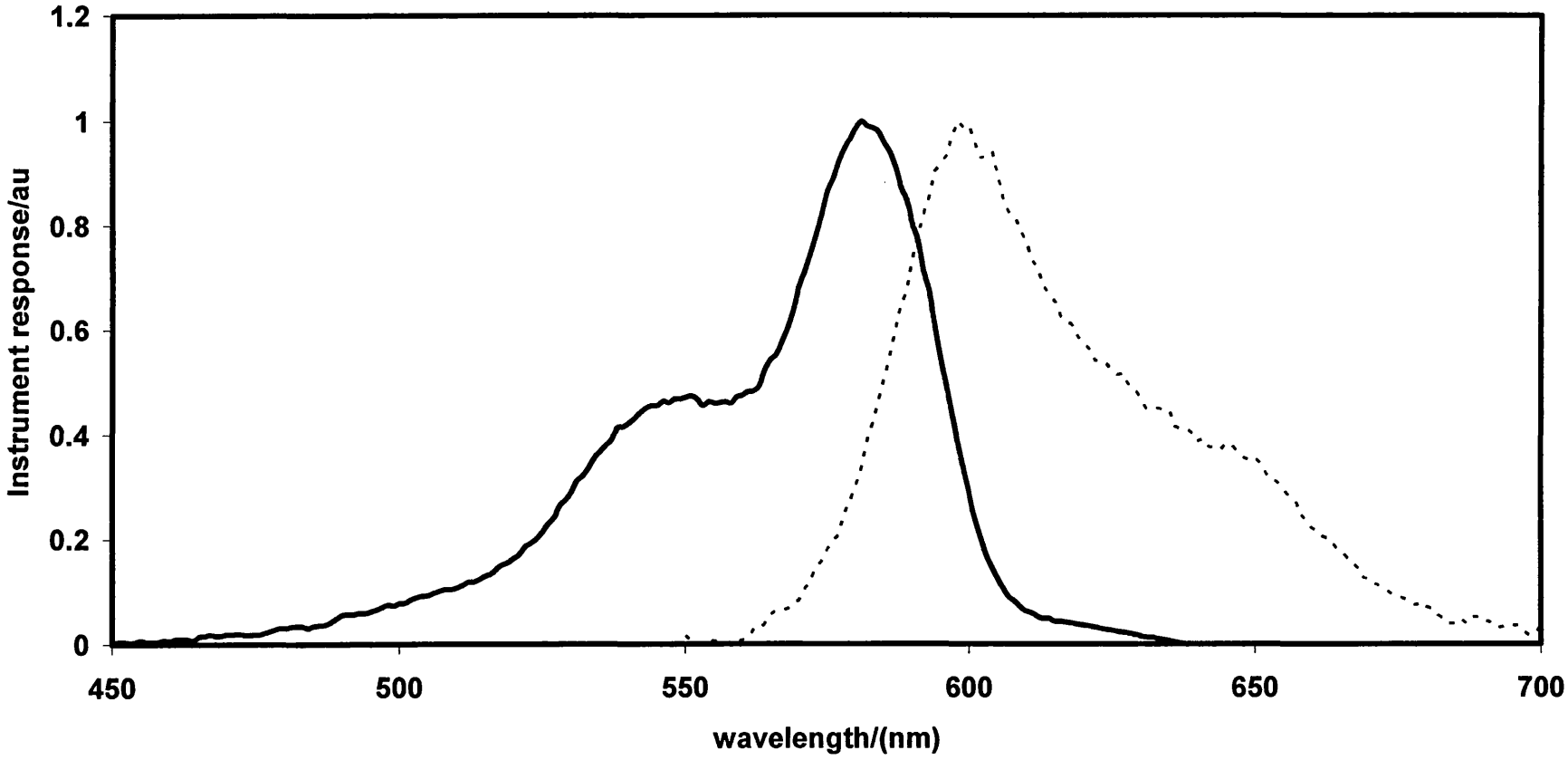

Figure 4.13: Normalised 77 K excitation (solid line) and emission (dashed line) spectra for 6-Me in EPA.

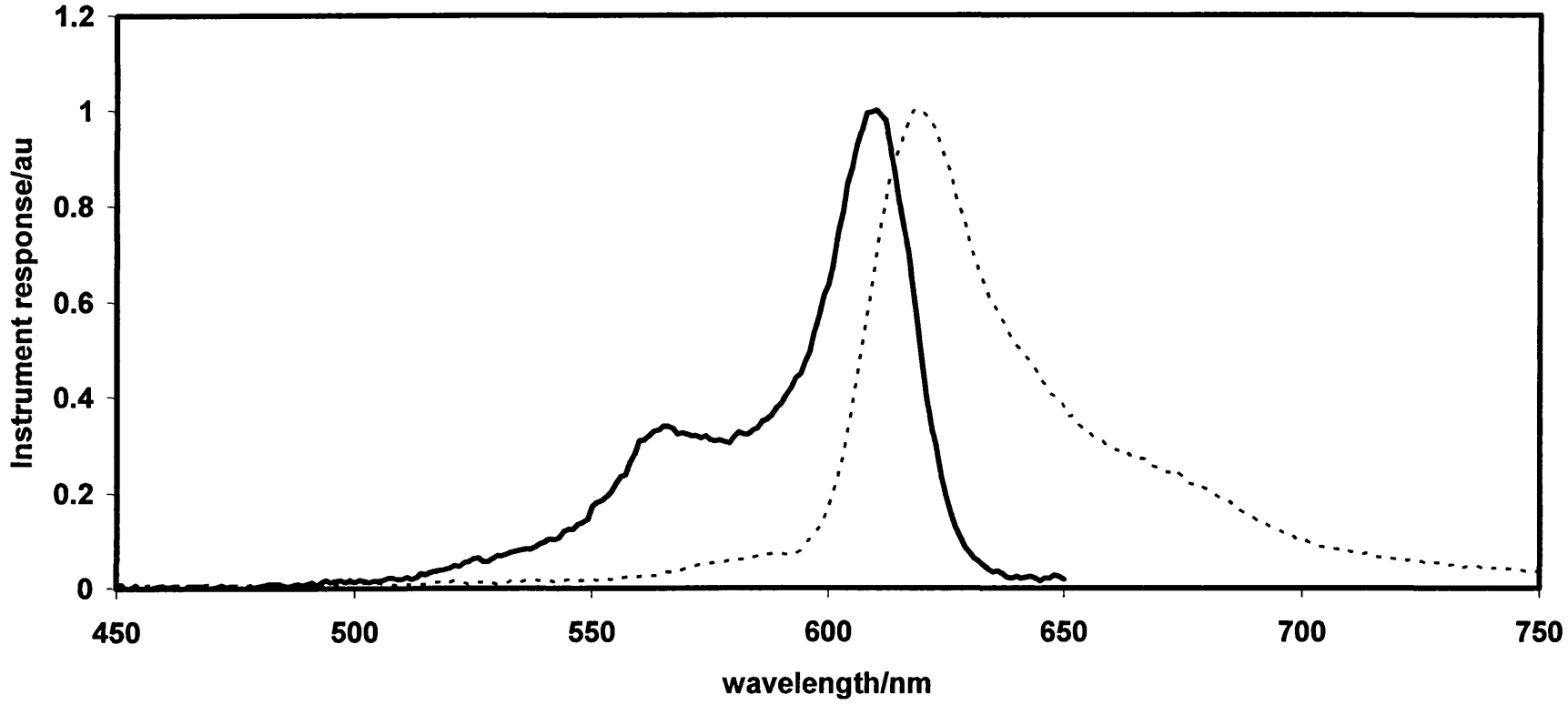

Figure 4.14: Normalised 77 K excitation (solid line) and emission (dashed line) spectra for 6-Ph in EPA.

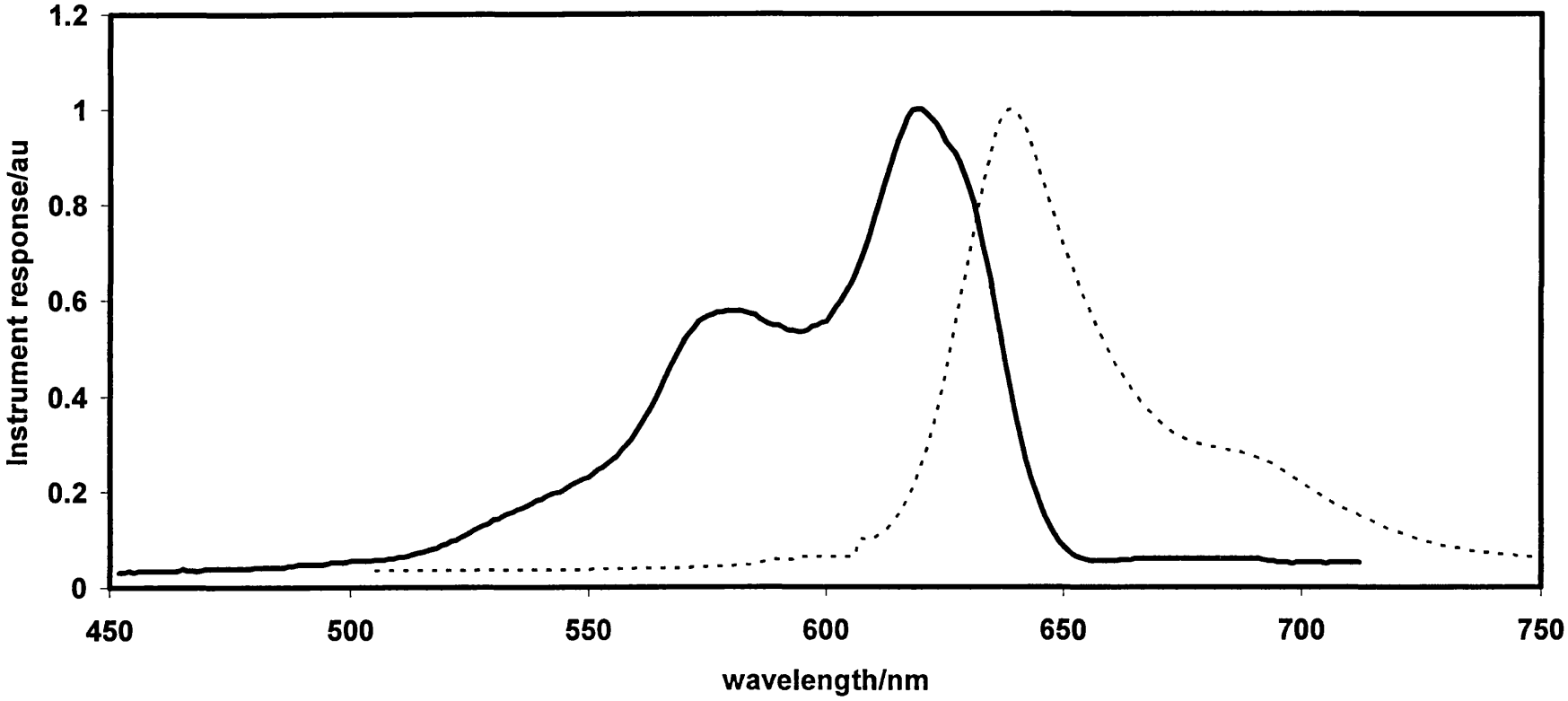

Figure 4.15: Normalised 77 K excitation (solid line) and emission (dashed line) spectra for 6-CO_2Et in EPA.

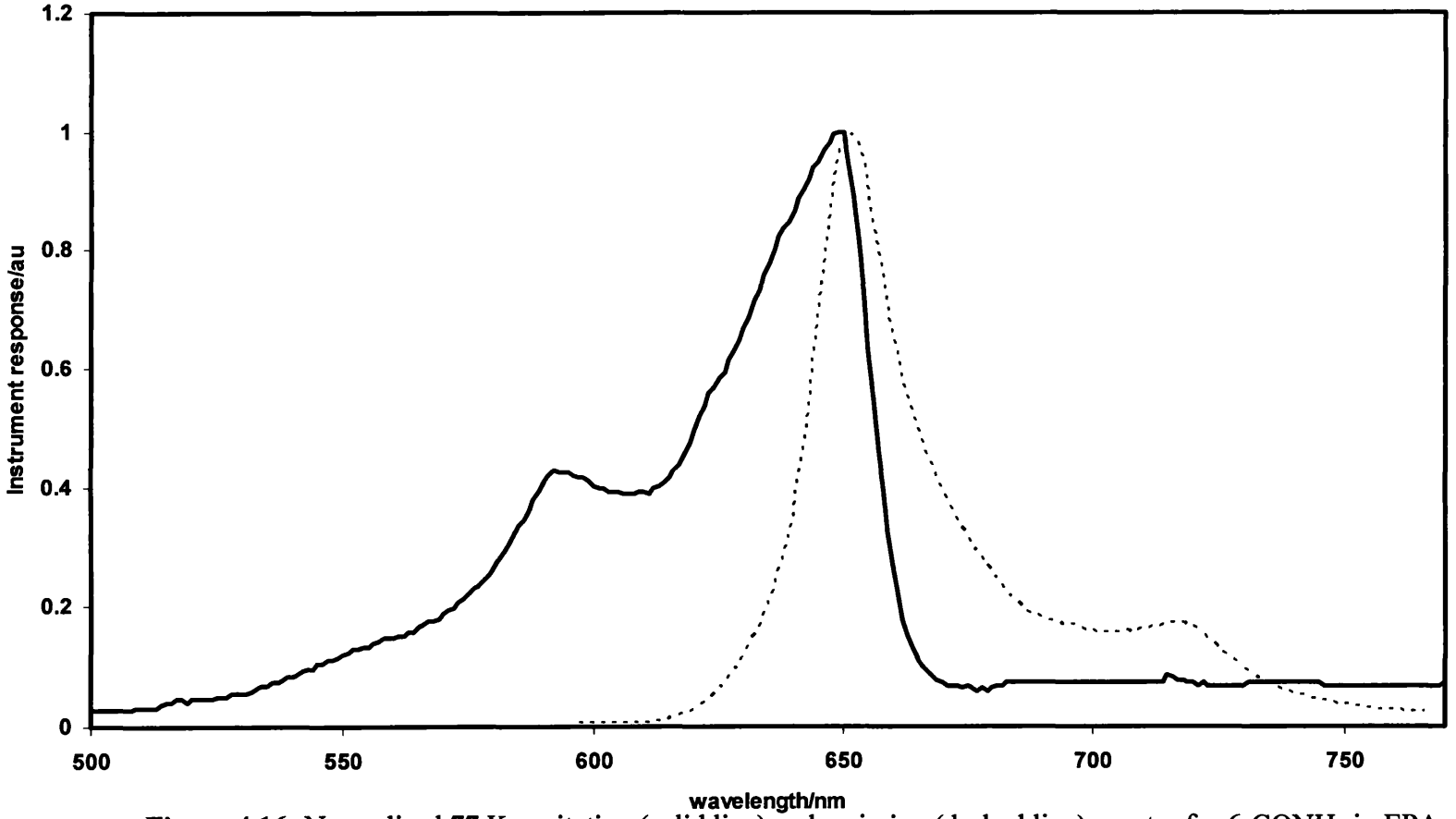

Figure 4.16: Normalised 77 K excitation (solid line) and emission (dashed line) spectra for 6-$CONH_2$ in EPA.

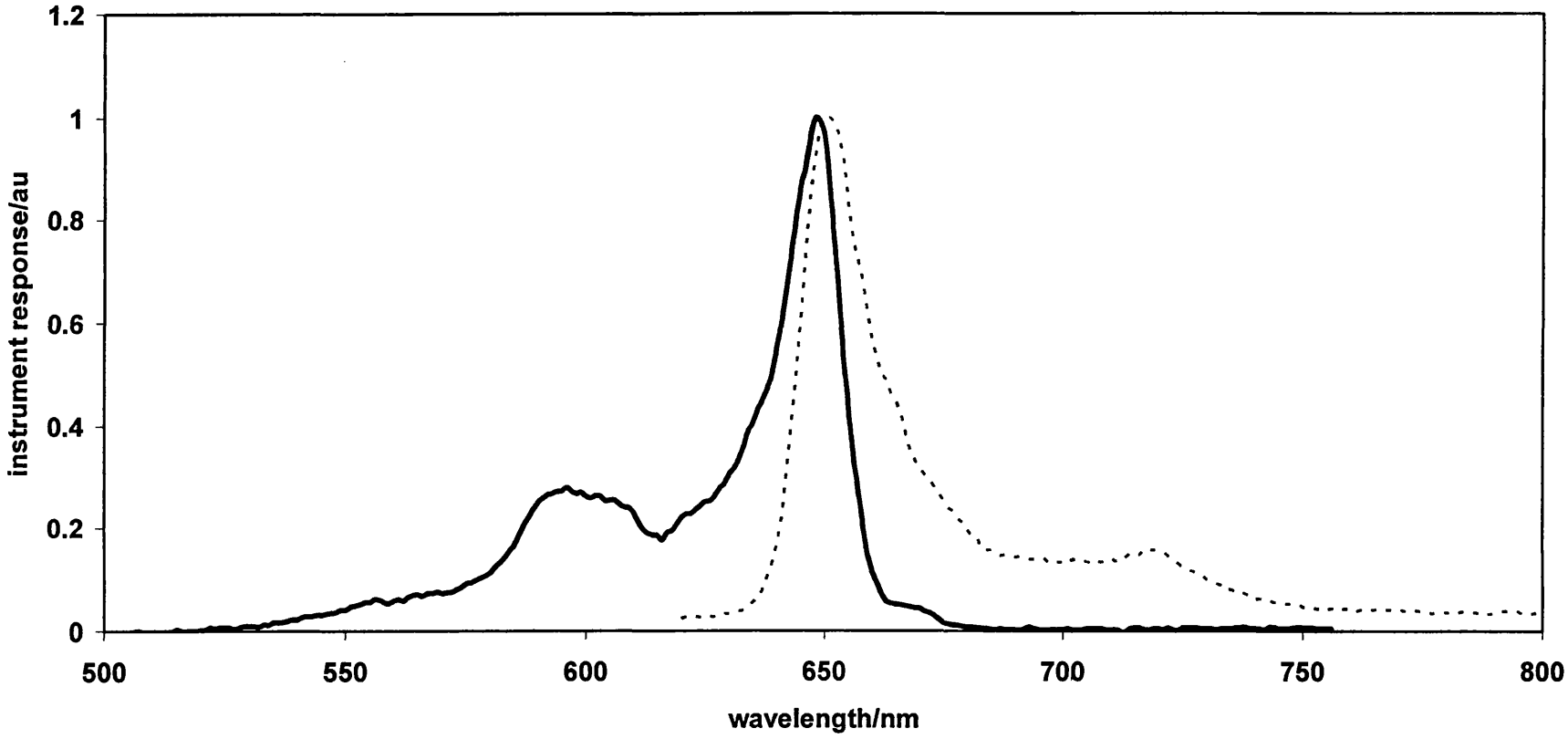

Figure 4.17: Normalised 77 K excitation (solid line) and emission (dashed line) spaectra for 6-CN dye in EPA.

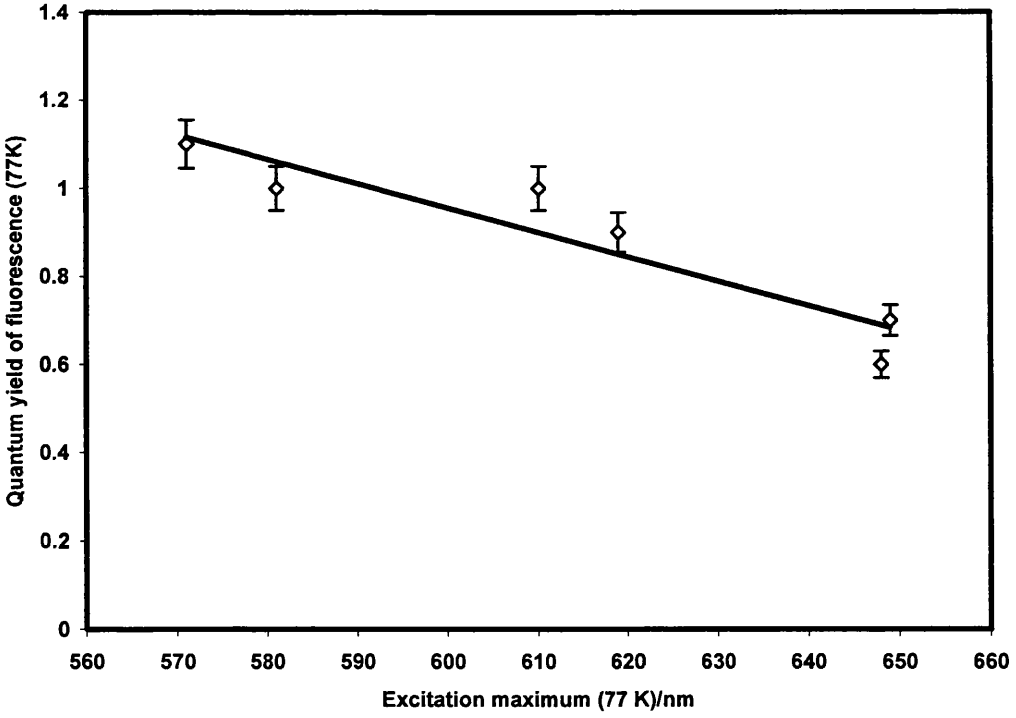

Figure 4.18: Correlation between Φ_{fl} and excitation maximum at 77 K.

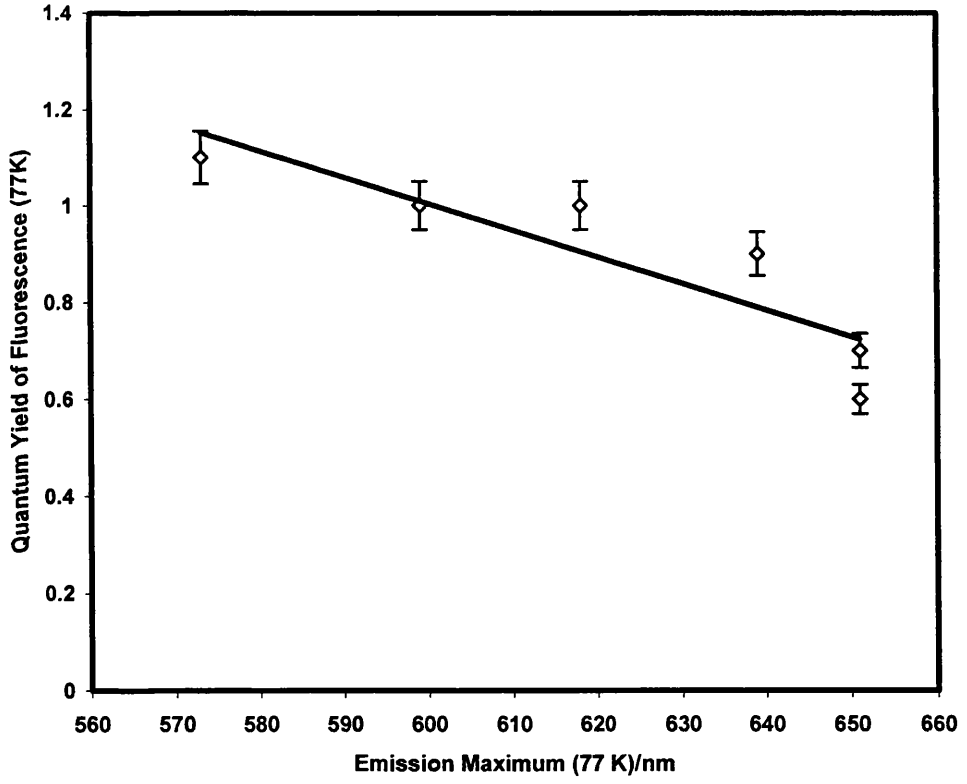

Figure 4.19: Correlation between Φ_{fl} and emission maximum at 77 K.

4.4 Room temperature absorption studies

4.4.1 Introduction

Magenta PT dyes are characterised by their high extinction coefficients (*ca.* 3.5-6.8 × 10^4 mol^{-1} dm^3 cm^{-1}) [1], broad absorption bands which show some vibrational fine structure in non-polar solvents, and a bathochromic shift in absorption maximum as solvent polarity increases [1-3].

Townsend [2] studied the interaction between PT dyes and their solvent media. Polar solvents containing a strong permanent dipole will have a greater interaction with the dissolved dye than non-polar solvents, and this interaction will be greater if the solute also has a permanent dipole. Minimisation of energy occurs as the polar solvent molecules arrange themselves around the solute, to give a ground state which is stabilised in comparison to that in a solvent of lower polarity. The Franck-Condon principle states that upon light absorption the transition between ground and excited states will occur so quickly that no reorganisation of the solvent can occur around the now excited solute. So a bathochromic shift in the spectrum, relative to an 'ideal' vapour state spectrum without solvent-solute interaction, will occur when the dye ground state is less polar than the excited state and a hypsochromic shift when the ground state is more polar than the excited state. The fact that polar solvents shift absorption maxima towards the lower energy part of the visible spectrum indicates that upon excitation the dipole moment is strengthened along the direction of the ground state dipole, an observation in accord with the M.O. calculations [2].

4.4.2 Experimental

All absorption spectra were recorded on a PC controlled Perkin Elmer Lambda 9 UV/Vis/NIR spectrophotometer using quartz 10 mm cuvettes.

4.4.3 Results and discussion

Figures 4.20-4.25 show normalised absorption spectra for the dye series in ten solvents of varying dielectric constant and polarisability. A summary of the absorption characteristics of the dyes studied is given in table 4.3.

Dye	min and max absorption wavelengths/nm (solvent shown in brackets)*	λ max variation across range of solvents (nm)	λ_{max} ethanol (nm)	Average $\varepsilon/10^4$ ($mol^{-1}dm^3cm^{-1}$)
6-OMe	528(1) → 554 (2)	26	546	5.12(±0.62)
6-Me	542(1) → 576 (2)	34	562	6.03(±0.46)
6-Ph	561(1) → 597 (2)	36	584	5.42(±0.46)
6-CO_2Et	584(1) → 622 (3)	26	606	6.61(±0.68)
6-$CONH_2$	596(1) → 630 (3)	34	623	6.50(±0.60)
6-CN	622(1) → 647 (2)	25	633	5.03(±0.44)

*(1, methylcyclohexane; 2, dimethylsulphoxide; 3, 1-chloronaphthalene)

Table 4.3: Summary of RT absorption maxima and extinction coefficients.

The average extinction coefficient has been calculated through considering the absorption spectra in the ten different solvents.

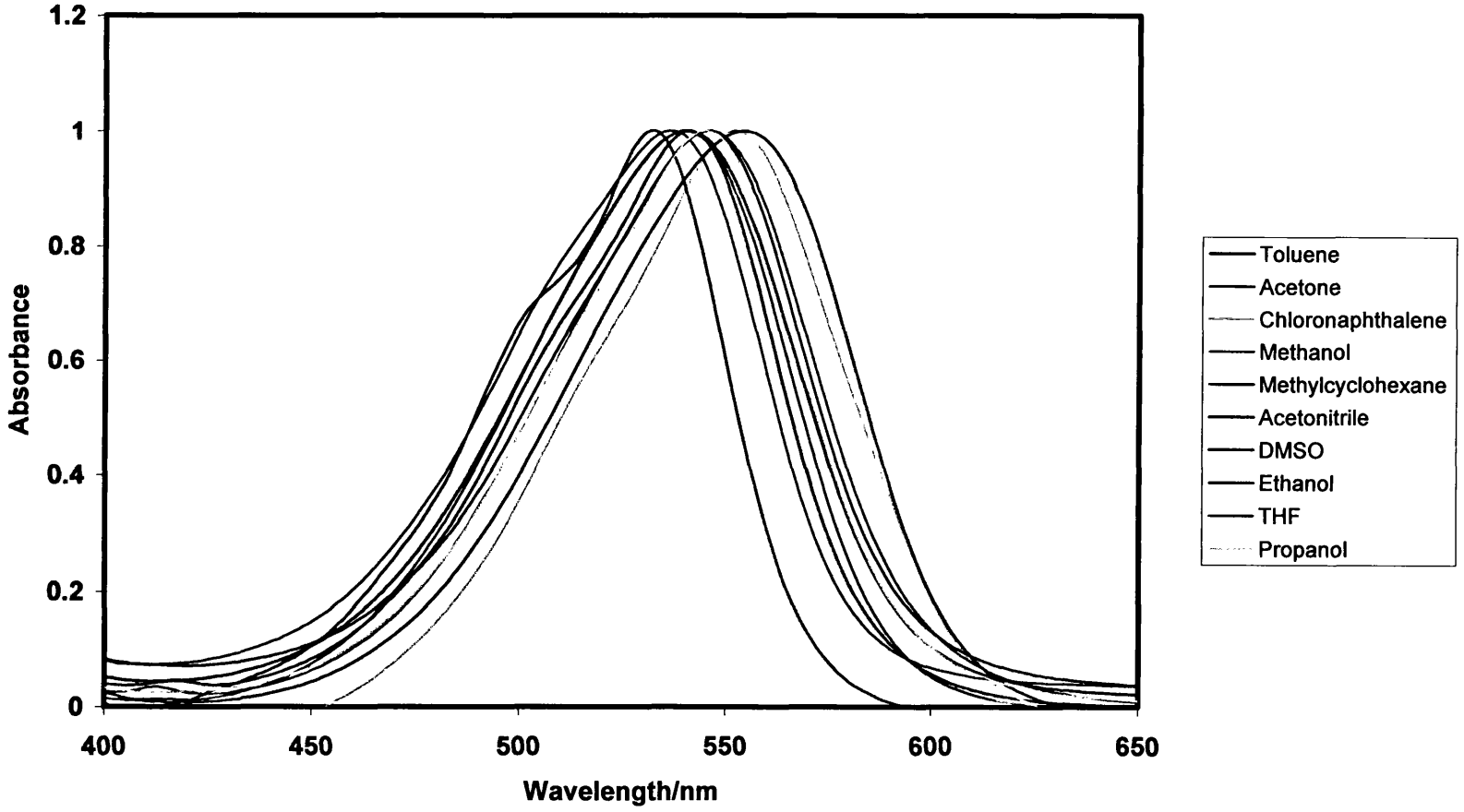

Figure 4.20: Normalised absorption spectra of 6-OMe in 10 solvents of varying dielectric constant.

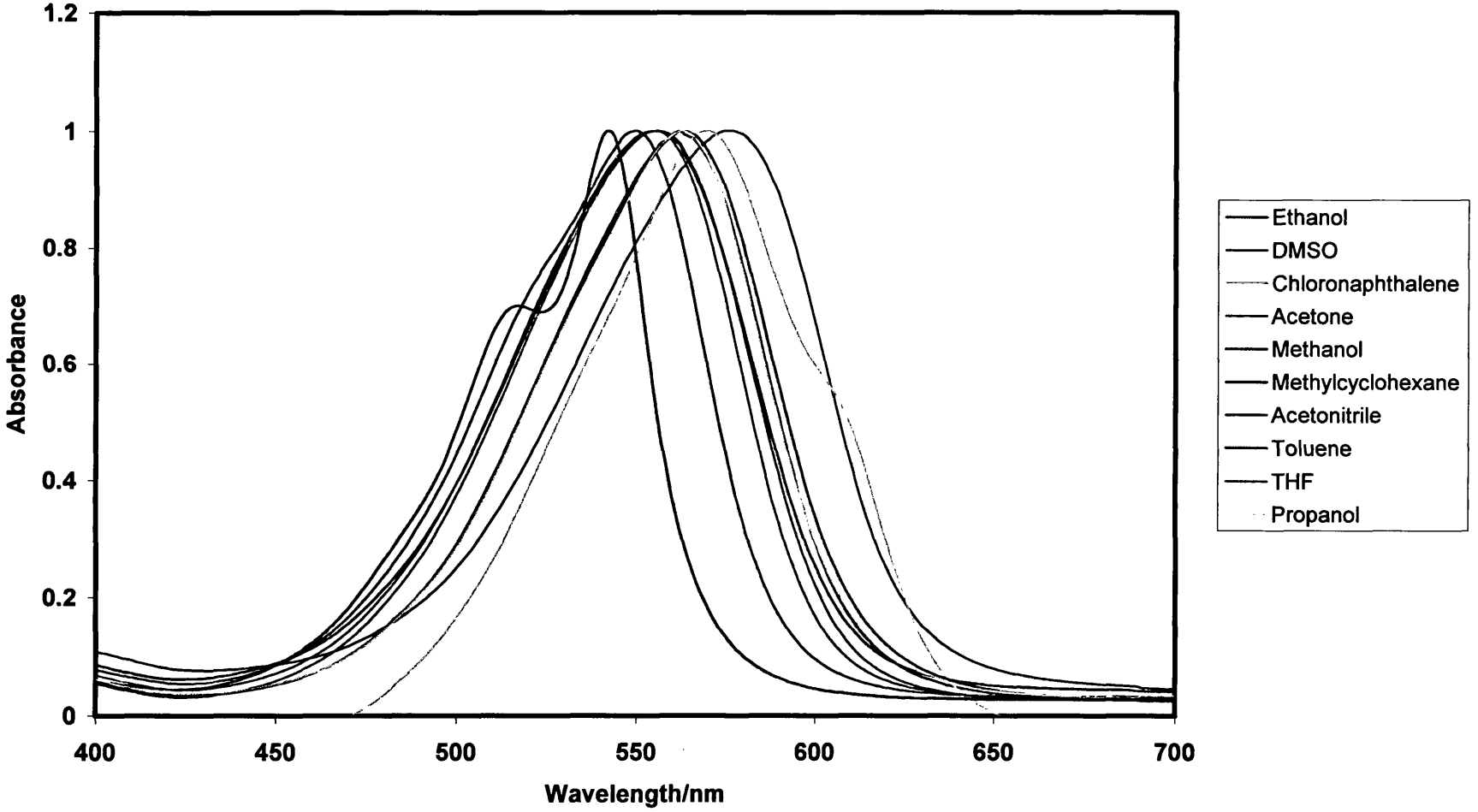

Figure 4.21: Normalised absorption spectra of 6-Me in 10 solvents of varying dielectric constant.

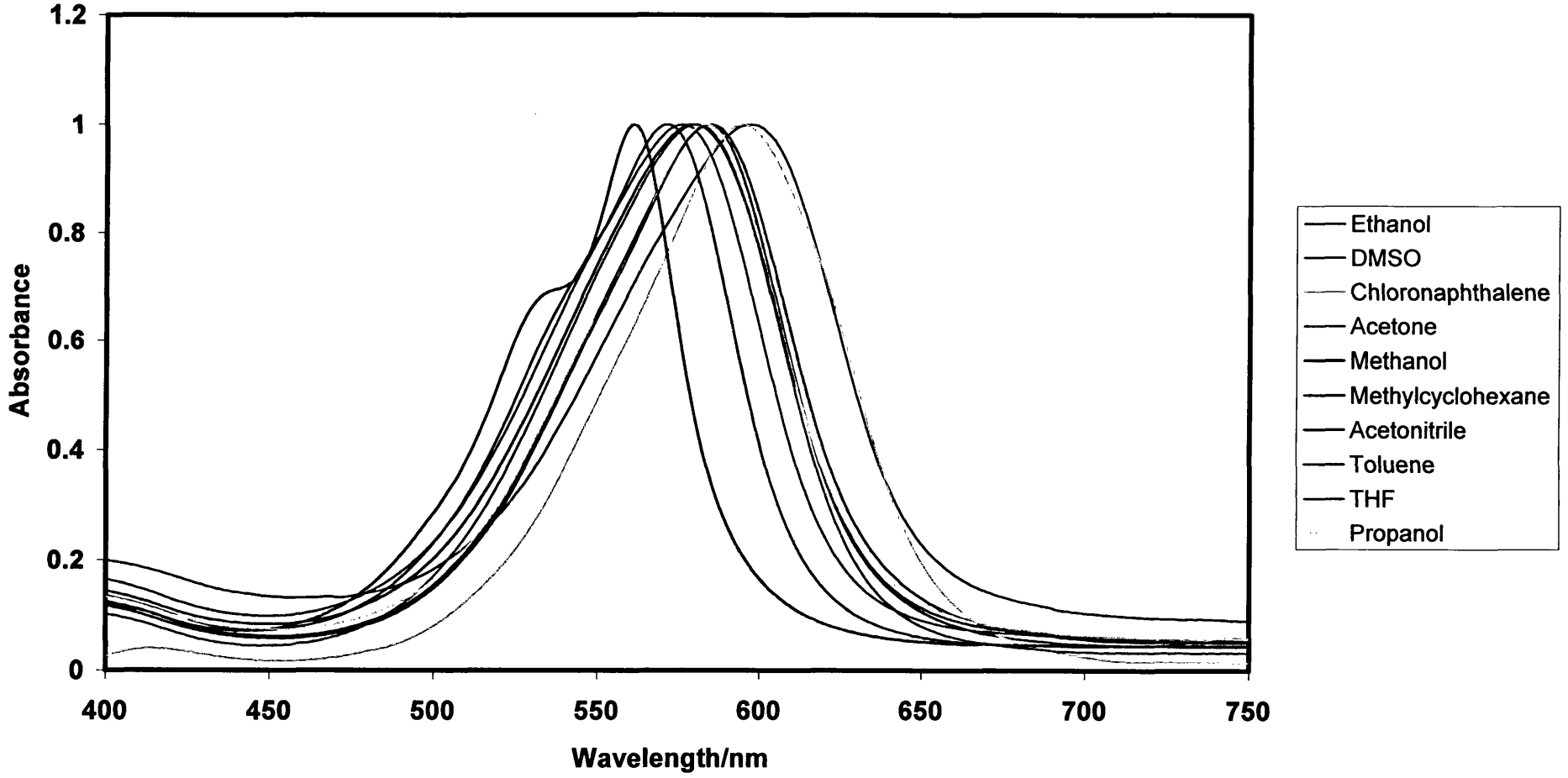

Figure 4.22: Normalised absorption spectra of 6-Ph in 10 solvents of varying dielectric constant.

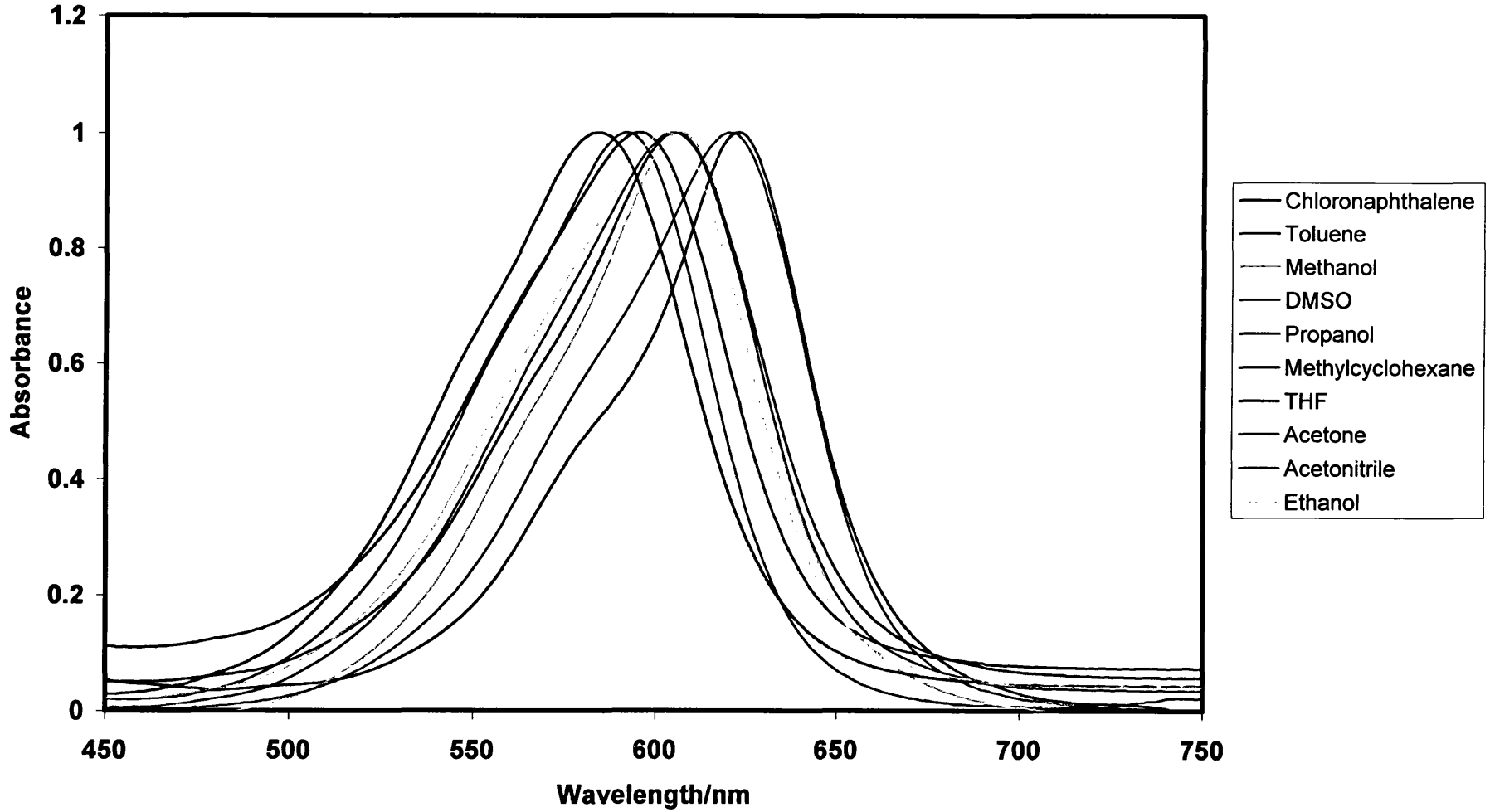

Figure 4.23: Normalised absorption spectra of 6-CO_2Et in 10 solvents of varying dielectric constant.

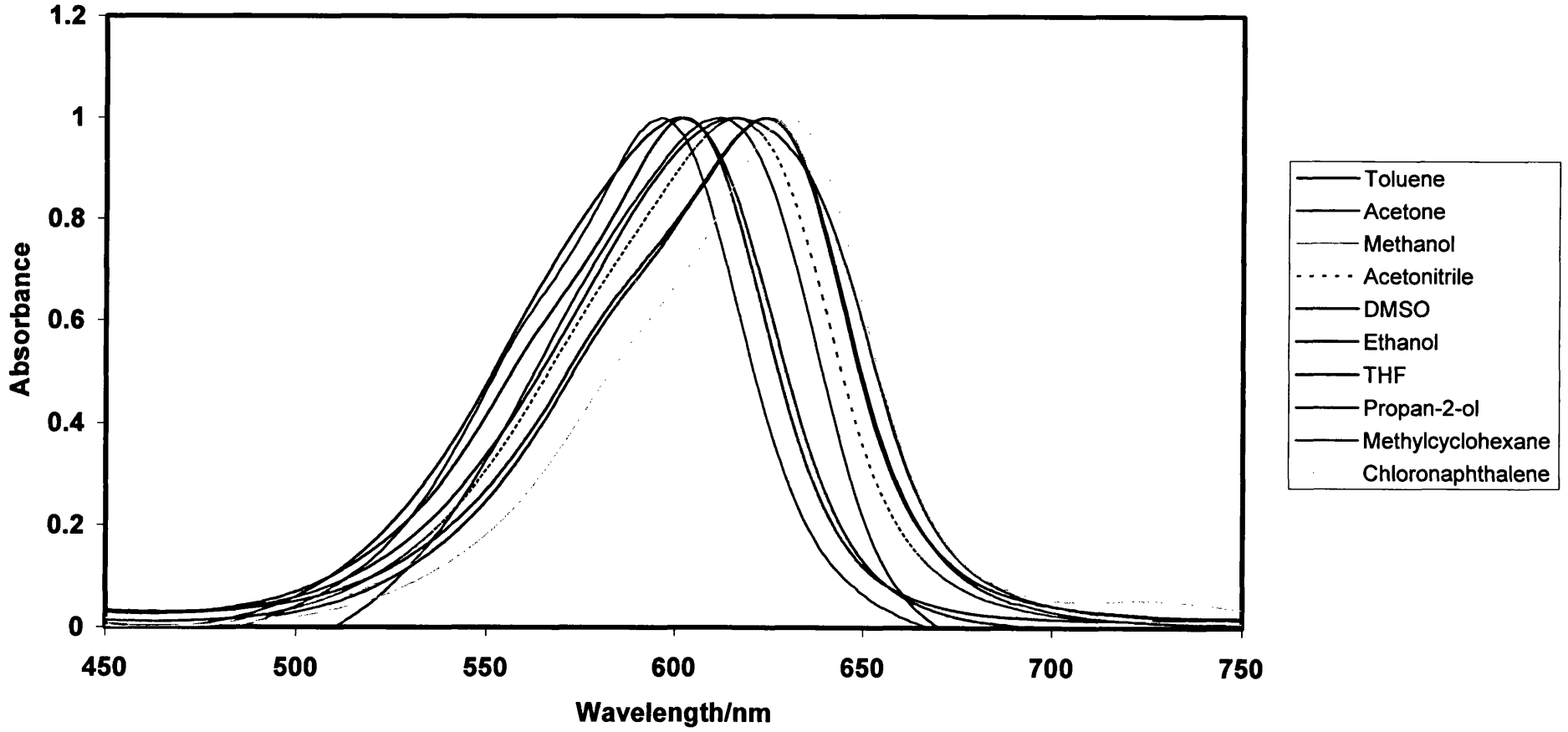

Figure 4.24: Normalised absorption spectra of 6-$CONH_2$ in 10 solvents of varying dielectric constant.

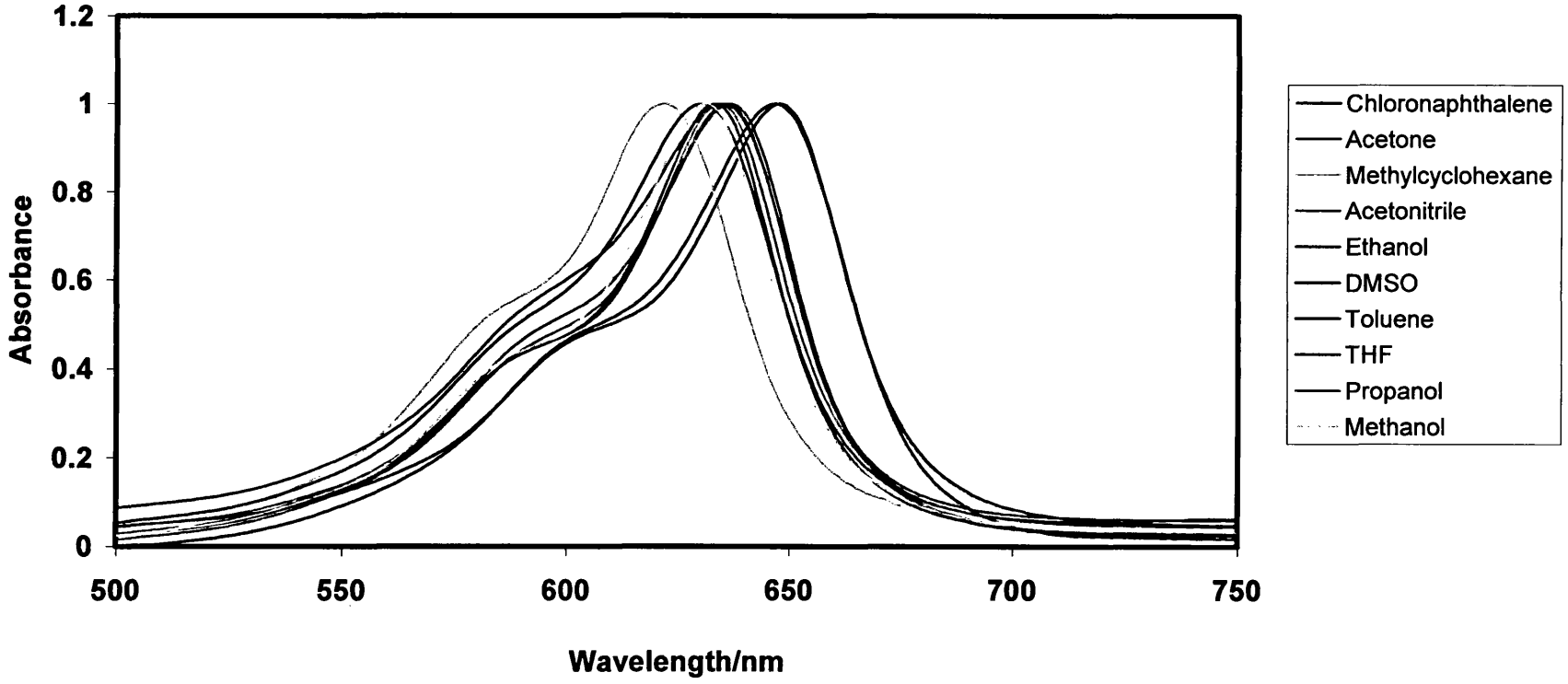

Figure 4.25: Normalised absorption spectra of 6-CN in 10 solvents of varying dielectric constant.

The vibrational transitions are generally resolved more clearly in non-polar solvents, particularly where the R_6 group is electron donating (note 6-OMe, 6-Me and 6-Ph dyes in methylcyclohexane), for 6-CN the vibronic structure remains resolved even in polar solvents.

Figure 4.26 below shows the correlation between dielectric constant and absorption maximum for 6-CN and 6-Me.

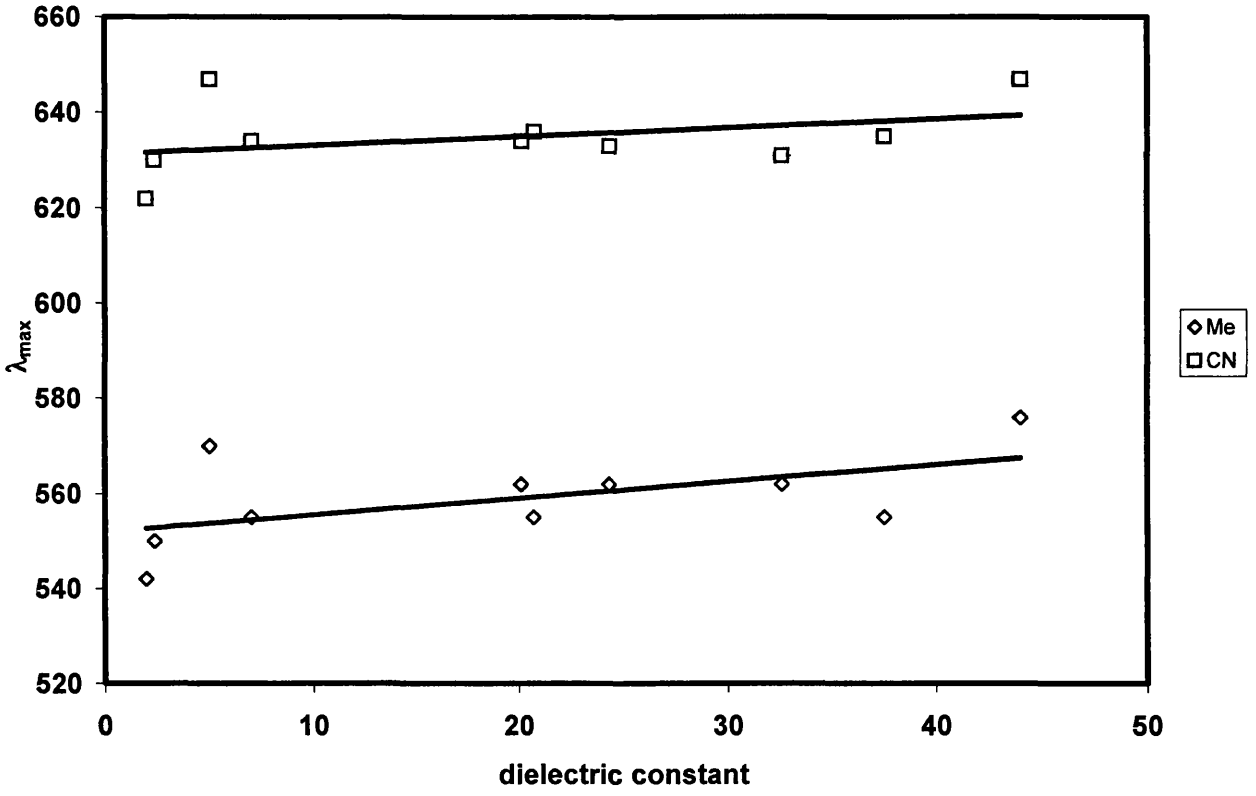

Figure 4.26: Correlation between absorption maximum and dielectric constant for 6-CN and 6-Me.

There is good correlation between the solvent dependent absorption maxima and the solvent polarity as measured by the E_T (30) solvent polarity scale [16] (figure 4.27).

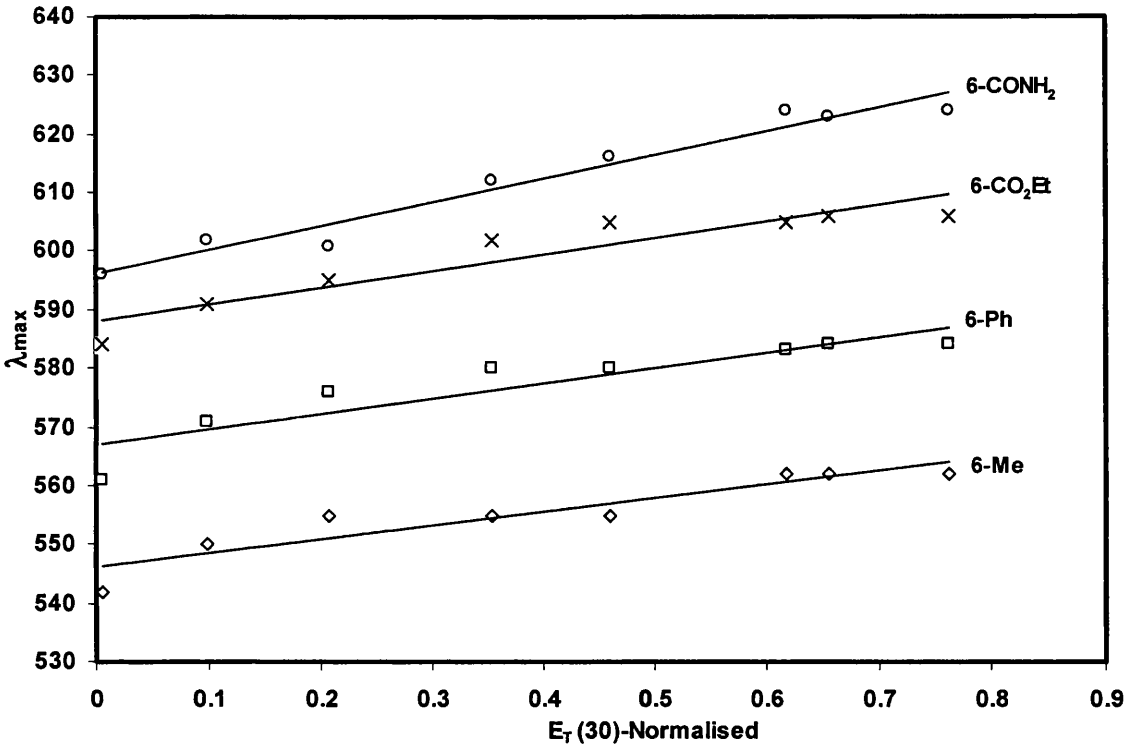

Figure 4.27: Correlation between absorption maxima and normalised E_T (30) values (Where tetramethylsilane = 0 and H_2O = 1) for four of the dyes studied. E_T (30) values for chloronaphthalene were not available. The point for DMSO has been removed as the E_T (30) data cannot be used, possibly due to water being present in the solvent.

4.5 Room temperature fluorescence

4.5.1 Introduction

Room temperature quantum yields for magenta PT dyes in typical fluid solutions are ~1×10^{-4} [3]. These low quantum yields can be attributed to radiationless deactivation of dye excited states at room temperature by molecular flexion around the azomethine bond. Quantum yields as low as this present some experimental problems arising from interference from scatter light, Raman bands, and even minor fluorescent impurities. Workers in Kodak Ltd. have been using *p*-dodecylphenol as a high viscosity solvent for fluorescence studies of flexible dyes and that has been the solvent of choice for the work presented here.

4.5.2 Experimental

All room temperature (22-24°C) emission experiments were carried out using a Perkin Elmer MPF 44E fluorimeter. Emission spectra for samples with low quantum yields of *ca.* 10^{-4} are difficult to obtain; in an attempt to increase the quantum yield, the viscous solvent PDP (*p*-dodecylphenol) was used. Due to the low emission yields it was not practical to use optically dilute solutions and therefore all samples and standards were prepared to give optical densities of 0.3 at the excitation wavelengths. However all emission spectra were corrected for the quantum efficiency of photomultiplier response and for self-absorption.

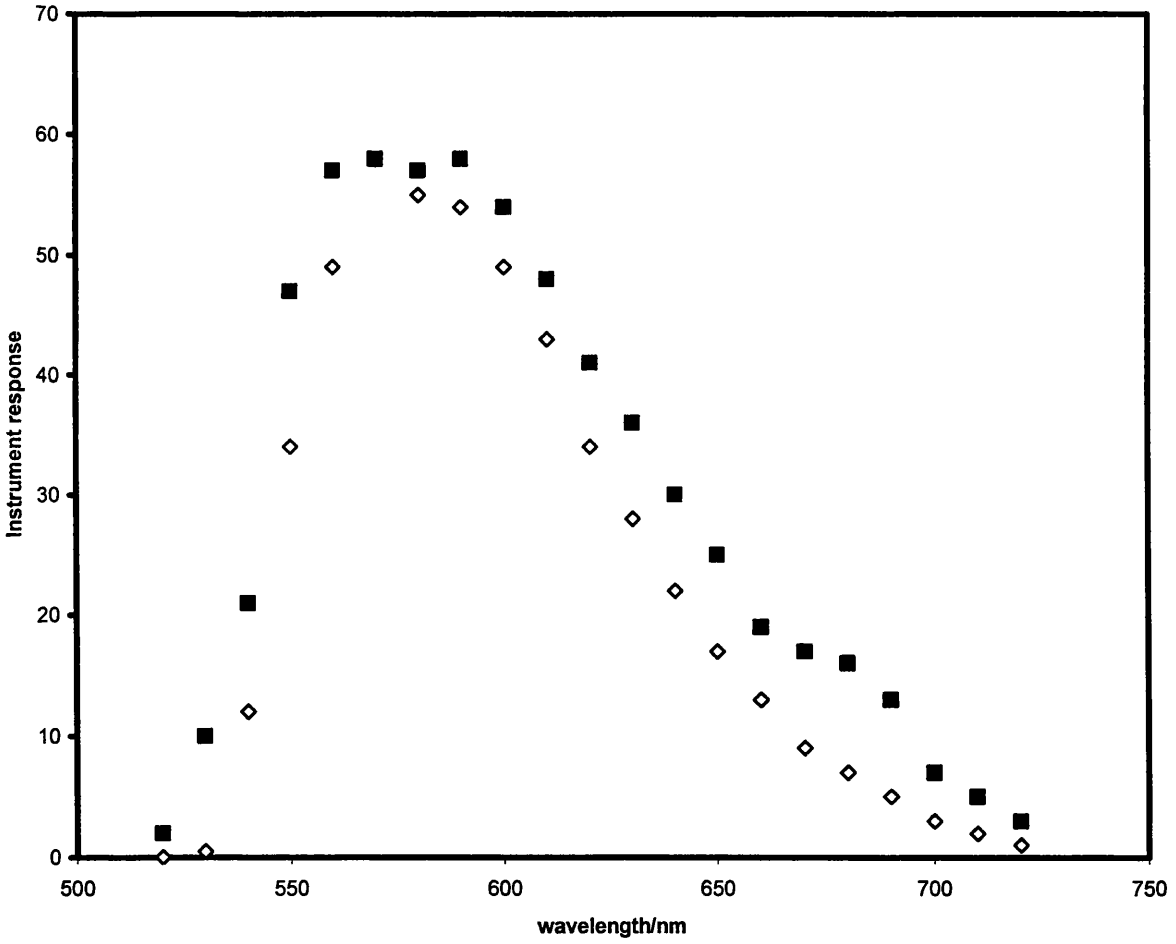

Figure 4.28: Corrected for photomultiplier response (filled squares) and uncorrected (unfilled diamonds) emission spectra for 6-Me PT dye.

Rhodamine B (in degassed ethanol) was used as the quantum yield standard ($\Phi_{f\,l}$= 0.61 [13]) and emission and excitatation slits were 5 nm in all cases. Absorption spectra were recorded using a PC controlled Perkin Elmer Lambda 7 UV/Vis

spectrophotometer. Corrections for the conversion of wavelength into frequency were used in order to ensure that calculations of the radiative rate constants, k_{rad}, using the Strickler-Berg equation [17] were correct. (Note section 2.3.3).

4.5.3 Results and discussion

A summary of singlet state characteristics is shown below and the normalised emission spectra for the series are shown in figure 4.29.

Dye	λ_{max} emission (nm)	Calculated k_{rad} ($\times 10^8 s^{-1}$)	Relative ϕ_{fl} ($\times 10^{-4}$)	Calculated τ_{rad} ($\times 10^{-9}$ s)	Calculated τ_s (ps)
6-OMe	575	2.4	6.3	4.2	2.7
6-Me	601	2.1	3.7	4.8	1.8
6-Ph	619	1.9	2.0	5.2	1.0
6-CO_2Et	625	2.1	2.3	4.7	1.1
6-$CONH_2$	663	1.6	6.3	6.1	3.9
6-CN	657	1.1	3.8	9.3	3.6

Table 4.4: Singlet state properties for the dye series (errors are estimated to be *ca.* ±20%) in PDP (*p*-dodecylphenol).

For most dyes the radiative rate constants are similar *ca.* 1.9×10^8 s^{-1}. However the value for 6-CN is significantly lower. The quantum yields measured are *ca.* five times higher than those reported previously using CCl_4 as solvent [3]. This can be attributed to the use of the more viscous solvent PDP which inhibits molecular motion, the main route of deactivation, and therefore increases the quantum yield of fluorescence. The most interesting feature of the data in table 4.4 is the variation in the calculated emission lifetime. The pattern seen in both the excited state vibrational spacing and Stokes shift is repeated here, with dyes bearing either electron donating or electron withdrawing substitutents showing relatively long lifetimes while those with electro-neutral substituents having significantly shorter lifetimes. There is a good correlation between emission maxima and singlet lifetimes. (Note figure 4.30)

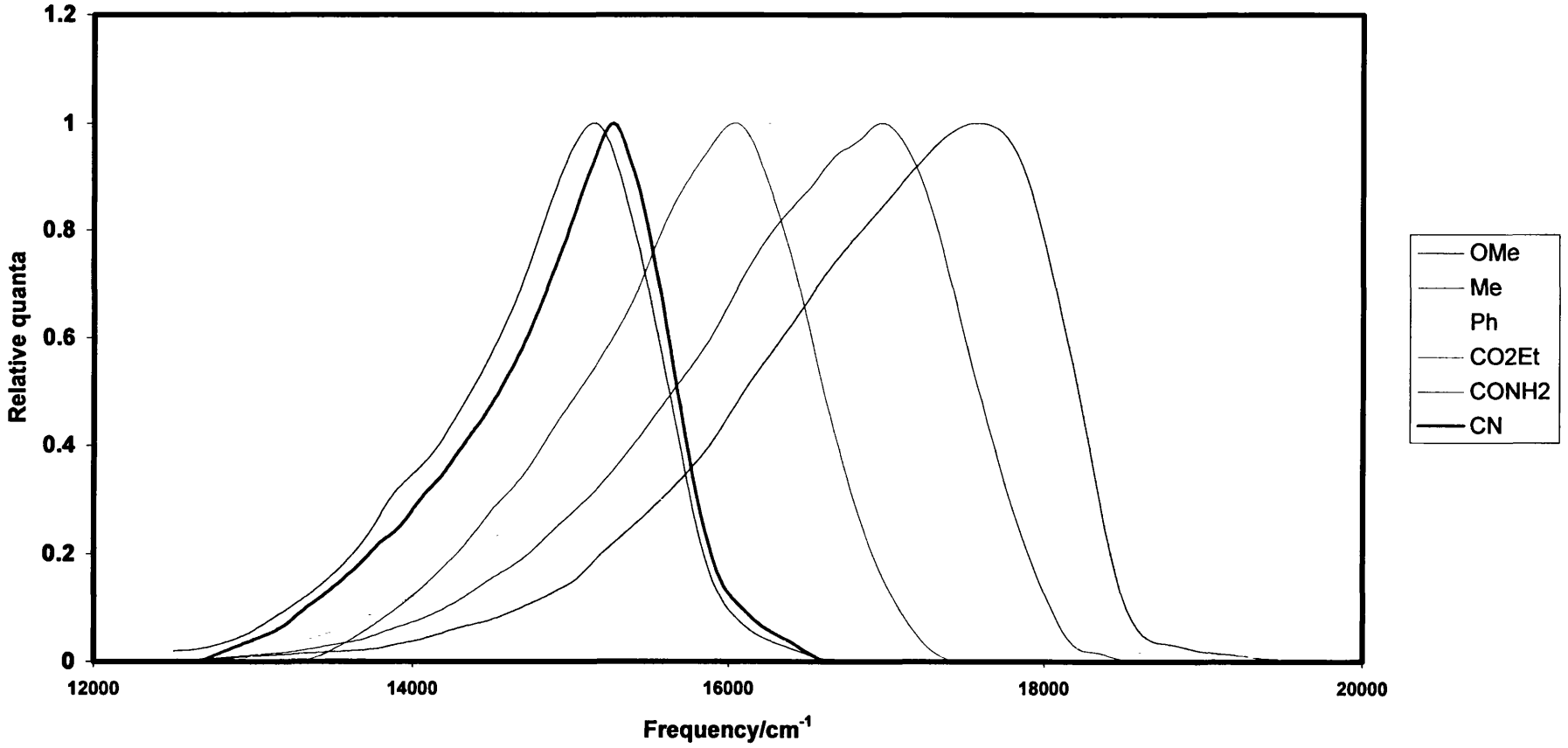

Figure 4.29: Normalised corrected room temperature emission spectra for the dye series in PDP.

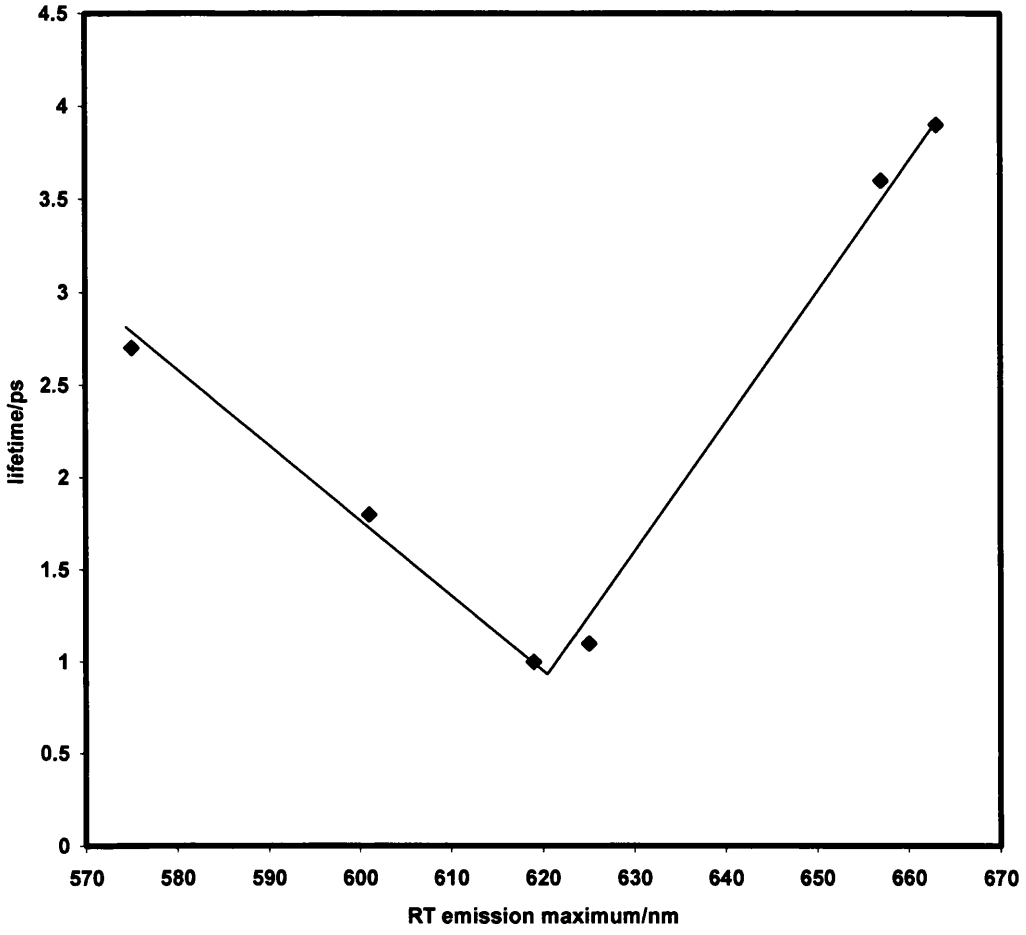

Figure 4.30: Correlation between singlet lifetime and emission maximum.

The data obtained from both the low temperature and room temperature studies can be used to contrast the effect that electron donating/withdrawing substituents have on the shape and position of the potential energy wells in the excited state.

A dye bearing a substituent which is strongly electron donating or withdrawing (*e.g.* 6-CN) appears to have a compressed potential energy well in the excited state, which leads to wider vibrational spacings and longer singlet lifetime. Conversely, a dye with a substituent such as 6-Ph which has little effect in terms of donating or withdrawing electron density appears to have a shallower well in the excited state, leading to a shorter singlet lifetime and also a shift in the excited state potential energy well (relative to the ground state) which is evident in a larger Stokes shift (note figure 4.31).

4.6 Single Photon Counting

4.6.1 Introduction

Previous work using picosecond single photon counting showed that the fluorescence decay of PT dyes is non-mono-exponential at temperatures ranging from 77-297 K. This was attributed to emission from different geometric configurations as the dye relaxes along the isomerisation coordinate. [10].

4.6.2 Experimental

All of the single photon counting experiments were undertaken at the University of Coimbra (see 2.3.4 for details). Due to the lack of sensitivity in the photomultiplier for regions above 600 nm, only the 6-OMe and 6-Me dyes provided useable data, as emission signals for the dyes which emitted in regions above this (*e.g.* 6-Ph, 6-CO_2Et, 6-$CONH_2$ and 6-CN) were masked by the excitation pulse. The lowest temperature which could be maintained with any stability was 173K at which temperature EPA is a glass, although not such a hard glass as is obtained at 77 K.

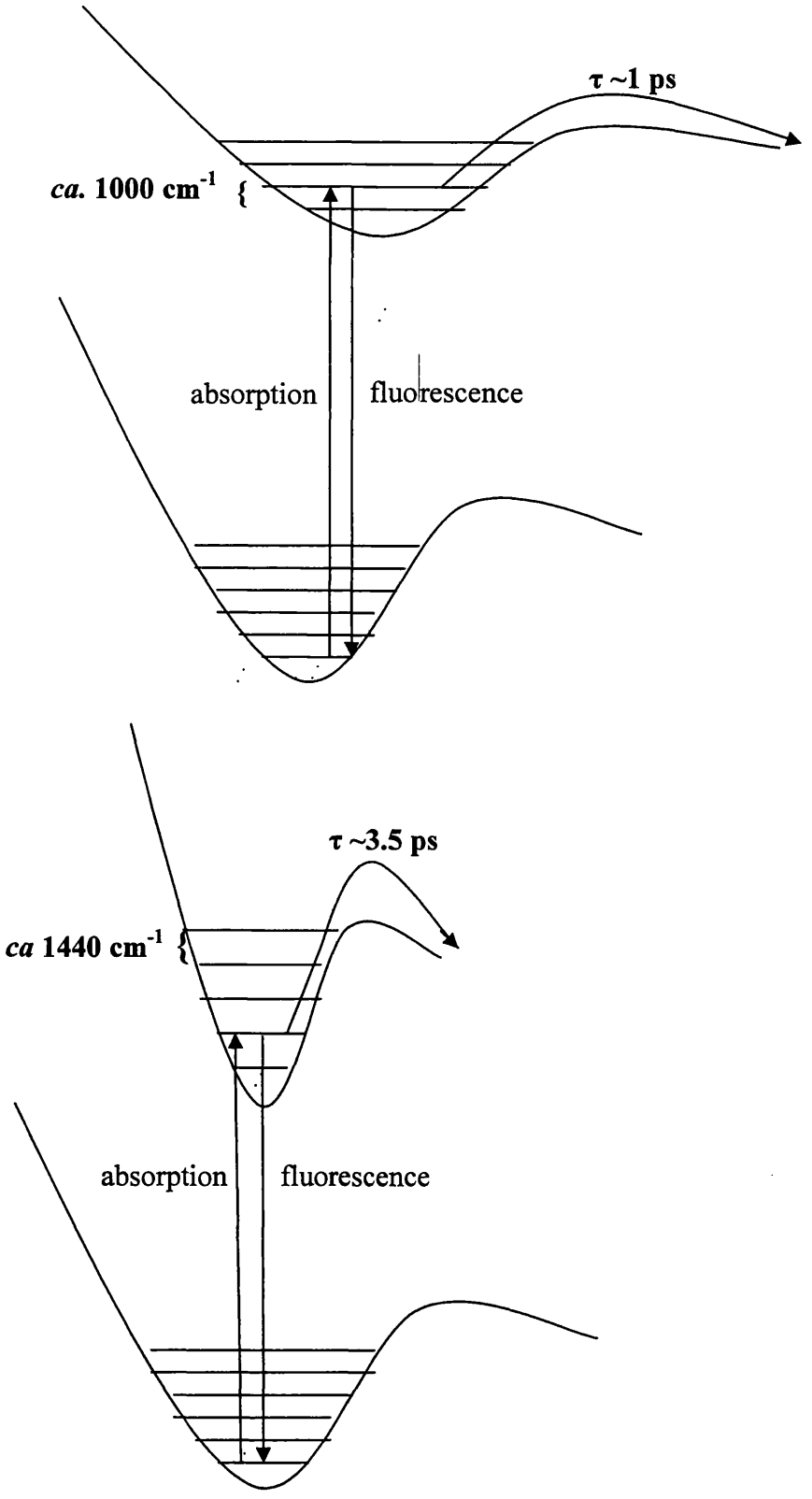

Figure 4.31: Potential energy curves for the 6-Ph (top) and 6-CN dyes (bottom).

4.6.3 Results and Discussion

Both dyes gave non-mono-exponential decays. The decay curves could be reasonably well modelled using a double exponential fit as shown in table 4.5. An example of the data obtained is given in figure 4.32.

Dye	t_1 (ns)	t_2 (ns)
6-OMe	0.36 (96.4%)	3.42 (3.6%)
6-Me	0.36 (88.6 %)	4.31 (11.4%)

Table 4.5: Single photon counting data.

While a double exponential analysis is experimentally convenient it is not clear what the two discrete emitting species could be. Furthermore it is generally found that emission across a distribution of emitting states often gives a decay curve which can be reasonally well fitted using a double exponential function. In the light of our knowledge of PT dye photophysics a distribution of emitting states across a potential surface is a more likely possibility.

With this in mind it is interesting to note that of the two dyes studied it is the 6-Me which shows greatest deviation from a mono-exponential decay and, if a distribution is an approporiate interpretation, therefore the widest distribution of emitting states. This would seem to be consistent with the general trend of the 6-Me dye having the shallower, looser, excited state potential energy surface of the two dyes.

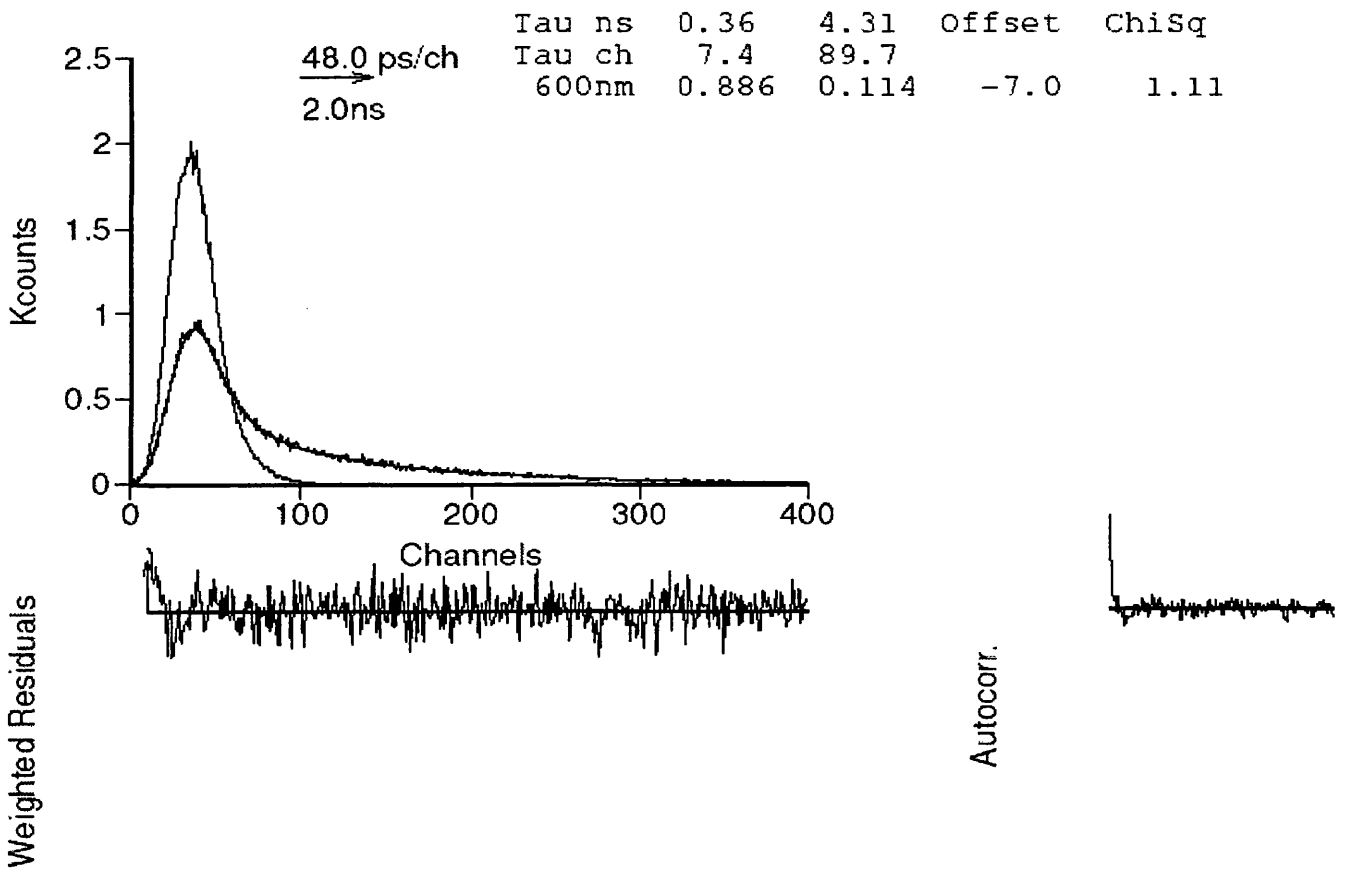

Figure 4.32: Single photon counting data for 6-Me in EPA at 173 K. Excitation wavelength is 580 nm; emission wavelength is given, as is the distribution fitted to two exponentials and the weighted residuals.

4.7 Conclusions

Electron donating substituents in the 6-position push dye hue bathochromically for the complete dye series at RT and 77 K.

At 77 K there is some evidence to support the notion that electron withdrawing and donating moieties have a similar effect on the excited state potential energy well by compressing it and therefore widening the vibrational intervals.

Room temperature dye hue is clearly affected by solvent polarity, with solvents of increasing polarity comparatively stabilising the excited singlet state pushing dye hue toward the red.

Room temperature fluorescence quantum yields are low for the entire series ranging from 2-6.8 $\times 10^{-4}$, but at 77 K these increase to between 0.6 and 1. These data support the proposal that deactivation of excited states of PT dyes is primarily driven by the flexibility around the azomethine bond, which results in $anti_{(\text{excited state})}$-$syn_{(\text{ground state})}$ isomerisation. This flexibility and configuration change cannot occur at 77 K resulting in deactivation *via* a radiative transition.

The RT singlet lifetimes also suggest that the potential energy surface of the excited state is more compressed in dyes which contain R_6 substituents that significantly donate/withdraw electron density from the pyrazolotriazole ring system.

Singlet photon counting experiments for two magenta PT's imply that the kinetics of singlet decay are complex, but at a temperature of 173 K they may be fitted to a double exponential expression.

4.8 References

1) J.Bailey, *J. Chem. Soc. Perkin Trans. 1,* **1977**, 2047.

2) S.M.Townsend, *PhD Thesis*, **1992**, University of Wales Swansea.

3) P.Douglas, *J. Photogr. Sci.* **1988**, 36, 83.

4) K.Furuya, N.Furutachi, S.Oda and K.Maruyama, *J. Chem. Soc. Perkin Trans. 2*, **1994**, 531.

5) R.J.Berry, *PhD Thesis*, **1998,** University of Wales Swansea.

6) N.J.Turro, *Modern Molecular Photochemisty*, **1991,** University Science Books, USA.

7) P.W.Atkins, *Physical Chemistry,* 1st Ed., **1978**, Oxford University Press, UK.

8) C.Reichardt, *Solvents and Solvent effects in Organic Chemistry,* 2nd Ed., **1988,** VCH, Germany.

9) G.U.Bublitz and S.G.Boxer, *J. Am. Chem. Soc.*, **1998**, 120, 3988.

10) P.Douglas, S.M.Townsend, P.J.Booth, B.Crystall, J.R.Durrant and D.R.Klug, *J. Chem. Soc. Faraday Trans.*, **1991**, 87, 3479.

11) J.N.Demas and G.A Crosby, *J. Phys. Chem.*, **1971**, 75, 991.

12) D.F.Eaton, *Pure Appl. Chem.*, **1988**, 60, 1107.

13) C.A.Parker, *Photoluminescence of Solutions*, **1968**, Elsevier, UK.

14) R.P.Wayne, *Photochemistry*, **1971**, Butterworth & Co., England.

15) D.Magde, J.H.Brannon, T.L.Cremers and J.Olmsted, *J. Phys. Chem.*, **1979**, 75, 991.

16) C.Reichardt, *Chem. Review*, **1994**, 94, 2319.

17) S.J.Strickler and R.A.Berg, *J. Chem. Phys.*, **1962,** 814.

Chapter 5

pK_a equilibria, influence of protonation on the isomerisation kinetics, and oxygen quenching of isomerisation of PT dyes

5.1 Introduction

There has been much work into the mechanisms of *syn-anti* photoisomerisation of PT dyes, and the reverse thermal reaction [1-6].

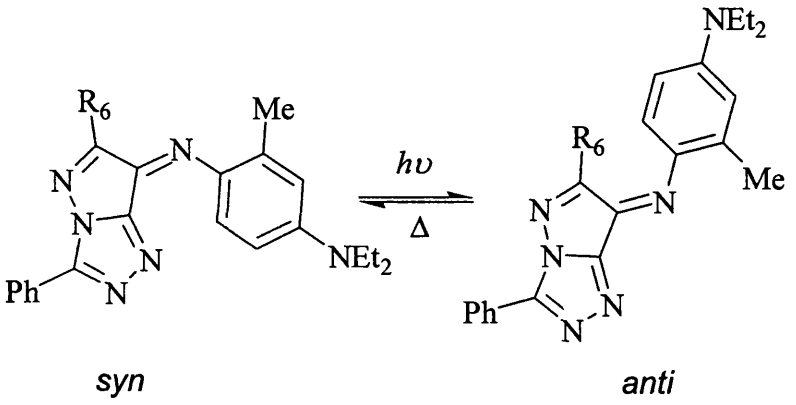

Figure 5.1: Photoisomerisation and thermal equilibrium of a PT dye

Three mechanisms for isomerisation about the azomethine bond have been proposed:

1) rotation;
2) inversion;
3) a biradical mechanism.

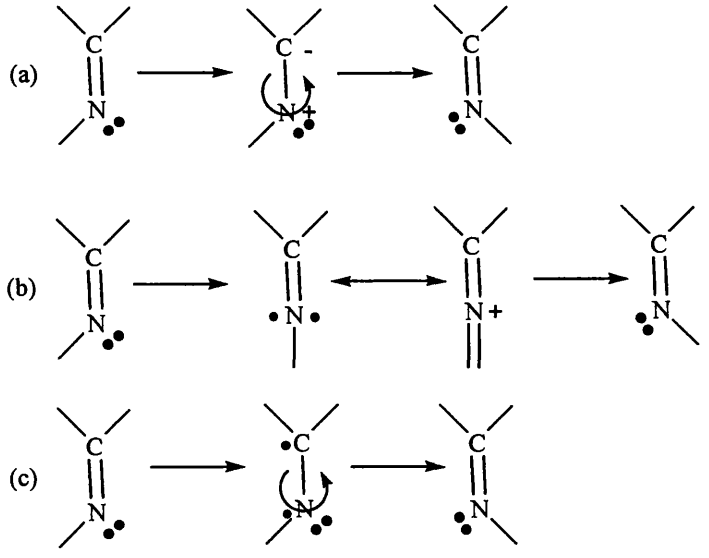

Figure 5.2: Isomerisation mechanisms for azomethine dyes;
(a) rotation, (b) inversion, (c) biradical mechanism [5].

The rotation mechanism is driven by heterolytic cleavage across the azomethine bond. The inversion mechanism is reliant on the rehybridisation of the nitrogen sp^2 state to an sp state, which results in the movement of electron density from the nitrogen into delocalisation across the aminophenyl developer. The biradical mechanism is caused by homolytic fission which enables rotation to occur. A number of studies including measurement of volumes of activation, substituent and solvent effects suggest the inversion mechanism as most likely [4, 5, 7].

X-ray crystallography shows that the 6-Me PT dye exists in the *syn* conformation in its solid state [8], and NOE studies have shown that the 6-H dye exists as the same conformer in solution [9]. It is reasonable to assume this is the case for all of the dyes discussed here.

The site of protonation of these dyes has also been studied by NMR and UV/Vis spectroscopy [9], with two protonation sites identified. The first protonation occurs at the azomethine nitrogen and the second, at higher proton concentrations, at the phenylamine nitrogen. The first protonation occurs at the azomethine bond, and since this is the site of isomerisation protonation affects the isomerisation kinetics [10].

5.2 Experimental

5.2.1 pK_a and protonation studies

Absorption spectra were recorded using a Perkin Elmer Lambda 9 UV/Vis/NIR spectrophotometer and a 1 cm quartz cuvette.

Spectral titrations were carried out on dye solutions at concentrations of *ca.* 2×10^{-5} mol dm^{-3} by the addition of µl amounts of either trifluoroacetic acid (TFAA) or hydrochloric acid. The acid was added using a µl Hamilton syringe to give in all cases a final acid concentration which was significantly greater than that of the dye. All solvents were either 99%+ or Analar grade. A variety of solvents was used including chloroform stabilised with amylenes. Initially there was a concern because of an inability to reproduce earlier work using chloroform as solvent [9], but dye protonation equilbria are strongly solvent dependent and it was discovered that previous workers had used Spectrosol grade chloroform [9] which is stabilised by

ethanol, and it was then possible to reproduce their results when using this solvent. While attempting to find reasons for this discrepancy with previous work some experimental runs were repeated with acid added by weight from a glass pipette in order to confirm that any interaction between the acid and the metal syringe needle was not an important factor. In all cases the results from addition by weight corresponded to those from addition by volume.

5.2.2 Isomerisation kinetics

Nanosecond flash photolysis experiments were carried out as described in section 2.3.5. Difference spectra were obtained by measuring the change in absorbance at 10 nm intervals. When the transient isomer is absorbing less light than the initial species then the absorbance is negative. The wavelength chosen for monitoring the isomerisation kinetics was set at *ca.* 50 nm to the red of the room temperature absorption maximum, where the unstable isomer absorbance is at its peak. Slit width was set at 4 nm. Room temperature experiments were at 23(±2) °C. For the Arrhenius plots, the 1 cm quartz cuvette was held in a Beckmann temperature control unit which is precise to ±0.1 °C.

5.3 Protonation equilibria

A simple acid-base equilibrium between proton and dye is as follows:

$$\text{Dye } H^+ \leftrightarrow \text{ Dye} + H^+ \qquad \textbf{5.1}$$

with the acid concentration equilibrium constant:

$$K_a = \frac{[Dye][H^+]}{[DyeH^+]} \qquad \textbf{5.2}$$

incorporating activity terms:

$$K_a = \frac{a_{Dye}\, a_{H+}}{a_{DyeH+}} \qquad \textbf{5.3}$$

At comparatively low proton concentrations ($<1 \times 10^{-4}$ mol dm^{-3}) in water, activity coefficients are ≈ 1; so that activity can be well approximated by concentration. Therefore equilibrium constants can be discussed in terms of concentration, so that:

$$pK_a = pH + \log ([\text{Dye } H^+]/[\text{Dye}]) \qquad \textbf{5.4}$$

However the situation is different in non-aqueous media where activity and concentration are not so easily related. In non-aqueous solutions, where activity coefficients are not readily available pK_a is difficult to determine. Therefore throughout this work data are reported in terms of the easily accessible experimental value P_{acid50} which is the negative log of the acid concentration when the dye is 50% protonated.

In this work the linear method previously used by Couture [10] to analyse absorbance titration data was initially used. This was developed further by using the sigmoidal curve fit of Jandel Scientific's Table Curve 2D computer programme (TC2D) to calculate P_{acid50} values and the number of protons involved in the transition. The Jandel Scientific programme gives a fit to the data in the form of the equation [11]:

$$y = a + \frac{b}{1 + \exp\frac{(-(x-c))}{d}} \qquad \textbf{5.5}$$

This equation can be expressed in terms of absorbance to give the P_{acid50} value:

$$\text{Absorbance} = A_{noacid} + \frac{A_{acid} - A_{noacid}}{1 + \exp^{2.303}\left[\frac{([acid] + P_{acid50})}{1}\right]} \qquad \textbf{5.6}$$

For a single protonation the denominator in the exponential term is one, and the factor of 2.303 is necessary to convert natural logarithms to log to base ten as used in pH.

5.4 Results and discussion

5.4.1 Protonation equilibria and acid induced degradation

The dyes can be placed in two groups depending upon the effect of the addition of acid to solutions of the dyes. The 6-OMe, 6-Me, 6-H and 6-Ph PT dyes show reversible protonation equilibria while the 6-CO_2Et, 6-$CONH_2$ and 6-CN dyes undergo an irreversible reaction.

5.4.2 pK_a transitions of 6-OMe, 6-Me, 6-H and 6-Ph PT dyes

Figures 5.3-5.6 show pH titrations for the 6-OMe, 6-Me, 6-H and 6-Ph dyes in dichloromethane. Spectra for the addition of small amounts of acid show a pH reversible shift in λ_{max} to higher wavelength, an increase in ε_{max} and a reasonable isosbestic point. Upon further additions of acid the shift in λ_{max} continues in part but the isosbestic point is lost, and at even higher acid concentrations the dye irreversibly degrades. This behaviour has been shown to be due to a combination of two protonations with the second leading to irreversible degradation. The first protonation causes the shift in λ_{max} seen in figures 5.3-5.6, and the combination of a second protonation and resultant degradation causes the loss of the isosbestic point at higher acid concentration [8].

Figure 5.7 shows a simple linear analysis in order to compare the P_{acid50} values obtained when plotting the absorbance values before and after the isosbestic point is lost in order to observe the effect that a second protonation equilibrium has on P_{acid50}. Analysis including the absorbance values after the isosbestic point is lost results in a decrease in P_{acid50} of around 10%. This can be accounted for by an overlap in the first and second protonation equilibria. Therefore in order to maintain accuracy all of the values quoted in table 5.1 are calculated while the isosbestic point is present, therefore only taking into account the equilibrium of the first protonation.

For all of these dyes addition of an organic base, such as tetrabutylammonium hydroxide, resulted in the dye reverting to its original unprotonated form and provided not too much acid was added and the solution was not left at low pH for any length of time the resulting absorption spectra were identical to the initial spectra when no acid was added.

The increase in resolution of the vibrational bands in the protonated species is interesting. It seems likely that protonation will limit the range of twisted conformations which can be adopted by the dye around the azomethine bond, and a narrowing of vibrational bandwidths would be consistent with this.

Curve fitting analysis of acid concentration against absorbance change at a specific wavelength (usually the λ_{max} for the protonated dye) enables a value of P_{acid50} to be obtained (figure 5.8) .The plot itself is obtained by measuring the absorbance of the dye when the first protonation is complete (λ_{max} of protonated dye), and then the absorbance at that wavelength when less acid is present so that a plot of absorbance against acid concentration can be obtained. Table 5.1 displays values for P_{acid50} and n (the number of protons involved in the 1st protonation step.)

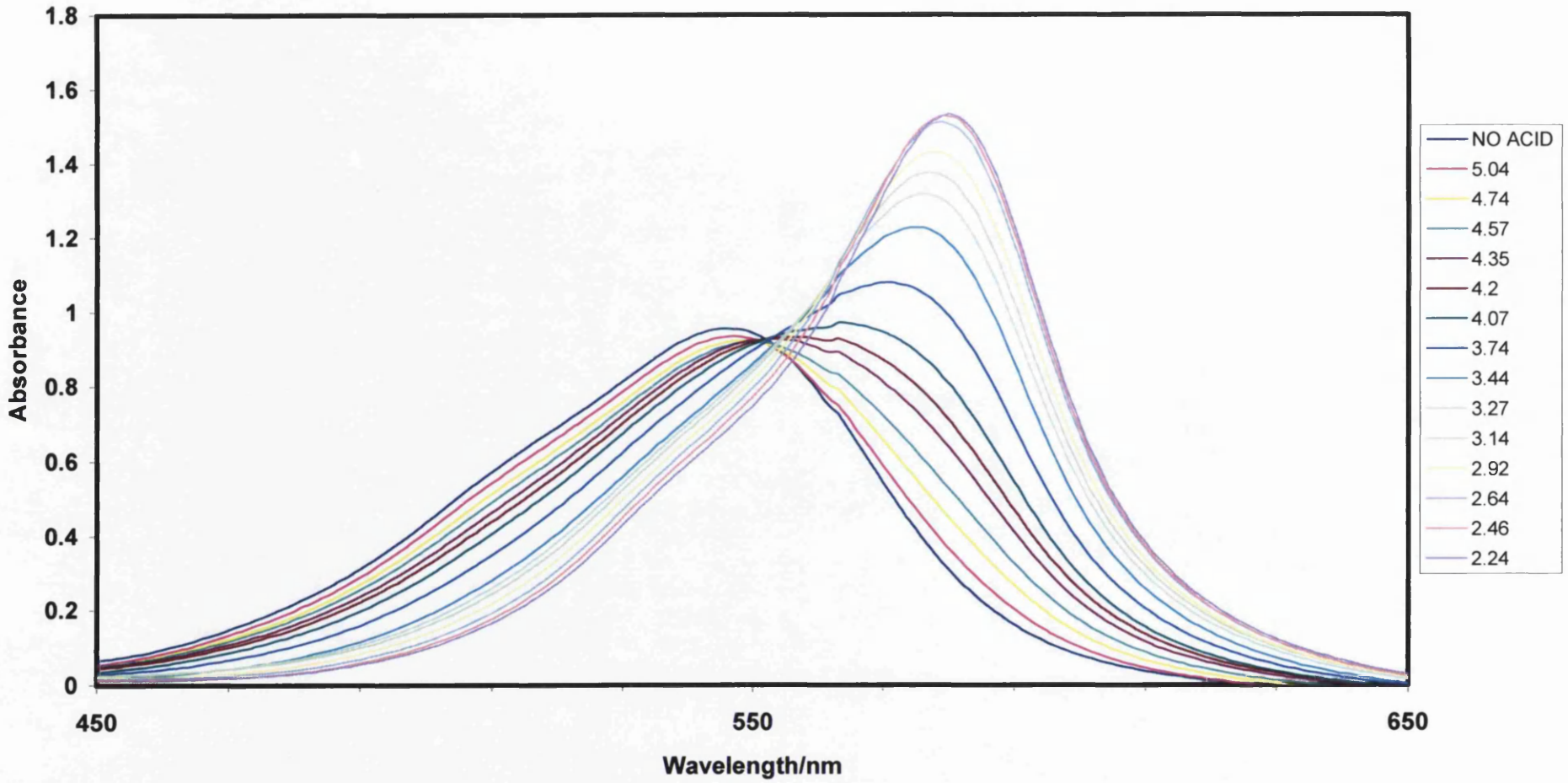

Figure 5.3: Effect of acid on the absorption spectrum of 6-OMe in dichloromethane (-log [acid] values are given in the key).

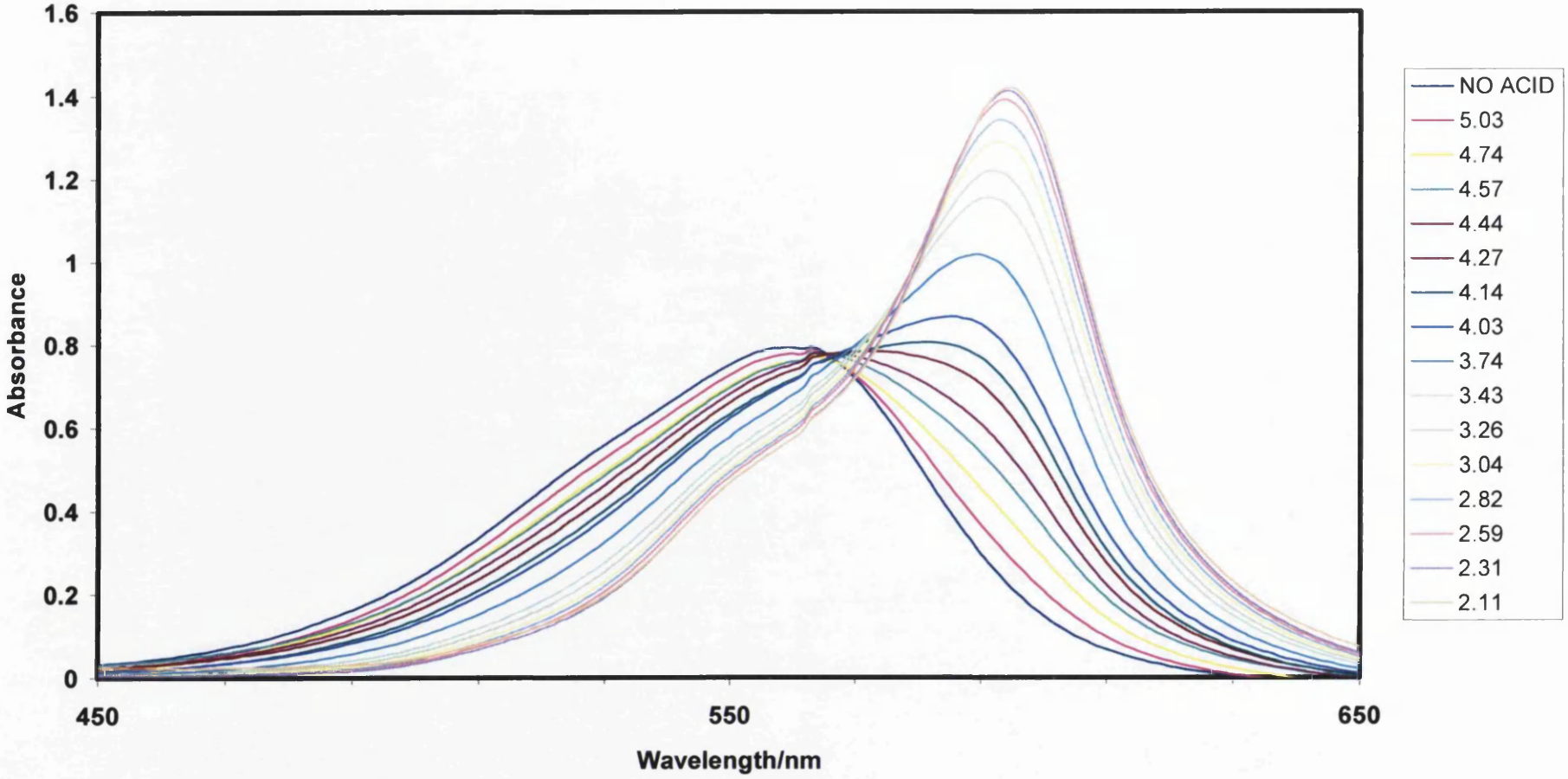

Figure 5.4: Effect of acid on the absorption spectrum of 6-Me in dichloromethane (-log [acid] values are given in the key).

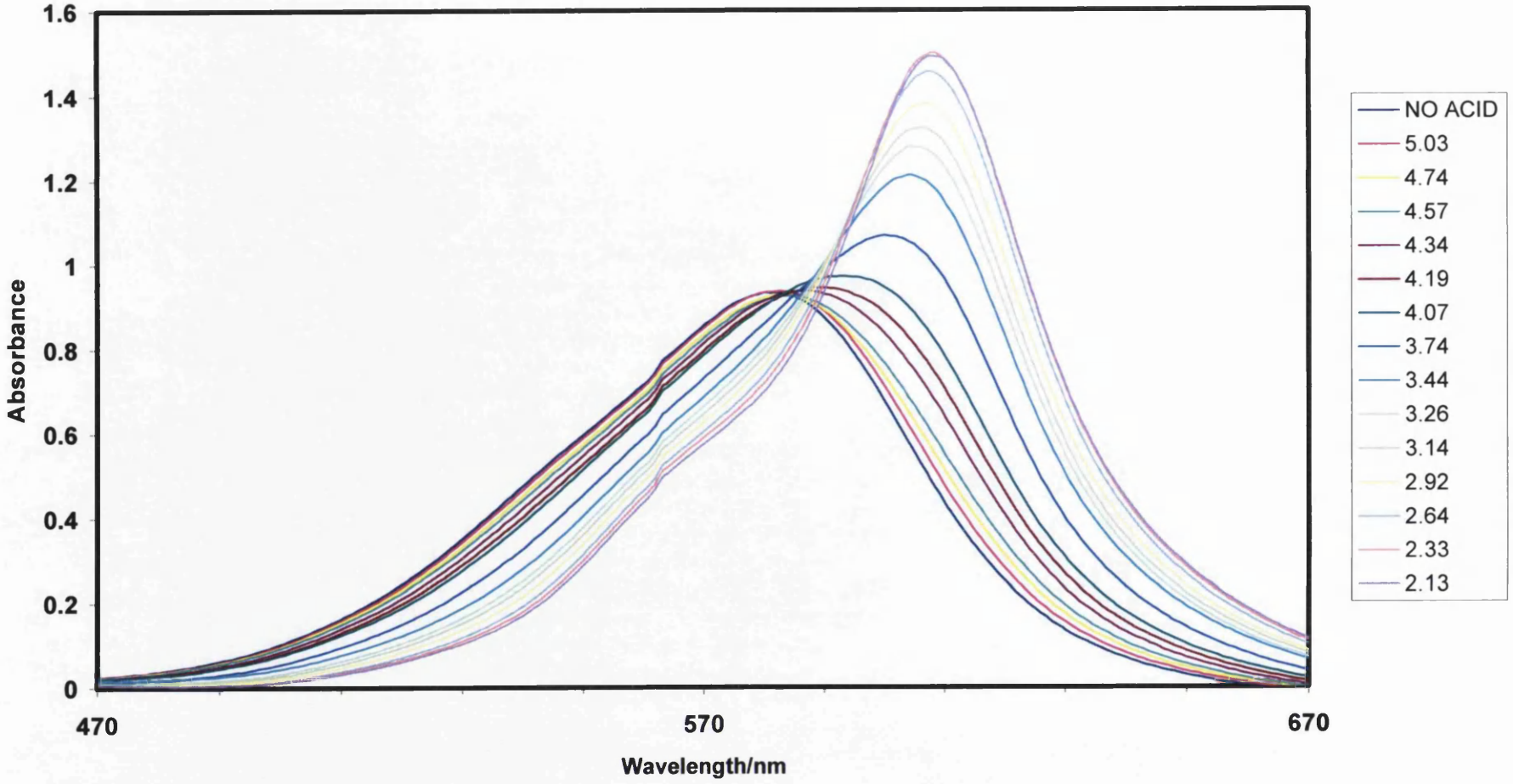

Figure 5.5: Effect of acid on the absorption spectrum of 6-Ph in dichloromethane (-log [acid] values are given in the key).

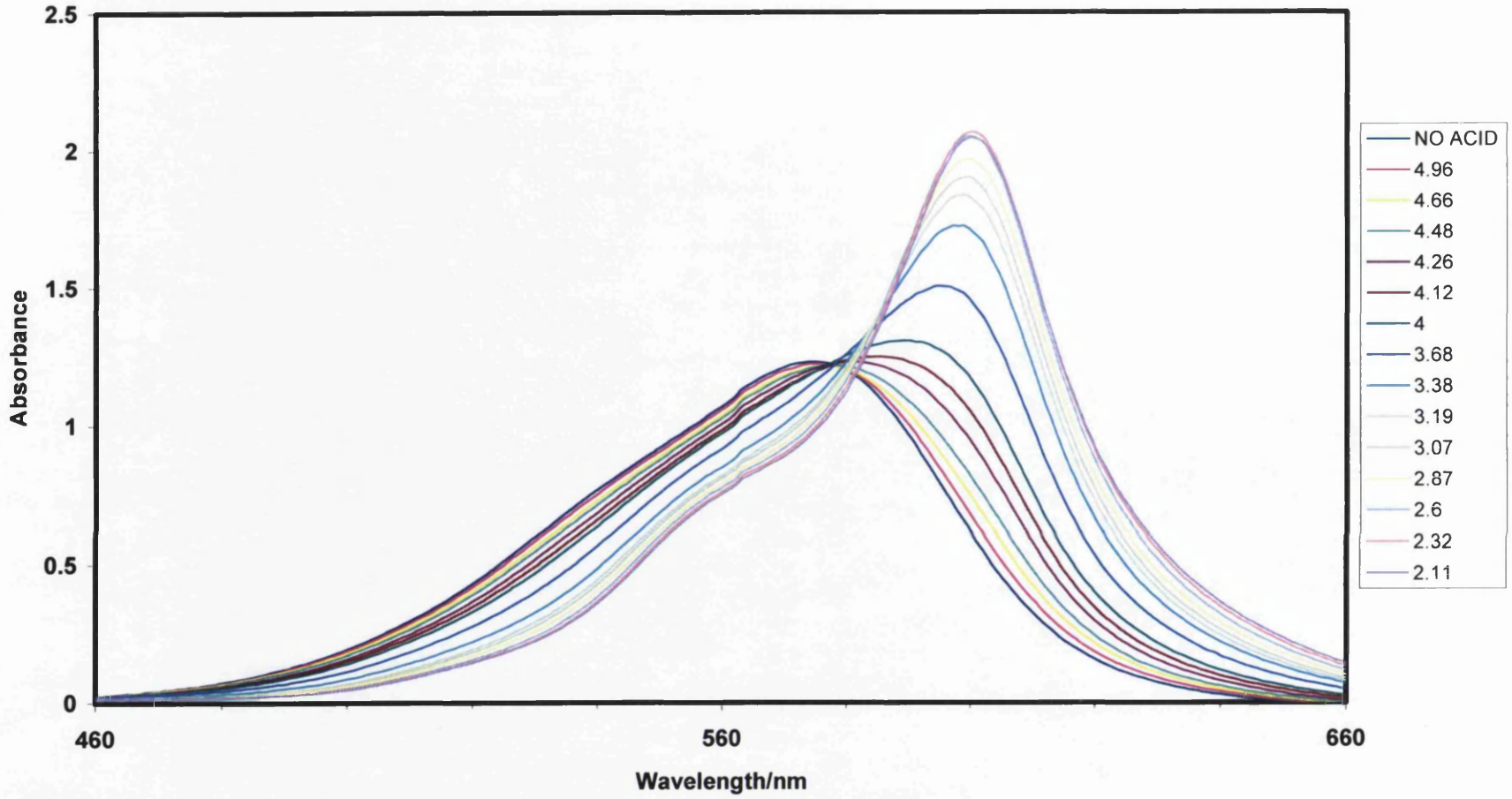

Figure 5.6: Effect of acid on the absorption spectrum of 6-H in dichloromethane (-log [acid] values are given in the key).

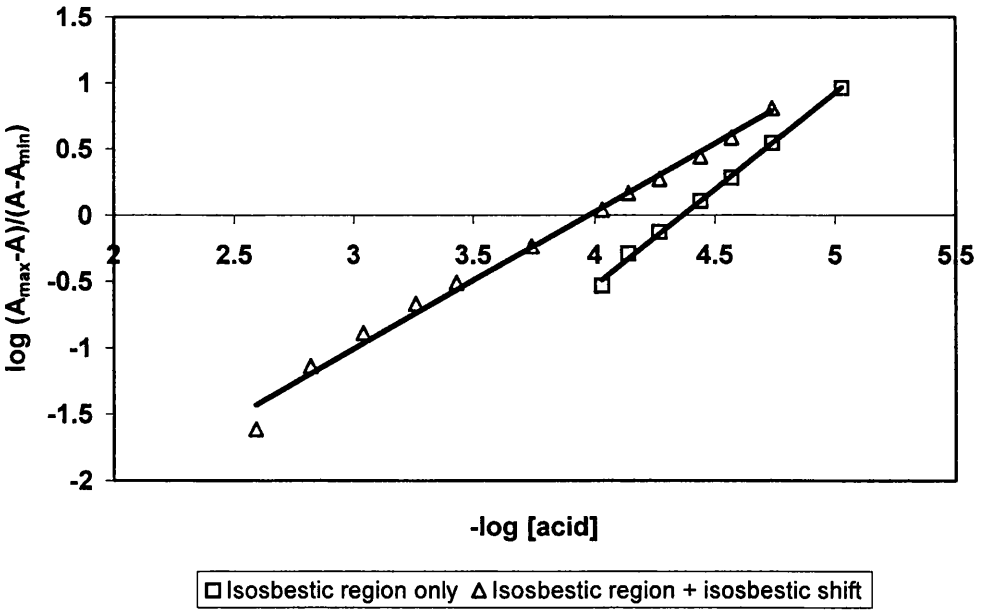

Figure 5.7: Comparison of data from the linear analysis of two different regions of the titration spectra. (Triangles-slope of 1.03, squares-slope of 1.46.)

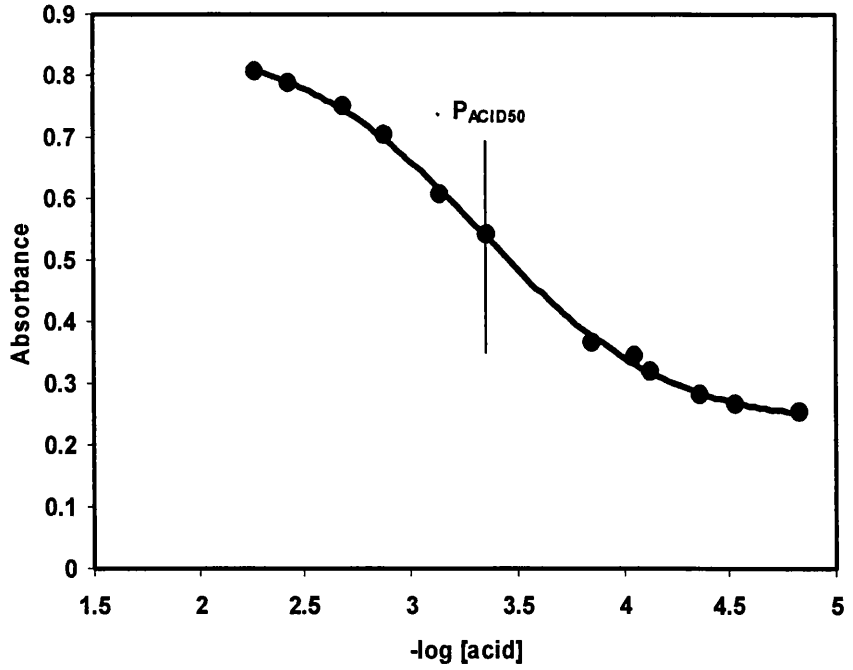

Figure 5.8: Typical sigmoidmal curve fit data. Analysis of the change in absorbance of 6-H in chloroform/TFAA at 602 nm (λ_{max} of protonated dye). $P_{acid50} = 3.3$.

Solvent media	6-OMe		6-Me		6-Ph		6-H	
	P_{acid50} (±0.1)	n (±0.1)	P_{acid50} (±0.1)	n (±0.1)	P_{acid50} (±0.1)	n (±0.1)	P_{acid50} (±0.1)	n (±0.1)
Dichloromethane[a]	4.1	1	4.2	1	3.8	1	3.8	1.1
Chloroform[a]	3.7	0.9	3.7	0.9	3.6	1	3.3	1
Dibutylphthalate[a]	1.5	1	1.7	1.1	1.5	1.1	1.5	1
THF[a]	0.2	1.5	0.2	1.5	0.2	1.7	0.3	1.6
EtOH/H_2O (95:5)[b]	-	-	1.7	1	-	-	1.7	1.3
EtOH/H_2O (9:1)[b]	-	-	1.3	1	-	-	1.4	1.1

Table 5.1: P_{acid50} data for the dye series ([a] TFAA used,[b] HCl used).
n is the best fit for the no. of protons involved in the transition.

P_{acid50} is strongly solvent dependent with more polar solvents giving both lower P_{acid50} values than dichloromethane or chloroform, and in some cases, notably when using THF as solvent, giving n values from curve fitting significantly higher than 1. It is difficult to unravel the variation in specific solvent dye interactions in these polar solvents especially as the medium changes as acid is added. One factor which will contribute is protonation of the solvent itself *e.g.* THF has a pK_a = -2.1 [12] which, although very low is still important because of the very high solvent concentration.

However as table 5.1 shows, for any given solvent there is no significant difference in the P_{acid50} value for any of the dyes studied, and with the exception of THF as solvent n is close to one.

5.4.3 Effect of protonation on the 6-CO_2Et, 6-$CONH_2$ and 6-CN dyes

For 6-CO_2Et, 6-$CONH_2$ and 6-CN dyes there is no characteristic red shift upon addition of acid. For these dyes the absorption maximum shifts to the blue and addition of base does not reverse the effect. Figure 5.9 shows, for comparison the effect of additions of acid to the spectra of both the 6-Ph dye (figure 5.9(a)) and 6-CN dye (figure 5.9 (b)). Although this has not been examined in detail it is thought it could be due to hydrolysis of the 6-position substituent to give the 6-COOH dye. Because of this behaviour no further protonation work was carried out using these dyes.

5.5 Effect of acid on isomerisation kinetics

5.5.1 Difference spectra

Figures 5.10 and 5.11 show the isomer difference spectra and isomer decay curves for the 6-H and 6-Ph dyes in methylcyclohexane with no acid present. The isomer signal from 6-H is much stronger than that from 6-Ph; furthermore the lifetime of the unstable isomer is much greater for the 6-H dye which back-reacts over a timescale of seconds than for 6-Ph which decays over the millisecond time scale [5]. These differences in behaviour are probably due to the small steric effect of the H substituent and the long lifetime of the 6-H dye unstable isomer makes this dye suitable for a study of the effect of protonation on the isomerisation of PT dyes.

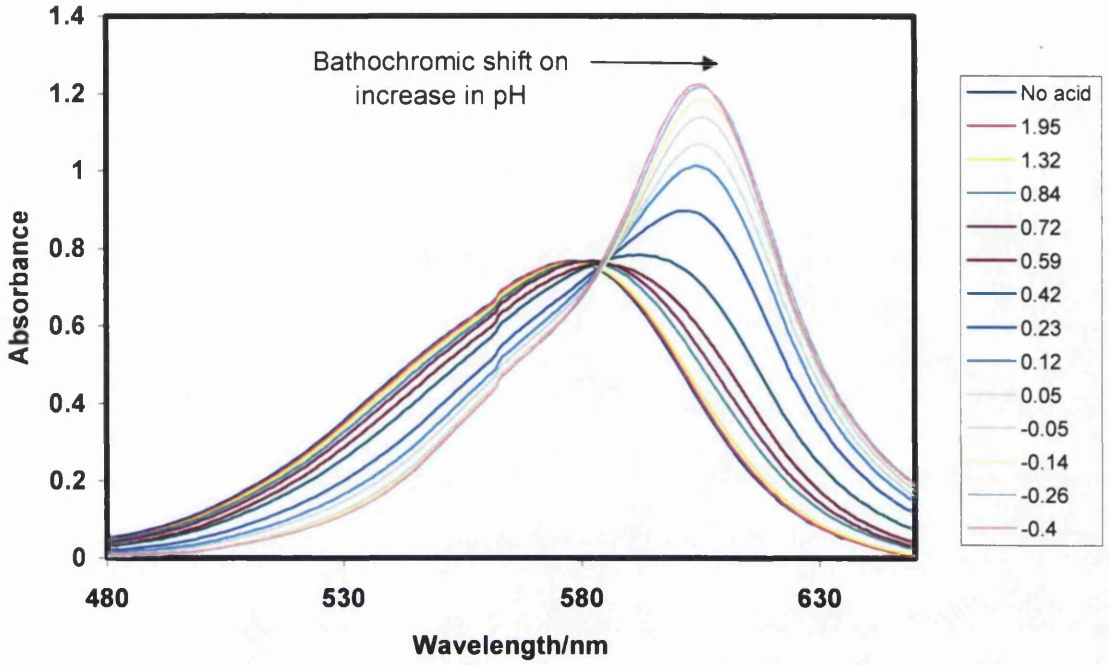

Figure 5.9(a): Effects of acid on the absorption spectrum of 6-Ph in THF (-log [acid] values are given in the key).

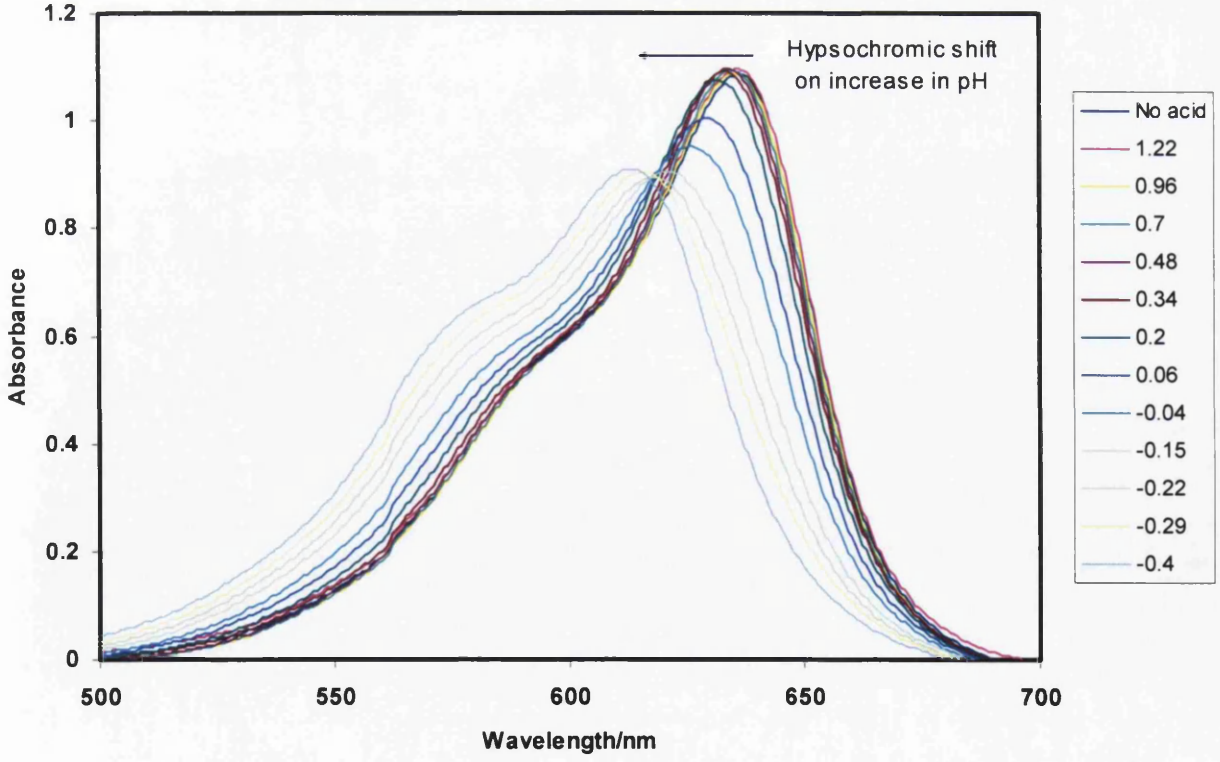

Figure 5.9(b): Effects of acid on the absorption spectrum of 6-CN dye in THF (-log [acid] values are given in the key).

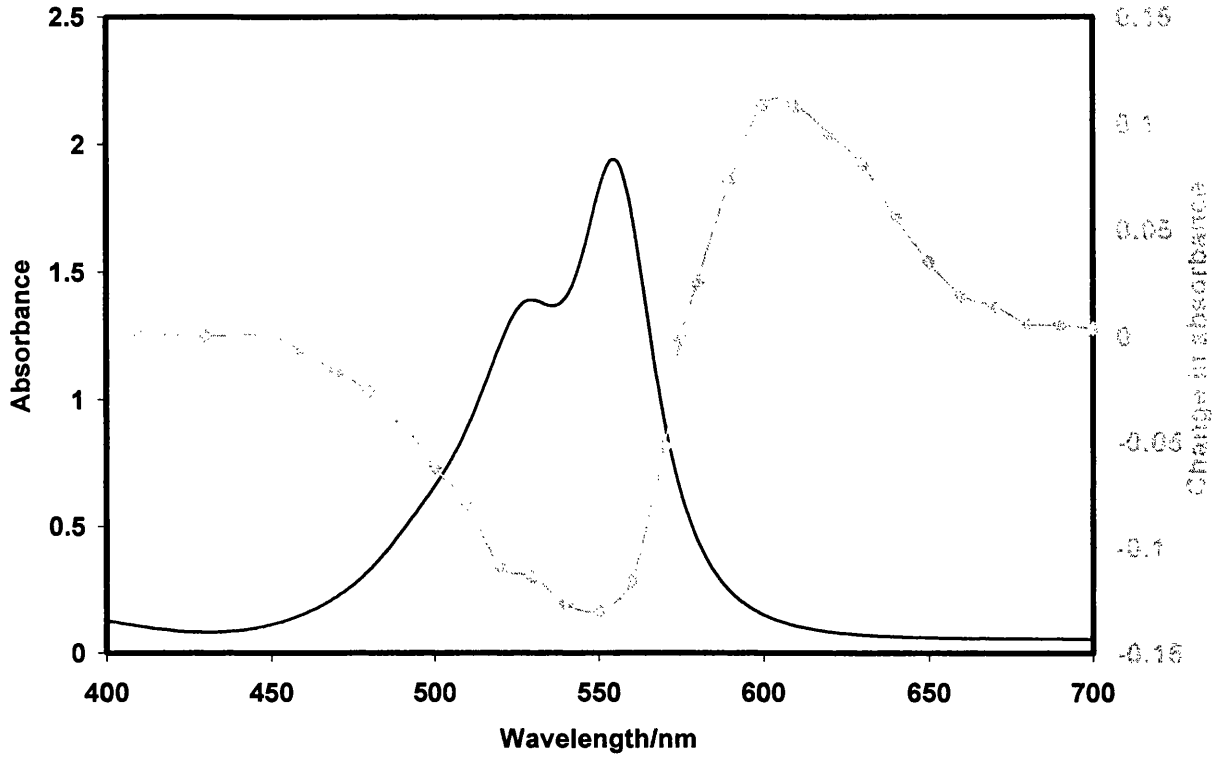

Figure 5.10: Absorption and isomer difference spectra for 6-H in methylcyclohexane.

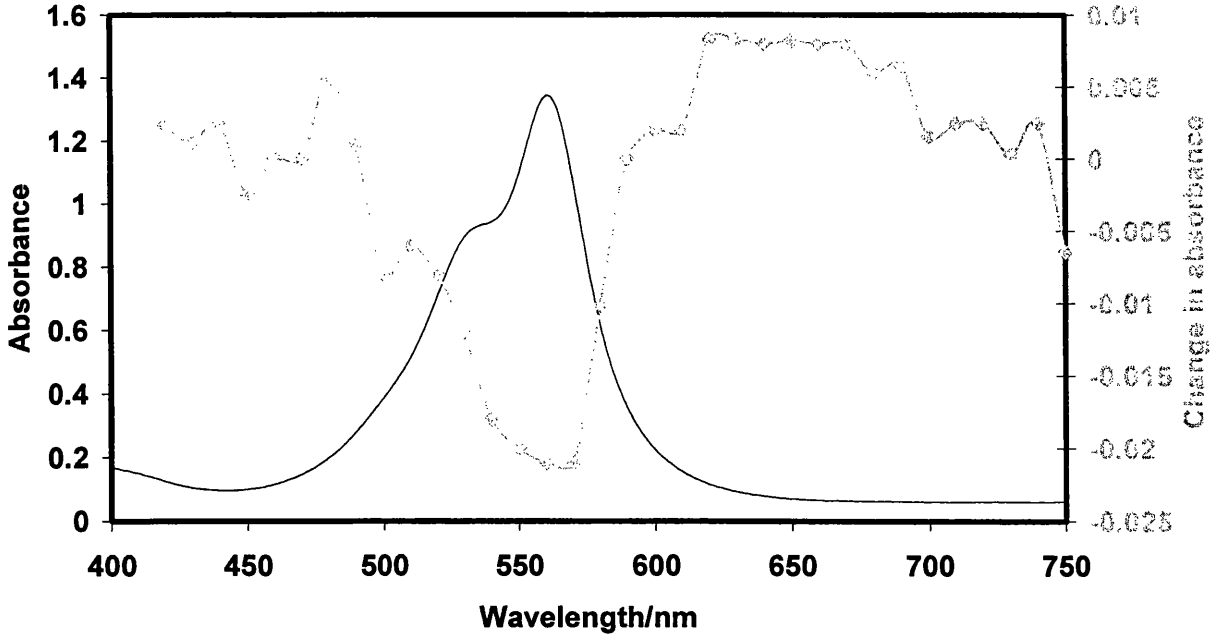

Figure 5.11: Absorption and isomer difference spectra for 6-Ph in methylcyclohexane.

5.5.2 Effect of acid on difference spectra

Addition of acid does not seem to have the same effect on the *anti* isomer absorption spectrum as is seen for the stable *syn* isomer. This is clear from the isomer difference spectra shown in figure 5.12, where even high concentrations of acid do not result in the well defined bathochromic shift characteristic of protonation of the *syn* isomer (see figures 5.3-5.6).

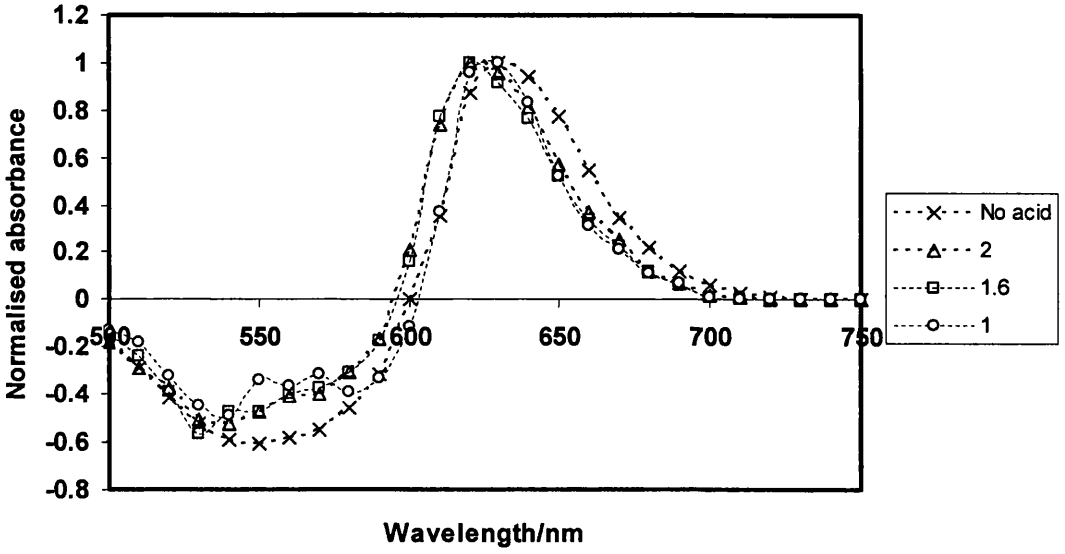

Figure 5.12: Acid effect on isomer difference spectra for the 6-H dye in chloroform, with varying amounts of TFAA added (-log [acid] values are shown).

In fact the spectra suggest that protonation of the *anti* isomer causes both a narrowing of the absorption band and a shift in λ_{max} to the blue.

5.5.3 Kinetics of the thermal back reaction

Figure 5.13 shows the effect of acid on the isomerisation kinetics of the 6-H dye in a number of solvents.

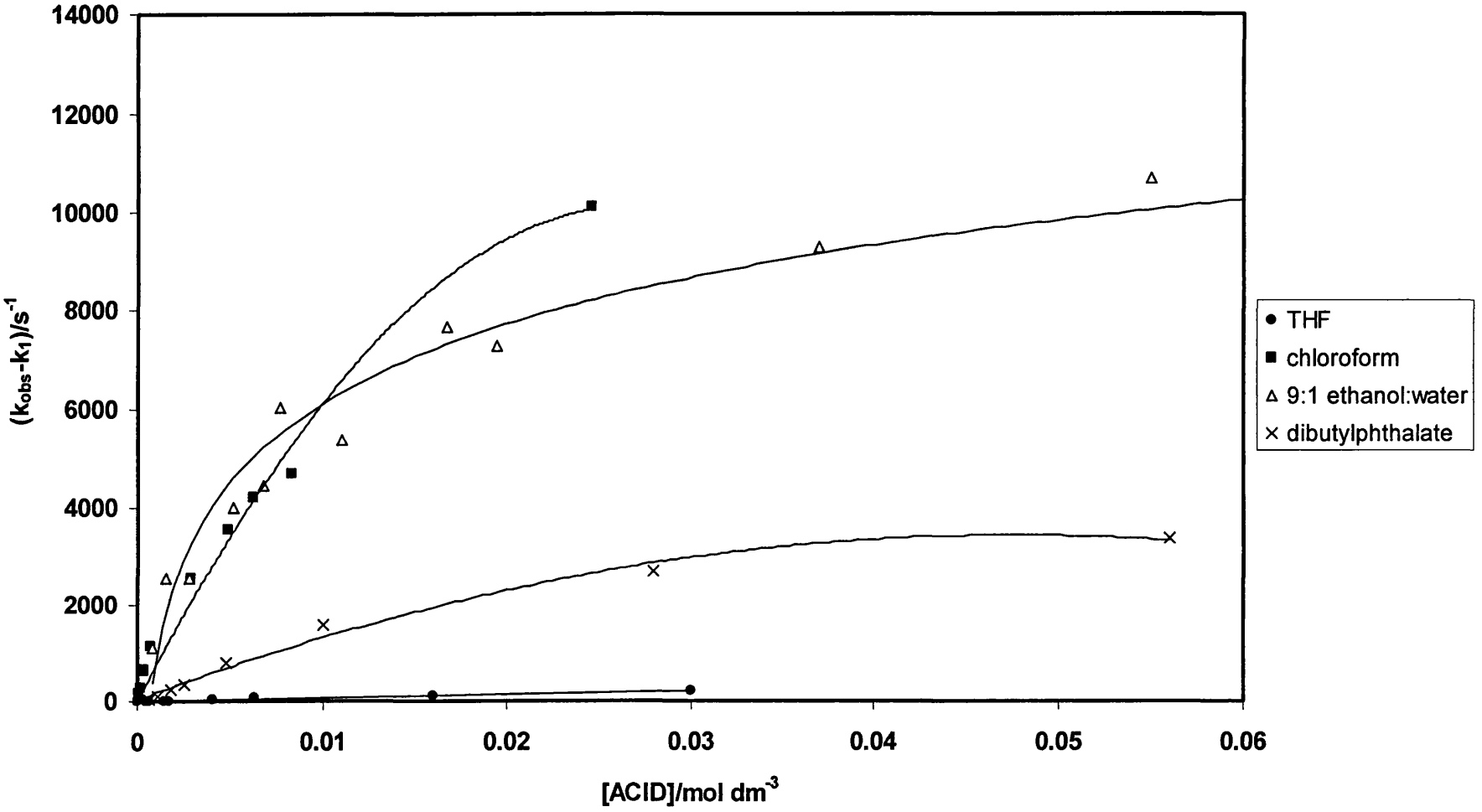

Figure 5.13: The effect of acid on the rate of isomerisation (k_{obs}-k_1) of the 6-H dye in various solvents.

Initially addition of acid causes a rapid increase in isomerisation rate but this effect levels off at high acid concentrations.

The kinetic scheme below has been postulated to describe the catalytic effect of an increase in proton concentration on the rate of isomerisation [10].

$$DYE_{syn} \xrightarrow{h\upsilon} DYE_{anti} \qquad \textbf{5.7}$$

$$DYE_{anti} \xrightarrow{k_1} DYE_{syn} \qquad \textbf{5.8}$$

$$DYE_{anti} + H^+ \overset{fast}{\leftrightarrow} DYEH^+_{anti} \qquad \textbf{5.9}$$

$$K = \frac{[DYEH^+_{anti}]}{[DYE_{anti}][H^+]} \qquad \textbf{5.10}$$

$$DYEH^+_{anti} \xrightarrow{k_3} \begin{matrix} DYEH^+_{syn} \\ \updownarrow \\ DYE_{syn} + H^+ \end{matrix} \quad fast \qquad \textbf{5.11}$$

$$k_{obs} = \frac{k_3 - k_1}{1 + \frac{1}{K[H^+]}} + k_1 \qquad \textbf{5.12}$$

$$\frac{1}{k_{obs} - k_1} = \frac{1}{K(k_3 - k_1)[H^+]} + \frac{1}{k_3 - k_1} \qquad \textbf{5.13}$$

The kinetic scheme above assumes that the protonated *anti* form of the dye relaxes to the protonated *syn* conformer (k_3). However the equilibrium between the non-protonated and protonated forms of the isomers is expected to occur much faster than the isomerisation and so the essence of the reaction is isomerisation from one equilibrium mixture of protonated and deprotonated dye in the *anti* conformation to an equilibrium mixture of protonated and deprotonated dye in the *syn* conformation.

k_1 (equation 5.8) is the rate of isomerisation with no acid present, while k_{obs} increases with addition of acid until it approaches the limiting value k_3 corresponding to all *anti* dye in the protonated form The catalytic effect of proton addition is clear as even at low acid concentrations the observed rate constant quickly reaches the limiting rate k_3. Figure 5.14 gives a plot of $1/(k_{obs} - k_1)$ against $(1/[H^+])$ giving a straight line with the slope $1/[K(k_3-k_1)]$ and intercept of $1/(k_3-k_1)$.

The effect of acid can also be modelled using a curve fit analysis in essentially the same way as the pH dependent spectra. This is shown in figure 5.15. The same sigmoidal shape is evident, as seen previously in figure 5.7 for a simple absorption titration for the *syn* isomer in the same solvent system. The same expression as used for the *syn* isomer can be used but in this case c is equal to P_{acid50} for the *anti* isomer.

$$y = a + \frac{b}{1 + \exp\frac{(-(x-c))}{d}} \qquad \textbf{5.14}$$

(where a is k_{obs}, b is [acid] and c is P_{acid50}).

Table 5.2 summarises the kinetic data and the P_{acid50} values for both the *syn* and *anti* isomers, using the sigmoidal fit method.

Solvent	$P_{acid\ 50}$ DYE_{anti} (±0.1)	$P_{acid\ 50}$ DYE_{syn} (±0.1)	k_1/s^{-1} (±0.2)	$k_3/x10^3\ s^{-1}$ (±5%)
Chloroform	1.6	3.3	2.9	33
9:1 EtOH:Water	2.2	1.4	2.7	10
THF	0.4	0.3	2.4	0.4
dibutylphthalate	1.8	1.5	3.2	1.7

Table 5.2: Summary of kinetics for the effect of acid on the isomerisation of 6-H in a variety of solvents.

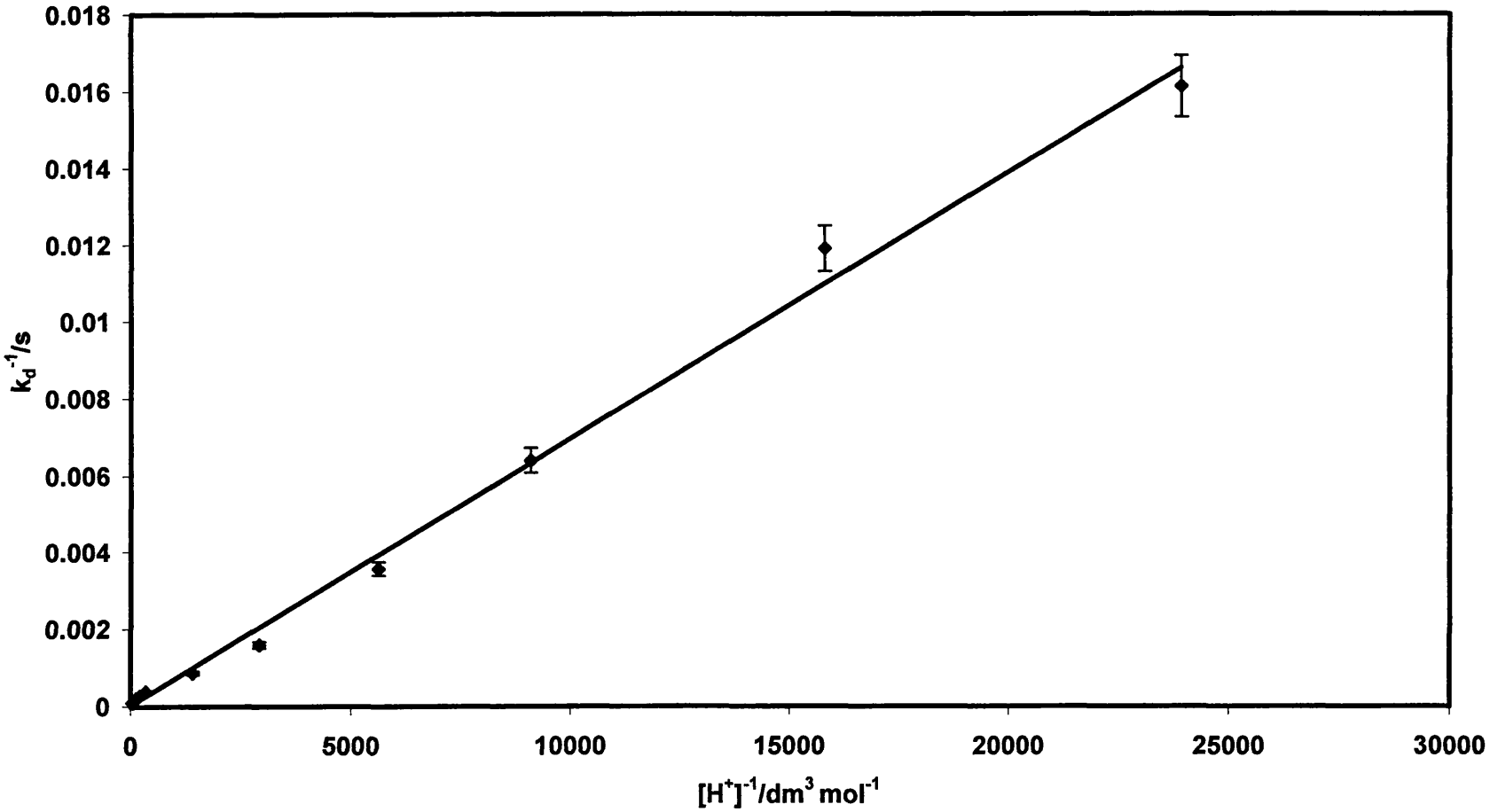

Figure 5.14: Linear relationship between reciprocal of acid concentration and reciprocal rate of isomerisation ($k_d = k_{obs}-k_1$) for 6-H in $CHCl_3$/TFAA.

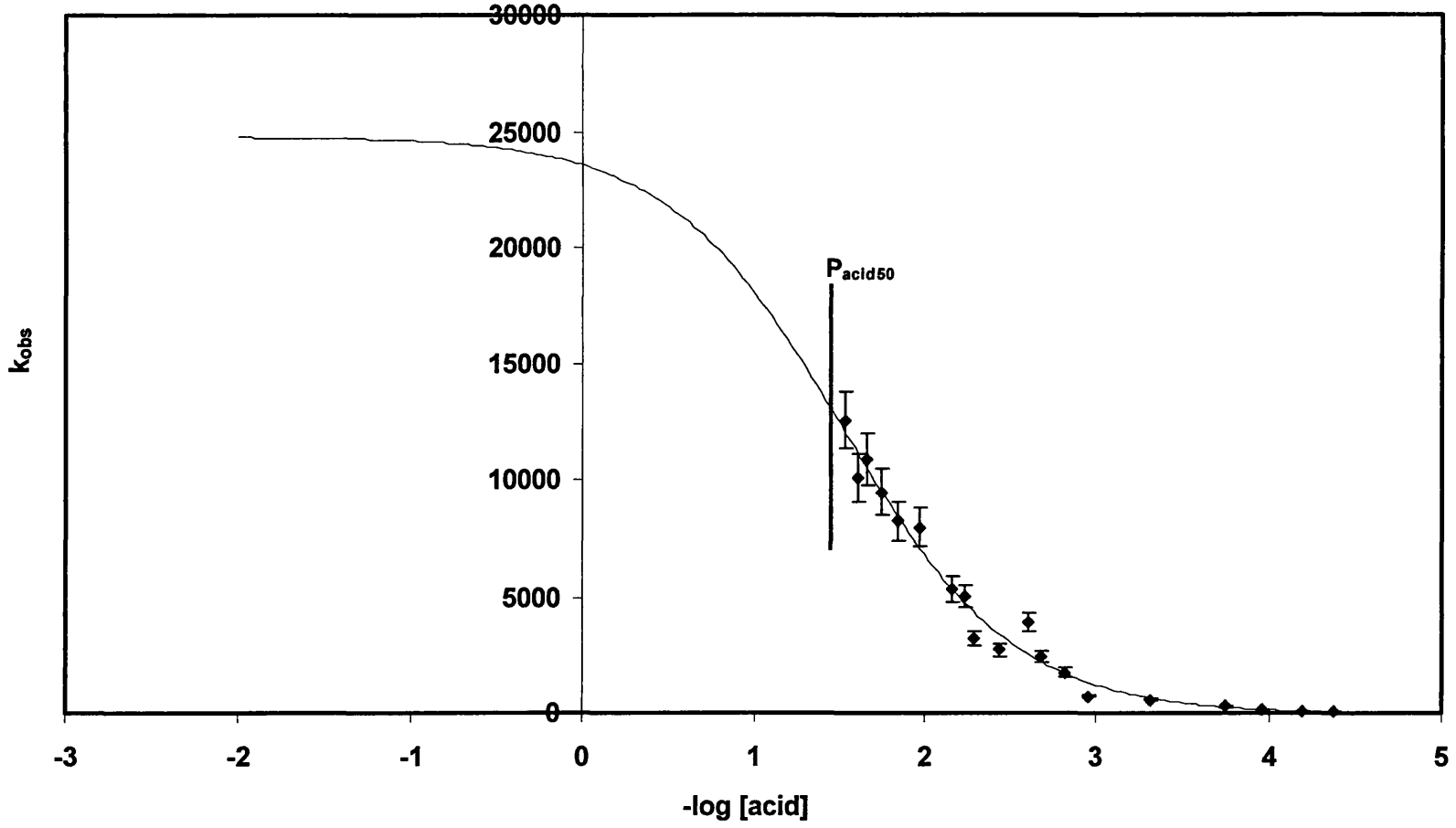

Figure 5.15: Sigmoidal kinetic relationship between acid concentration and the rate of isomerisation for 6-H in $CHCl_3$/TFAA.

Figure 5.16 displays typical Arrhenius data for the 6-H dye. Thermodynamic parameters for two solvent systems are summarised in table 5.3. A high pre-exponential factor for the protonated form of the dye in ethanol:water was measured, suggesting that the isomerisation occurs *via* a singlet state mechanism [5]. The lower pre-exponential factor measured for both dye forms in chloroform may suggest the possibility of a triplet biradical.

	$CHCl_3$/TFAA		**EtOH-H_2O (9:1, v-v)/HCl**
	DYE	**$DYEH^+$**	**$DYEH^+$**
log A (± 0.4)	10.8	11	13.6
$\Delta G^{\ddagger}$/ kJ mol^{-1}(± 1)	60.1	38.5	50
$\Delta H^{\ddagger}$/ kJ mol^{-1}(± 1.5)	61.5	40.3	52
$\Delta S^{\ddagger}$/J mol^{-1} K^{-1}(± 3)	-4.6	-6.1	7

Table 5.3: Summary of thermodynamic parameters for 6-H.

Unfortunately the data reported here do not take into account the temperature effects on the equilibrium between protonated and unprotonated dye. In order to investigate this further data need to be obtained, particularly full sigmoidal plots (note figure 5.15) at varying acid concentration for temperature effects on the rate of isomerisation.

Even so the free energy decrease when comparing protonated and non-protonated forms compares with work by Hessler *et al.* where a value of the free energy decrease of around 12 kJ mol^{-1} was measured when the imine group of a phenylguanidinium salt was protonated [10, 13]. This process is thought to occur *via* a rotation mechanism [14].

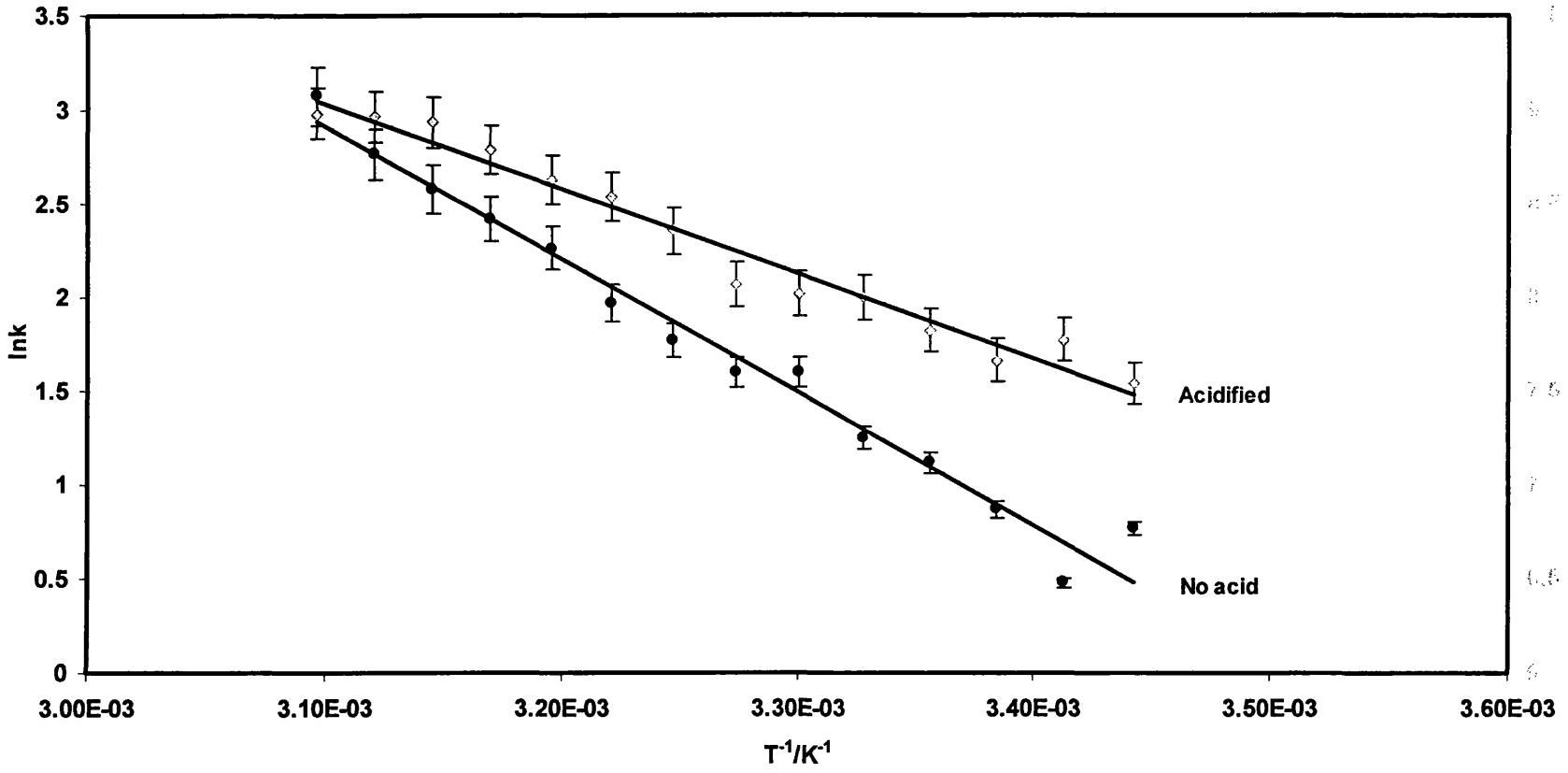

Figure 5.16: Arrhenius plots for isomerisation kinetics for the 6-H dye in acidified chloroform (-log [acid] = 2.4; *syn* dye in predominantly protonated form) and chloroform with no acid added.

5.6 Oxygen quenching of isomer yield

Oxygen is an efficient quencher of triplet states, and oxygen quenching of a photochemical transient can often be used to determine whether or not the transient originates from the singlet or triplet state.

In previous work White [15] found that both UV and visible light-induced isomerisations of the 6-H and 6-Me dyes were not oxygen quenched while UV induced isomerisation of 6-CO_2Et was. White has suggested [15] that the behaviour of the 6-CO_2Et dye is due to excitation of a localised triplet state on the carbonyl group of the ester which undergoes intramolecular energy transfer into the PT triplet levels. The 6-H dye does not have such a substituent-localised triplet state and this, he suggests, is why the isomer ratio is independent of excitation wavelength. Douglas found a small but reproducible oxygen quenching effect for the visible induced isomerisation of a number of PT dyes including 6-Me [16]. These previous workers used broad band flash excitation, and it was considered worthwhile to examine the effect of monochromatic visible and UV excitation from a Nd/YAG laser. Table 5.4 collects data from White, Douglas and this work.

Dye		Excitation wavelength or wavelength range (nm)	Abs(N_2)/Abs (air)
6-CO_2Et		**532**	**1.13 (0.04)**
		>400 [15]	1.00(0.05)
		335	**1.90 (0.12)**
		>330 [15]	1.40 (0.05)
		>300 [15]	2.6 (0.3)
		>200 [15]	3.8 (0.3)
6-H		>400 [15]	1.0 (0.05)
		>330 [15]	1.0 (0.05)
		>300 [15]	1.0 (0.05)
		>200 [15]	1.0 (0.05)
6-Me		>400 [15]	1.07 (0.02)
		620 [16]	1.07 (0.04)

Table 5.4: The effect of varying the excitation wavelength on the ratio: isomer yield in solution under nitrogen/isomer yield in air-equilibrated solution. (Numbers in bold represent this work.)

The results obtained here using monochromatic excitation confirm those obtained previously. For all dyes photoisomerism due to visible excitation, either broad band or monochromatic, is quenched slightly by oxygen while for the 6-CO_2Et dye UV induced photoisomerisation is significantly quenched by oxygen. These results confirm that there is some triplet formation upon visible excitation and, assuming dynamic quenching, that the triplet lifetime is sufficiently long to be quenched by oxygen at *ca.* 1×10^{-3}mol dm^{-3} (assuming a concentration of oxygen in air equilibrated ethanol of 2×10^{-3} mol dm^{-3} [17]). The direct isomerisation quantum yields of PT dyes are generally small, while triplet-sensitised quantum yields of isomersation are much higher [16]. Since, for visible excitation, oxygen quenching removes only a small fraction of the isomer yield, triplet quantum yields from visible excitation are themselves probably only small. Estimating the triplet lifetime from these data is difficult because the quantum yield is not known but a minimum lifetime of a few ns is implied by the fact that oxygen at *ca.* 1×10^{3} mol dm^{-3} quenching at a diffusion controlled rate constant of *ca.* 1-3 $\times 10^{10}$ s^{-1} does give a measurable decrease in isomer yield. Triplet lifetimes could be much higher but if this is the case then the yield must be less than a few percent otherwise these triplet states would be easily detected by ns flash photolysis and to date there are no reliable reports of the direct detection of PT dye triplet states in flash photolysis even though a number of workers have looked for them by this method [2, 3, 17].

5.7 Conclusion

The rate at which PT dyes back-isomerise from the less stable *anti* isomer to *syn* following flash excitation can be catalysed by the addition of acid. In chloroform the rate of isomerisation for the 6-H dye increases by a factor of around 10000 when the concentration of acid is raised to *ca.* 0.02 mol dm^{-3}. A kinetic analysis shows this effect to arise from protonation of the azomethine bond, and that the protonated dye isomerises much fast that the unprotonated dye.

The protonation equilibria are not significantly affected by the R_6 substituent (which controls dye hue) but are very dependent upon solvent.

For the 6-H dye using kinetic data and transition state theory to calculate the ground state barrier to isomerisation together with the minimum energy difference between syn and anti isomers from NMR studies gives a barrier height > *ca.* 70 kJ mol^{-1}. This can be compared to a triplet energy of *ca.* 110 kJ mol^{-1}. It is known that this dye will isomerise from the triplet state but it is still not clear whether the well in the triplet state PE curve associated with isomerisation is deep enough to bring triplet and ground state surfaces into contact (note figure 5.17).

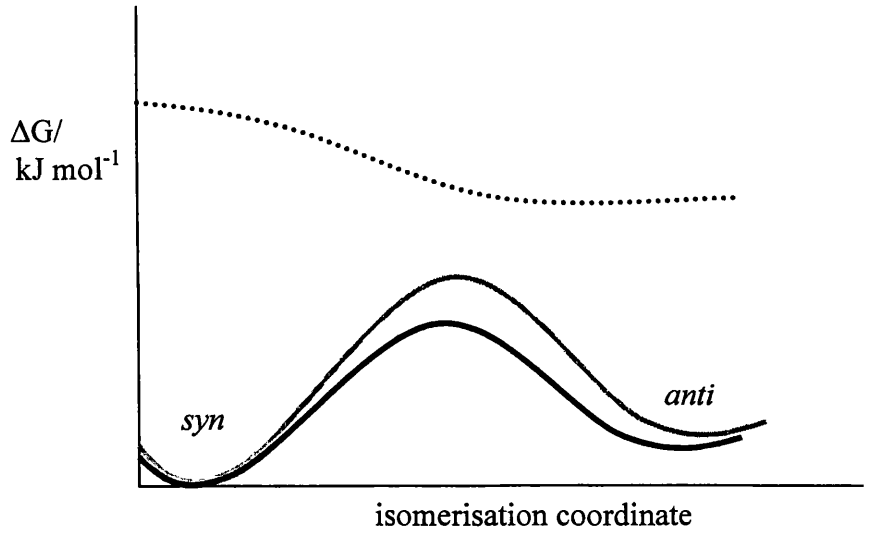

Figure 5.17: Proposed potential energy surfaces for the triplet (dotted line) and protonated (bold black line) and unprotonated (bold grey line) ground states of the 6-H dye [5].

Isomerisation yield can be quenched by oxygen. Although the effect is generally small this is strong evidence for triplet state formation in fluid solution. The size of the effect together with the inherently low quantum yield for isomerisation suggest a low triplet quantum yield. The fact that the triplet state is quenched suggests a lifetime of at least a few ns. The failure to detect the triplet state directly by ns flash photolysis also suggests the combination of a low triplet yield and a lifetime less than *ca.* 100 ns.

5.8 References

1) A.Padwa and F.Albrecht, *J. Am. Chem. Soc.*, **1974**, 96, 4849.

2) W.G.Herkstroeter, *J. Am. Chem. Soc.*, **1973**, 95, 8686.

3) W.G.Herkstroeter, *J. Am. Chem. Soc.*, **1976**, 98, 330.

4) T.Asano, T.Okada and W.G.Herkstroeter, *J.Org. Chem.* **1989**, 54, 379.

5) P.Douglas and D.Clarke *J. Chem. Soc. Perkin Trans. 2*, **1991**, 1363.

6) P.Douglas, J.D.Thomas, H.Strohm, C.Winscom, D.Clarke and M.S.Garley, *Photochemical and Photobiological Sciences,* **2003**, 2, 563.

7) F.Wilkinson, D.R.Worrall, R.S.Chittock, *Chem. Phys. Letters*, **1990**, 174, 416

8) Chapter 3 of this work.

9) P.Douglas, C.Couture, D.Clarke, D.Reed, I.H.Sadler and T.Wear, *J. Chem. Soc. Perkin Trans. 2*, **1994**, 1295.

10) C.Couture, *MPhil Thesis,* **1992**, University of Wales Swansea.

11) L.Nicholls, *Private communication.*

12) C. H. Rochester, *Acidity Functions*, Academic Press, London, 1970.

13) H.Kessler and D.Liebfritz, *Tetrahedron*, **1969**, 25, 5127.

14) H.Kessler, *Angew. Chem. Internat. Edit.,* **1968**, 7, 898.

15) M.White, *MPhil Thesis,* **2004,** University of Wales Swansea.

16) P.Douglas, *J. Photogr. Sci.,* **1988**, 36, 83.

17) S.M.Townsend, *PhD thesis,* **1992**, University of Wales Swansea.

Chapter 6

Triplet energies and singlet oxygen quenching rate constants of PT dyes

6.1 Introduction

For many dyes and polyaromatic hydrocarbons photo-induced fading through the self-sensitised generation of singlet oxygen ($^1O_2$) [1-4] is an important photodegradation route. It has been suggested that this route might also be important for PT dyes and azomethine dyes in general [5-9]. The relevant photochemistry is given in figure 6.1.

Schmidt and Schweitzer [2] and Gorman and Rodgers [3] supply a detailed discussion of the characteristics of singlet oxygen, while Wilkinson *et al.* provide a comprehensive summary of the rate constants for the decay and reactions of the lowest electronically excited state of molecular oxygen in solution [4].

The essential characteristics of ground state and singlet oxygen of relevance to the work presented here are as follows. The spin forbiddenness of both radiative and non-radiative routes of deactivation of $^1O_2$ result in comparatively long lifetimes in solution (*ca.*10 μs in ethanol, *ca.* 60 μs in acetonitrile) [2] . Chemical quenching of $^1O_2$ can lead to oxidation and dye degradation and therefore affect the light fastness of photographic systems (note figure 6.1).

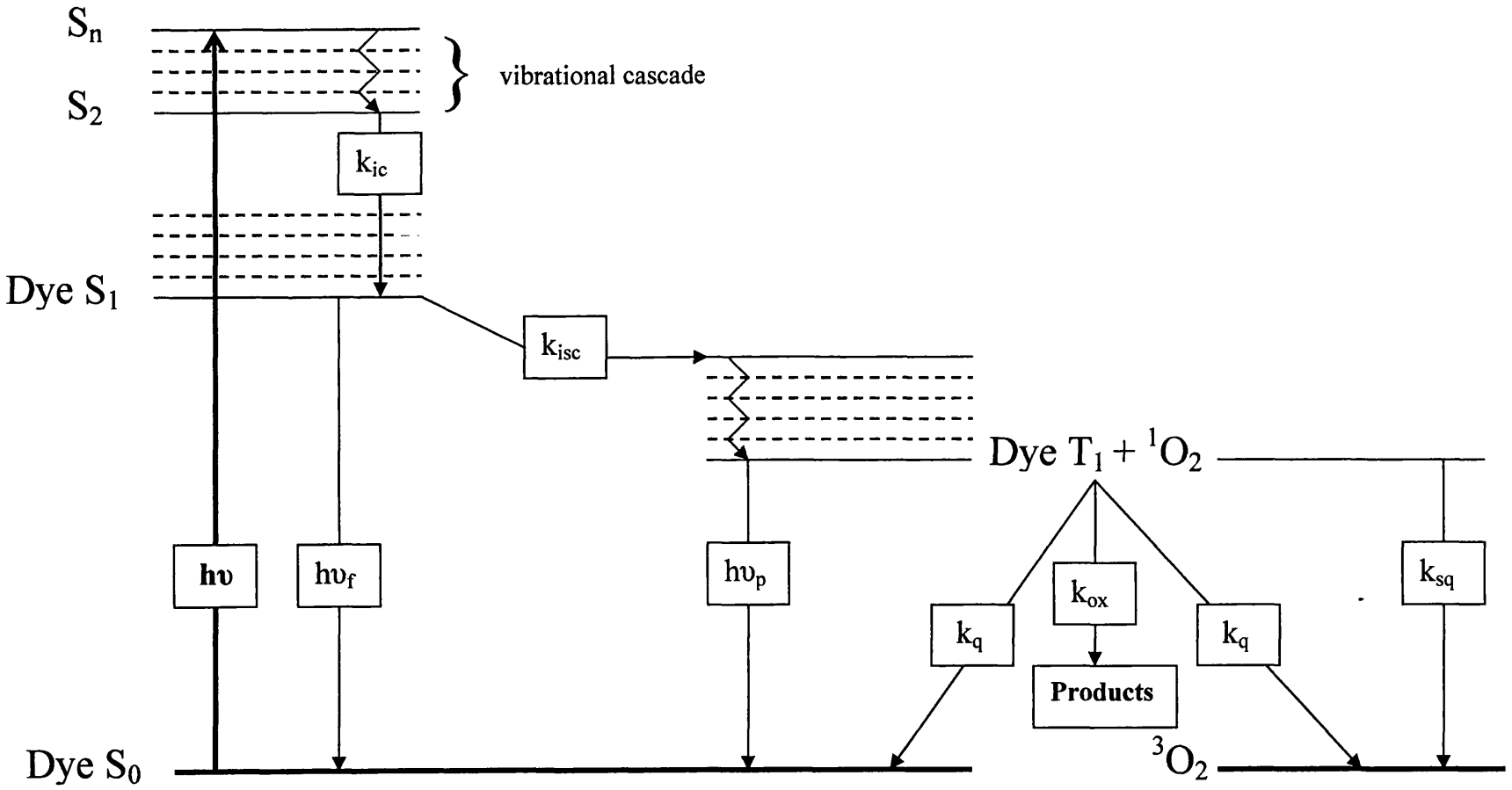

Figure 6.1: Mechanisms for deactivation of dye excited states and reaction with singlet oxygen.

k_i = rate constant for internal conversion, k_{isc} = rate constant for intersystem crossing, $k_{reverseisc}$ = rate constant for reverse intersystem crossing, $h\upsilon_f$ = fluorescent emission, $h\upsilon_p$ = phosphorescent emission, k_q = physical rate constant for quenching of singlet oxygen by dye, k_{sq} = rate constant for solvent quenching of singlet oxygen, k_{ox} = rate constant for dye destruction by reaction with $^1O_2$.

The amount of singlet oxygen produced will depend upon the triplet characteristics of the dye. One of the key considerations is the energy of the triplet state, whether it lies 'above' or 'below' that of singlet oxygen. A dye with a triplet energy (E_T) significantly higher than 94.7 kJ mol^{-1} would be expected to be a more efficient singlet oxygen sensitiser than one with a triplet energy less than 94.7 kJ mol^{-1}.

The rate constant for energy transfer quenching of singlet oxygen by the dye will also depend on the energy for the dye triplet state. Dyes with triplet state energies less than singlet oxygen are expected to be efficient singlet oxygen quenchers, while those with triplet energies significantly greater than 94.7 kJ mol^{-1} are expected to show low singlet oxygen quenching rates.

6.2 Triplet Energy Estimations

6.2.1 Indirect Measurements of E_T by energy transfer

Measuring PT dye triplet energies is difficult for the following reasons.

a) The dyes do not phosphoresce and hence the triplet energies cannot be measured directly [10,11].
b) Triplet state yields and lifetimes are such that there have been no reliable reports of detection of dye triplet states by direct excitation using flash photolysis.
c) The short triplet lifetimes preclude triplet state detection by energy transfer in fluid solution, although triplet state involvement in sensitiser quenching is indicated by efficient triplet-sensitised syn-anti isomerisation [10,12-16].

It is, however possible to use triplet-triplet energy transfer rate constants to make an estimate of dye triplet energies. If the E_T of the donor lies above that of the acceptor then the rate of energy transfer will occur at close to the diffusion controlled limit, which can be calculated using the Stokes-Einstein relationship. However, if the acceptor E_T lies above that of the donor then the rate of energy transfer will be well below that of a diffusion controlled process. Therefore by using donors or sensitisers of known triplet energy (such as porphyrins, naphthalocyanines and phthalocyanines), it is possible to estimate the dye triplet energy by a consideration of the rate of energy transfer between sensitiser and dye.

The kinetic scheme is summarised below [17]:

$$\text{SENS } S_0 + h\upsilon \longrightarrow \text{SENS } S_1^* \qquad \textbf{6.1}$$

$$\text{SENS } S_1^* \xrightarrow{\text{isc}} \text{SENS } T_1^* \qquad \textbf{6.2}$$

$$\text{SENS } T_1^* \xrightarrow{k_{relax}} \text{SENS } S_0 \qquad \textbf{6.3}$$

$$\text{SENS } T_1^* + \text{DYE } S_0 \xrightarrow{k_q} \text{SENS } S_0 + \text{DYE } T_1^* \qquad \textbf{6.4}$$

isc - intersystem crossing; k_{relax} - rate constant for radiationless decay; k_q - rate constant for quenching; * - signifies an excited state.

If the triplet lifetime of a sensitiser is measured as a function of dye concentration then the following expressions can be used to obtain the quenching rate constant.

$$d[\text{SENS}]/dt = k_{relax}[\text{SENS } T_1^*] + k_q[\text{DYE}][\text{SENS } T_1^*] \qquad \textbf{6.5}$$

and therefore:

$$k_{obs} = k_{relax} + k_q[\text{DYE}] \qquad \textbf{6.6}$$

A plot of k_{obs} against [DYE] is linear, k_q is given by the slope and k_{relax} is the intercept.

Balzani proposed the following general kinetic scheme for the energy transfer process

$$\text{SENS } T_1^* + \text{DYE } S_0 \underset{k_{-d}}{\overset{k_d}{\rightleftharpoons}} [\text{SENS } T_1^* \bullet\bullet\bullet\bullet \text{DYE } S_0] \underset{k_{-en}}{\overset{k_{en}}{\rightleftharpoons}} [\text{SENS } S_0 \bullet\bullet\bullet\bullet \text{DYE } T_1^*] \underset{k_d}{\overset{k_{-d}}{\rightleftharpoons}} \text{SENS } S_0 + \text{DYE } T_1^* \qquad \textbf{6.7}$$

where k_d is the diffusion controlled rate constant and k_{en} is the pre-exponential factor for the forward energy transfer.

From this he derived the following equation which gives the variation in rate constant for energy transfer, between an excited state donor, D* (in our case a triplet sensitiser)

and ground state acceptor, A (in our case a PT dye), as a function of donor and/or acceptor excited state energies, and the "reorganizational energy" for the process.

$$k_q = \frac{k_d}{1+\exp(\Delta G/RT)+(k_{-d}/k_{en})\exp\left[\frac{\Delta G+(\ln 1/2)\Delta G^{\ddagger}(0).\ln[1+\exp(-\Delta G \ln 2/\Delta G^{\ddagger}(0))]}{RT}\right]} \quad \textbf{6.8}$$

Where: k_q is the observed quenching rate constant,; k_d is the rate constant for diffusion controlled encounter between ground state dye and excited state sensitiser; k_{-d} is the rate of separation of the encounter pair which, as obtained from geometric arguments, is *ca.* $1.15k_d$ [18,19]. k_{en} is the pre-exponential factor for the forward energy transfer as given by, $k_{en} = k_{trans}.k_BT/h$ (where k_{trans} is the transmission coefficient, and k_B and h the Boltzmann and Planck constants respectively), ΔG is the difference in energy of the two states involved, *i.e.* $E_{A^*} - E_{D^*}$; and $\Delta G^{\ddagger}(0)$ is the reorganisational energy for the energy transfer process. When ΔG is adequately large and negative then equation 6.8 reduces to give equation 6.9

$$k_{q(max)} = k_d/(1+ k_{-d}/k_{en}) \quad \textbf{6.9}$$

where $k_{q(max)}$ is the maximum observed rate constant. The experimental method used is to measure k_q for a range of sensitisers of varying triplet energy but other molecular properties as similar as possible and then to analyse the variation in k_q with sensitiser triplet energy using equation 6.8. In order to estimate triplet energies for the dyes of interest here, which can be estimated to be *ca.* 90-120 kJ mol^{-1} [5, 9, 11] triplet energy transfer measurements were obtained using a series of porphyrin, phthalocyanine and naphthalocyanine sensitizers.

A similar approach was used by Herkstroeter [11] for studies of yellow, magenta and cyan azomethines, and Douglas *et al.* for studies of magenta PT dyes [10], although in these studies a simplified form of the Balzani equation, the Sandros equation (equation 6.10) was used.

$$k_{ET} = k_{diff}/(1+e^{\Delta G/RT}) \quad \textbf{6.10}$$

However Berry *et al.* [9] used the full Balzani equation for work with cyan indoaniline azomethines, as did Abu-Hasanayn and Herkstroeter [20] with yellow dicarbonyl azomethines. It is from these studies that the triplet energies given in table 1.1 in the introduction are taken.

6.2.2 Experimental

The sensitisers chosen for the energy transfer studies were as follows:

Sensitiser	Triplet energy/kJ mol^{-1}
PdTPP [21]	174
ZnTPP [22]	153
TPP [23]	139
ZnP [24]	109
CAP [1]	105
GaNC [23]	81
SnNC [23]	79

Table 6.1: Triplet energies of the sensitisers used.
SnNC - tin naphthalocyanine, GaNC - gallium naphthalocyanine,
CAP - chloroaluminium phthalocyanine, ZnP - zinc phthalocyanine,
TPP - tetraphenylporphyrin, ZnTPP – zinc tetraphenylporphyrin,
PdTPP - palladium tetraphenylporphyrin.

Nanosecond flash photolysis experiments were carried out using 532 or 355 nm radiation from an Nd/YAG laser (Spectron Lasers) and an Applied Photophysics Laser Kinetic Spectrometer. The unfocussed excitation beam was ~ 1 cm in diameter, with a pulse duration of ~ 16 ns, and pulse energy of 15 mJ. Samples were contained in 1 cm or 0.5 cm cells and the transmission monitored at 90^0 to the excitation pulse. Transient kinetic data were recorded on a Gould OS4072 digital oscilloscope and transferred *via* a Picolog data logger to a PC for kinetic analysis. A pulsed xenon arc source was used as monitoring beam for studies in the microsecond time domain, and either this lamp in continuous mode, or a stabilized 100 W tungsten lamp, was used

for studies in the millisecond time range. All energy transfer studies were carried out using solutions deoxygenated by purging with nitrogen.

Choice of solvent was dictated by dye and sensitiser solubility. In particular SnNC and GaNC are insoluble in most solvents and show a propensity to aggregate even in solvents in which they appear to dissolve [17]. In order to prepare solutions of SnNC and GaNC free of aggregation these sensitisers were dissolved in 1-chloronaphthalene with refluxing at 180°C for 2 hours. The 6-CN dye has poor solubility in ethanol and therefore acetone was used as solvent for studies with this dye. For energy transfer studies with 1-chloronaphthalene as solvent 532 nm excitation was used; for energy transfer studies in other solvents 355 nm excitation was used. For porphyrin sensitisers the decay of sensitiser triplet states was followed at the triplet-triplet absorption maximum, *ca.* 450 nm, while for phthalocyanine and naphthalocyanine sensitisers recovery of the ground state absorption was used. Error estimates are given as one standard deviation.

6.2.3 Results and discussion

In all cases the only transients observed were those due to the triplet state of the sensitiser and the isomer of the dye which is formed as a result of both triplet sensitized isomerisation and direct isomerisation by dye absorption of some of the excitation pulse. No long-lived products other than the dye isomer, and no obvious degradation of either dye or sensitiser was observed.

Typical kinetic data are shown in figure 6.2 and table 6.2 collects quenching rate constants for all of the dye-sensitiser combinations used. For high energy sensitisers the rate constants are essentially independent of sensitiser energy and constant at *ca.* 1/3-1/2 of the full diffusion controlled rate constants, k_d, as calculated using the simple Stokes-Einstein relationship, which, for the three solvents, used are: ethanol 5.8×10^9; acetone 2.2×10^{10}; 1-chloronaphthalene 2.2×10^9 mol dm^{-3} s^{-1} at 22°C [25]. For lower energy sensitisers the rate constants decrease with decreasing sensitiser energy.

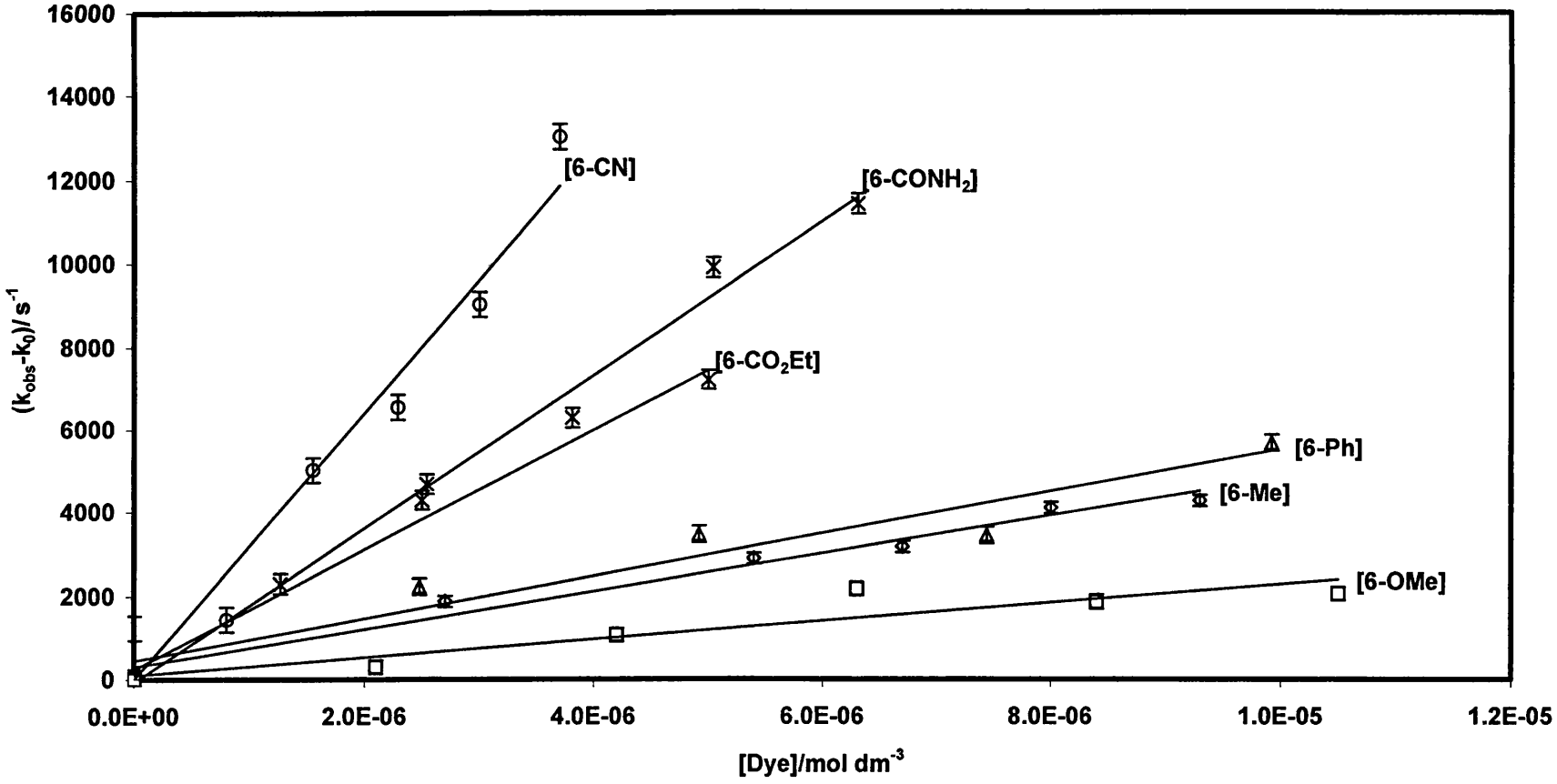

Figure 6.2: (k_{obs}-k_0) vs [dye] for quenching of ZnPC. k_{obs} is the observed first order rate constant in the presence of dye while k_0 is in the absence of dye.

Dye	λ_{max} energy/ kJ mol^{-1}	k_q/ 10^9 mol dm^{-3} s^{-1} SnNC (E_T = 79 kJmol^{-1})	GaNC (E_T = 81 kJmol^{-1})	CAP (E_T = 105 kJmol^{-1})	ZnPC (E_T =109 kJmol^{-1})	TPP (E_T =139 kJmol^{-1})	ZnTPP (E_T =153 kJmol^{-1})	PdTPP (E_T = 105 kJmol^{-1})	k_{en}/ 10^9 s^{-1}	E_T / kJ mol^{-1}
6-OMe	219	*<0.1*	*<0.1*	0.42 (±0.07)	0.22 (±0.05)	1.85 (±0.12)	2.42 (±0.26)	2.96 (±0.14)	5.0	**112** 114.5‡
6-Me	213	*<0.1*	*<0.1*	0.31 (±0.05)	0.45 (±0.04)	2.72 (±0.39)	2.27 (±0.26)	2.40 (±0.20)	5.0	**111.5** 113‡
6-Ph	205	*<0.1*	*<0.1*	0.36 (±0.05)	0.51 (±0.06)	2.04 (±0.16)	1.53 (±0.44)	2.25 (±0.04)	5.0	**111** [110, 2] 112.5‡
6-CO_2Et	197 *193*	*<0.1*	*0.22 (±0.09)*	1.22 (±0.39)	1.85 (±0.10)	2.45 (±0.26)	2.34 (±0.20)	2.63 (±0.31) *0.60(±0.08)*	3.4	**106** [103, 3]# 108‡ *84*
6-$CONH_2$	192	*<0.1*	*<0.1*	0.37 (±0.06)	1.44 (±0.23)	1.52 (±0.34)	2.20 (±0.13)	2.65 (±0.17)	4.0	**109** [108, 2] 109.5‡
6-CN	*188 *185*	*0.08 (±0.06)*	*0.14 (±0.05)*	*1.40 (±0.18)*	*3.21 (±0.37)	*3.00 (±0.51)	*3.96 (±0.28)	*2.65 (±0.20)	*4.4	***107** *[106,1] *104.5‡ *84*

Table 6.2: Summary of energy transfer kinetics and triplet energy estimations for the dye series.
Data in italics are for 1-chloronaphthalene as solvent. *With acetone as solvent. For all other data ethanol was the solvent. Where an upper limit is given no measurable energy transfer was observed. E_T values in bold are for $\Delta G^{\ddagger}(0) = 0$, those in parentheses are for cases were the data were consistent with $\Delta G^{\ddagger}(0) \neq 0$ (for these entries the first number is E_T and the second is $\Delta G^{\ddagger}(0)$). ‡data from analysis of ZnPC quenching data using k_{en} average and $\Delta G^{\ddagger}(0) = 0$.
#obtained including data for quenching of $^1O_2{}^*$ with $k_q = 1 \times 10^8$ mol dm^{-3} s^{-1}.

All data was fitted using Jandel and microsoft Excel computer programmes. k_{en} values and other parameters for energy transfer quenching by the dye series are collected in table 6.2. There is little variation in k_{en} with dye-sensitiser combinations with k_{en} = 3.4-5 × 10^9 s^{-1}. This gives a value for k_{trans} of only *ca.* 0.001, but values of this magnitude are common for triplet-triplet energy transfer rate constants and are taken to reflect the stringent orbital overlap criterion for such processes [19, 20]. In analyzing the data to obtain ΔG and $\Delta G^{\ddagger}(0)$ it is important to note that there are relatively few data points which explore the region in which ΔG is small and positive, and therefore determination of $\Delta G^{\ddagger}(0)$ is difficult. However, for none of the data for quenching of porphyrin or phthalocyanine sensitisers in ethanol or acetone is it necessary to invoke a $\Delta G^{\ddagger}(0)$ value much greater than a few kJ mol^{-1}.

The largest value necessary to give a good fit to the data is 3 kJ mol^{-1}, and that is for the 6-CO_2Et dye when we include the quenching rate for singlet oxygen from previous work is included as a data point in the analysis [5]. This generality of behaviour with regard to both k_{en} and $\Delta G^{\ddagger}(0)$ is apparent in figure 6.3 which shows data for all dyes in the form of log k_q vs ΔG plots using best fit dye triplet energies. The lines are theoretical curves for the average k_{en} value, with $\Delta G^{\ddagger}(0)$ = 0, and the Stokes-Einstein diffusion rate constants for ethanol and acetone. Triplet energies of the dyes, calculated for both $\Delta G^{\ddagger}(0)$ =0, and where appropriate $\Delta G^{\ddagger}(0) \neq 0$, are included in table 6.2.

Of all the sensitisers used ZnPC gives the greatest dye to dye variation in k_q, and analysis of rate constants for quenching of this one sensitiser using the Balzani equation give estimates of dye triplet energies in which experimental variations are minimised. Values calculated in this way, with $\Delta G^{\ddagger}(0)$ = 0, are also included in table 6.2. They differ little from those calculated for each dye from the Balzani equation, but they do show a somewhat wider spread of energies.

In an attempt to obtain energy transfer data with lower energy sensitisers studies were carried out using tin and gallium naphthalocyanines in 1-chloronaphthalene. Only 6-CO_2Et and 6-CN gave measurable quenching constants with these sensitisers, and of these only 6-CN gave measurable quenching for both ^{3}SnNC* and ^{3}GaNC*. In order

to estimate $k_{q(max)}$ for these reactions k_q for quenching of $^3PdTPP^*$ by dye 6-CO_2Et was measured in 1-chloronaphthalene. The k_{en} value obtained in this way is *ca.* 1/5 of that for the other sensitisers in ethanolic or acetone solutions, and the quenching rate constants are very high considering the low energies of $^3SnNC^*$ and $^3GaNC^*$. The highest triplet energies, *i.e.* those with $\Delta G^{\ddagger}(0) = 0$, consistent with these experimental data are 84 kJ mol^{-1}, much lower than those suggested by data in ethanol or acetone. The need to change solvent introduces the complicating factor of a shift in λ_{max}, and possibly dye triplet energy, to lower energy (see table 6.2), but, from the shift in $E_{\lambda max}$ this is estimated to be at most 4 kJ mol^{-1}, too small to cause the effect seen. The fact that k_{en} is solvent dependent may indicate that dye reorganisational energies are solvent dependent.

For the 6-OMe, 6-Me, 6-Ph and 6-$CONH_2$ dyes the quenching data in ethanol allows some confidence in the triplet energies, and the general observation of a low or zero $\Delta G^{\ddagger}(0)$ as given in table 6.2. For 6-CO_2Et previous data [5] supports the assignment of the triplet energy in ethanol as 103 kJ mol^{-1}, with $\Delta G^{\ddagger}(0) = 3$ kJ mol^{-1}. However, for 6-CN the E_T estimation in acetone relies heavily on just one data point close to $k_{q(max)}$, and it should be noted that these data could be fitted well using lower triplet energies provided $\Delta G^{\ddagger}(0)$ is increased to compensate (*e.g.* with $E_T = 84$ kJ mol^{-1} and $\Delta G^{\ddagger}(0) = 7$ kJ mol^{-1}). For this reason 107 kJ mol^{-1} is considered to be an upper limit for the triplet energy of 6-CN and 88 kJ mol^{-1} to be a reasonable estimate of the lower limit for E_T for this dye in acetone.

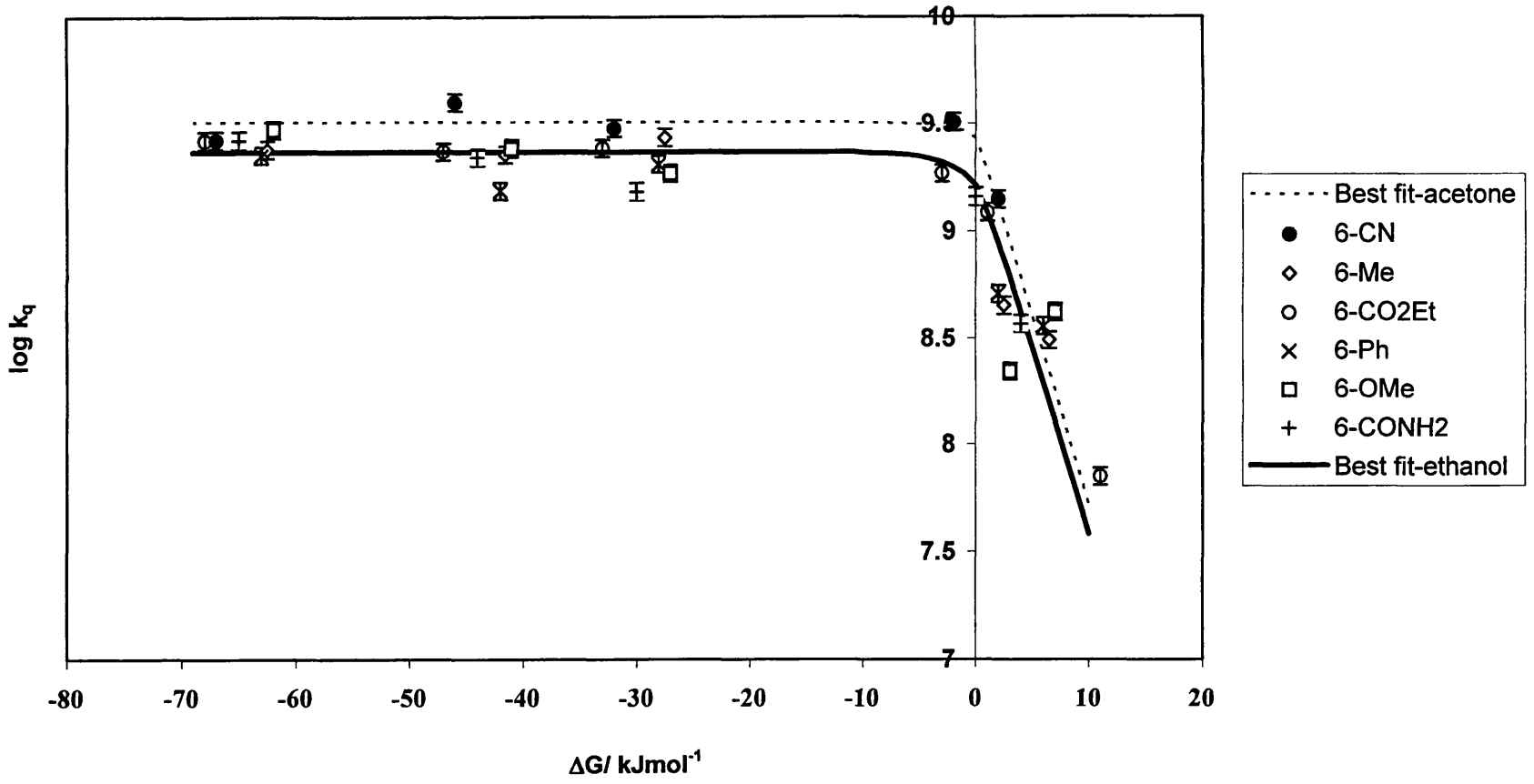

Figure 6.3: Log k_q against ΔG calculated using the E_T values given in table 6.2 with $\Delta G^{\ddagger}(0) = 0$. The lines are theoretical for $k_{en} = 4.5 \times 10^9$ s^{-1}, $k_{-d} = 1.15\ k_d$ and $\Delta G^{\ddagger}(0) = 0$. Solid line represents data for the 6-Me, 6-OMe, 6-Ph, 6-CO_2Et and 6-$CONH_2$ dyes with k_d (ethanol) = 5.8×10^9 mol dm^{-3} s^{-1}. Dashed line for data for 6-CN, with k_d (acetone) = 2.2×10^{10} mol dm^{-3} s^{-1}.

6.2.4 Correlation between absorption maximum and triplet energies of azomethine dyes

Figure 6.4 gives a plot of energy of λ_{max} against triplet energies for azomethine dyes for which these data are available in the literature. (While λ_{max} corresponds to the most probable transition rather than the 0-0 transition, it is both experimentally easily accessible and it is the technologically more relevant property.) The data show a reasonable correlation between absorption energy and triplet energy if the higher of the two triplet state energies obtained for the yellow azomethines, *i.e.* those accessible by adiabatic energy transfer, are used. The relationship between dye triplet state energy and dye singlet state energy is given by equation 6.11.

$$E_T = 0.69(\pm 0.04)\, E_{\lambda max} - 33(\pm 9)\ \text{kJ mol}^{-1} \qquad \textbf{6.11}$$

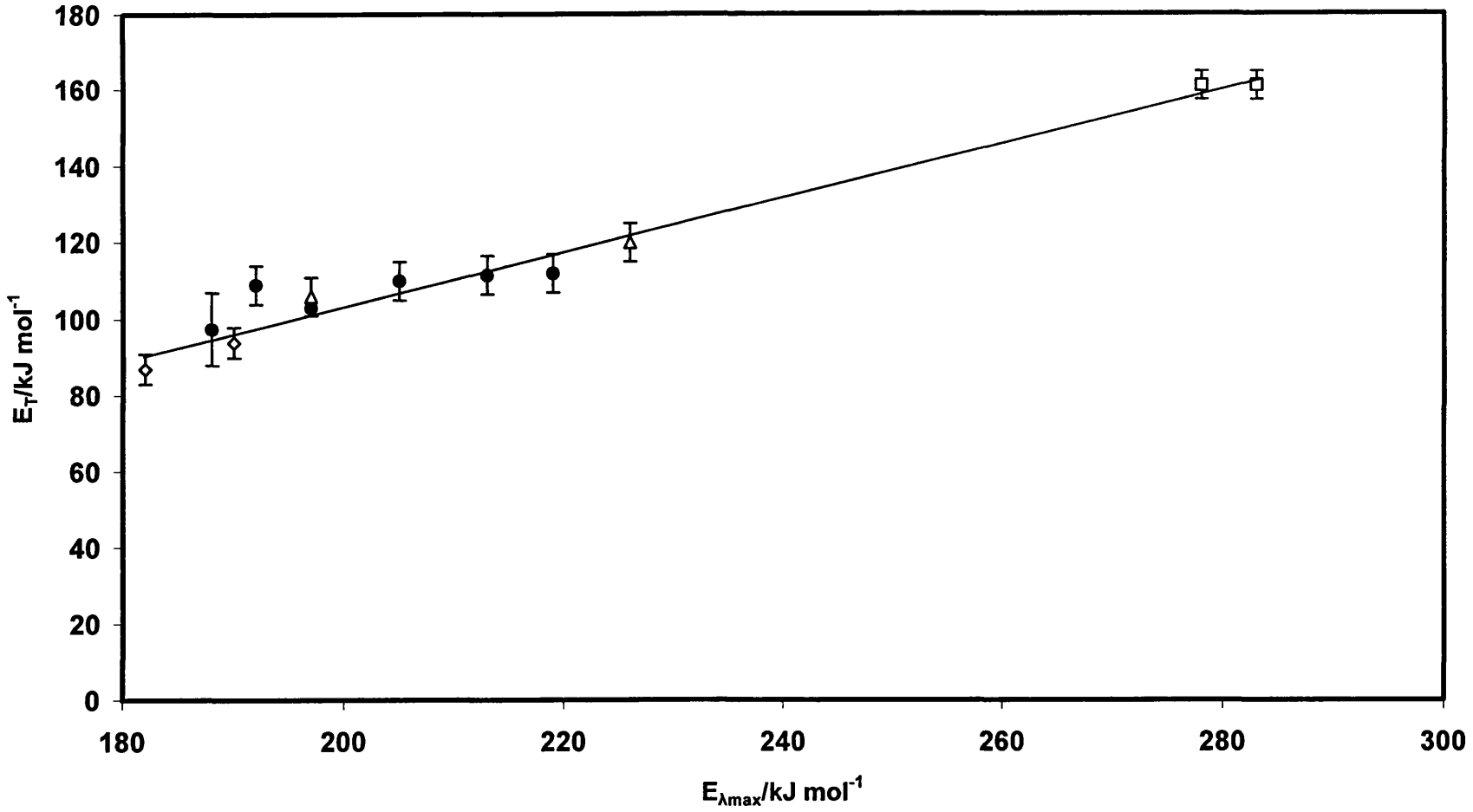

Figure 6.4: Triplet energy against $E_{\lambda max}$ for azomethine dyes. Cyan indoanilines [9] (diamonds); magenta/cyan pyrazolotriazoles [5] (triangles); yellow dicarbonylazomethines [20] (squares); magenta/cyan pyrazolotriazoles, this work (filled circles).

6.3 Quenching of singlet oxygen by PT dyes

6.3.1 Introduction

The main routes of physical quenching of $^1O_2$ are by either a charge transfer or energy transfer mechanism. Charge transfer mechanisms generally predominate when a molecule has a triplet energy significantly higher than that of $^1O_2$ and also a low oxidation potential which encourages exciplex formation.

For molecules which have E_T close to, or below 94.7 kJ mol^{-1}, the mechanism of energy transfer generally predominates and follows a similar pattern as given previously (note section 6.2.1). $^1O_2$ behaves as a sensitiser (such as a porphyrin or phthalocyanine) and reactions will proceed at close to the diffusion controlled limit. When considering a dye series of known triplet energies a clear pattern should emerge, that as the dye E_T moves further from the energy level of singlet oxygen so too should the rate of quenching decrease in magnitude.

It must be noted that the interaction between singlet oxygen and a quencher cannot always be explicitly classed as 'charge transfer' or 'energy transfer'. Rajadurai and Das [26], when discussing the physical quenching of nickelocene attributed both energy and charge transfer as components of the quenching process .

Encinas *et al.* [27] detailed the mechanism for quenching of singlet oxygen by hydroxylamines, with the formation of a free radical being important in the charge transfer interaction.

A comprehensive overview of singlet oxygen quenching by hydrazines was undertaken by Clennan *et al.* [28]. In a more complete description of the charge transfer process, the mechanism was characterized as a 'contact charge transfer spin-orbit coupling induced process', whereby the singlet and triplet state oxygen-hydrazine complexes are coupled *via* spin-orbit interaction, which then dissociate to form ground state oxygen and hydrazine.

Darmanyan *et al.* [29] described the charge transfer relationship between singlet oxygen and amines/aromatic hydrocarbons as occurring *via* reversible charge transfer involving an exciplex.

Recent work, measuring the rate of singlet oxygen quenching for a range of cyanine dyes [30] compared the rate of quenching and absorption maxima, and the rate of quenching and dye oxidation potentials. Smith *et al.* [6] measured the quenching rate constants for a number of azomethine dyes with absorption maxima stretching from yellow to cyan. He concluded that a combination of charge transfer and energy transfer mechanisms contributed to the quenching process. An investigation of the triplet states of yellow dicarbonyl azomethine dyes concluded that interaction between dye triplet states and $^1O_2$ occurred *via* energy and electron transfer reactions [20].

In further work on the mechanism of the physical quenching of singlet oxygen by PT dyes, it was found that the 6-CO_2Et dye isomerised as a consequence of quenching singlet oxygen (Quenching rate = 6 (±1) × 10^7 $mol^{-1}dm^3$ sec^{-1} [31]). It is known that for this dye isomerisation can be triplet sensitised. This isomerisation process, combined with the absence of any transients during photolysis experiments support an energy transfer mechanism in this case.

$^1O_2^* \rightarrow {}^3O_2$ **6.12**

$^1O_2^* + DYE \rightarrow {}^3O_2 + ISOMER$ **6.13**

$^1O_2^* + ISOMER \rightarrow {}^3O_2 + DYE$ **6.14**

$ISOMER \rightarrow DYE$ **6.15**

6.3.2 Experimental

Singlet oxygen yields were obtained using an Applied Photophysics laser flash photolysis equipment using the third harmonic of a Nd:YAG laser (Spectra Physics) with excitation wavelength of 355 nm. The phosphorescence of singlet oxygen was monitored at 1270 nm. Phenalanone (concentration *ca.*1 × 10^{-5} mol dm^{-3}) in air equilibrated acetonitrile (τ $^1O_2$ = 60μs[2]) was the sensitiser used to generate $^1O_2$, and dye was added to provide a concentration range of 1-8 ×10^{-5} mol dm^3.

The kinetic traces at various dye concentrations were then used to calculate k_q. Each trace is an average of 32 'shots'. Examples of the traces obtained are shown in figures 6.5 and 6.6.

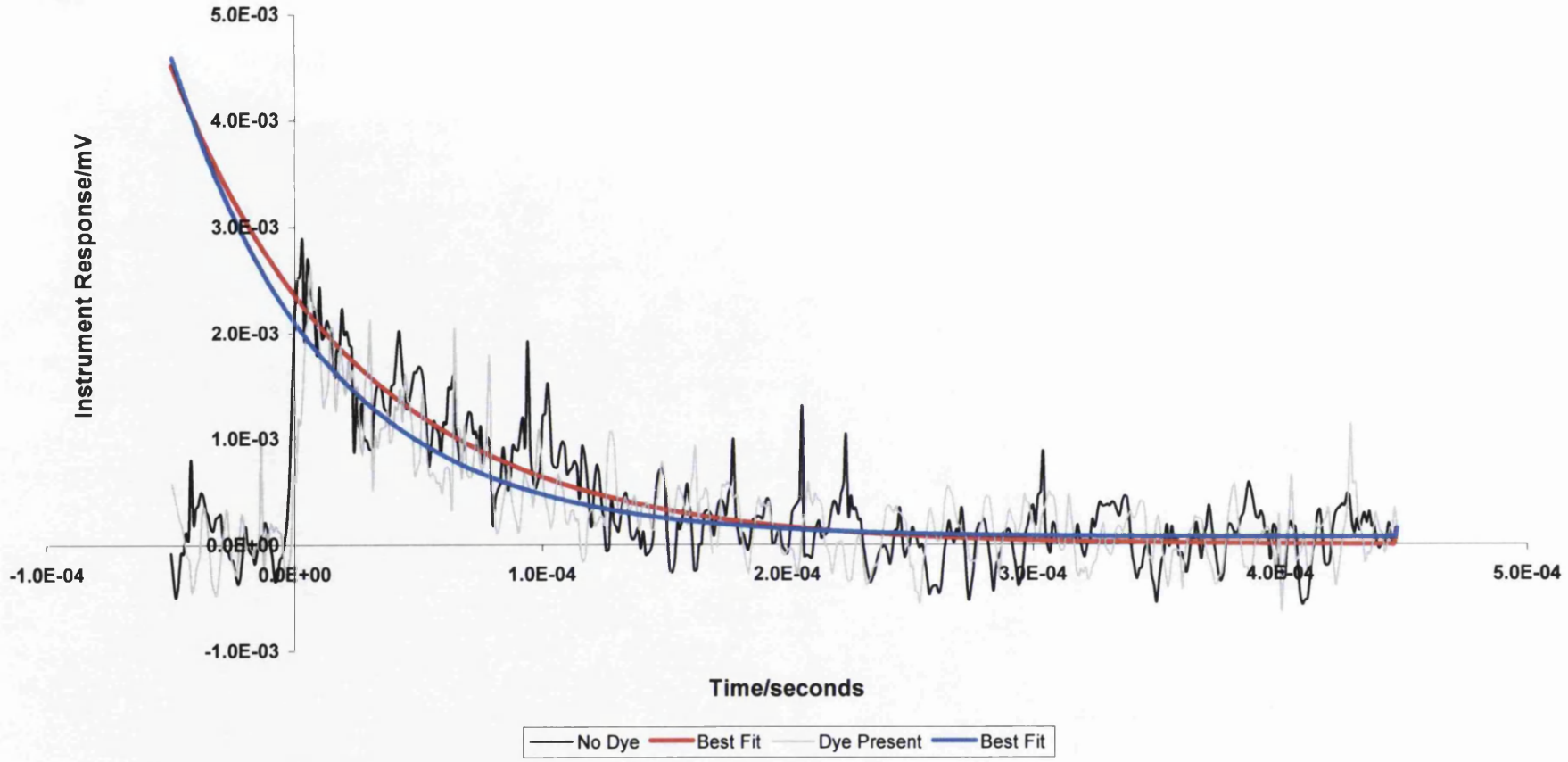

Figure 6.5: Oxygen luminescence decay curves at 1270 nm. The dye present is 6-OMe, at a concentration of *ca*.8 $\times 10^{-5}$moldm^3. Note that there is not a large difference in the decay shape of both traces, implying a comparatively slow rate of quenching $^1O_2$ by the dye.

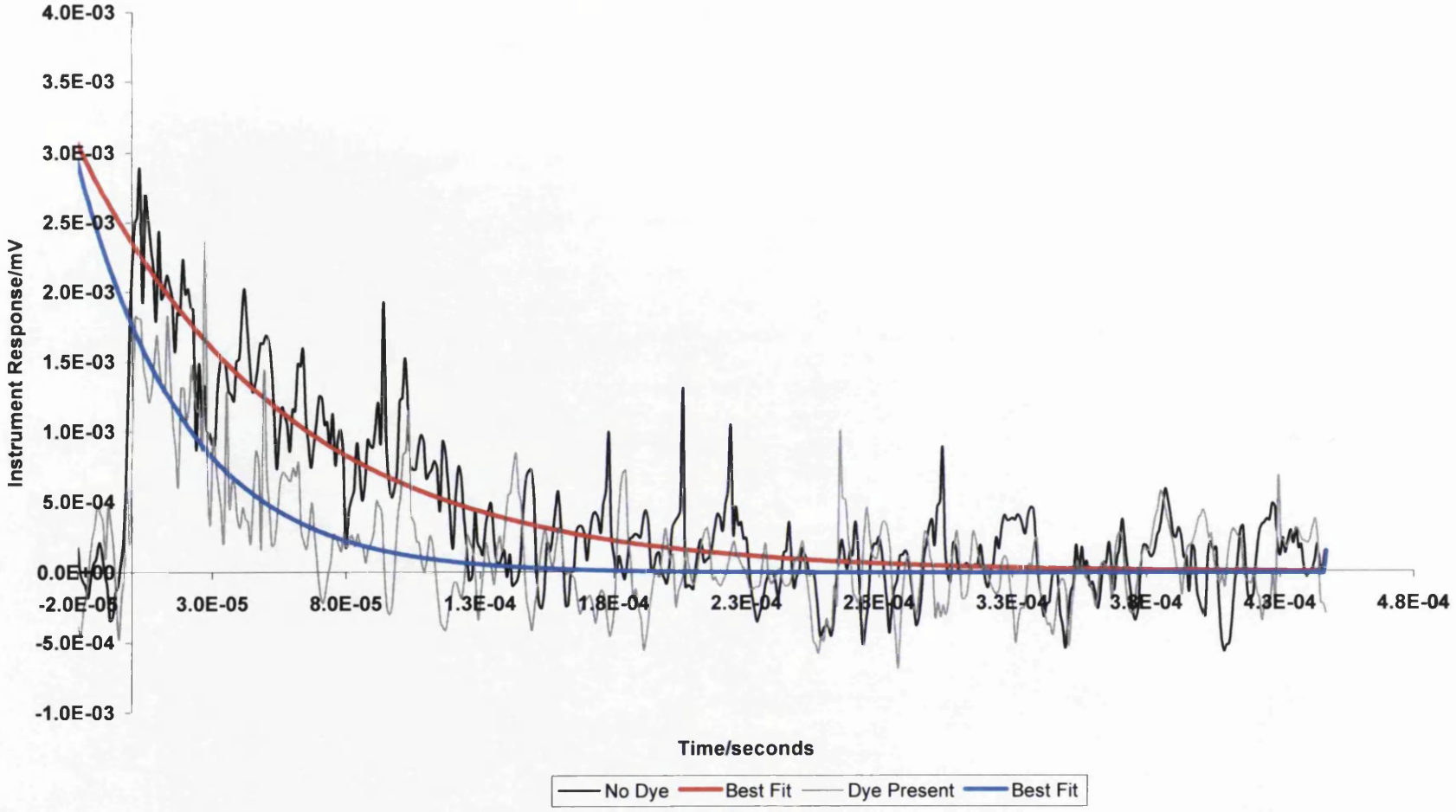

Figure 6.6: Oxygen luminescence decay curves at 1270 nm. The dye present is 6-CN, at a concentration of *ca.*8 × 10^{-5}mol dm^{-3}. This dye quenches $^1O_2$ at a faster rate than the 6-OMe dye shown in figure 6.5.

6.3.3 Results and discussion

Figure 6.7 gives plots of the rate constant for the decay of singlet oxygen against dye concentration: as dye concentration increases, so too does the rate of quenching $^1O_2$. Table 6.3 gives measured oxygen quenching rate constants. In general as the dye absorption maximum moves toward the cyan, and dye triplet energy decreases the quenching rate increases. Also included in table 6.3 are the expected rate constants calculated using the Balzani equation with the kinetic parameters, k_d, k_{en}, k_{-d}, used in the triplet energy transfer studies described in section 6.2.3

Dye	E_T (kJ mol^{-1})	λ_{max} (nm)	Observed k_q ($\times 10^8$) (mol^{-1} dm^3 s^{-1})	Calculated k_q ($\times 10^8$) (mol^{-1}dm^3 s^{-1})
6-OMe	**112**	541	0.13 (±0.08)	0.02
6-Me	**111.5**	555	0.89 (±0.20)	0.03
6-Ph	**111**	580	0.43 (±0.13)	0.03
6-CO_2Et	**106**	605	1.98 (±0.14)	0.19
6-$CONH_2$	**109**	616	1.02 (±0.12)	0.06
6-CN	**107**	635	1.36 (±0.15)	0.04

Table 6.3: Summary of $^1O_2$ quenching kinetics for the dye series. E_T values taken from table 6.1.

In general as dye triplet energy decreases the quenching rate increases. The value for 6-CO_2Et is also in good agreement with previous recorded values [5] of 2 (±0.2) × 10^8 and 9 (±5) × 10^8 mol^{-1} dm^3 s^{-1} for the quenching rate constant of this dye. Previous work, using both steady state and flash photolysis methods gave only an upper limit for 6-Me of 6 × 10^7 mol^{-1} dm^3 s^{-1} [5], which is slightly lower than the value of 8.9(±0.2) × 10^7 mol^{-1}dm^3 s^{-1} measured here.

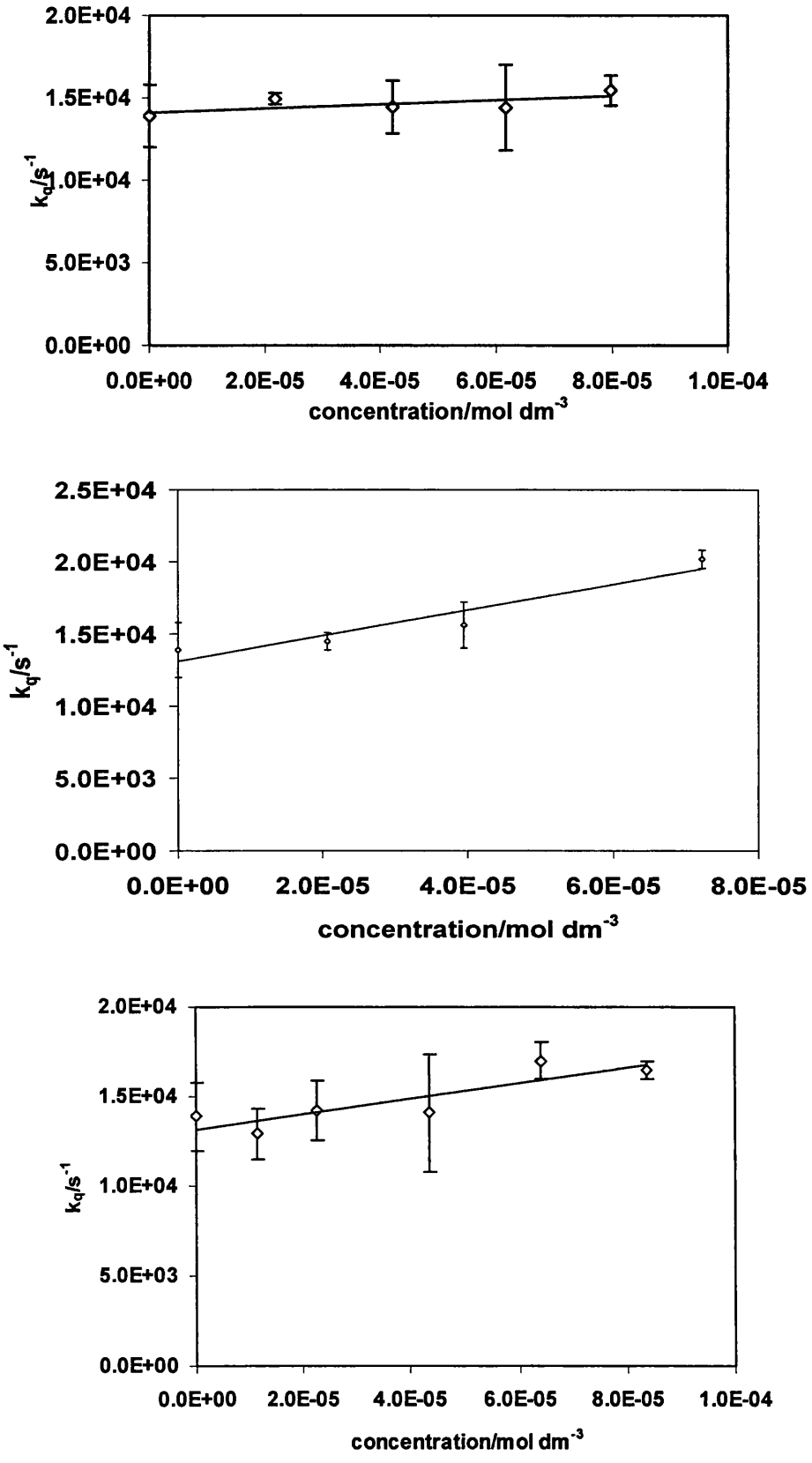

Figure 6.7: $^1O_2$ quenching data of the dye series.
6-OMe (top), 6-Me (middle), 6-Ph (bottom).

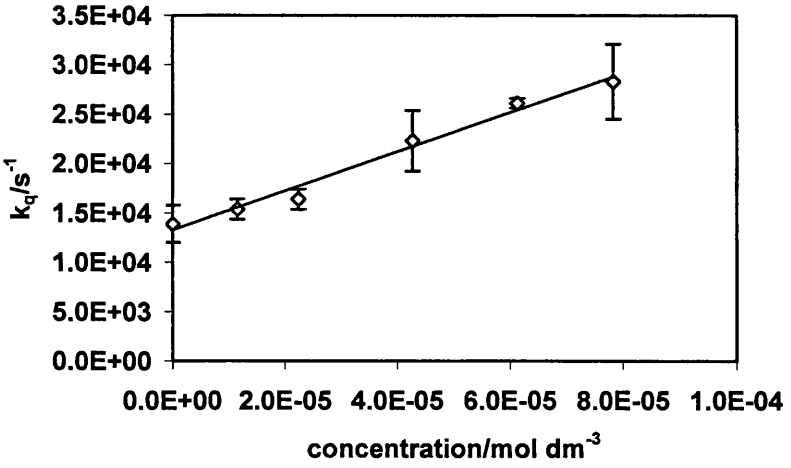

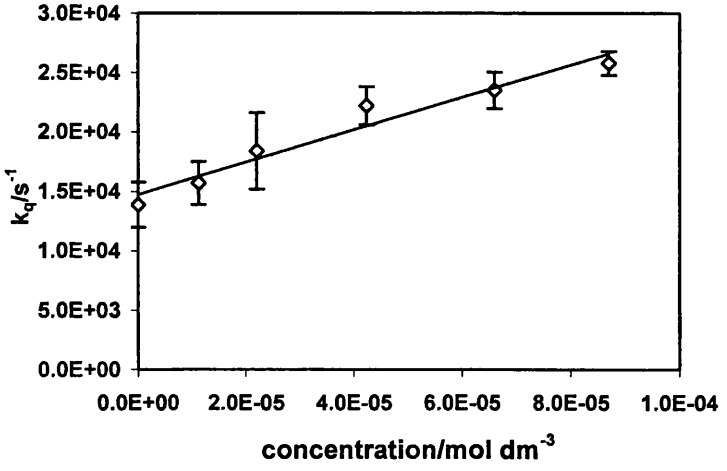

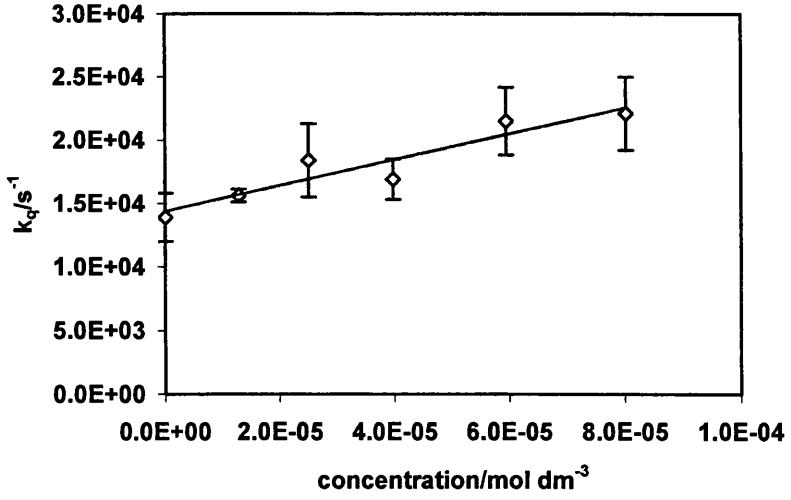

Figure 6.7: $^1O_2$ quenching data of the dye series.
6-CO_2Et (top), 6-$CONH_2$ (middle), 6-CN (bottom).

Smith *et al.* [6] discussed the relationship between absorption maxima and quenching rate constants, noting that a plot of absorption band energy against quenching efficiency had a very shallow slope (-0.09 mol/kcal), much less than would be expected if the energy of the state involved in energy transfer changed in parallel with the absorption maximum and the reaction followed the Arrhenius equation (-0.73 mol/kcal). Kanofsky *et al.* [30] in discussing singlet oxygen quenching by cyanine dyes also found a shallow slope for the same plot, reporting values of -0.11 mol/kcal.

The relationship between absorption maxima and quenching efficiencies for the PT dye series is given in figure 6.8. (The predicted slope of -1/2.3RT is also shown.) The slope of −0.11 mol/kcal is in excellent agreement with the work of both Smith and Kanofsky.

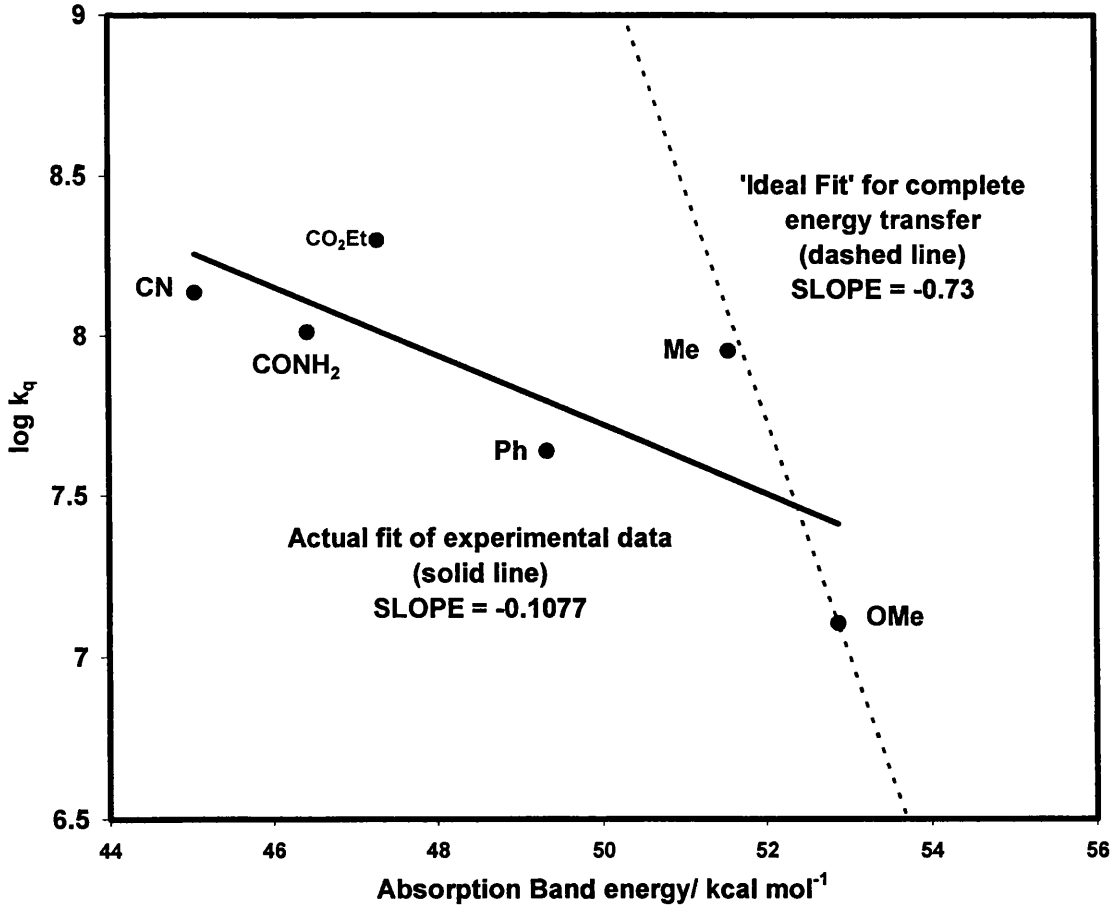

Figure 6.8: The relationship between absorption band energy (obtained from λ_{max} in acetonitrile) and quenching efficiency. Note that energy values are given in kcal/mol to enable ease of comparison with previous work [6, 30].

6.4 Correlating singlet oxygen quenching data and triplet energy transfer data

As table 6.3 shows a cursory comparison between observed quenching rate constants and those calculated using dye triplet energy and the Balzani equation with parameters appropriate for triplet energy transfer between dye and porphyrin/phthalocyanine sensitisers indicated that the observed rate constants are much higher than expected using this calculation. This discrepancy may arise because of changes in quenching mechanism or changes in the Balzani parameters. There is no evidence for electron transfer products arising from dye quenching of singlet oxygen and therefore the Balzani parameters have been looked at.

One of the key components in the Balzani equation is the term used for the diffusion controlled rate constants k_d and k_{-d}. Generally k_d is obtained from Stokes' law and the following expression

$$k_d = 8RT/3\eta \qquad \textbf{6.17}$$

(where η is the viscosity, R the gas constant and T the temperature).

However, Ware [31], whilst measuring the diffusion controlled rate of singlet state quenching by oxygen in various solvents, concluded that k_d is higher than that given by the simple Stokes equation because of the high mobility of the small O_2 molecule. He calculated that the diffusion controlled limit of $^1O_2$ quenching in common organic solvents at room temperature is 3×10^{10} mol dm^{-3} s^{-1} [2, 31]. Changing k_d alone is not enough to bring the singlet oxygen data in line with triplet sensitiser quenching. However an examination of the Balzani equation shows that the maximum possible rate constant is given by equation 6.9 :

$$k_{q(max)} = k_d/(1+ k_{-d}/k_{en}) \qquad \textbf{6.9}$$

and as this equation shows k_{en} can also be a significant factor in determining the rate constant. In particular the ratio of k_{en} to k_{-d} influence the highest rate constant obtainable. If $k_{en} >> k_{-d}$ then the maximum rate constant is the diffusion controlled rate constant, if $k_{en} = k_{-d}$ then the maximum rate constant is ½ that for diffusion

control, and if $k_{en} << k_{-d}$ the maximum rate constant will be significantly less than that for diffusion control. In the triplet sensitiser study k_{en} was found to be similar in value to k_{-d}, and the transmission coefficients for these reactions were therefore typically *ca.* 0.001. However examination of a range of reactions in which oxygen acts as a quencher [25] shows that such reactions often have rate constants as high as k_{-d} obtained for oxygen by Ware, and, as equation 6.9 shows, this necessarily means that both $k_{en} >> k_{-d}$ and the transmission coefficient is much greater than the value of 0.001 for quenching of porphyrin and phthalocyanine sensitisers by PT dyes. It would appear then that for many excited state reactions involving oxygen both k_{en} and the transmission coefficient are significantly higher than those from triplet-triplet energy transfer. Using these ideas we have correlated the triplet sensitiser quenching data have been correlated with the singlet oxygen quenching data by using higher k_d and k_{en} values for the latter. Table 6.4 displays the values used for the best fit, while figure 6.9 shows typical data, obtained for the 6-CN dye.

Dye	**E_T (kJ mol^{-1})**	**$\Delta G^{\ddagger}$ (kJ mol^{-1})**	**k_{en}^{*} ($\times 10^9$ s^{-1})**	**k_d^{*} ($\times 10^9$ s^{-1})**	**$k_{en}^{\#}$ ($\times 10^{11}$ s^{-1})**	**$k_d^{\#}$ ($\times 10^{10}$ s^{-1})**
6-OMe	112	7	5	5.8	2	3
6-Me	111.5	15	8	5.8	4	3
6-Ph	111	8	4	5.8	1.2	3
6-CO_2Et	106	5	5	5.8	1	3
6-$CONH_2$	109	6	4	5.8	0.8	3
6-CN	107	2	20	5.8	4	3

Table 6.4: Best fit values for the six dyes studied. * denotes values used for porphyin and naphthalocyanine sensitisers, # for $^1O_2$ as sensitiser. Average k_{en} for the former = 7.7×10^9 s^{-1}, average k_{en} for the latter = 2.2×10^{11} s^{-1}.

Figure 6.10 shows a Balzani plot using singlet oxygen only as sensitiser and the dye series as quenchers using the average k_{en} value from table 6.4. The reasonable fit further underlines the need for an increase in k_{en} values when using singlet oxygen as a sensitiser.

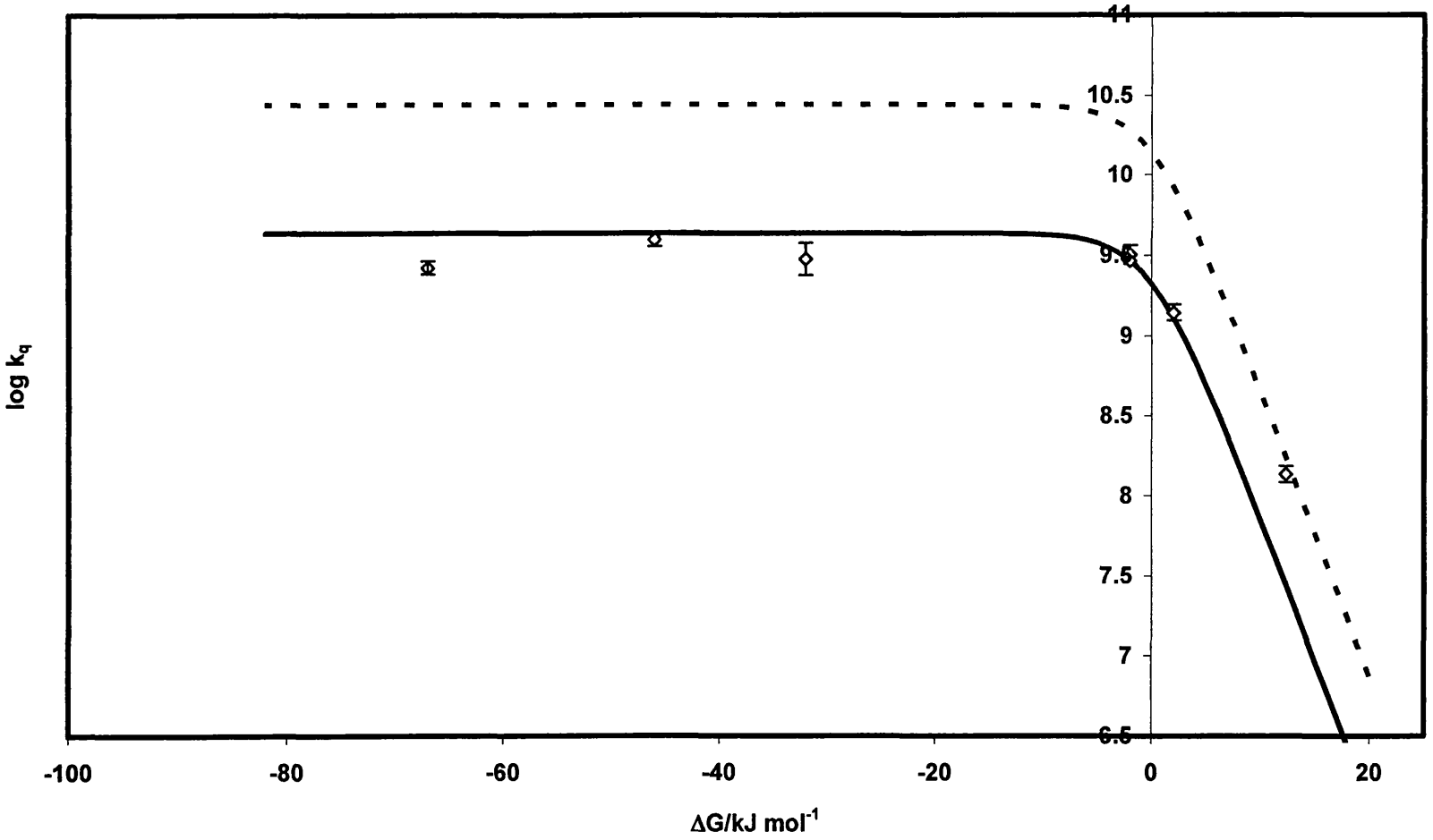

Figure 6.9: log k_q against ΔG for 6-CN using an E_T value of 107 kJ mol^{-1} and $\Delta G^{\ddagger}$ of 2 kJ mol^{-1}, k_{diff} of 5.8×10^9 mol dm^{-3} s^{-1} and k_{en} of 2×10^{10}s^{-1} (solid line) and k_d of 3×10^{10} mol dm^{-3} s^{-1} and k_{en} of 4×10^{11} s^{-1} (dashed line).

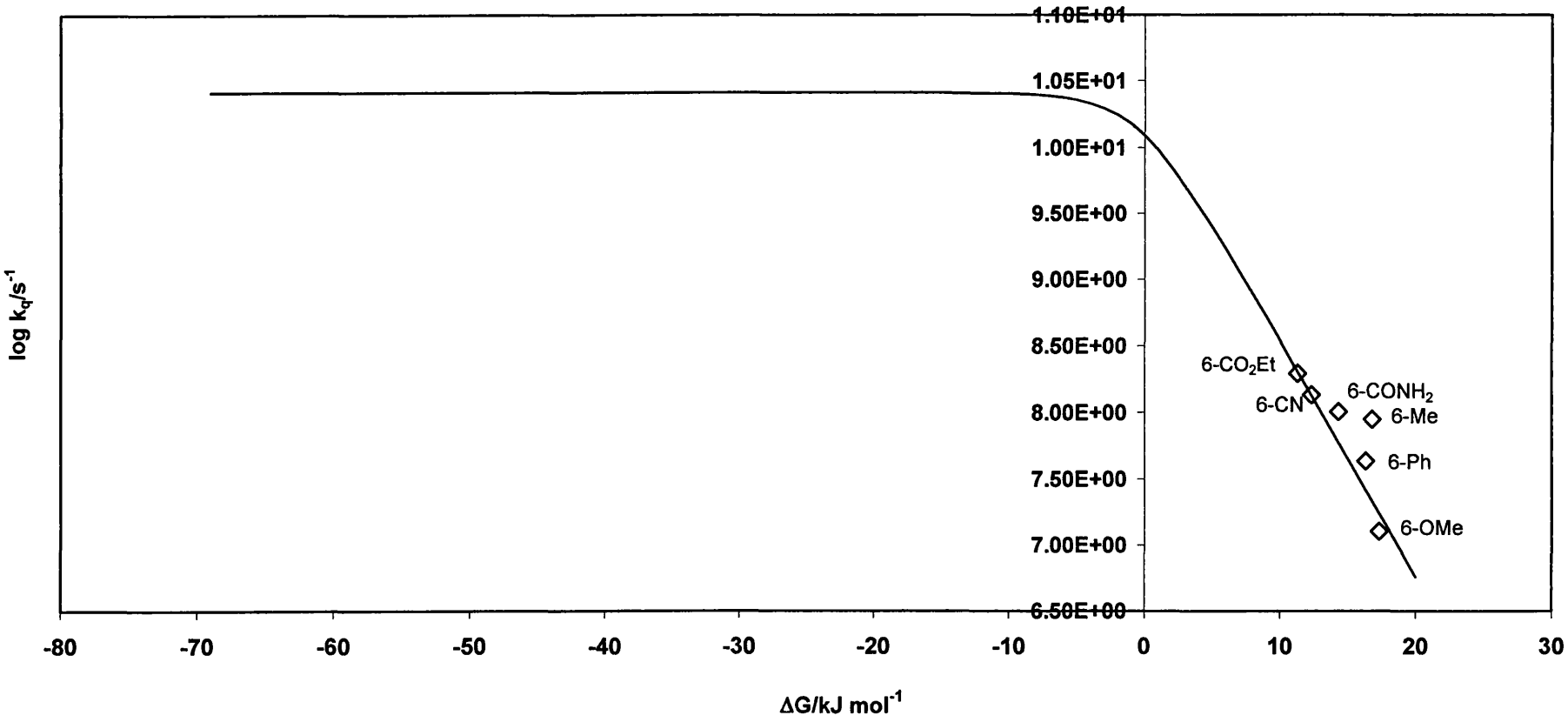

Figure 6.10: log k_q against ΔG calculated using the E_T values given in table 6.4 with $\Delta G^{\ddagger}(0) = 0$. The lines are theoretical for $k_{en} = 2.2 \times 10^{11}\ s^{-1}$, $k_{-d} = 1.15\ k_d$ and $\Delta G^{\ddagger}(0) = 0$. The line of best fit is given for $k_d = 3 \times 10^{10}$ mol $dm^{-3}\ s^{-1}$.

6.5 Quantum Yields of singlet oxygen production

Several attempts were made to measure the singlet oxygen production of the dye series. Direct irradiation, even with a high intensity Xenon Arc lamp did not yield measurable amounts of singlet oxygen (measured by monitoring the loss of DPBF as a singlet oxygen acceptor). Singlet oxygen luminescence techniques were also not sensitive enough to measure any production of $^1O_2$. Therefore only an upper limit can be given for the quantum yields of singlet oxygen production by the dye series, of $<1 \times 10^{-4}$ [32].

6.6 Conclusions

Triplet energy transfer measurements from porphyrin and phthalocyanine sensitisers indicate the triplet energies of six pyrazolotriazole azomethine dyes with absorption maxima in ethanol of 546-633 nm lie in the range 115-88 kJ mol^{-1}. The energy transfer rates can be well approximated using the Balzani equation with a zero or small reorganization energy, and a transmission coefficient *ca.* 1/1000 that of the fully adiabatic value of k_BT/h. Comparison of all the available data on triplet energies of azomethine dyes suggests a relationship between the dye absorption energies and dye triplet energies of the form: $E_T = 0.69(\pm0.04)(E_{\lambda max}) - 33(\pm9)$ kJ mol^{-1}.

The rate of oxygen quenching by the dye series is in the range 0.13-1.89 $\times10^8$ kJ mol^{-1}. The correlation between absorption energy and quenching rate constant reveals that complete energy transfer between dye and $^1O_2$* does not occur.

In order to correlate singlet oxygen quenching data and triplet energy transfer data the values for k_{en} and k_d need to be altered in order to compensate for mobility of the comparatively small $^1O_2$ molecule (when compared to the bulkier porphyrin and naphthalocyanine sensitisers).

The quantum yield of $^1O_2$ production could not be measured leading to an estimate of $<1 \times10^{-4}$ for the dye series.

6.7 References

1) N.J.Turro, *Modern Molecular Photochemisty*, **1991,** University Science Books, USA.

2) C.Schweitzer and R.Schmidt, *Chem. Rev.*, **2003**, 1685.

3) A.A.Gorman and M.A..Rodgers, *Handbook of Organic Photochemistry,* **1989**, CRC Press Inc., USA, Chapter 10.

4) F.Wilkinson, W.P.Helman and A.B.Ross, *J. Phys. Chem. Ref. Data*, **1995**, 24, 663.

5) P.Douglas, S.M.Townsend, R.Ratcliffe, *J. Imag. Sci.*, **1991**, 35, 211.

6) W.F.Smith Jr.,W.G.Herkstoeter and K.L.Eddy, *J. Am. Chem. Soc.*, **1975**, 97, 2764.

7) W.F.Smith Jr.,W.G.Herkstoeter and K.L.Eddy, *Photogr. Sci. Eng.*, **1976**, 20, 140.

8) Z.Kucybala, I.Pyszka, B.Marciniak, G.Hug, *J. Chem. Soc. Perkin Trans. 2*, **1999**, 2147.

9) R.J.Berry, P.Douglas, M.S.Garley, T.Jolly, D.Clarke, H.Moglestue, H.Walker, C.J.Winscom, *J. Photochem. Photobiol. A : Chem.*, **1999**, 120, 33.

10) P.Douglas, *J. Photogr. Sci.*, **1988**, 36, 83.

11) W.G.Herkstroeter, *J. Am. Chem. Soc.*, **1975**, 97, 3090.

12) W.G.Herkstroeter, *J. Am. Chem. Soc.*, **1976**, 98, 6210.

13) F.Wilkinson, D.R.Worrall, R.S.Chittock, *Chem. Phys. Letters*, **1990**, 174, 416.

14) F.Wilkinson, D.Worrall, D.McGarvey, A.Goodwin, A.Langley, *J. Chem. Soc. Faraday Trans.*, **1993**, 89, 2385.

15) W.G.Herkstroeter, *J. Am. Chem. Soc.*, **1973**, 95, 8686.

16) W.G.Herkstroeter, *J. Am. Chem. Soc.*, **1976**, 98, 6210.

17) R.J.Berry, *PhD Thesis*, **1998**, University of Wales Swansea.

18) K.Sandros, *Acta Chem. Scand.*, **1964**, 27, 3021.

19) V.Balzani, F.Bolletta, F.Scandola, *J. Am. Chem. Soc.*, **1980**, 102, 2152.

20) Faraj Abu-Hasanayn and W.G.Herkstroeter, *J. Phys. Chem. A*, **2001**, 105, 1214.

21) J.R.Darwent,, P.Douglas, A.Harriman, G.Porter, M.C.Richoux, *Coord. Chem. Rev.*, **1982**, 83-126.

22) D.J.Quimby, F.R.Longo, *J. Am. Chem. Soc.*, **1975**, 97, 5111.

23) W.E.Ford, B.D.Rikter, M.A.J. Rodgers, *J. Am. Chem. Soc.*, **1989**, 111, 2362.

24) P.S.Vincette, E.M.Voight, K.E.Rieckhoff, *J. Chem. Phys.*, **1971**, 55, 4131.

25) S.Murov, I.Carmichael and G.Hug, *Handbook of Photochemistry*, 2nd Ed., **1993**, Marcel Dekker Publishers, USA.

26) S.Rajadurai and P.K. Das, *Journal of Photochemistry*, **1987**, 37, 33.

27) M.V.Encinas, E.Lemp and E.A Lissi, *J. Chem. Soc. Perkin Trans. 2*, **1987**, 1125.

28) E.L.Clennan, L.J.Noe, E.Szneler and T.Wen, *J. Am. Chem. Soc.*, **1990**, 112, 5080.

29) A.P.Darmanyan, W.S.Jenks and P.Jardon, *J. Phys. Chem. A*, **1998**, 102, 7420.

30) J.R.Kanofsky and P.D.Sima, *Photochemistry and Photobiology*, **2000**, 71, 361.

31) W.R.Ware, *J. Phys. Chem.*, **1962**, 66, 455.

32) R.Ratcliffe, *Fourth International Conference on Mechanisms of Reactions in Solution, University of Kent at Canterbury*, **1986**, Poster abstract no. 60.

Chapter 7

Fade studies in preformed dye coatings

7.1 Quantum Yields of fade

7.1.1 Introduction

Although determining the photophysical and photochemical properties of image dyes in solution is important, it is also vital to compare these characteristics to the behaviour of these dyes in photographic environments *i.e.* suspended in an emulsion and coated onto a transparent base so as to mimic a photographic coating. Once a coating of the model dye has been made it is possible to measure one of the most important physical characteristics of an image dye, its light fastness.

Smith *et al.* [1] measured the fading efficiencies of pyrazolone dyes in oil-in-gelatin dispersions, and they concluded that this dye class fades *via* a triplet and singlet state mechanism. More recently Townsend [2] studied the fade characteristics of a ballasted PT dye with and without a stabiliser present using both SANS (Simulated Artificial North Sky) and HID (High Intensity Daylight) techniques. Kucybala *et al.* [3] studied the bleaching of azomethine dyes in solution and this work supported Smith's assumption that photofading was dependent on both the triplet and singlet states of the dye. Interestingly it also showed that when isomerisation about the azomethine bond is prevented/restricted then photofading occurs at a faster rate, implying that when this route of deactivation is not present, self-sensitising fading processes are more likely to occur.

Parmar [4] used rapid fade and HID techniques to measure the effect of aggregation at the oleophilic-aqueous interface on dye light stability. He concluded that aggregation does not have a great effect on lightfastness in either oxidative or reductive conditions, and that for oxidative conditions an important parameter is the rate at which oxygen diffuses through the air-gelatin interface.

7.1.2 Experimental

In order to compare the light fastness of the dye series, as well as trying to deduce whether the primary fade mechanism of the dyes is oxidative or reductive, the dyes were incorporated into an oil in gelatin emulsion, coated onto a transparent base and subjected to high intensity light under a nitrogen or oxygen atmosphere at different humidities. The optical density was monitored regularly at set time intervals in order to calculate the quantum yield of fade.The experimental details for the set up of the rapid fade are found in the experimental chapter, this includes details of any filters used, as well as the calibration of the light source in order to maintain constant photon flux for all of the coatings studied.

The preformed dye coatings were prepared as follows. 10 g of 2.5% gelatin w/w was added to 40 ml of 4% sodium dodecylsulphate solution and the resultant solution was gently warmed until all of the gelatin had melted.

35 mg of PT dye was then mixed well with 200 mg of *p*-dodecylphenol (PDP); 2 ml of ethyl acetate was added and the resultant solution was warmed on a hotplate, taking care that the ethyl acetate did not completely evaporate. 20 g of the gelatin-surfactant melt was then added to this dye-coupler solution, and together the mixture was ultrasonically dispersed using a soniprobe (Dawes 7530A) at full power (*ca.* 6 amps) for 5 minutes.

This dispersion was then kept warm in a custom made block (*ca.* 22°C), then 0.1 ml of hardener was added for each 3 ml portion of solution. Around 0.8 ml of this solution was then injected out onto an estar® base which was clamped onto a custom made PC controlled SSC (small scale coater). The coating was then 'rolled' onto the transparent base using a 100 μm roller. The coating was then left to dry at room temperature (20-22°C). Coatings for four of the dyes were made (6-OMe, 6-Me, 6-CO_2Et, 6-$CONH_2$). The 6-Ph dye could not be coated onto the estar base as it crystallised out of the gelatine melt immediately and not enough 6-CN dye was available for coating by this process.

The preformed coatings were then subjected to irradiation from a high intensity 'rapid fade' light source (details of which are given in Chapter 2) and the quantum yield of fade (Φ_{fade}) calculated by measuring the decrease in absorbance maxima as a function of time. Results from a typical example of a PT dye coating fade are shown below.

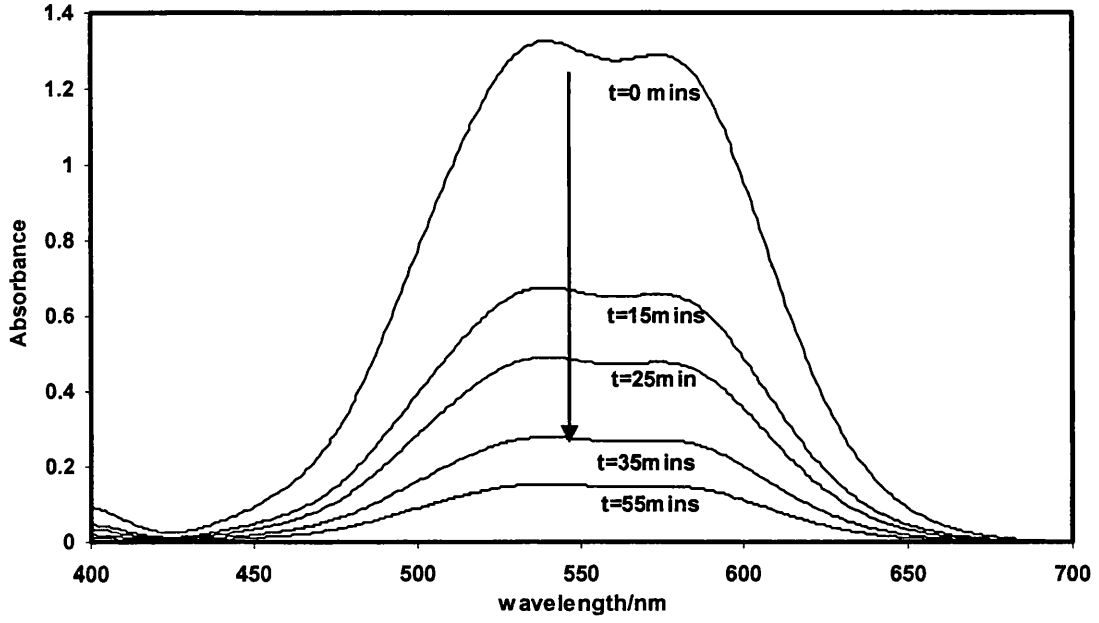

Figure 7.1: Absorbance spectra for a preformed coating of 6-Me, subjected to rapid fade in a 'dry oxygen' atmosphere.

In order to measure the Φ_{fade} a computer program was used [5] which takes into account the experimental data (time and absorbance of the sample) and the following expressions [4]:

$$\Phi_{fade} = \frac{R_{loss}}{I_a} \qquad 7.1$$

where R_{loss} is the rate at which degradation of dye molecules occurs and I_a is the rate at which photons are absorbed.

R_{loss} is obtained from the initial rate of loss of absorbance R_{OD}, usually measured over the first 10% of fade, the dye extinction coefficient, ε, and the irradiation area A_{irr}. (A factor of 1000 is necessary to rationalise for the units of ε.)

$$R_{loss} = \frac{R_{OD} \cdot A_{irr}}{1000\varepsilon} \qquad \textbf{7.2}$$

R_{loss} is the no. of molecules destroyed per unit time, and R_{OD} is the initial rate.

It must be noted that it is assumed that the no. of photons absorbed remains the same throughout the initial fade. This cannot be the case as the absorbance is decreasing as a result of dye degradation. However due to high concentrations of the coatings this does not lead to significant errors in the calculations.

7.1.3 Results and Discussion

Typical experimental data are shown for four of the dye series in figures 7.2-7.5, and the data are summarised in table 7.1. The quantum yields of fade are, as expected, very low.

Dye	E_T (kJ mol^{-1})	λ_{max} (nm)	Observed k_q ($x10^8$) ($mol^{-1}dm^3$ s^{-1})	Relative ϕ_{fl} ($\times 10^{-4}$)	Calculated τ_s (ps)	Φ_{fade} Dry nitrogen ($\times 10^{-7}$)	Φ_{fade} Wet nitrogen ($\times 10^{-7}$)	Φ_{fade} Dry oxygen ($\times 10^{-7}$)	Φ_{fade} Wet oxygen ($\times 10^{-7}$)
6-OMe	112	541	0.13 (±0.08)	6.3	2.7	8.9	2.9	110	100
6-Me	111.5	555	0.89 (±0.20)	3.7	1.8	0.3	0.2	27	35
6-CO_2Et	106	605	1.98 (±0.14)	2.3	1.1	0.9	1.9	5	4
6-$CONH_2$	109	616	1.02 (±0.12)	6.3	3.9	1.2	2.0	9	7

Table 7.1: Quantum yields of fade for preformed coatings and other relevant photochemical characteristics.

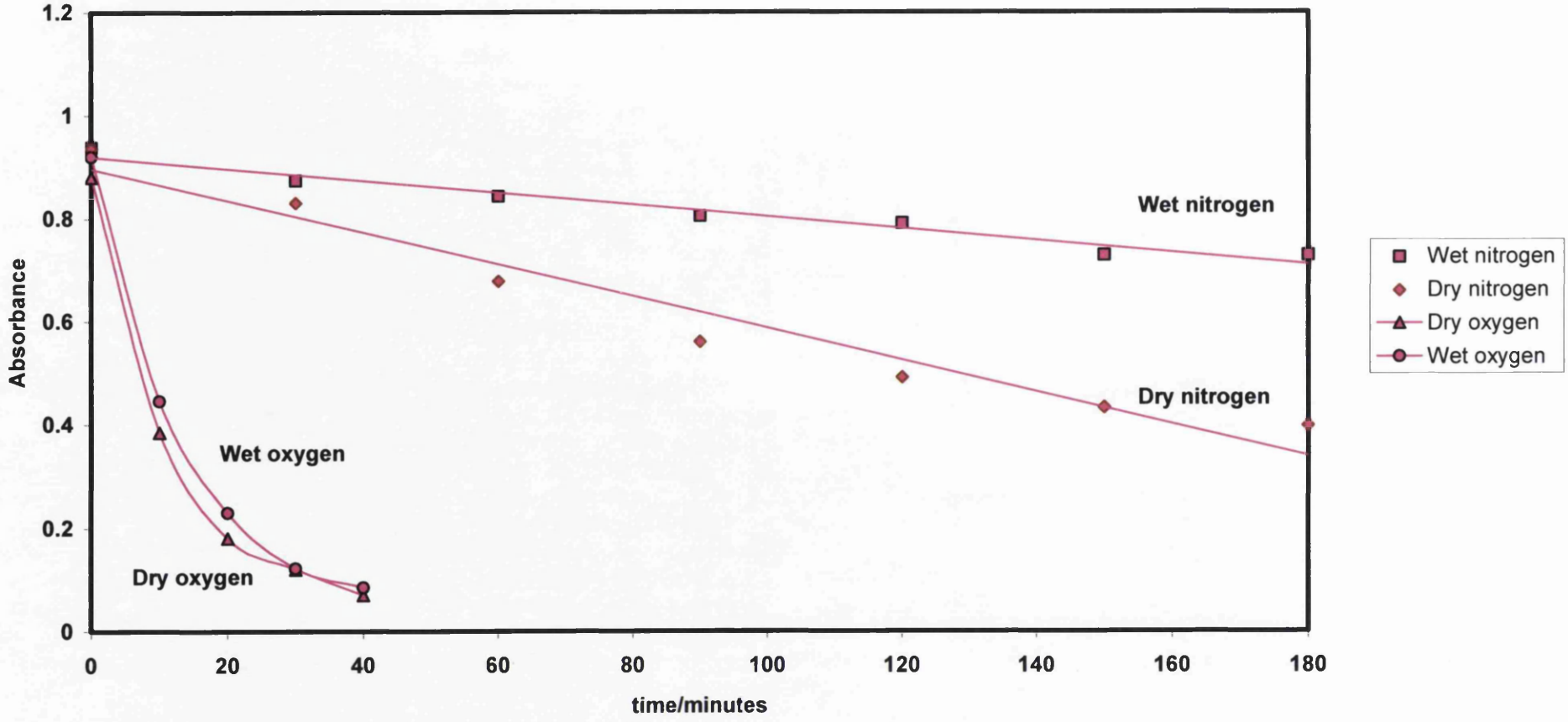

Figure 7.2: Fade of 6-OMe under varying atmospheric conditions in "rapid fade" apparatus.

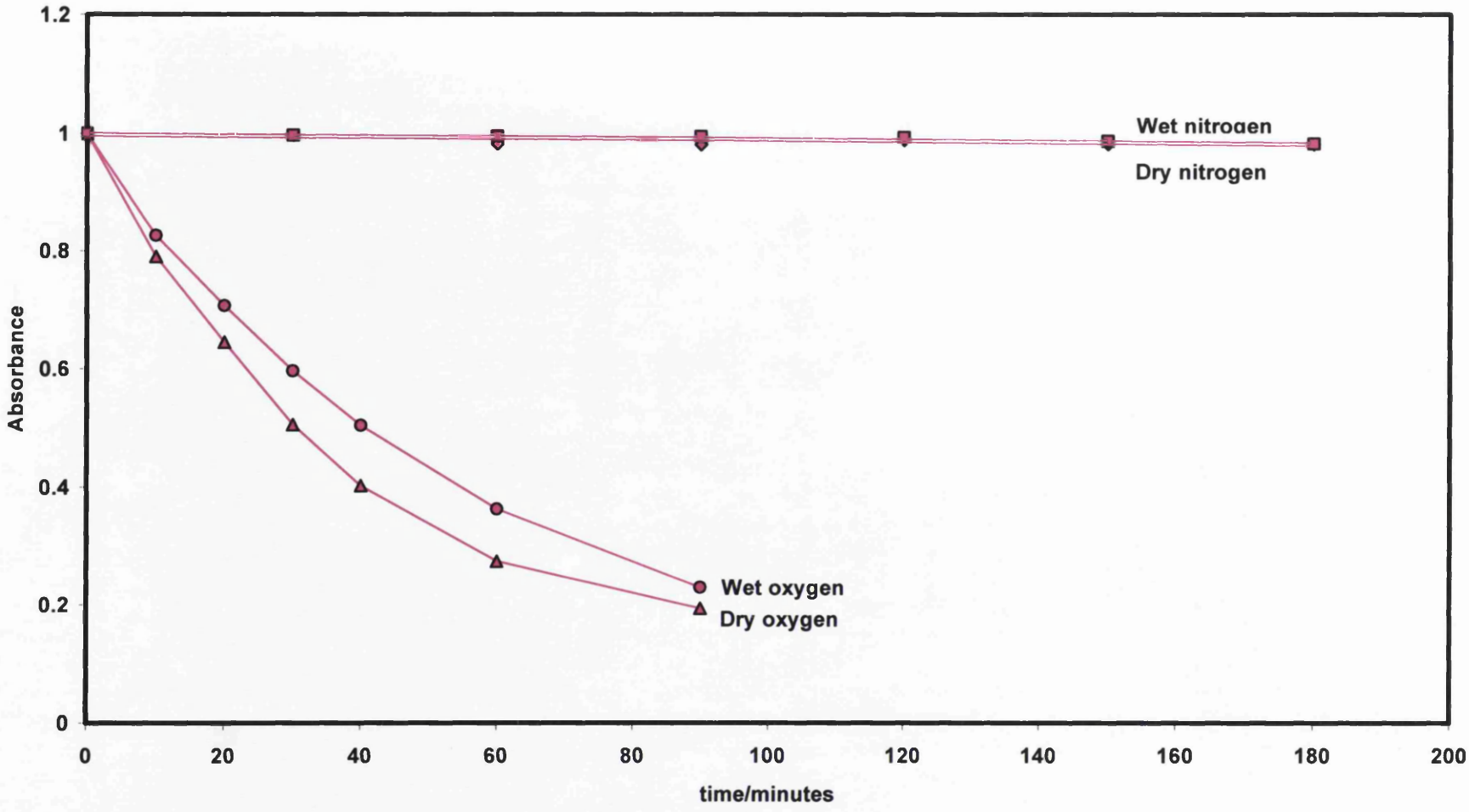

Figure 7.3: Fade of 6-Me under varying atmospheric conditions in "rapid fade" apparatus.

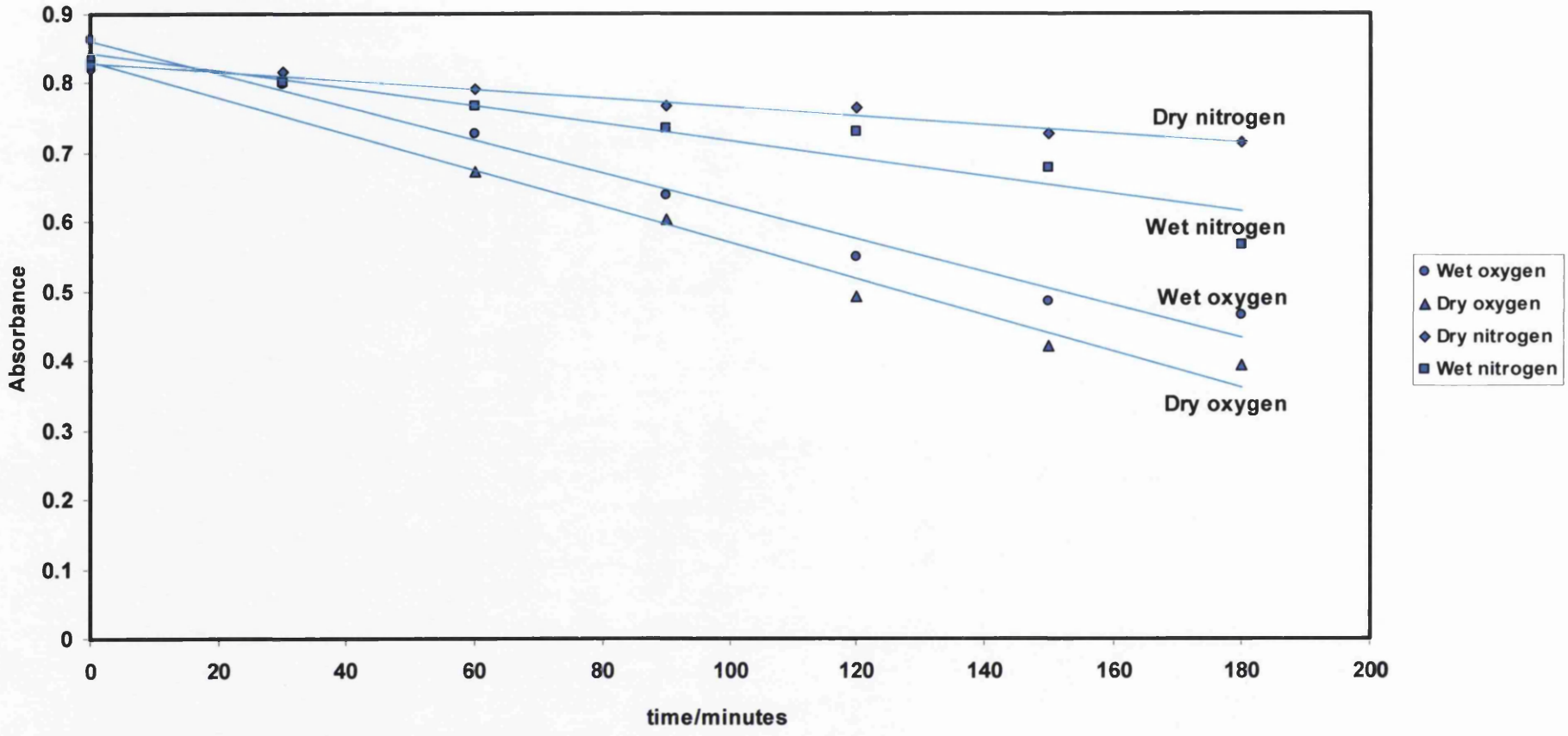

Figure 7.4: Fade of 6-CO_2Et under varying atmospheric conditions in "rapid fade" apparatus.

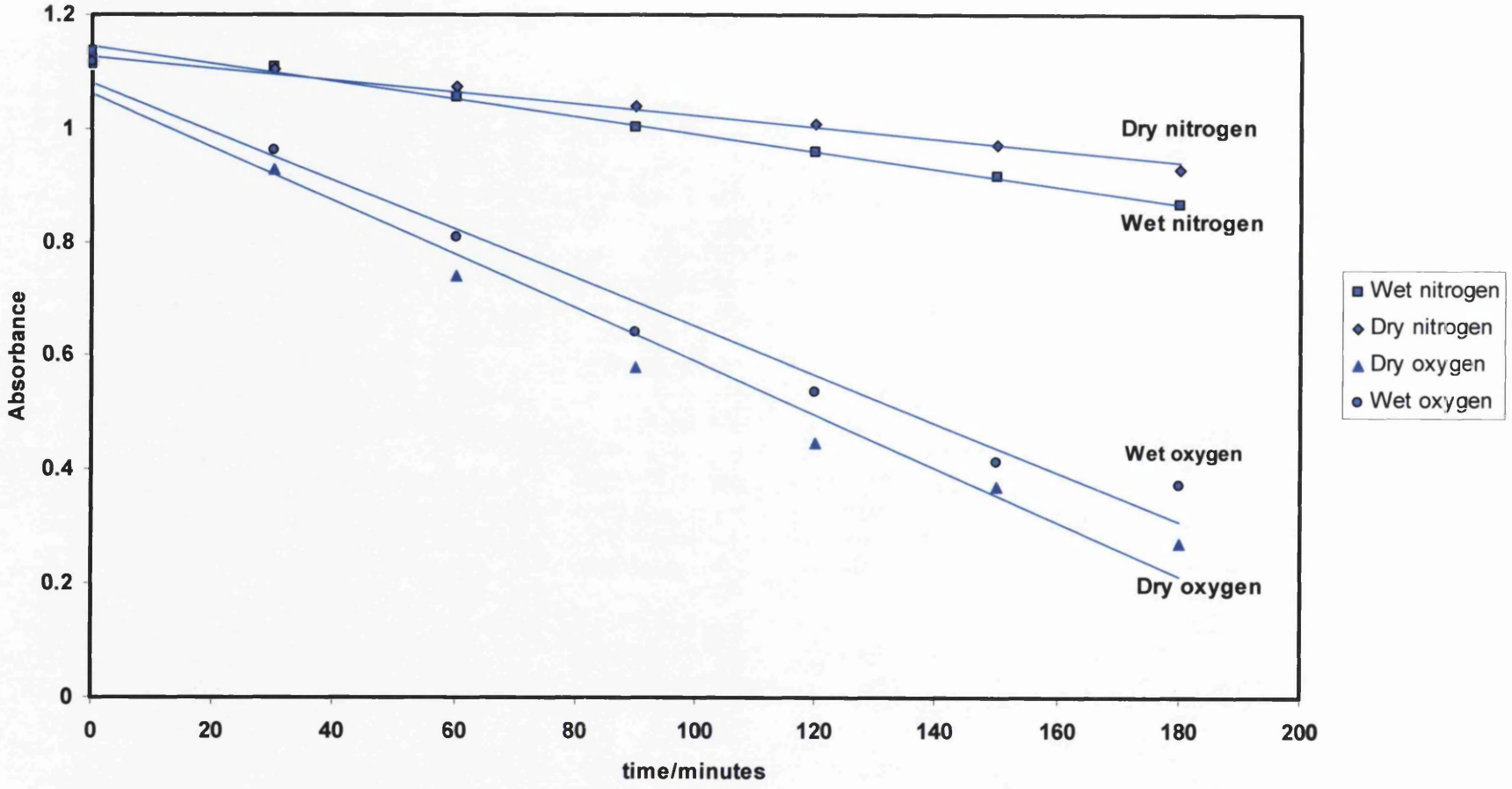

Figure 7.5: Fade of 6-$CONH_2$ under varying atmospheric conditions in "rapid fade" apparatus.

An important question which these data might shed some light on is which excited states, singlet or triplets, are involved in dye photodegradation. It was hoped that a comparison of fade data with excited state properties such as lifetimes and energies would show correlations which might indicate which states are involved.

7.3.1.1 Fade rates under nitrogen

Only for the 6-OMe dye is there any significant difference in quantum yield under wet or dry nitrogen, and even here it is only a factor of three. There is no correlation between quantum yield and dye triplet energy, dye singlet energy or quantum yield; but rather intriguingly there is a correlation with the calculated singlet lifetime (see table 7.1). With only four data points it is difficult to draw definitive conclusions but the data suggest that under nitrogen dye fade goes *via* a singlet state mechanism and the fade rate is dependent upon the singlet state lifetime. It is interesting to note that fading of the 6-Me dye is insensitive to whether the nitrogen is wet or dry, but dyes at the extremes of the absorption range show reversed sensitivities *i.e.* for the magenta 6-OMe the fade under dry nitrogen is *ca.* three times that under wet nitrogen while for cyan 6-CO_2Et and 6-$CONH_2$ dyes the quantum yields under wet nitrogen are *ca.* twice those under dry nitrogen.

7.3.1.2 Fade rates under oxygen

The fade rate under oxygen is an order of magnitude greater than that under nitrogen. Whether the fading is carried out under dry or wet oxygen makes little difference to the fade rate. The data show correlations between quantum yield of fade under oxygen and dye triplet energy, but not calculated singlet lifetime, or the calculated rate constant for generation of singlet oxygen from triplet dye. The *ca.* twenty fold variation in fade rate across the dye series is difficult to rationalise in terms of variation in singlet state energy, but could be understood in terms of a self-sensitised triplet mechanism in which quenching of singlet oxygen by dye is a determining factor.

The relatively high triplet energies suggest that all of the dyes will be comparably efficient at generating singlet oxygen from dye triplet, but they show very different singlet oxygen quenching rate constant. In the absence of data to the contrary the gross assumption will be made then that the quantum yield of singlet oxygen production is similar for all four dyes. Once generated, singlet oxygen can decay via three routes: reaction with the dye with a rate constant k_r, physical quenching by the dye with a rate constant k_q, or deactivation by either physical or chemical reaction with other materials such as coupler solvent *etc.* The quantum yield of fade is then given by:

$$\Phi_{fade} = \Phi^1 O_2 \left[\frac{k_r[Dye]}{k_d + k_r[Dye] + k_q[Dye]} \right] \qquad \textbf{7.3}$$

In the oil droplet of the photographic emulsion the concentration of dye is so high that quenching by dye could well be the limiting reaction which determines the lifetime of singlet oxygen in the droplet. If $k_q[Dye] > k_d$, and $k_r[Dye]$ then this gives:

$$\Phi_{fade} = \Phi^1 O_2 \frac{k_r}{k_q} \qquad \textbf{7.4}$$

and a plot of quantum yield of fade against $1/k_q$ gives a zero intercept and slope of quantum yield of singlet oxygen generation $\times$ k_r. Such a plot is shown in figure 7.6. The data are consistent with this interpretation, which of course requires that k_r for the dyes does not vary significantly. Using a singlet oxygen generation quantum yield of *ca.* 1×10^{-4} as the upper limit gives the lower limit of k_r to be 1×10^6.

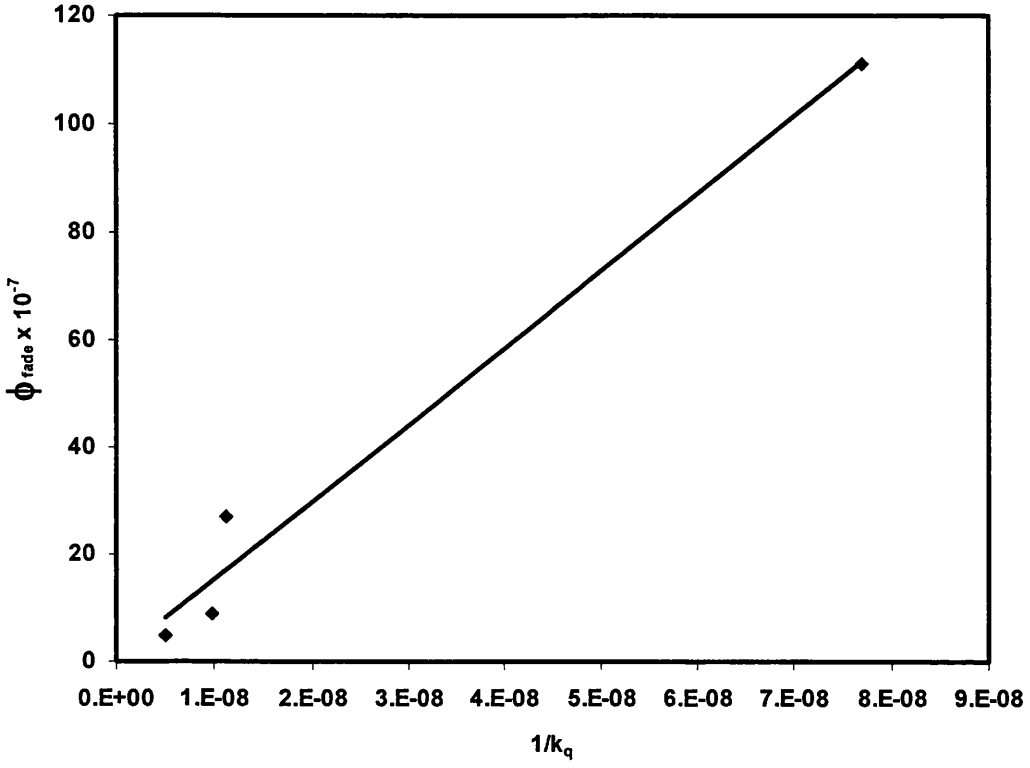

Figure 7.6: Correlation between the reciprocal of the $^1O_2$ quenching rates and Φ_{fade} in dry oxygen.

7.4 Conclusions

The quantum yield of fade of four PT dyes in model photographic coating has been determined for fading under wet and dry nitrogen and wet and dry oxygen. The quantum yield of fade under oxygen is about an order of magnitude higher than that under nitrogen.

Under nitrogen the fading of the 6-Me dye is insensitive to whether the nitrogen is wet or dry, but dyes at the extremes of the absorption range show reversed sensitivities *i.e.* for the magenta 6-OMe the fade under dry nitrogen is *ca.* three times that under wet nitrogen while for cyan 6-CO_2Et and 6-$CONH_2$ dyes the quantum yields under wet nitrogen are *ca.* twice those under dry nitrogen. The variation of quantum yield of fade with those photochemical parameters of the dyes discussed suggests that under nitrogen fading occurs *via* a singlet state route and that the quantum yield of fade is determined by the singlet state lifetime. Under oxygen whether the gas is wet or dry does not make a significant difference to fade efficiency. In this case the variation in quantum yield of fade with those photochemical parameters discussed earlier in the thesis suggests that fading under oxygen goes *via* a self-sensitised triplet state mechanism. Here, because of the high dye concentration in the oil droplet in the photographic dispersion the lifetime of singlet oxygen is determined primarily by the rate of quenching by dye, and it is the variation in the efficiency of this "self-protection" that determines the relative fade efficiencies of PT dyes.

7.5 References

1) W.F.Smith Jr.,W.G.Herkstoeter and K.L.Eddy, *Photogr. Sci. Eng.*, **1976**, 20, 140.

2) S.M.Townsend, *PhD Thesis*, **1991**, University of Wales Swansea.

3) Z.Kucybala, I.Pyszka, B.Marciniak, G.Hug, *J. Chem. Soc. Perkin Trans. 2*, **1999**, 2147.

4) C.K.Parmar, *PhD thesis,* **2001**, Imperial College of Science, Technology and Medicine.

5) Computer program developed by C.Winscom, Kodak Ltd.

APPENDICES CONTENTS

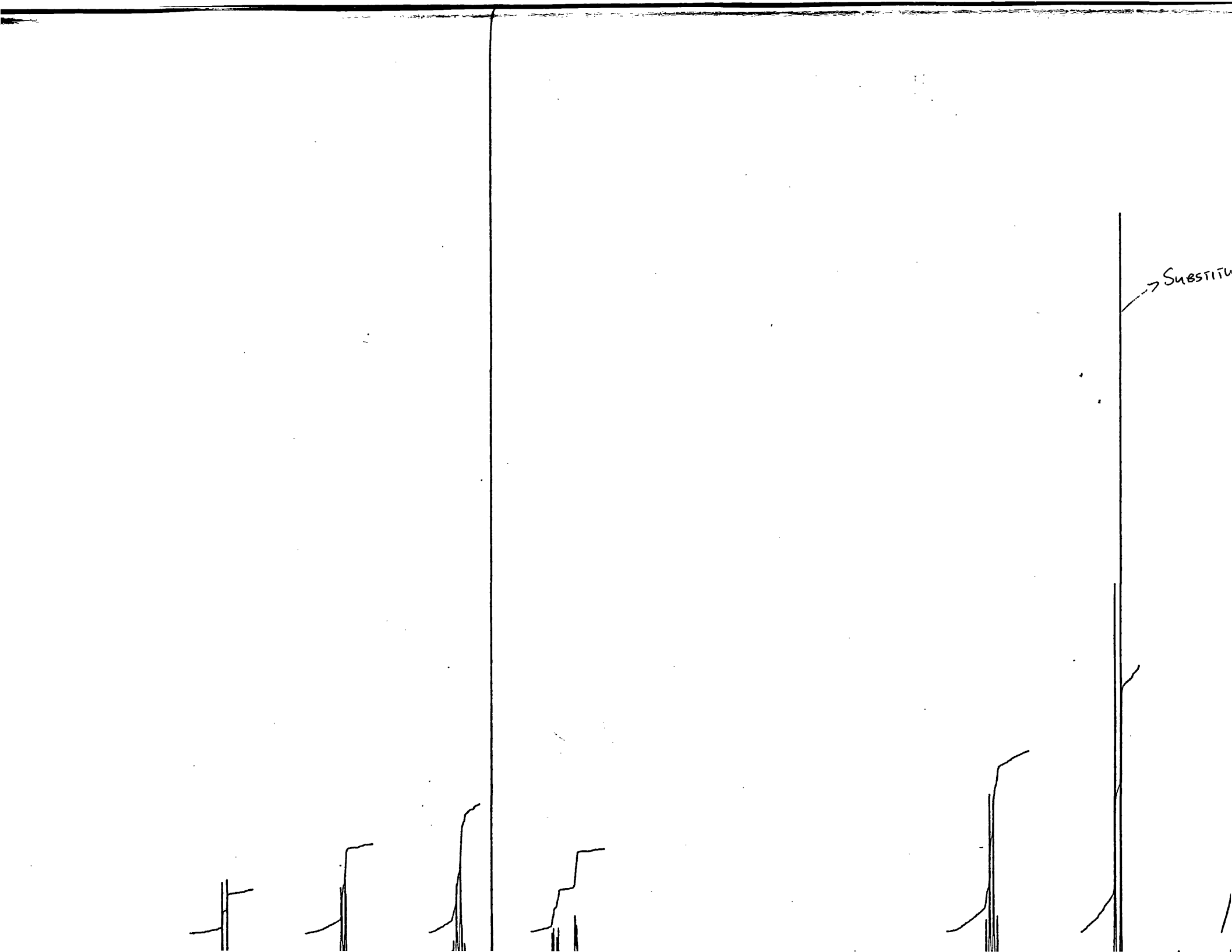
Substitu

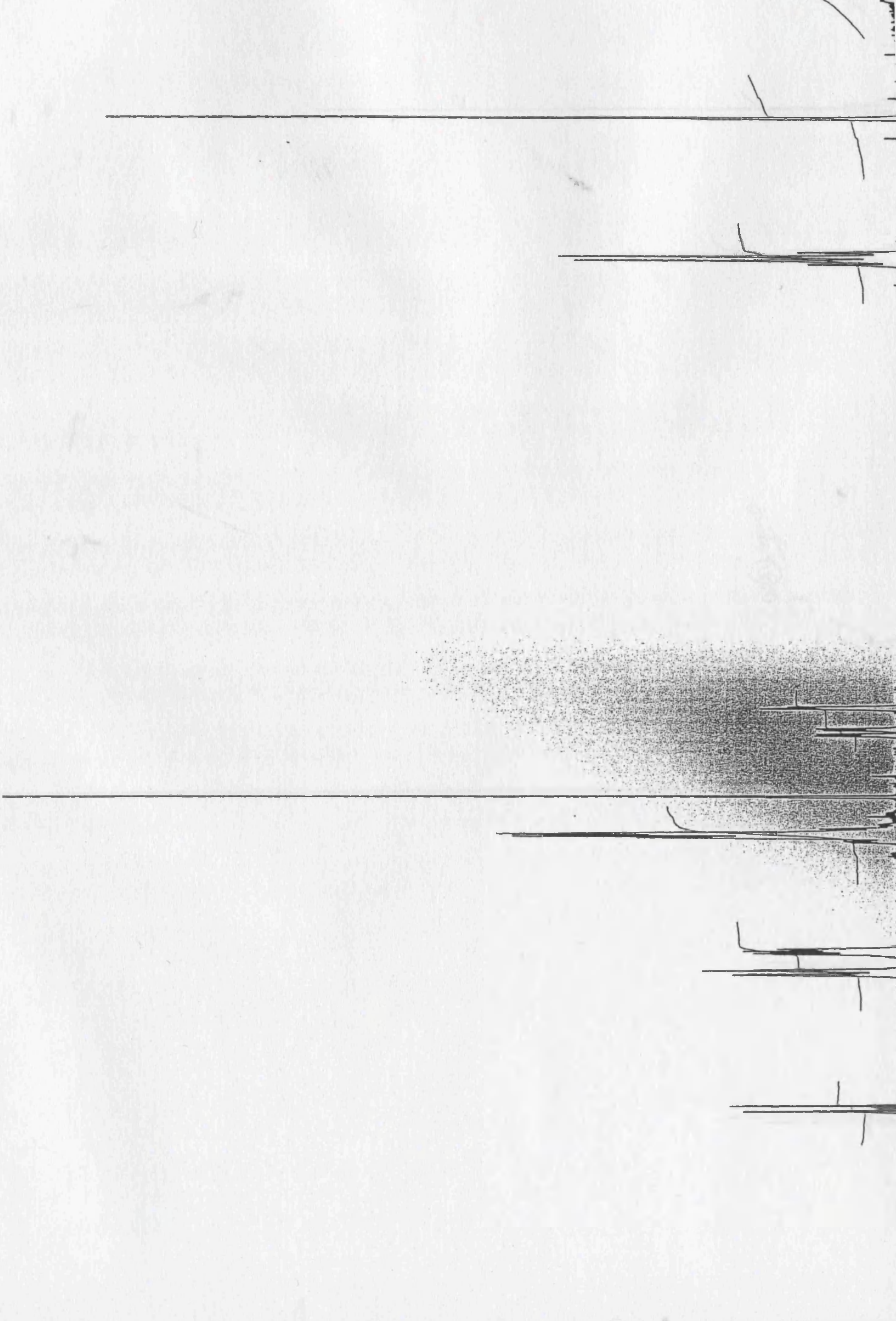


(CH3)2group.

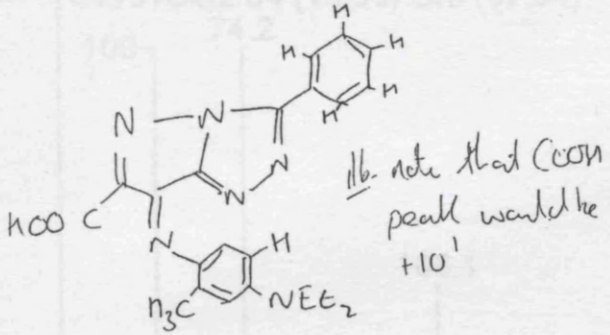

11b. note that COOH peak would be +10'

SOLVENTS PEAKS

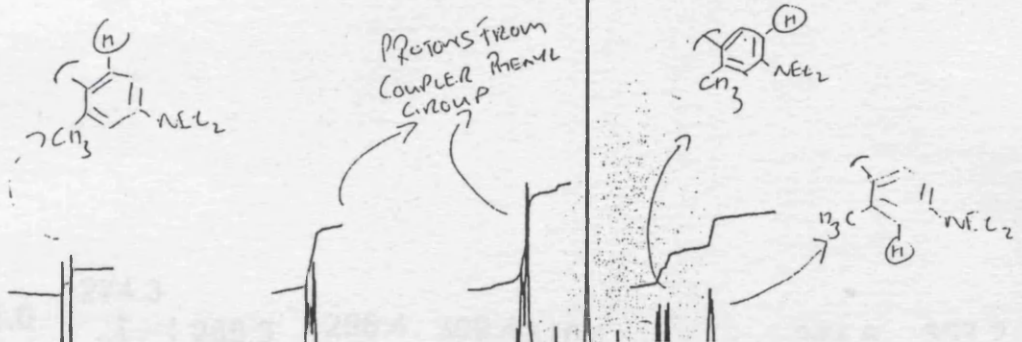

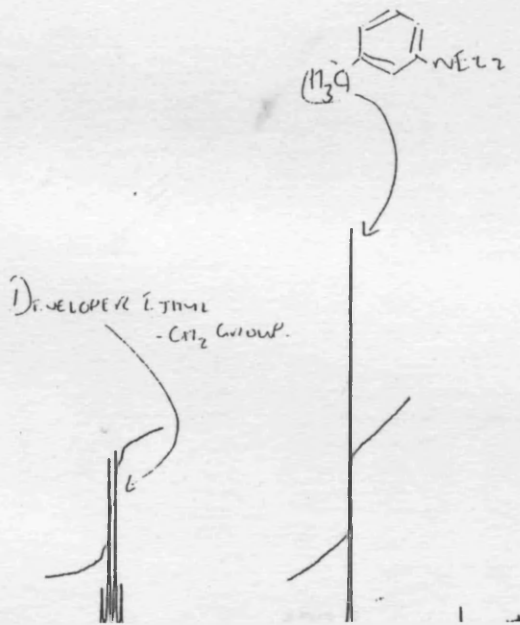

JTME MW=372?
Thomas
SW01DO2 64 (1.290) Cm (57:64)

EPSRC National Centre, Swansea
QUATTRO

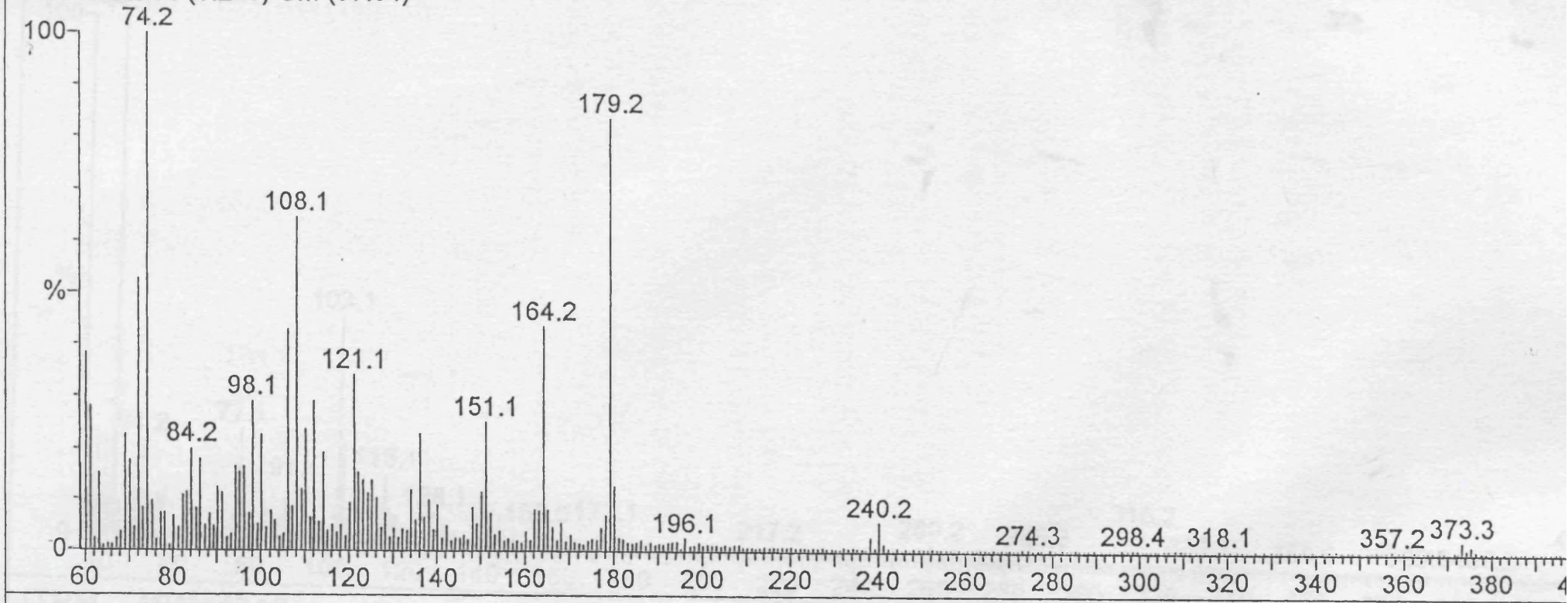

JTME MW=372?
Thomas
SW01DO2 64 (1.290) Cm (57:64)

EPSRC National Centre, Swansea
QUATTRO

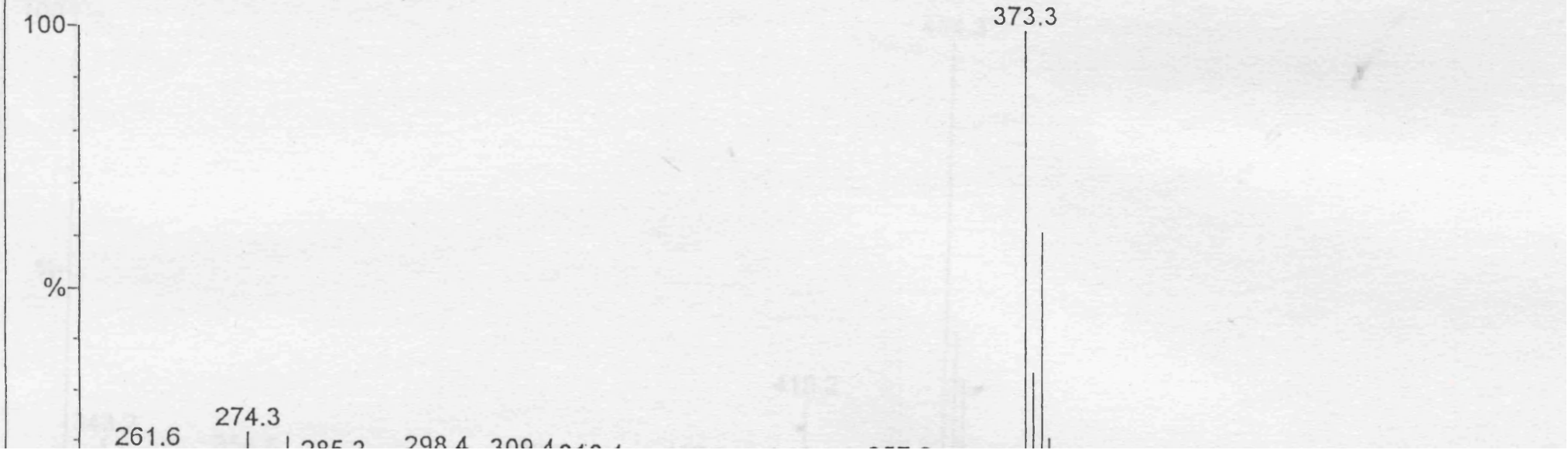

JTPM MW=434?

Thomas

SW04DOU 140 (2.592) Cm (136:140)

EPSRC National Centre, Swansea

QUATTRO

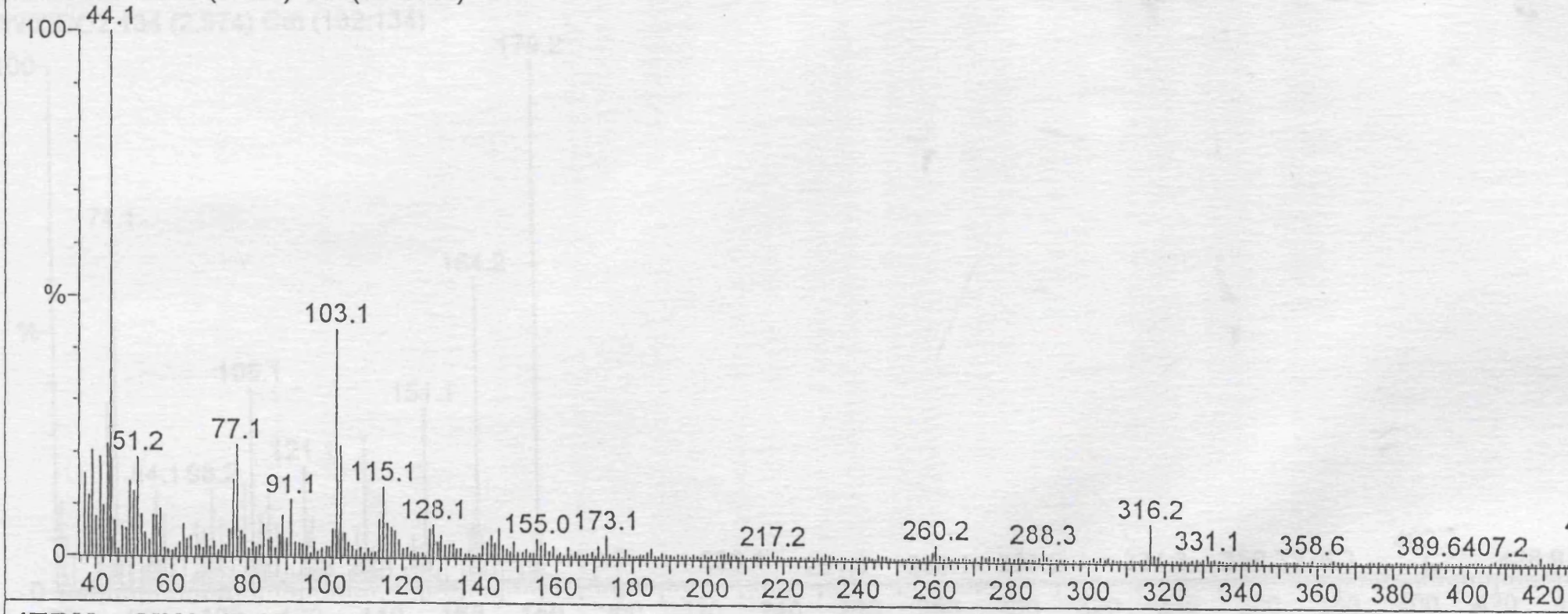

JTPM MW=434?

Thomas

SW04DOU 140 (2.592) Cm (136:140)

EPSRC National Centre, Swansea

QUATTRO

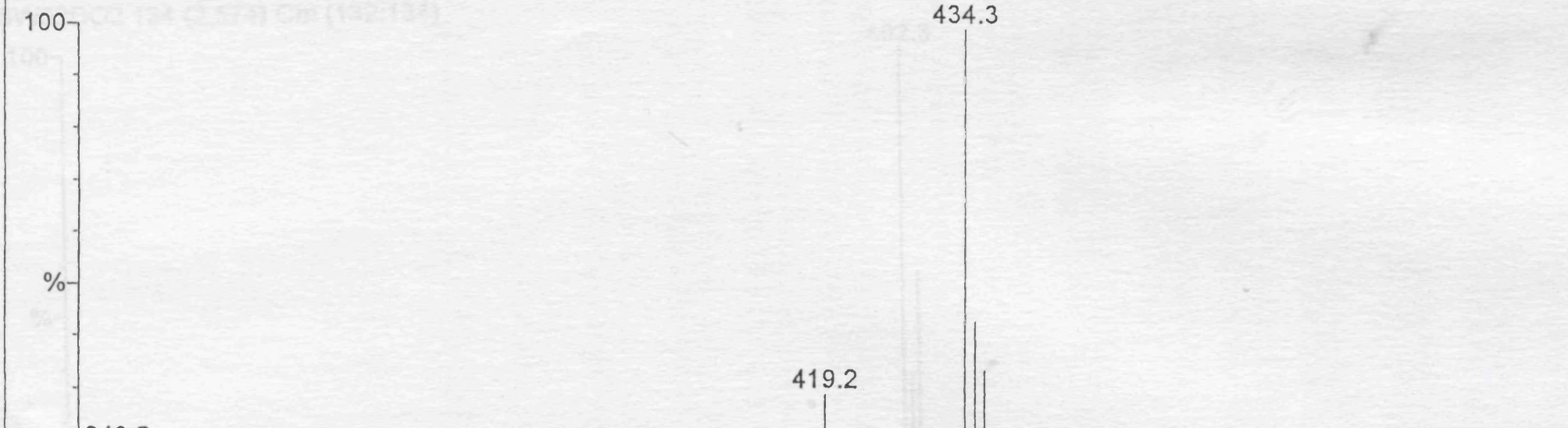

JTAMIDE MW=401?
Thomas
SW02DO2 134 (2.574) Cm (132:134)

EPSRC National Centre, Swansea
QUATTRO

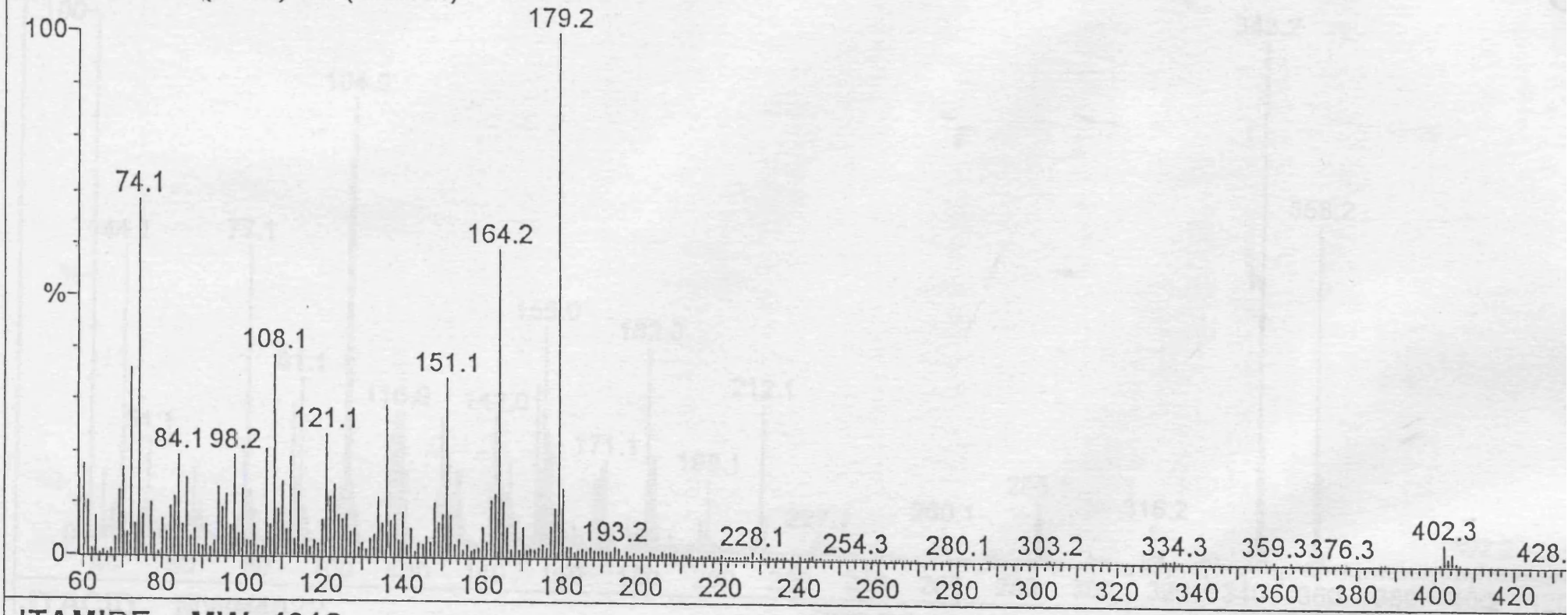

JTAMIDE MW=401?
Thomas
SW02DO2 134 (2.574) Cm (132:134)

EPSRC National Centre, Swansea
QUATTRO

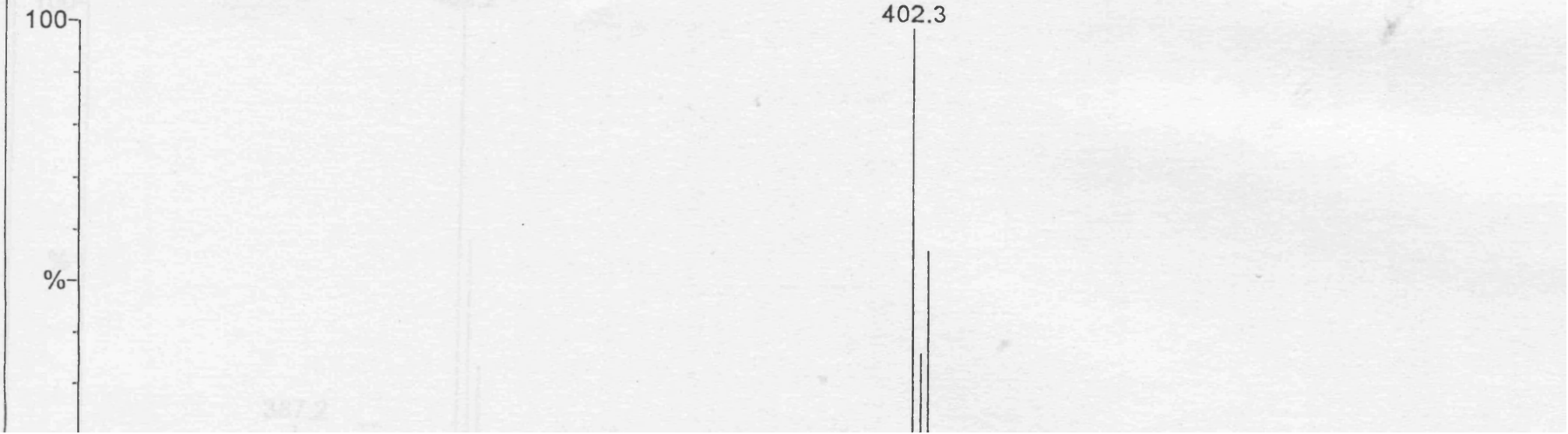

JTACID MW=402?

Thomas

SW03DOU 137 (2.537) Cm (136:137)

EPSRC National Centre, Swansea
QUATTRO

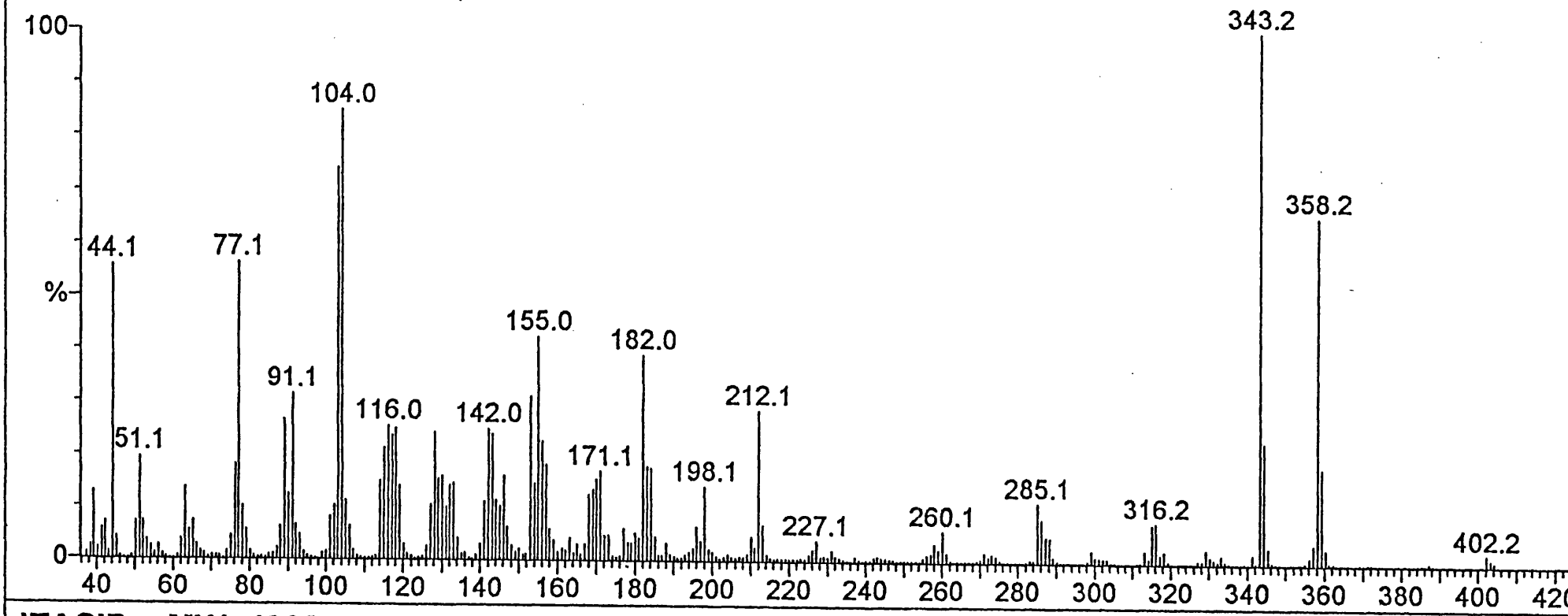

JTACID MW=402?

Thomas

SW03DOU 137 (2.537) Cm (136:137)

EPSRC National Centre, Swansea
QUATTRO

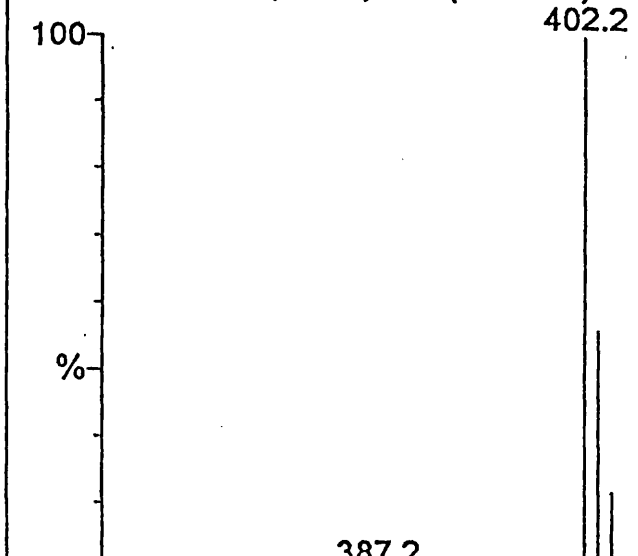

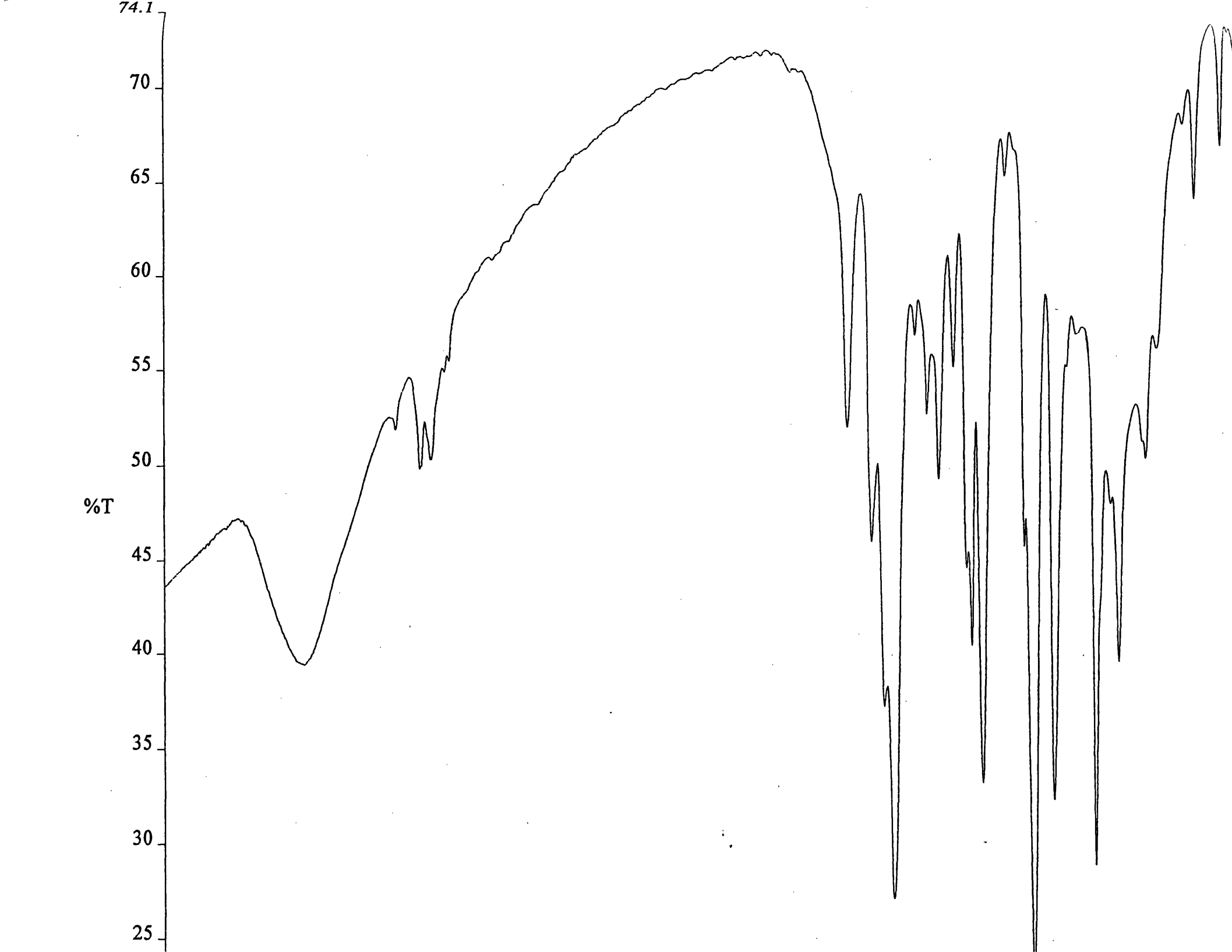
74.1
70
65
60
55
50
%T
45
40
35
30
25

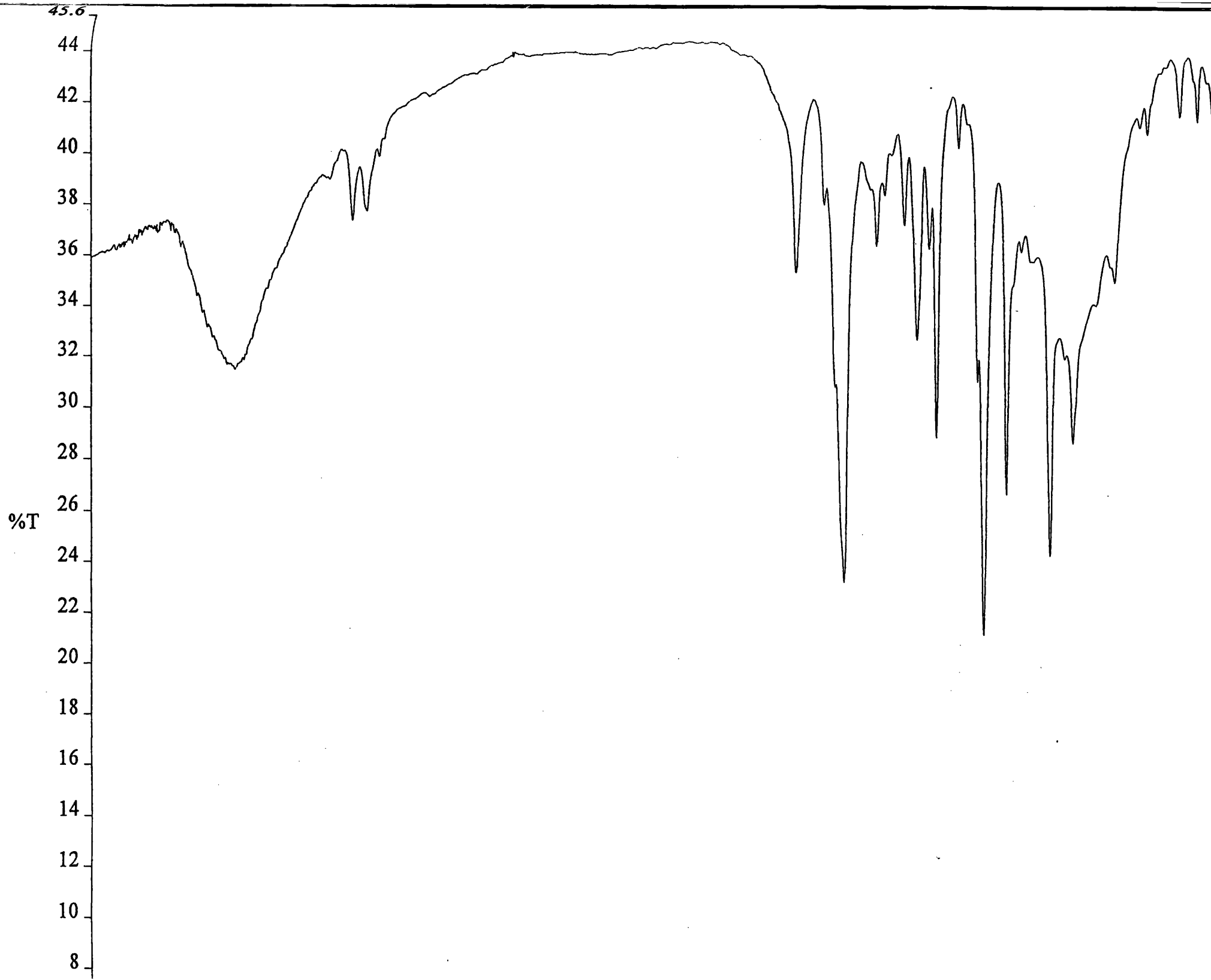
45.6
44
42
40
38
36
34
32
30
28
26
24
22
20
18
16
14
12
10
8
%T

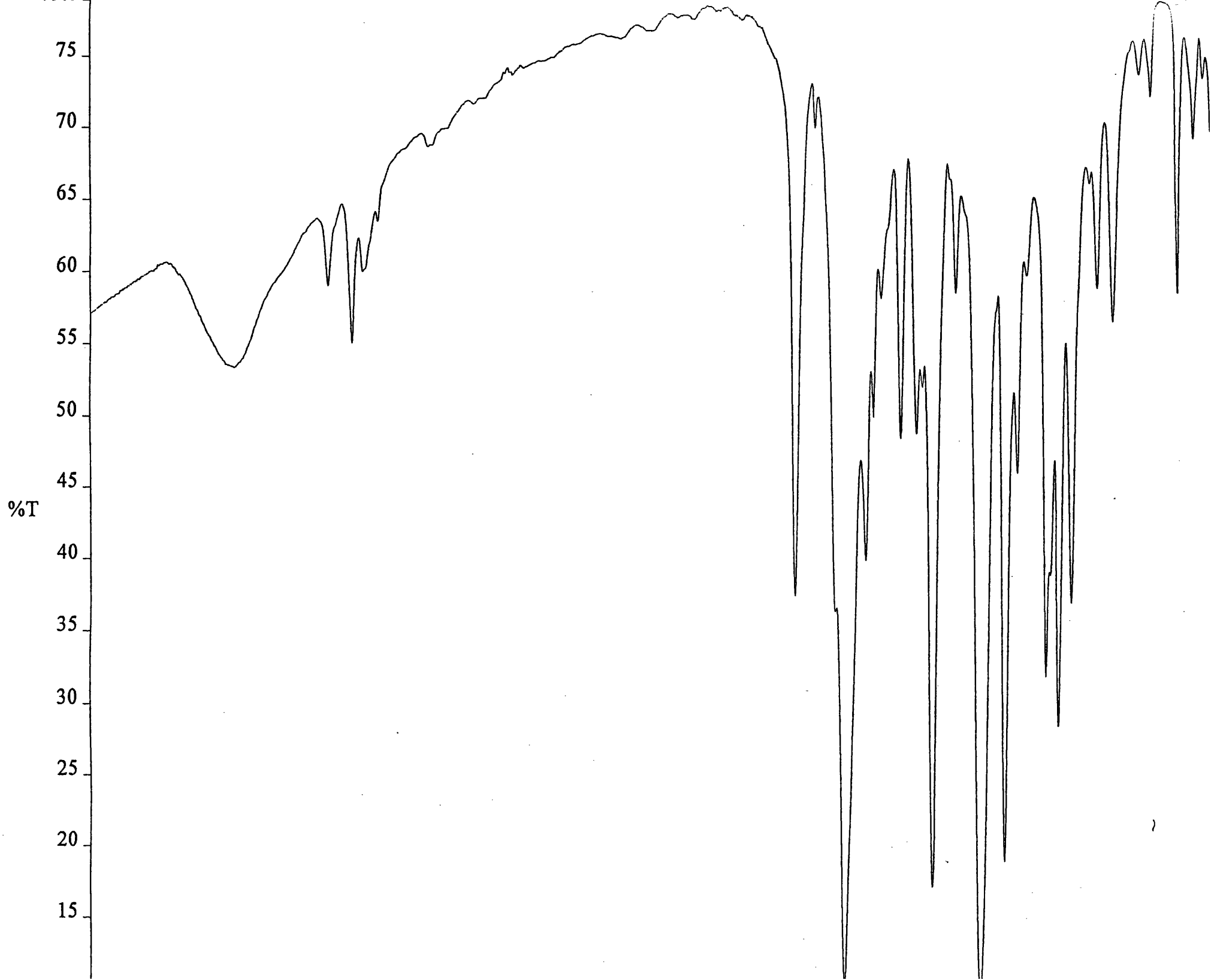
75
70
65
60
55
50
45
%T
40
35
30
25
20
15

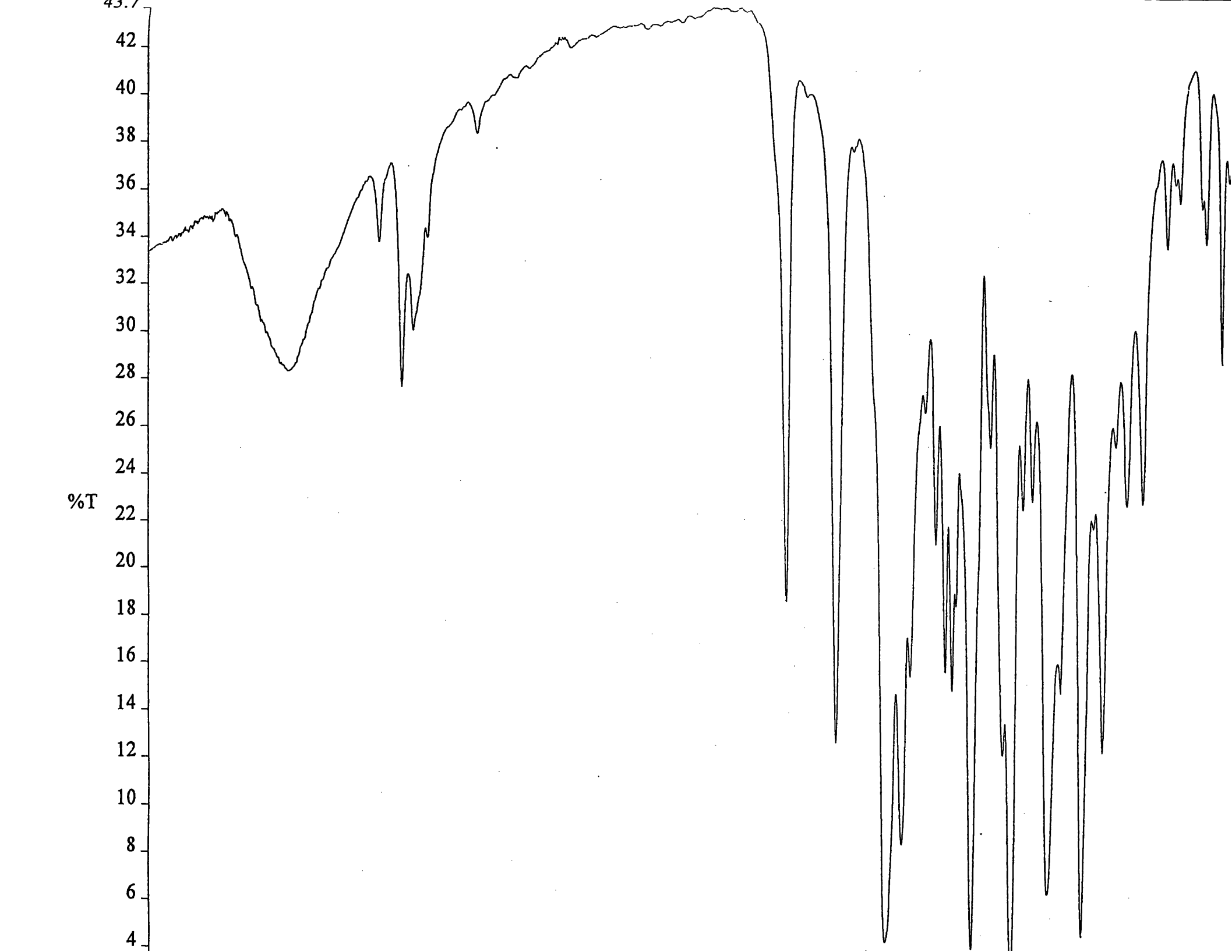
43.7
42
40
38
36
34
32
30
28
26
24
%T
22
20
18
16
14
12
10
8
6
4

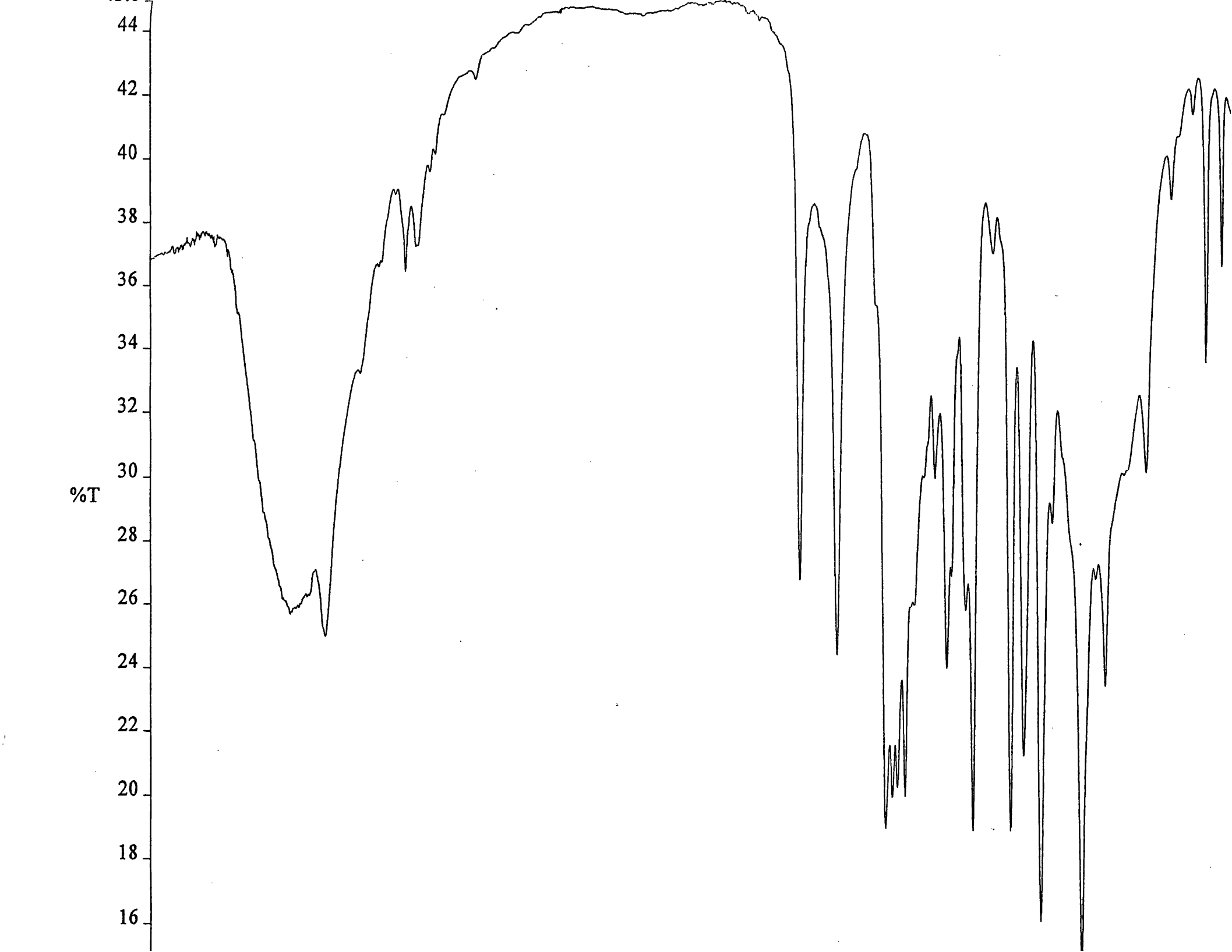
44
42
40
38
36
34
32
30
%T
28
26
24
22
20
18
16

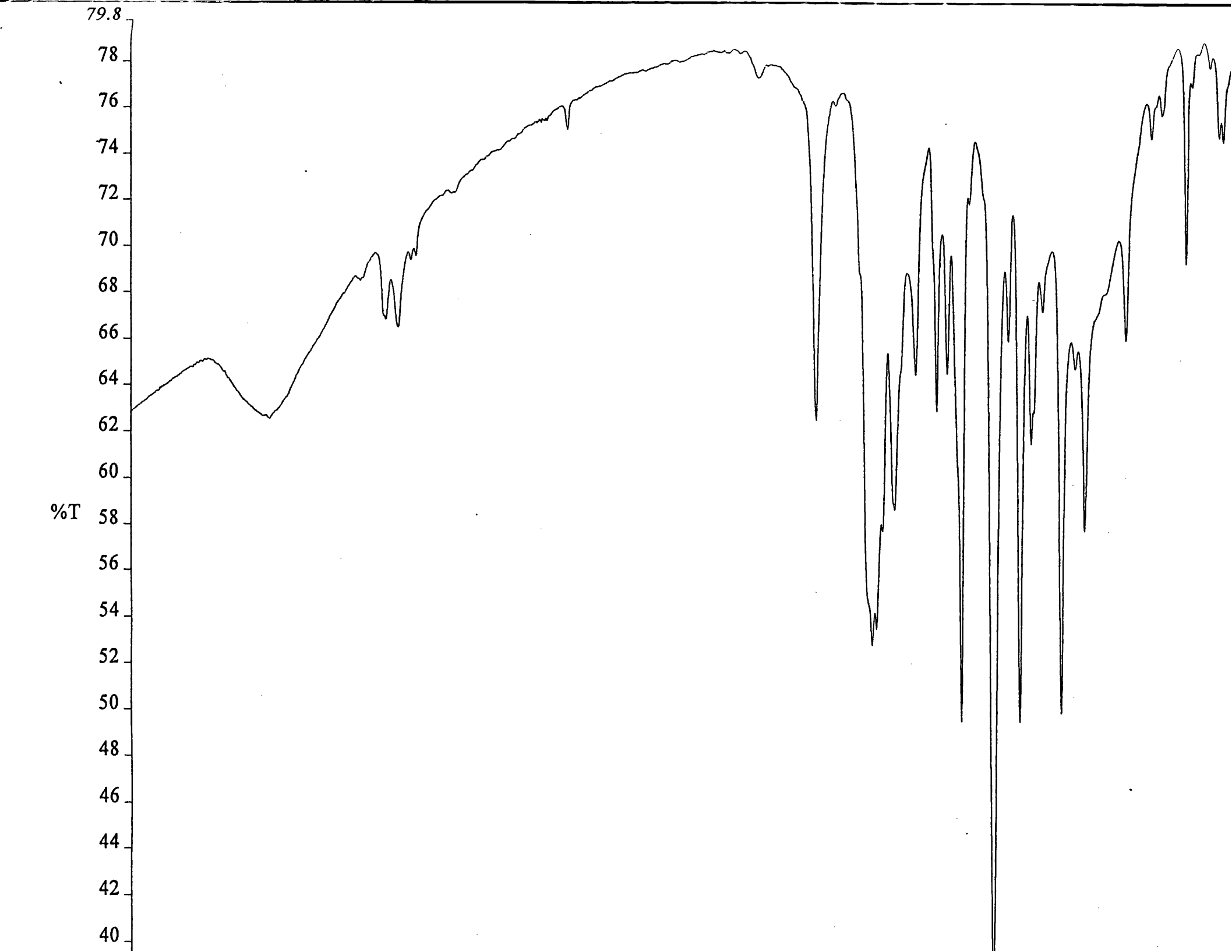
79.8
78
76
74
72
70
68
66
64
62
60
%T
58
56
54
52
50
48
46
44
42
40

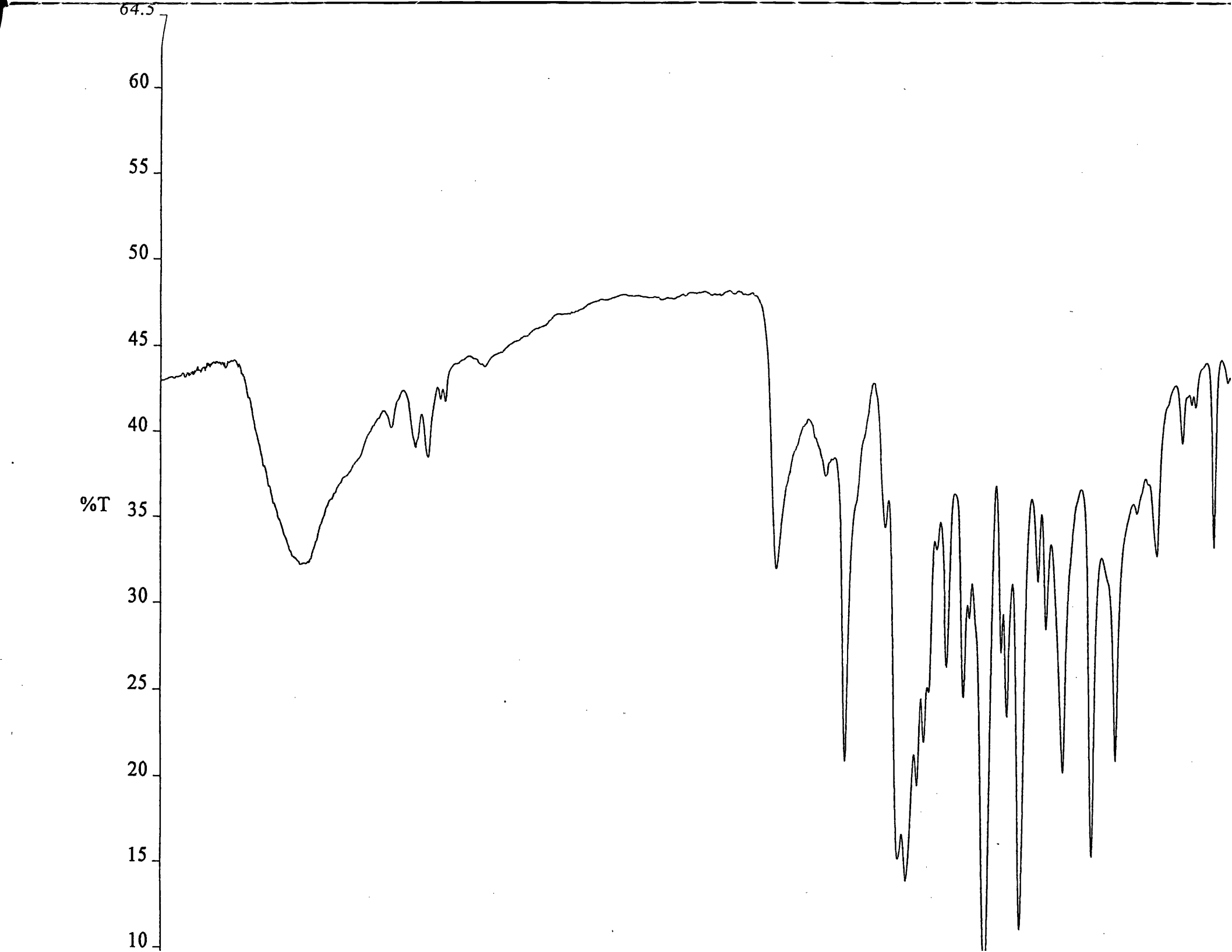
64.5
60
55
50
45
40
%T
35
30
25
20
15
10